8-12-2016

Synthesis and Determination of Optical Properties of Selected Pentamethine Carbocyanine Dyes

Tyler L. Dost
tdost1@gsu.edu

SYNTHESIS AND DETERMINATION OF OPTICAL PROPERTIES OF SELECTED PENTAMETHINE CARBOCYANINE DYES

by

TYLER L. DOST

Under the Direction of Maged Henary, Ph.D.

ABSTRACT

This thesis begins with a brief review about the role and importance of the small molecules containing fluorine atoms in medicine and imaging. Then, the first part of the thesis will discuss the synthesis, purification and characterization of pentamethine cyanine dyes. The structure identification of the final dyes is done by using ^{1}H NMR, ^{13}C NMR, ^{19}F NMR, and mass spectrometry. The studies performed after full characterization were the determination of optical and physicochemical properties. After these properties were performed, the fluorophores were evaluated to be good candidates for *in vivo* testing.

INDEX WORDS: near-infrared, preoperative medicine, fluorophore, intraoperative imaging, cyanine, fluorescence

SYNTHESIS AND DETERMINATION OF OPTICAL PROPERTIES OF SELECTED PENTAMETHINE CARBOCYANINE DYES

by

TYLER L. DOST

A Thesis Submitted in Partial Fulfillment of the Requirements for the Degree of

Master of Science

in the College of Arts and Sciences

Georgia State University

2016

SYNTHESIS AND DETERMINATION OF OPTICAL PROPERTIES OF SELECTED PENTAMETHINE CARBOCYANINE DYES

by

TYLER L. DOST

Committee Chair: Maged Henary

Committee: Markus Germann

Alfons Baumstark

Electronic Version Approved:

Office of Graduate Studies

College of Arts and Sciences

Georgia State University

August 2016

DEDICATION

Zu meinem Papa : Sie geben mir den Antrieb und die Kraft , alles zu tun ich träumen konnten zu tun und meine Ziele zu erreichen . Vielen Dank.

ACKNOWLEDGEMENTS

Firstly, I would like to thank my committee for allowing me the opportunity to present my work and give a good reflection of the help that they have given me. I would especially like to thank Dr. Maged Henary, who has not only been my PI for 4 years, but a mentor and a leader in research. I would like to thank Dr. Alfons Baumstark for talking with me for hours and hours about classes, work, my future, and what is truly important in this world. You also guided me through what is right and wrong in this strange world of academics and research. And I would also like to thank Dr. Gigi Ray who looked after me not only as a professor through classes, making sure I got into research and helping me to set my coursework, but also as a friend.

A giant thank you to my lab mates and group members: Cory, Andy, Eddie, and Matt. Thank you to all of my friends in chemistry. To Lizzy, Alex, Jalisa, Crystal, Jeff and Zeus. I am the youngest of us all and you guys have looked after me like a younger brother. I am truly honored and grateful that you keep me around and that you helped me through my Master's degree. You are some of the best friends someone could ask for and you were only right around the corner at all times.

To Momma BH, There is no way I can thank you for instilling in me your passion of chemistry. I now love the subject and (just about) everything that comes with it. You were a wonderful teacher and the best example to push me into the subject I will be dealing with for the rest of my life.

To my family: There aren't enough words to say in this language, but thank you so much for the love and support shown to me. I do this so you can say "my son/brother" is doing something with his life. And finally to Meghan, you pushed and pushed me and I am a better person having

someone like you who cares. I could always complain or show off or brag or even just talk to you and even when you had no idea what I was talking about, you listened and you gave the best advice.

TABLE OF CONTENTS

ACKNOWLEDGEMENTS ..... **ii**

LIST OF TABLES ..... **vii**

LIST OF FIGURES ..... **viii**

LIST OF SCHEMES ..... **xi**

1 INTRODUCTION: THE ROLE OF Small molecules containing fluorine Atoms IN MEDICINE AND IMAGING **1**

1.1 Atomic Fluorine **1**

1.2 Common Reactions Involving Fluorine **3**

1.3 Fluorine in Medicine **5**

1.3.1 Metabolic Oxidation ***7***

1.3.2 Electronic Considerations ***10***

1.3.3 Size Considerations ***14***

1.4 Fluorine Incorporated into Imaging Agents **16**

1.4.1 Coumarin ***17***

1.4.2 Fluorescein/Rhodamine ***18***

1.4.3 BODIPY ***20***

1.4.4 Near-Infrared (NIR) ***22***

1.5 Imaging Techniques for Early Disease Detection **25**

1.6 Fluorine in Positron Emission Tomography (PET) 25

1.7 Fludeoxyglucose (^{18}F-FDG) and Other Tagged Molecules for Imaging Including Synthesis 28

1.8 Conclusion 31

1.9 REFERENCES 32

2 Synthesis and Characterization of Pentamethine Carbocyanine fluorophores 35

2.1 Introduction: Intraoperative Imaging 35

2.2 Rationale 37

2.3 Synthesis and Optical Property Determination of Halogenated Pentamethine Dyes 38

2.3.1 Synthesis of Pentamethine Fluorophores 39

2.3.2 Optical Properties 40

2.3.3 Physicochemical Properties 43

2.3.4 Conclusions 45

2.3.5 Experimental Details 45

2.4 Synthesis and Optical Properties of Asymmetric Pentamethine Cyanine Dyes 52

2.4.1 Introduction 52

2.5 Results and Discussion 53

2.5.1 Synthesis 53

2.5.2 Optical Properties Study *55*

2.5.3 Physicochemical *58*

2.5.4 Conclusion *60*

2.5.5 Experimental Details *61*

2.6 Synthesis and Optical Properties of Near-Infrared Pentamethine Dyes with N-Substituted Pentanoic Acid Groups **65**

2.6.1 Synthesis and Purification of Pentamethine Dyes *66*

2.6.2 Optical Properties and Physicochemical Calculations *67*

2.6.3 Conclusions *69*

2.6.4 Experimental Details *70*

2.6.5 References *74*

APPENDICES **76**

Chapter 1 ..... **76**

Appendix A.1 ^{1}H NMR Spectra *76*

Appendix A.2 ^{13}C NMR Spectra *96*

Appendix A.3 ^{19}F NMR Spectra *109*

Appendix A.3 Mass Spectra *112*

Appendix A.4 Absorbance and Fluorescence Spectra *116*

Appendix B.4 Physicochemical Properties *119*

LIST OF TABLES

Table 1. The half-lives and positron energies of several radionuclides that can used for PET and SPECT scans 27

Table 2. Optical Properties of 700 nm Emitting NIR Fluorophores, **14**-**28**.[a] 41

*Table 3. A comparison of symmetrical and unsymmetrical pentamethine cyanine dyes **11 a-c** and **10 a-c**. The novel dyes optical properties were performed in polar protic and aqueous solvents* 57

Table 4. A comparison of symmetrical and asymmetric pentamethine cyanine dyes **11 d-f** and **10 d-f**. The novel dyes optical properties were performed in polar protic and aqueous solvents. 58

Table 5. The HOMO/LUMO levels and energy calculated using Spartan '14. 58

Table 6. The optical property data collected from compounds **4a-f** in two solvents..... 69

LIST OF FIGURES

Figure 1. The relative sizes of stilbene and decafluorostilbene calculated using Spartan.[5] 1

Figure 2. A flow diagram outlining the effects of adding fluorine on drug leading to final consequences 3

Figure 3. Examples of fluorination reactions involving alkanes or aromatic reactions.[8,9] 4

Figure 4. Examples of an addition (top), allylic substitution (middle), and nucleophilic substitution and rearrangement (bottom) reactions involving a fluoride ion.[8,9] 5

Figure 5. The four most successful pharmaceutical drugs featuring fluorine.[1] 6

Figure 6. The drug Aprepitant, **5**, with a fluorine atom strategically blocking a potential metabolic oxidation site. The red circle highlights the sites blocked from metabolic oxidation.[13] 8

Figure 7. Ezetimibe, **6**, uses the fluorine molecule to block the para-position from metabolic oxidation.[14] 9

Figure 8. Three compounds, **2**, **3**, and **7**, in the statin class of compounds that feature and require a para-fluorophenyl group.[15,16] 10

Figure 9. The parent molecule (top, **8**) and the FDA approved drug derivative, Fulvestrant (bottom, **9**).[18] 11

Figure 10. Vandetanib, **10**, and AV-45 derivatives, **11**, use the fluorine atom to tailor lipophilicity of the overall compounds or of certain parts of the compound.[21] 13

Figure 11. Norfloxacin, **12**, Delafloxacin, **13**, Sparfloxicin, **14**, and 5,8-difluoro-1-(4-methoxybenzyl)-4-oxo-N-phenyl-1,4-dihydroquinioline-3-carboxaminde, **15**.[19-20] 14

Figure 12. Nilotinib, **16**, is a compound that inhibits a tyrosine kinase inhibitor in patients with chronic myelogenous leukemia.[24] 15

Figure 13. Lapatinib, **17**, utilizes fluorine as an essential size requirement for potency. [25] 16

Figure 14. Two Coumarin dyes, **18** and **19**, featuring fluorine atoms that fluoresce at around 450 nm.[29] 18

Figure 15. Fluorescein, **20**, and fluorine containing derivatives, **21**-**23** showing decreased photobleaching and comparable quantum yield.[33] 19

Figure 16. Several rhodamine derivatives featuring fluorine and trifluoroethyl groups, compounds **24-27**.[34] 20

Figure 17. The general structure of a BODIPY dye, **28**.[37] 21

Figure 18. Two examples of BODIPY dyes **29** and **30** featuring fluorine or trifluoromethyl groups outside of the basic structure. [37] 22

Figure 19. The general structure of the cyanine dye class.[35] 23

Figure 20. Representative carbocyanine dyes featuring the fluorine atom, **31**-**34**.[7,38-40] 24

Figure 21. The annihilation pathway undergone by an ^{18}F atom as well as the gamma ray pathways picked up by a surrounding PET detector. 26

Figure 22. Examples of compounds from sources **35-38** respectively.[42,45,46] 28

Figure 23. The synthesis of radiolabel ^{18}F-FDG.[53] 29

Figure 24. Examples of synthetic routes to derive radiolabeled compounds, **39**-**42**, from unlabeled precursors.[49-52] 30

Figure 25. An illustration of a system of NIR cameras visualizing dyes to be used intraoperatively. 36

Figure 26. Photodegradation profile in light and dark conditions of a select subset of NIR fluorescent contrast agents. The absorbance values for the individual fluorophores were measured (at the wavelength of maximum absorption) at different intervals to determine the percentage of absorption remaining. 43

Figure 27. HOMO/LUMO calculations of compounds **10f** and **11f**. Both the energy gap and the energy levels differ significantly between the symmetric and asymmetric compounds. 60

Figure 28. The HOMO (top) LUMO (bottom) 68

LIST OF SCHEMES

Scheme 1. A standard route taken to make cyanine dyes with longer chain lengths. 23

Scheme 2. Synthesis of 700 nm Emitting Pentamethine Cyanines Featuring Neutral (X = H) and Electron-Withdrawing (X = F, Cl, Br, CF3) Moieties, compounds **14**-**28**. [Owens, 2016 #69] .. 39

Scheme 3. Synthetic routes taken to obtain symmetrical (A.) and unsymmetrical pentamethine cyanine dyes (B.). i. acetic acid (25mL), reflux, 72hr; ii. acetonitrile, reflux, 24hr; iii. sodium acetate, acetic anhydride, RT, 20min; iv. sodium acetate, acetic anhydride, 60 ^{o}C, 20 min; sodium acetate, acetic anhydride, 60 ^{o}C, 30 min. 54

Scheme 4. The synthetic route used to obtain compounds **4 a**-**f** from the starting material phenyl hydrazines **1**. 66

1 REVIEW: THE ROLE OF SMALL MOLECULES CONTAINING FLUORINE ATOMS IN MEDICINE AND IMAGING

1.1 Atomic Fluorine

The growing importance of the fluorine atom incorporated into molecules in medicine is undeniable. During the past 20 years, publications, patents and medically viable fluorine-containing compounds have been published at a rapid rate with three of the top ten and four of the top twenty blockbuster drugs containing fluorine somewhere on the molecule. These four drugs alone account for 16.7 billion dollars in income since 2011. [1] The utilization of the fluorine atom and its use as a functional group is very attractive in the medical field for many reasons. Firstly, the fluorine atom is the second smallest "functional group". Its size falls between that of a hydrogen atom and a hydroxyl group. Accompanying that, the trifluoromethyl group is similar in size to a methyl, 2.107 Å vs. 1.715 Å,[2] however, the trifluoromethyl group occupies more space than an isopropyl group in terms of single-bond rotational barriers.[3,4] As shown in Figure 1 below, modeling studies performed reveal the relative sizes and electrostatic potentials of these groups on a stilbene ring.

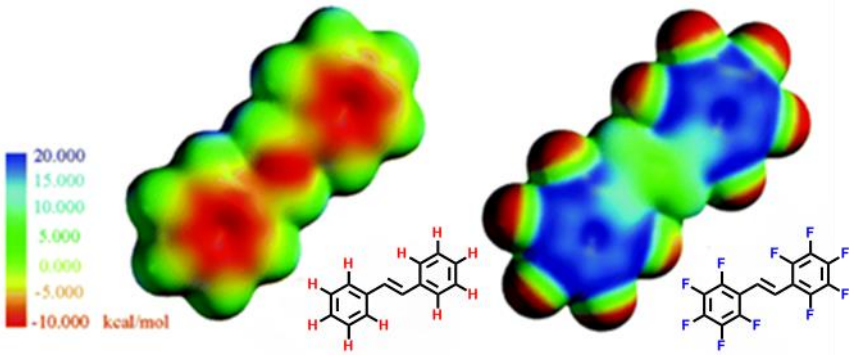

Figure 1. The relative sizes of stilbene and decafluorostilbene calculated using Spartan.[5]

Advantages accompanying the size of fluorine, it being the smallest halogen, allows for it and its "methyl" form to fit into smaller pockets of space in comparison to the other halogens and their corresponding groups. A second advantage is the atom's electronegativity. Fluorine is the most electronegative atom with a value of 4.0 on the scale developed by Linus Pauling. This value translates into several key physical and chemical properties. The C-F bond is considered the strongest bond in organic chemistry due to the electronegativity difference between the two atoms.[6] The electronegative nature of fluorine changes the dipole moment and direction of molecules as well as changing the pK_a of the molecule. The consequences stemming from the addition of a fluorine atom's size and electronegativity included on a pharmaceutical are drug distribution, drug receptor binding and potency. A third advantage of the fluorine atom regarding its use in medical and biomedical imaging applications is its ability to increase lipophilicity. The tuning of lipophilicity allows researchers to allow for the compounds to be absorbed and transported *in vivo* faster and more easily. This stems from the fact that the C-F bond is more hydrophobic than that of the C-H bond.[7] The most important reason that fluorine is featured in about 25% of all pharmaceutical drugs on the market is metabolic oxidation and the role the fluorine atom plays into blocking sites from this process. These last two properties of a fluorinated compound determine how the body reacts to the compound in ways such as the clearance rate and route of the molecule as well as the toxicity of the molecule on living and tissue.

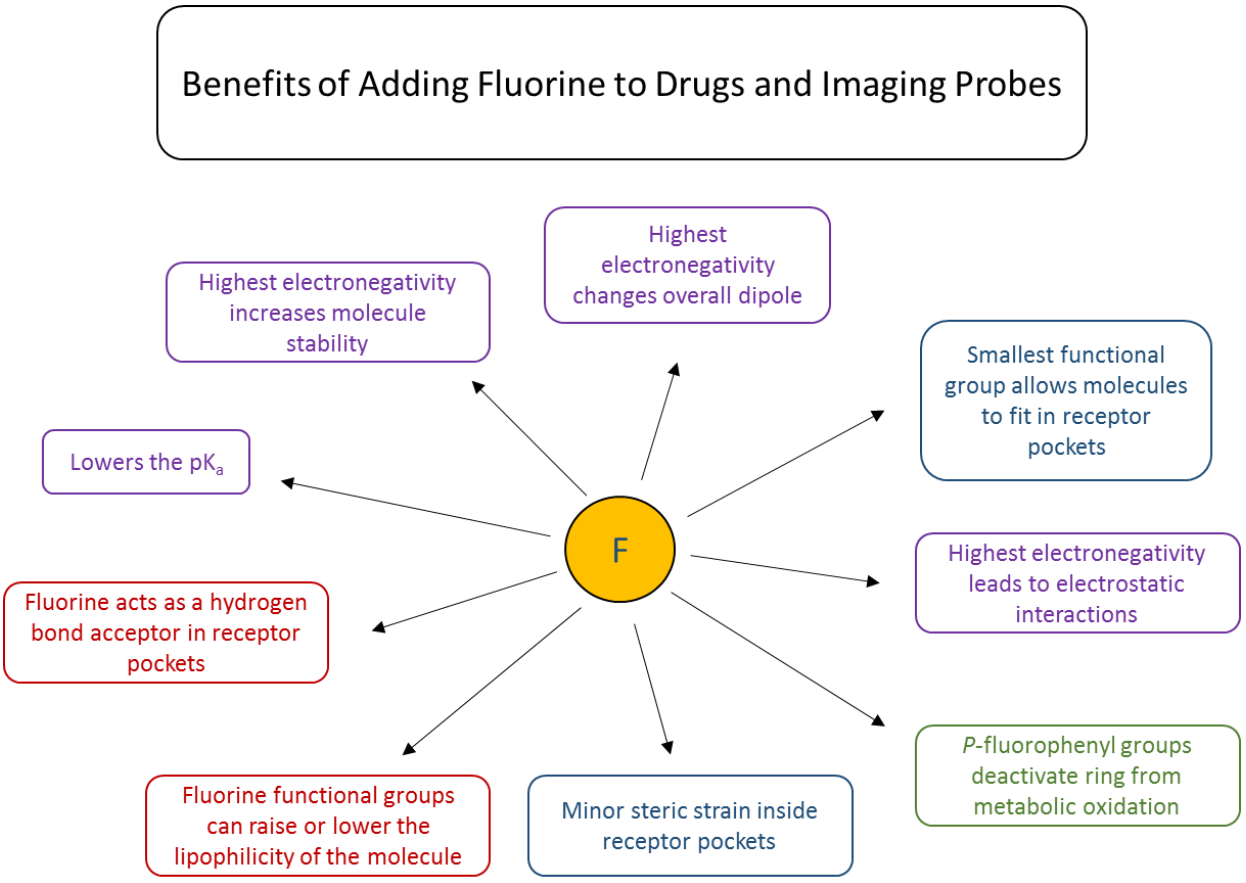

Figure 2. A flow diagram outlining the effects of adding fluorine on drug leading to final consequences.

1.2 Common Reactions of Incorporating Fluorine to Small Molecules

To synthesize drugs and pharmaceuticals containing the fluorine atom, and other fluorine containing functional groups, it is important to understand the reactions involving fluorine. Here, three reactions involving fluorine on saturated alkyl systems are described. The first reaction is one that is performed in industrial large scale settings and involves hydrogen fluoride (HF). This reaction uses it as a nucleophilic substitute for other halogens; this process is somewhat limited to allylic and benzylic halogens.[8] Two examples of this reaction are shown in Figure 3, reactions 1 and 2. Another reaction commonly used to incorporate fluorine is the basic Friedel-Crafts (FC)

alkylation. Hydrogen fluoride in this case acts as both the FC catalyst and the fluorinating agent itself to prepare trifluormethylated aromatic systems. The carbon tetrachloride reagent, in Figure 3, equation 3 below, replaces a hydrogen on the benzene ring, followed by the substitution of fluorine for the three chlorine atoms. A third reaction that requires a Lewis acid catalyst is referred to as the Swarts reaction. This involves a metal fluoride species acting as the catalyst in removing a previous halide and substituting it with a fluorine atom after a four-member intermediate is formed.[9] These three examples involve saturated alkyl or aromatic systems and examples are shown below.

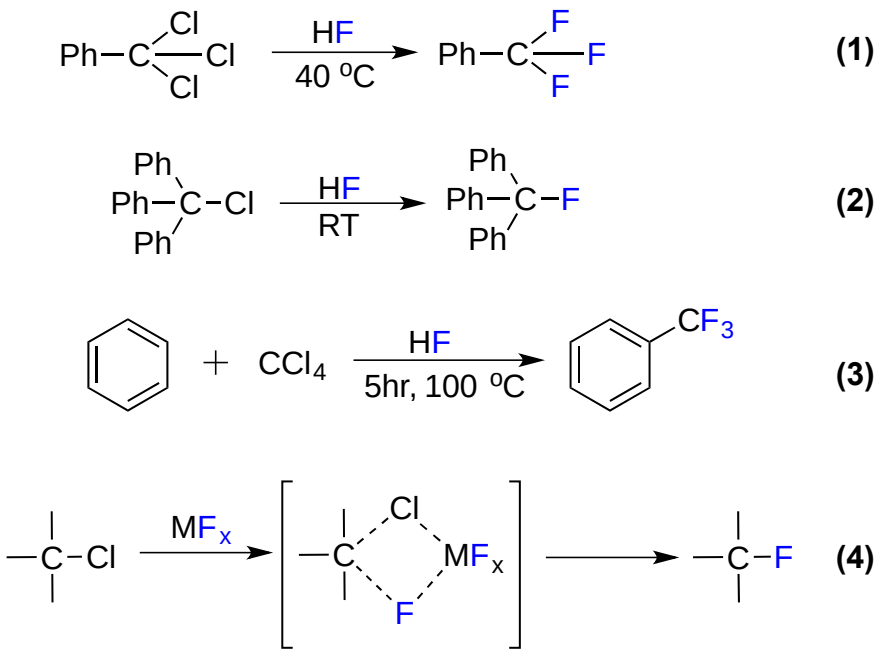

Figure 3. Examples of fluorination reactions involving alkanes or aromatic reactions.[8,9]

Substitution or addition/elimination reactions can also occur on unsaturated alkyl chains at vinylic or allylic positions. A fluorine anion, usually stemming from some metal complex, acts as the nucleophile and attacks the alkene system. This reaction can occur directly at the point of

unsaturation as well as at allylic or vinylic positions. Examples of these reactions are shown in Figure 4 as well as a rearrangement reaction. These are just basic reactions involving fluorine, synthesis of several fluorine containing drugs are visualized later in this review.

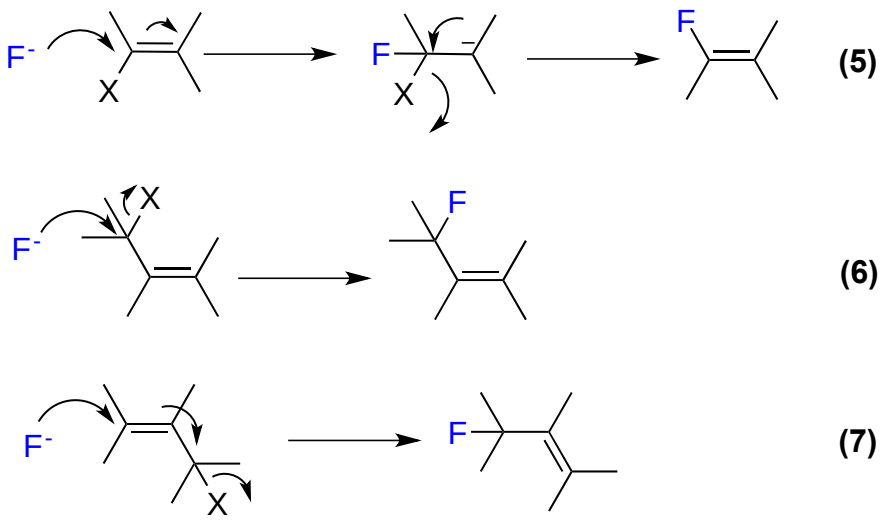

Figure 4. Examples of an addition (top), allylic substitution (middle), and nucleophilic substitution and rearrangement (bottom) reactions involving a fluoride ion.[8,9]

With the emergence of fluorine incorporated into drugs and its apparent positive effects on the compounds, fluorinating reagents such as alkyl chains, heterocycles and fluorine-metal complexes are all commercially available and readily obtained for continuing syntheses.[9]

1.3 Fluorine Role in Medicine

As alluded to earlier, four compounds in the top 20 of the highest grossing pharmaceuticals feature fluorine: Lipitor, **1**, Advair Diskus, **2**, Crestor, **3**, and Lexapro, **4**.[1] These drugs treat high cholesterol, asthma, high cholesterol, and depression and anxiety disorders respectively; it is obvious that these drugs are used by patients in every demographic and their functions effect millions of people worldwide. Shown in Figure 5 below, these compounds represent only a fraction

of new pharmaceuticals that contain at least one fluorine atom. In fact, in 2007 alone, 9 of the 19 drugs approved by the FDA contained fluorine.[10] As seen in Figure 5 outlining the structures of the four drugs, a parafluorophenyl group is present in three of the molecules and at least one fluorine atom exists on all four. In this sections, drugs and pharmaceuticals will be described and categorized in detail as outlined in Figure 2. Compounds that feature fluorine for each reason in the chart above will be explored for the research done and the process leading researchers to apply fluorine groups onto their lead compounds.

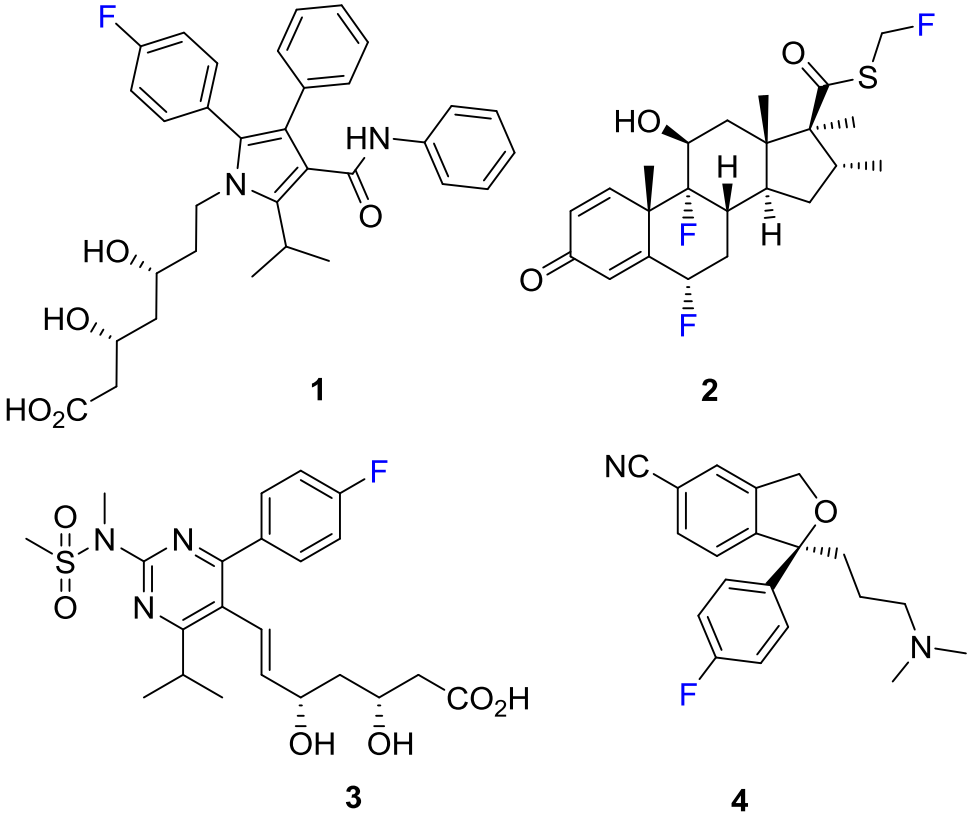

Figure 5. The four most successful pharmaceutical drugs featuring fluorine.[1]

1.3.1 Metabolic Oxidation

As previously mentioned, a large reason to incorporate the fluorine atom, especially on aromatic ring systems is to combat the effect of metabolic oxidation. This process occurs when drugs are taken into the body; this a natural reaction from the body on drugs when taken is to eliminate them as quickly as possible. The P450 monooxygenase protein accomplishes this by oxidizing CH bonds, generally at the para-position on a benzene ring featured in most drugs. The addition of an atom or group stops this pathway as the molecule may not fit into the active site of the monooxygenase.; the electron withdrawing nature of the fluorine atom deactivates other positions on the ring against this particular metabolic pathway as well.[4] Slowing the P450 protein and its function allows for the drug to remain in the body longer, which in turn increases its potency and viability as a drug. Examples exist of compounds which have very quick bodily clearances, but when fluorine is incorporated, the rate at which the compound is cleared slows by as much as 10^8-fold.[3] And while the main function of the P450 protein is to speed up metabolism, this process can take a pharmaceutically active compound and turn it toxic.[11] For many of the potential pharmaceutically viable compounds, clearance rate and clearance mechanism creates concerns when designing and synthesizing molecules for use in the body. Fluorine and chlorine can block this process from happening, but due to its minimal size and steric perturbation in active sites, fluorine is the preferred atom over chlorine. Many therapeutics highlighted in this introduction share this common theme: a parafluorophenyl group. The protection afforded by the halogen reduces the toxicity of the compound and can make these compounds useful in activation sites in proteins ect.[4,12] The strategy of para-fluorination has been thoroughly investigated and has been frequently used in drug design.[11]

Aprepitant, **5**,[13] serves as an example of a para-fluorine atom serving the purpose of blocking oxidative metabolism and lowering oxidation potential elsewhere on the ring. This drug was approved by the FDA in 2003 for the purpose of preventing chemotherapy-induced nausea and vomiting. The 3,5-bis-(trifluoromethyl)phenyl group is a common feature with other NK_1 receptor antagonists and improves the penetration of the drug into the central nervous system.[13] The *p*-fluorophenyl group blocks the 4-position from oxidation as well as deactivating the remainder of the ring positions.

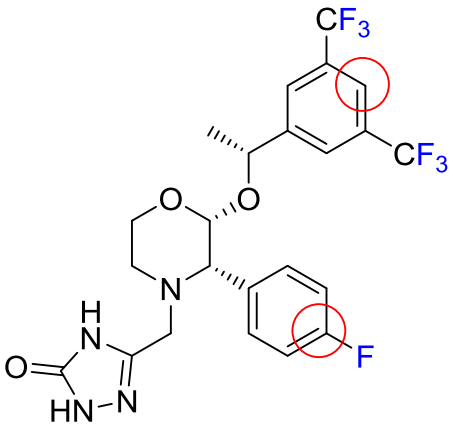

5

*Figure 6. The drug Aprepitant, **5**, with a fluorine atom strategically blocking a potential metabolic oxidation site. The red circle highlights the sites blocked from metabolic oxidation.*[13]

Ezetimibe, **6**,[14] is another drug to combat cholesterol; the drug features a fluorinated phenyl ring to block other sites on the ring from metabolic oxidation as well. Figure 7 shows the structure of Ezetimibe and highlights the blocking of sites due to the fluorine atoms. The compound utilizes the fluorine atoms as this defense against aromatic hydroxylation as well as yielding a derivative that exhibited improved pharmacokinetic properties that also increases the activity of the drug significantly. Another benefit of the fluorine atoms is that they increase the polarity of the overall

molecule. More polar molecules are more susceptible glucuronidation, a process which generally inactivates drugs. However in the case of Ezetimibe, the glucuronidation actually improves the activity of the drug by recirculating the drug to the site of activation and increases the residence time in the area of interest. Therefore the use of fluorine, with its chemical properties, increases lipophilicity and polarity as well as blocking the oxidation sites, displays to researchers the advantages of using this atom, highlighted explicitly by the fact that once fluorine atoms were added to the drug, it displayed a 50-fold increase in activity over the parent atom.

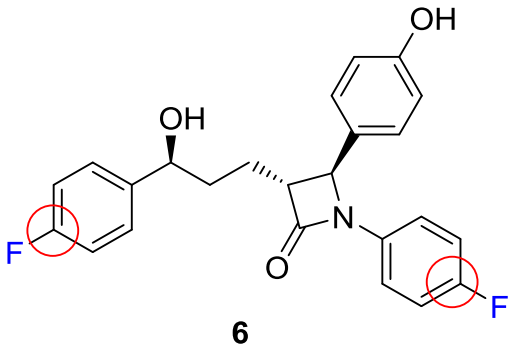

6

*Figure 7. Ezetimibe, **6**, uses the fluorine molecule to block the para-position from metabolic oxidation.*[14]

Synthetic Statins are a class of drugs that require 4-fluorophenyl groups as structural requirements for biological activity. Figure 8 shows Pitavastatin, **7**, atorvastatin (lipitor), **1**, and rosuvastatin (crestor), **3**, as three examples of this synthetic class of drugs. These drugs all combat cholesterol problems by inhibiting the HMG-CoA reductase. All of these compounds feature a parafluorophenyl moiety as studies have shown that substitutions with this group greatly surpasses the potency of all other functional groups tested.[15,16]

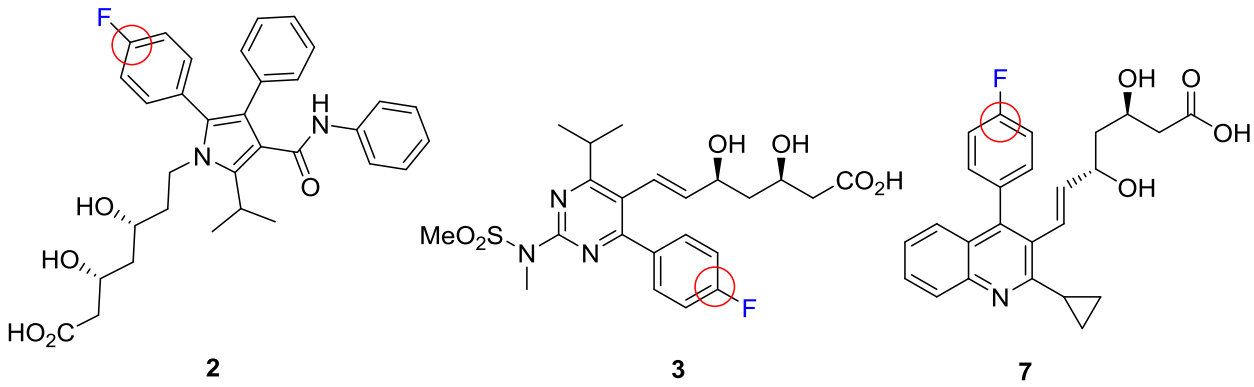

*Figure 8. Three compounds, **2**, **3**, and **7**, in the statin class of compounds that feature and require a para-fluorophenyl group.*[15,16]

Rosuvastatin spawned from the idea of replacing complex and larger functional groups and heteroatoms with simpler, achiral alternatives. The addition of the pyrimidine ring compared to other synthetic statins, compare with Lipitor, **1**, improved activity for inhibiting the targeted reductase. The fluorophenyl group on this molecule is a structural requirement as mentioned above as well as deactivating the ring against the P450 monooxygenase. Pitavastatin is the last statin-type drug to enter the market and is completely synthetic. The cyclopropyl group, differing from rosuvastatin, translates to a high resistance to metabolism along with the 4-fluorophenyl group on the heterocycle.[17]

1.3.2 Electronic Considerations

While deactivating the drug against this metabolic process is possibly the most important consequence of adding fluorine to drugs, it remains only one of the reasons. Electronic considerations such as electronegativity, pK_a modification and lipophilicity tailoring are also reasons that pharmaceutical chemists utilize fluorine as a functional group. Electronegativity has

several effects on a molecule including molecule and bond stability, overall dipole of a molecule and electrostatic interactions with receptor sites. A few drug examples detailed above utilized these properties in combination with blocking metabolic sites, however, below are examples of compounds that feature fluorine for these reasons alone.

An example not involving oxidation but instead that of functional group modification toward fluorine is Fulvestrant, **9**. ICI 164,384, **8**, the original derivative was developed for the treatment of breast cancer, specifically to combat negative side effects of the receptor modulator tamoxifen. Tamoxifen increased risk of the metastasis of associated tumors. The parent molecule did not display enough potency *in vivo* to represent viable clinical consideration, however after fluorination of the drug, the derivative, showed a 5-fold increase in intrinsic potency. The addition of terminal pentafluoroethyl group as opposed to ethyl end-chain increases the strength of the bonds and makes the compound more stable as well as increasing hydrogen bonding with the receptor, increasing metabolic stability during estrogen receptor (ER) binding.[18]

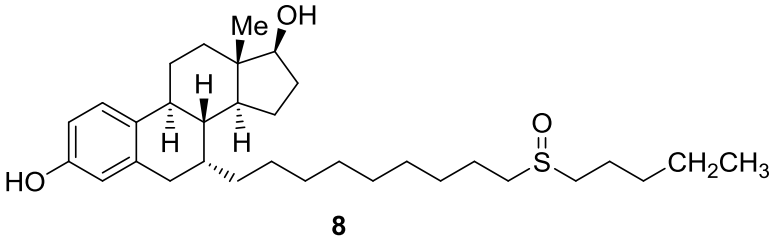

8

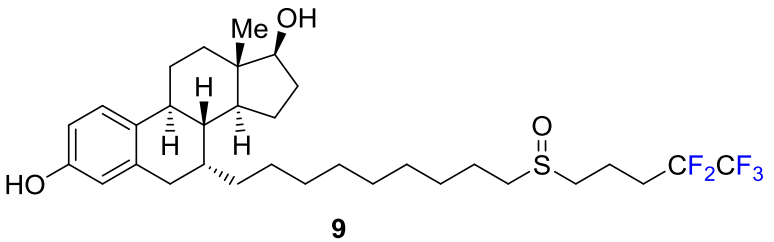

9

*Figure 9. The parent molecule (top, **8**) and the FDA approved drug derivative, Fulvestrant (bottom, **9**).*[18]

Multiple drugs rely on fluorine to alter the lipophilicity of the compound in an attempt to increase drug uptake through a cell membrane. While fluorination of an aromatic or π-system increases the lipophilicity, fluorination and trifluoromethylation of an n-alkyl chain actually shows a decrease in lipophilicity. Vandetanib, **10**, [19] a drug discovered to act as an antagonist of the vascular endothelial growth factor receptor (VEGFR) and is used as an oral kinase inhibitor for thyroid tumors, represents an example of a compound modified with fluorine to achieve the perfect lipophilicity level. Many derivatives of Vandetanib were tested to tailor the lipophilicity of the compound. Structure activity relationship tests showed that a halogen at the C-4' position was preferred and that a fluorine was preferred at the C-2' position. The fluorobromophenyl group was analyzed as a residue matching these two cases and shown that the fluorine atom is able to lead the fluorobromophenyl group deep into the protein's hydrophobic pocket, ultimately increasing the potency of the drug.[19]

Compound **11**, a specific derivative with 3 additional PEG groups added onto the chain, was tested, along with varying chain lengths for varying hydrophilicity. These compounds were being studied for amyloid beta plaque affinity in relation to combatting Alzheimer's disease. Compound **11**, also called AV-45, displayed good Aβ binding coupled with high blood brain barrier penetrations. A whole range of fluorine-ethylene glucol (FPEG) lengths were studied to find the greatest uptake depending on the logP (lipophilicity). The result shows only a minimal change in logP values when modifying the PEG length below n =5, however when the FPEG group was replaced with a hydroxyl group, there was a significant increase in lipophilicity as well as a decrease in potency.[20]

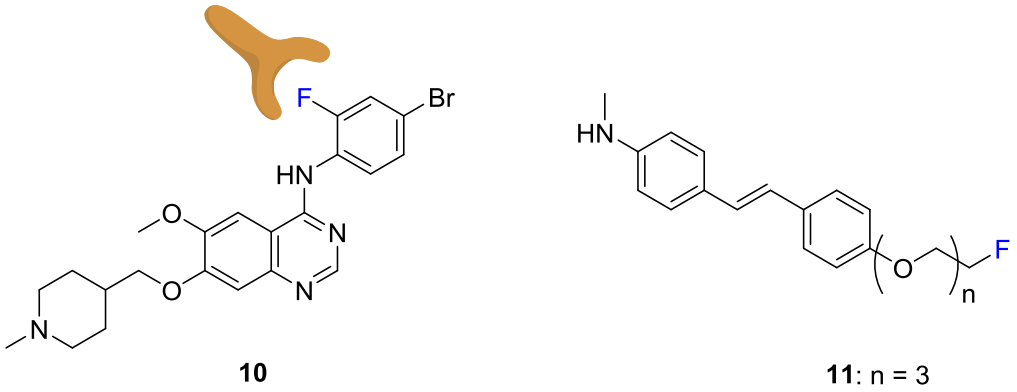

*Figure 10. Vandetanib, **10**, and AV-45 derivatives, **11**, use the fluorine atom to tailor lipophilicity of the overall compounds or of certain parts of the compound.*[21]

Fluorine containing quinolones and pyrimidoquinolines have been shown to exhibit anti-cancer properties.[21] Many groups have shown that the fluorine atom and trifluoromethyl substituent play major roles in anticancer, antimicrobial and antituberculosis effectivity of these compounds.[22,23] These base molecule can utilize a *p*-fluorophenyl group, however unlike the examples preceding, it its purpose is to serve as a hydrophobic group for pocket penetration as opposed to blocking metabolic oxidation. Examples of target pocket amino acids that attract the fluorine hydrophobic group include leucine and phenylalanine.[21] More specific examples of quinoline-based compounds are shown in Figure 11.

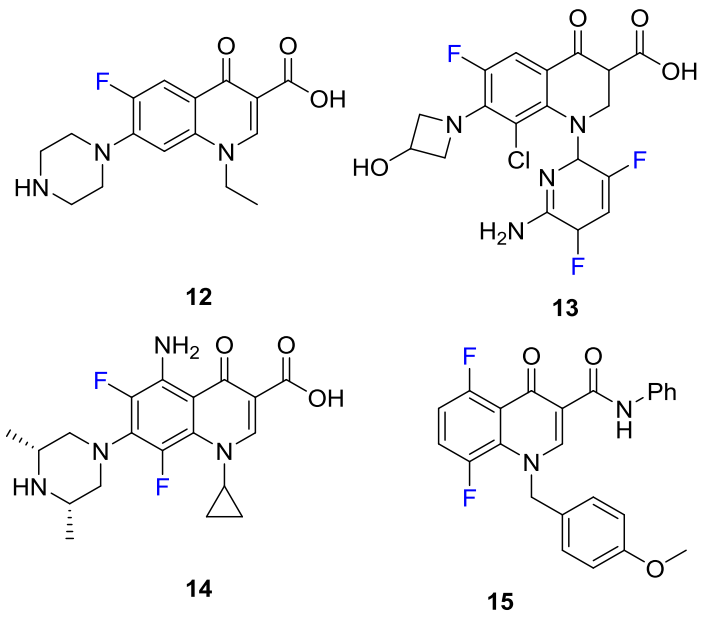

Figure 11. Norfloxacin, ***12****, Delafloxacin,* ***13****, Sparfloxicin,* ***14****, and 5,8-difluoro-1-(4-methoxybenzyl)-4-oxo-N-phenyl-1,4-dihydroquinioline-3-carboxaminde,* ***15****.*[19-20]

These examples of fluorinated therapeutics represent only a fraction of compounds available as drugs. Due to the extraordinary properties exhibited by the fluorine atom, drug designers continue to incorporate this atom into future lead compounds. In the next section, the benefits of the sizes of fluoro- and fluorine-containing functional groups will be discussed.

1.3.3 Size of Fluorine Atom Considerations

As mentioned previously, the size of fluorine containing functional groups are very unique. Structurally, they take up more room than a hydrogen but less than a hydroxyl group and many examples show that the substitution from hydroxyl to fluorine in very beneficial. The size of the functional groups can attribute to driving a compound into its target pocket. Once the molecule is inside the pocket, electronic characteristics of the fluorine then determine the potency and effectiveness of the drug.

In Figure 12, nilotinib, **16**,[24] a derivative of imatinib, is shown. The addition of the trifluoromethyl group resulted in the compound being 30 times more potent than the mother compound. Once inside the pocket of the Bcr-Abl kinase, the trifluoromethyl group interacts with side chains such as histidine and isoleucine. When another derivative featuring a methyl as opposed to the trifluoromethyl was tested, it showed a five-fold decrease in activity.

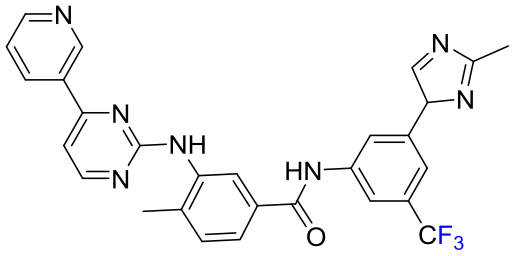

16

*Figure 12. Nilotinib, **16**, is a compound that inhibits a tyrosine kinase inhibitor in patients with chronic myelogenous leukemia.*[24]

A second compound that utilizes the size of fluorine is Lapatinib, **17**.[25] This compound is a human epidermal growth factor inhibitor and dual tyrosine kinase inhibitor for breast cancer and other solid tumors. Larger groups than the fluorophenyl and chlorophenyl groups yielded diminished the activity of the drugs. Other derivatives without the fluorine on the phenyl group also showed decreases in inhibition and hydroxyl and bromine groups, being larger than fluorine, exhibited reduced activity. This leads researchers to the conclusion that the fluorine is essential to fit into the binding pocket; x-ray crystallography also yielded the same conclusion; Figure 13 shows Lapatinib, **17**. [25]

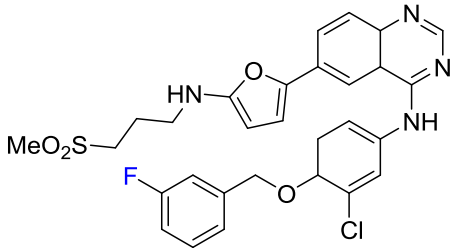

17

*Figure 13. Lapatinib, **17**, utilizes fluorine as an essential size requirement for potency.* [25]

Thus far, this review has highlighted therapeutic agents and pharmaceuticals that feature fluorine. This special atom has become more and more important in drug development in recent decades and will continue to be an essential building block when designing and synthesizing drugs. The benefits and characteristics of fluorine, whether size considerations, electronic characteristics or blocking of metabolic sites susceptible to the P450 monooxygenase, are undeniable in medicinal chemistry. Another faction of medicinal chemistry that utilizes fluorine is that of imaging agents. Where the previous compounds were synthesized in fighting and inhibiting disease, the next section will focus on compounds that image and detect these diseases.

1.4 Fluorine Incorporated into Imaging Agents

Imaging *in vivo* is another sector of medicine that has become more popular in recent time to assist in the fight against many diseases. These fluorine incorporated probes can exist to illuminate several ranges of light waves. A few different classes of probes including coumarin, fluorescein/rhodamine, BODIPY, and cyanine dyes will be explored for their benefits and shortcomings contributing to biological imaging.

1.4.1 Coumarin

The electromagnetic wave spectrum spans from high energy waves such as gamma rays to low energy waves such as radio waves. The visible light spectrum lies between the two extremes and usually is defined as having wavelengths of 400-600 nm. Dyes in this region are generally[26] used for surface imaging as they have more of a possibility of native tissue absorption in this range[27] than NIR dyes which absorb light at higher wavelengths. Because of this, very few examples of probes for biological imaging exist in this range. More examples of dyes that fluorescence in the visible light wavelength range for purposes other than biological/medical exist including solar cell construction.

One example that features a blue-light wavelength is the coumarin class. Coumarin fluorophores have been used for diagnosis and imaging of diseases such as cancer. Coumarin molecules are small and biocompatible, as well as having a relatively high light quantum yield compared to other fluorescent dye classes.[28] One example of a fluorine-incorporated visible light coumarin probe was discovered by Weissleder[29] and coworkers. The dye is shown below in Figure 14 and can be seen to have two fluorine atoms on the coumarin moiety, compounds **18** and **19**. The fluorophores with the fluorine substituents, in comparison to the other molecules presented shows a very comparable extinction coefficient, 19,000 to 16,000, while having a higher quantum yield, 49% to 41%.[29] The dyes effectively labeled the biological targets as well as featuring optical flexibility and fast reactivity with the targets.[29]

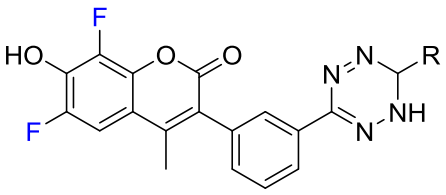

18: R = H
19: R = Me

*Figure 14. Two Coumarin dyes, **18** and **19**, featuring fluorine atoms that fluoresce at around 450 nm.*[29]

1.4.2 Fluorescein/Rhodamine

Fluorescein and rhodamine dyes consist of two important groups: the xanthene moiety which acts as the fluorophore and the benzene moiety which provides the photoinduced electron transfer (PeT). This PeT is a known mechanism in which the chromophore's fluorescence is quenched with the electron transfer from this benzene donor to the xanthene acceptor.[30,31] The mother compound of fluorescein has a carboxyl group at the 2 position of the benzene moiety and until recently, it was believed that this donor group was essential to the molecule; this is based on results replacing the COO- group with a hydrogen, reducing the quantum yield value by over 60%.[32] These two xanthene based dyes are seen as a highly tunable, therefore highly relied on, biological marker for DNA and proteins. These dyes do have some flaws including being very pH dependent due to the compounds being able to exist from neutral to dianionic as well as photobleaching. Another shortcoming stems from the wavelengths that these dyes absorb and fluoresce. Under 600 nm, where these xanthene dyes fluoresce, there is high interference from tissue autofluoresence. However, due to the high quantum yield and tunability, the dyes are still used as biological markers.

One research group, while synthesizing a host of fluorescein derivatives found some very interesting characteristics in the derivatives featuring fluorine. While exhibiting slightly less molar absorbtivity in comparison to the parent compound, the quantum yield values of select fluorinated xanthenes increased to nearly 100%. Another exciting fluorine-induced feature combats slightly one of the drawbacks of the class of compounds as a whole, photobleaching. The bleaching value reduced from 17 (fluorescence percentage loss after 33 minutes) to as little as 4. It is hypothesized that this phenomenon likely stems from the triplet state lifetime of the molecule. The fluorine molecules, at the 2' and 7' position, as shown in compounds **21-23**, shorten the triplet lifetime so that the reaction chance with its quencher is decreased.[33] A few of the compounds presented are shown below. Although these compounds were not tested *in vivo*, this study showed great promise of these compounds for use in bioconjugation in the future.

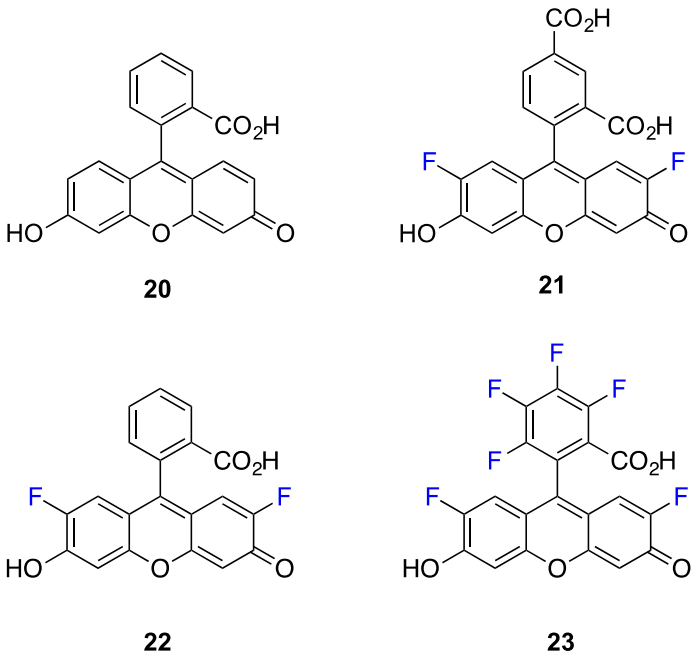

*Figure 15. Fluorescein, **20**, and fluorine containing derivatives, **21-23** showing decreased photobleaching and comparable quantum yield.*[33]

Rhodamine dyes, while having similar benefits and uses in molecular imaging, have similar shortcomings. The basic structure of rhodamine differs only in the two amine groups instead of the carbonyl and hydroxyl groups on the xanthene. Again, this shows a drawback to the compounds as they can exist as neutral, zwitterionic, cationic or dicationic, making the use of the dyes specific to a certain pH range. Similarly to the fluorescein dyes, researchers discovered increased quantum yield with fluorinated rhodamine dyes along with prolonged photostability and decreased photobleaching of the dyes. One particular research group, synthesizing and studying the dyes featured in Figure 16, found that their fluorine-incorporated rhodamines, **24**-**27**,[34] showed promise for stimulated emission depletion (STED) nanoscopy experiments, elucidating protein structures.

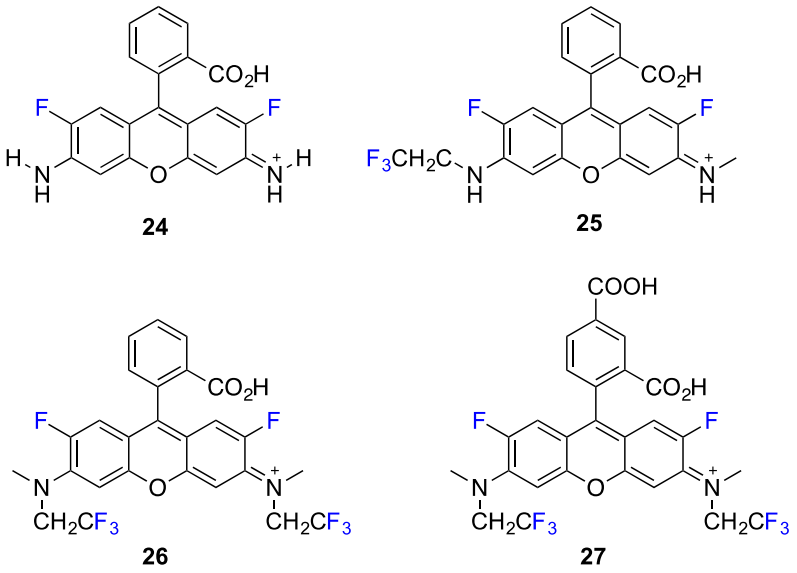

*Figure 16. Several rhodamine derivatives featuring fluorine and trifluoroethyl groups, compounds **24-27**.*[34]

1.4.3 BODIPY

The near infrared region of light on the electromagnetic spectrum lies at about 700-1000 nm. This region and its use in biomedical imaging presents a very unique range of compounds that can

be used and avoids several potential problems concerning body imaging. Body tissue inherently fluoresces light, called autofluoresence, at around 450-500 nm. Should the imaging agents fluoresce in this region, there would be a high background signal interface due to the autofluoresence. Thus, the use of a NIR filter essentially eliminates tissues from autofluoresence altogether.[35] This makes higher wavelength fluorescing molecules superior in terms of background to noise ratios and molecular brightness. The high end of the range exists around 1000nm due to water overtones that begin in this region. NIR light also has the ability to penetrate tissue for several centimeters.[36] This is due to the lower tissue absorbance and reduced scattering.

Many different classes of NIR fluorophores contain fluorine atoms. One of the most common types is the boron-dipyrromethine (BODIPY) dyes. Figure 17 shows the core structure of the BODIPY dye **28**; it is seen to have two fluorine atoms in the core structure with a host of possible alteration sites.

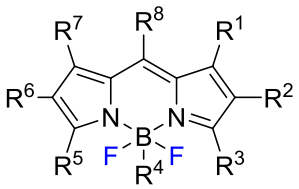

28

*Figure 17. The general structure of a BODIPY dye, **28**.*[37]

Although all BODIPY dyes feature fluorine off of its core boron, very few BODIPY dyes further incorporate fluorine into the design. Figure 18 gives two examples, compounds **29**, **30**, of continuing to add fluorine to the core structure, but the dyes were not tested for *in vivo* imaging purposes.

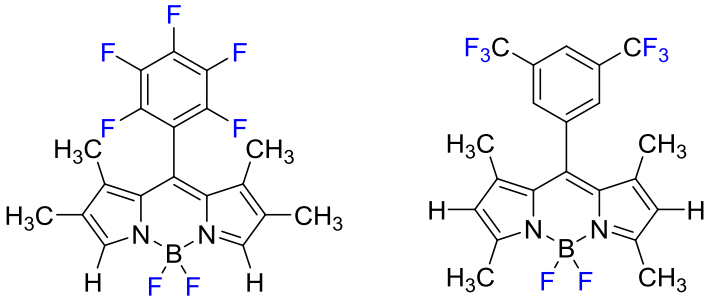

29 **30**

*Figure 18. Two examples of BODIPY dyes **29** and **30** featuring fluorine or trifluoromethyl groups outside of the basic structure.* [37]

1.4.4 Near-Infrared (NIR)

One class of NIR fluorophores that has yet to feature many lead compounds highlighting the fluorine atom for biological activity is the carbocyanine dye family. This family of dyes is often utilized in biomedical imaging as they have several benefits. One such benefit pertains to the non-toxic nature of the compounds to humans, making them great candidates for imaging in the human body. Indocyanine green, a dye currently FDA approved and used for medical imaging, remains one of the least toxic agents ever to be administered to humans.[35] These organic fluorophores also do not suffer from aggregation issues as intensely as other classes of dyes exhibit. Thirdly, researchers can easily tailor the wavelengths of carbocyanine: for each double bond added between the indole end units contributes to a wavelength increase of around 80-100 nm. This does increase hydrophobicity, however, these dyes also have the benefit of having many different sites of modulation. This hydrophobicity increase caused by a longer carbon chain can be potentially combatted by adding a sulfonate group or another hydrophilic functional group to any of these sites. The basic cyanine structure is shown below in figure 19.

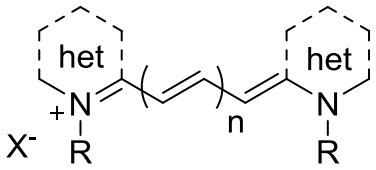

Figure 19. The general structure of the cyanine dye class.[35]

Cyanine dyes derive their names from the number of n-alternating double and single bonded carbons connecting the two heterocycles. For example, compounds with n = 1, 2, 3 would be named as trimethine, pentamethine and heptamethine respectively. The number of carbons not only correspond to wavelength, but also play a part in biodistribution in the body.

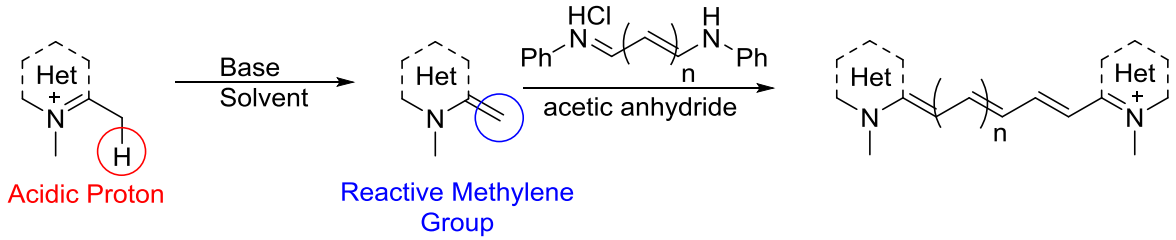

Scheme 1. A standard route taken to make cyanine dyes with longer chain lengths.

Scheme 1 shows a general route taken to synthesize these compounds. The quaternary heterocyclic amine allows the hydrogen atoms on the corresponding methyl group to be acidic. Deprotonation at this position can facilitate the formation of a reactive methylene group which, after the regeneration of the ammonium center, attacks the electrophilic position of the dianil compound which forms a half reacted intermediate. A second addition of the indolenine salt end unit affords the final compound.

Very few examples of carbocyanine dyes featuring the fluorine atom exist in literature. Four examples incorporating the fluorine atom on the dye molecules are dyes that selectively binds to G-quadruplex DNA, **31**,[38] compounds that target the thyroid and parathyroid glands, **32**,[7] a dye

which features a polyfluorinated bridge but no biological use, **33**, [39] and a squarine cyanine dye used for labeling oligonucleotides, **34**. [40] The G-quadruplex DNA binding dyes, when comparing the fluorine substituent to the hydrogen substituent, showed a high increase in the thermal stability of the telomeric quadruplex. For the endocrine targeting cyanines, the uptake of the fluorinated molecules more than doubled that of any other substituent studied in the article, including other halogens and electron donating groups. The fluorinated compounds were still observed *in vivo* after 4 hours showing a slow renal clearance rate. The fluorinated squarine dyes studied showed similar absorbance and fluorescence maxima in comparison to the hydrogen compliments, however they exhibited higher quantum yield values. The promising nature of these compounds for intraoperative imaging has lead researchers to begin exploring these dyes as dual-modal molecules.

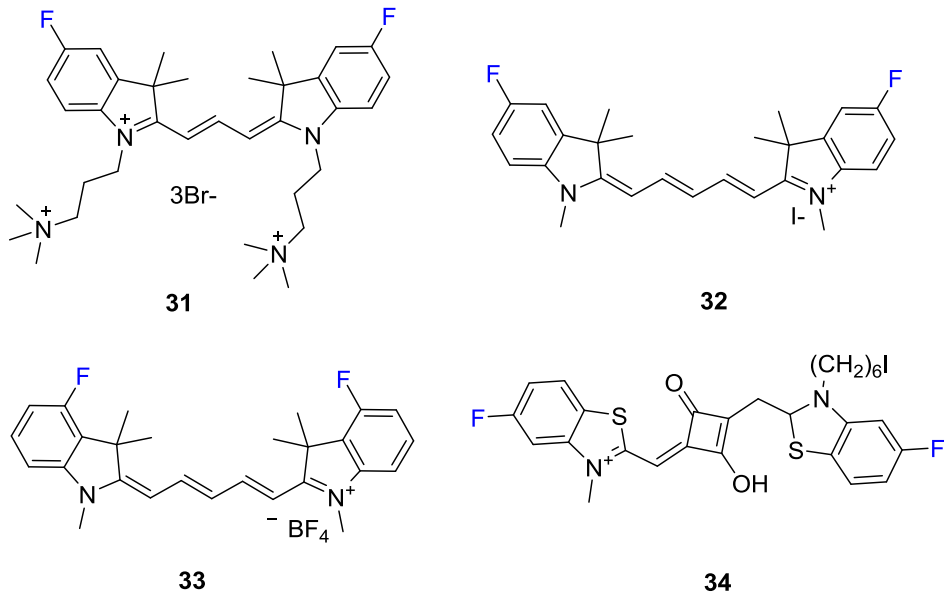

Figure 20. Representative carbocyanine dyes featuring the fluorine atom, ***31-34****.*[7,38-40]

1.5 Imaging Techniques for Early Disease Detection

Due to the increased success rate of both surgery and chemotherapy during the early stages of tumor development, a need for enhanced detection methods has emerged. Visualization of diseased tissues grants doctors and surgeons insight to the answers of important questions such as: where is the diseased tissue, how big is the diseased mass, and what is the best course of action to combat the issue? Depending on the stage at which some diseases such as cancer are detected, visualization of diseased tissues can help lead to curative measures.[36,41] Currently, many imaging methods are utilized in the healthcare industry including: magnetic resonance imaging (MRI), single-photon emission computed tomography (SPECT), positron emission tomography (PET), and electroencephalography (EEG). These imaging methods aid the healthcare professionals assess the situation and help them to define a course of action. For PET, SPECT and MRI techniques to be useful, imaging agents must be used that will bind to the tissues in question as well as give off energy in the form of positrons as emission radiation or radiative return, which is how the instrument obtains the visualization. Agents such as tagged proteins, nanoparticles and metal delivery systems have been explored for use in these types of imaging modalities, however small organic molecules are just starting to become popular in the realm of PET and SPECT imaging.

1.6 Fluorine in Positron Emission Tomography (PET)

Fluorine 18 has been heavily relied on for PET imaging. This could be attributed to fluorine's long half-life in comparison to other positron emitting atoms. ^{11}C, ^{13}N and ^{15}O have half-lives of 20, 10 and 2 minutes respectively, whereas ^{18}F has a half-life of 110 minutes. The ^{18}F atom decays into ^{18}O, a non-toxic, non-radioactive nucleus that, when is featured on a sugar molecule (FDG),

is excreted through the kidneys and liver .[14] This positron emitting isotope has driven the development of safe fluorinating contrast agents and binding modalities.[42]

^{18}F imaging agents currently are being developed for the visualization of cancer cells and for non-cancerous diseases such as Alzheimer's disease as well as other types of dementia.[43,44] Studies have used the fluorine atom as a substitute as a hydroxyl group, showing that structurally there is little difference between the two, however it has great effect in increasing the lipophilicity of the compound to facilitate the transport through the blood brain barrier (BBB).

PET and SPECT scans are presently the most sensitive molecular imaging techniques modalities.[36] The use of radioactive isotopes as labels for these imaging methods must be used with caution. The positron comes from the nucleus of the radionuclide and is annihilated with an electron once it moves away from the nucleus, a process that occurs almost immediately. The energies of the emitted positron determine the path length, with larger positron energies corresponding to larger distances traveled by the positron,[42] as visualized in Figure 21. After annihilation occurs, gamma waves are emitted at an almost 180^{o} angle and the waves trigger a response from the detector at 511 keV and an image is created.

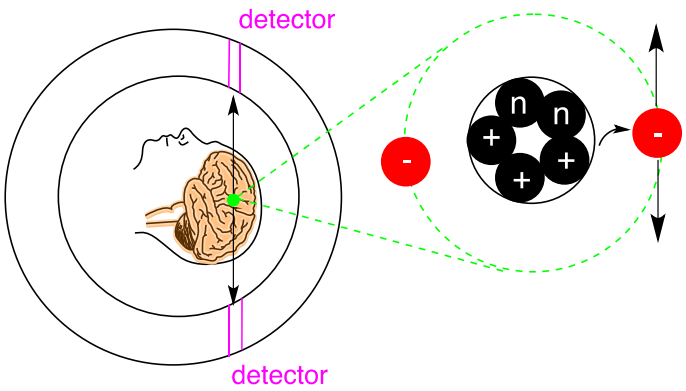

Figure 21. The annihilation pathway undergone by an ^{18}F atom as well as the gamma ray pathways picked up by a surrounding PET detector.

The two most common radionuclides used for PET imaging are ^{11}C and ^{18}F. These two labels have half-lives of 20.3 and 110 minutes respectively and have different imaging uses. ^{11}C commonly is used when labeling compounds with short half-lives *in vivo* or *in vitro*. This itself provides its own set of problems as its only useful for 20 minutes before half of the radiolabel has decayed. Although these compounds can be used past the half-life, it does rush the synthesis, purification and clinical use of the molecules. Another disadvantage to using the carbon radiolabel is that these compounds can only be produced and used in cyclotron and radiochemistry facilities. Therefore, for clinical uses, different professionals and a separate facility from the hospital must be utilized. The ^{18}F nuclide, with its longer half-life, no need for separate facilities and low positron energy, presents the best physical imaging characteristics. Table 1 shows information compiled by Simon Ametamey and coworkers about the common radionuclides, their half-lives and its positron energies.

Table 1. The half-lives and positron energies of several radionuclides that can used for PET and SPECT scans

Nuclide	Half-life (minutes)	Positron energy (MeV)
^{18}F	110	0.64
^{11}C	20.3	0.97
^{13}N	10	1.20
^{15}O	2	1.74
^{76}Br	972	4.0
^{124}I	60,192	2.14

Many examples exist of compounds, originally synthesized with a fluorine atom, becoming synthetically altered in such a way that it becomes a radiolabel. In a few instances, this involves converting the fluorine to fluorine-18 directly, however most of the synthetic routes involves including a bulky leaving group and then substituting this group with the nuclide. These radiolabels, depending on the makeup of the compound as a whole, can be modified to target most tissue types, proteins or *in vivo.* Studies report compounds that bind and image amyloid plaques, **35** and **36**, a common symptom/cause for Alzheimer's Disease,[45,46] and hypoxic cells, **37** and **38**, a major cause of cancer.[47,48] Figure 22 gives examples of the wide variety of compounds described above, all having ^{18}F present.

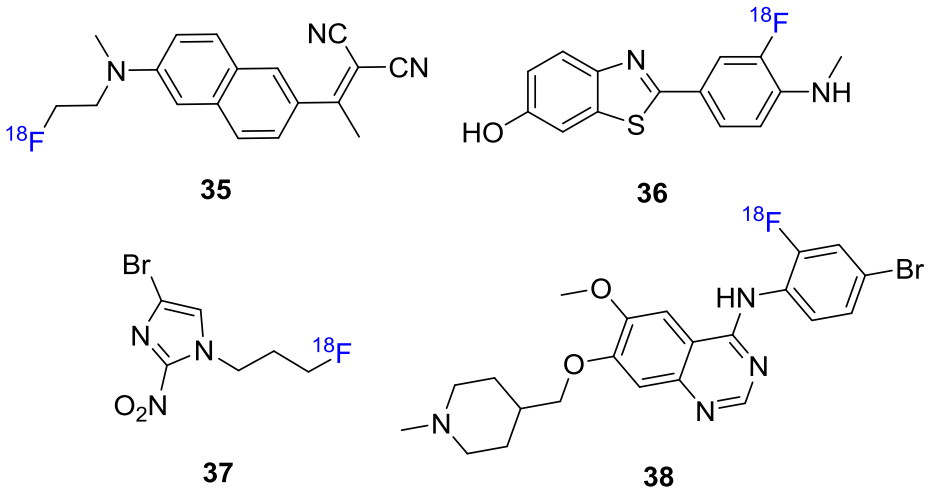

*Figure 22. Examples of compounds from sources **35-38** respectively.*[42,45,46]

1.7 Fludeoxyglucose (^{18}F-FDG) and Other Tagged Molecules for Imaging Including Synthesis

The synthesis of fluorine isotope labeled compounds is not as simple as replacing a fluorine with its radiolabel. Fluorine is a bad leaving group as explained by its small bond length, and high

bond strength with carbon and its size being so small. Therefore, usually to test effectiveness, the marker compound is synthesized with fluorine as a control or reference compound, [47,49-52] and then the actual radiolabeled compound is synthesized from an analog with a good leaving group in its place. Examples of leaving groups used as substitutes would be tosyl (OTs) groups or larger halogens such as bromine or iodine.[47,49-52] The standard for PET labels is fludeoxyglucose and it is the most successful and one of the few radiopharmaceutical currently in use. FDG, shown below with its synthesis, is an analogue of glucose where the d-hydroxyl group features an ^{18}F in its place. The synthesis of this compound comes from the electrophilic fluorination of a double bond and then hydrogenation to replace the non-radiolabeled fluorine atom with a hydroxyl group. Figure **23** while showing the final ^{18}F-FDG product, also describes the synthetic route taken to obtain this PET radiolabel.

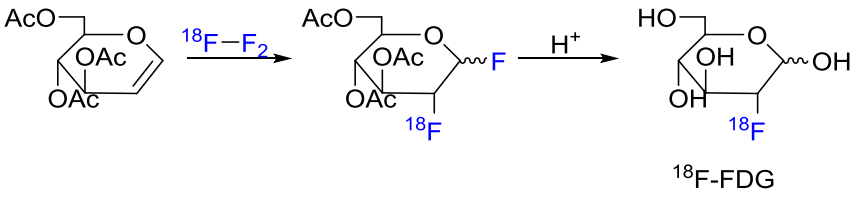

Figure 23. The synthesis of radiolabel ^{18}F-FDG.[53]

In the case of FDG, the reaction performed to obtain the fluorinated product is electrophilic fluorination. However for other examples of PET radiolabeled molecules, nucleophilic substitution reactions are performed to achieve the final product. A few of these examples are shown in Figure **24**. Examples of other classes of compounds turned PET labels are: glucoses, **39**,[49] caboximidamides, **40**,[51] hydroxynoraporphines, **41**,[52] BODIPY dyes, **42**,[50] and recently, cyanines.[54] These compounds feature this nucleophilic substitution reaction for a large, good leaving group such as tosyl groups being substituted with the radiolabeled ^{18}F. The reaction time

of this S_N2 reaction is generally around one minute which is helpful when remembering the half-life of the ^{18}F nuclide is 110 minutes. This leaves maximum amount of time to do *in vivo* testing of the label. In one particular example, the BODIPY dye, **42**, shown in figure 24, the radiolabel can still be seen prominently after 30 minutes and is beginning to be excreted with no release of free ^{18}F after 1 hour.[50] This example shows how even with small molecules not modeled after FDG, the PET radiolabels being developed exhibit promising signs of both their usefulness and non-toxicity. Examples of the synthetic processes used to obtain radiolabeled compounds mentioned above are laid out in Figure 24.

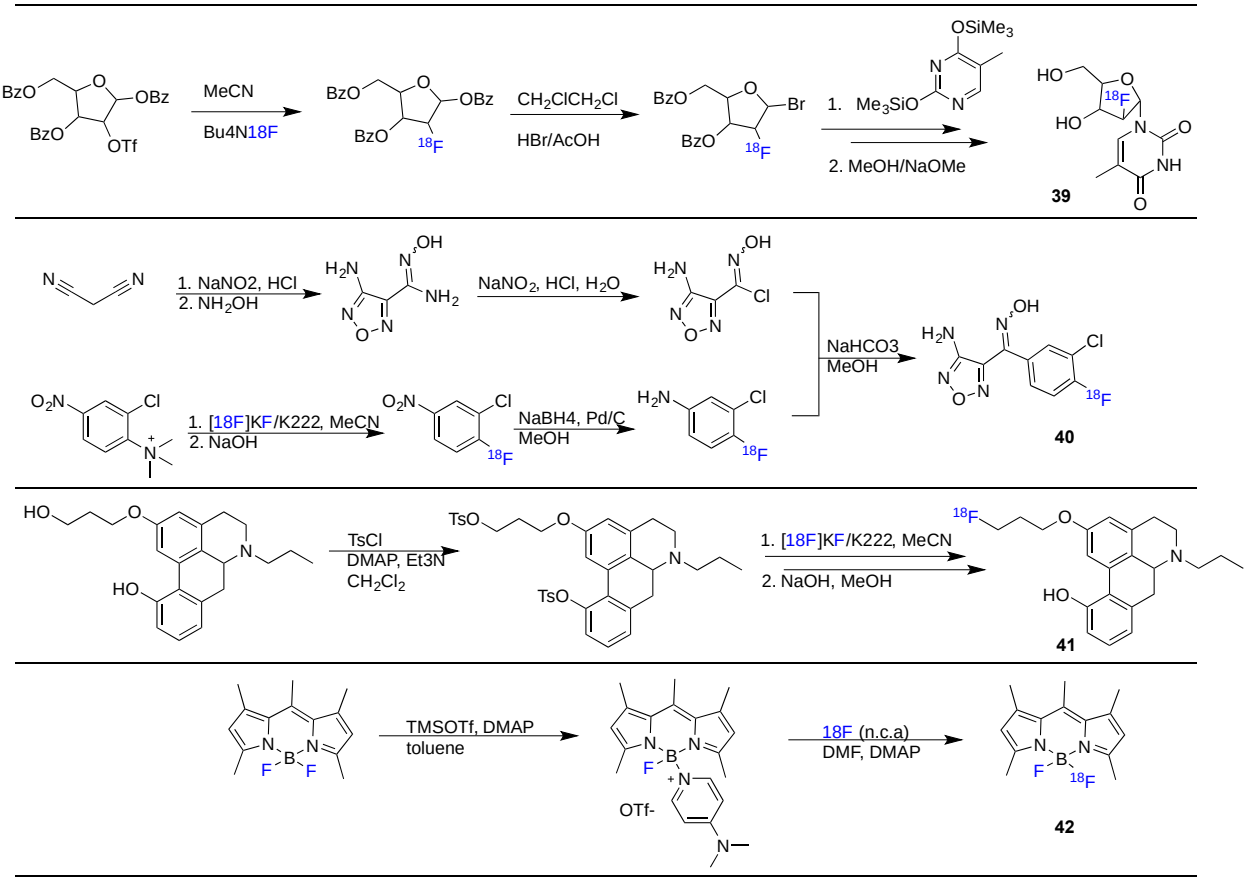

*Figure 24. Examples of synthetic routes to derive radiolabeled compounds, **39-42**, from unlabeled precursors.*[49-52]

1.8 Conclusion

The utilization of fluorine atoms in chemistry has increased in the past 30 years, and its viability in drug development and imaging has increased. Fluorine's many unique characteristics and properties lend to the use of this atom to combat many different problems medicinal chemists may face. The inherent size, electronegativity, and blocking of metabolic sites for drugs and shortening the triplet state for imaging chromophores can be solved singularly by the addition of fluorine atoms on a molecule. Similar to in medicine, the addition of fluorine atoms on a contrast agent is becoming increasingly relied on for biomolecular imaging and preventative medicine. Other forms of imaging are incorporating fluorine atoms as a radiolabel for an increased use of fluorescent probes for multimodal imaging. A unique opportunity presents itself for researchers when considering the addition of fluorine on drugs or imaging fluorophores: multipurpose molecules. Not only would the fluorinated chromophores be useful intraoperatively and for drug tracking in the body, the radiolabeled form could have usefulness as an ^{18}F-radiolabeled compound for PET and SPECT purposes. Through the research performed on small molecules containing fluorine atoms and functional groups containing fluorine, much has been learned about drug metabolic pathways and medical advancements both through drugs and imaging techniques.

1.9 REFERENCES

(1) *J. Chem. Ed.* **2010**, *87*, 1348.
(2) Uneyama, K. *Organofluorine Chemistry*; Blackwell Publishing Ltd, 2006.
(3) B Kevin Park, N. R. K., Paul M O'Neill *Annual Review of Pharmacology and Toxicology* **2001**, *41*, 443.
(4)Purser, S.; Moore, P. R.; Swallow, S.; Gouverneur, V. *Chemical Society reviews* **2008**, *37*, 320.
(5) Reichenbacher, K. S., H. I.; Hulliger, J. *Chem. Soc. Rev.* **2005**, *34*, 22.
(6) O'Hagan, D. *Chemical Society reviews* **2008**, *37*, 308.
(7) Hyun, H.; Park, M. H.; Owens, E. A.; Wada, H.; Henary, M.; Handgraaf, H. J. M.; Vahrmeijer, A. L.; Frangioni, J. V.; Choi, H. S. *Nat Med* **2015**, *21*, 192.
(8) Liang, T. N., C.; Ritter, T. *Angewandte Chemie International Edition* **2013**, *52*, 8214.
(9) Chambers, R. D. *Fluorine in organic chemistry*; CRC Press, 2004.
(10) Filler, R.; Saha, R. *Future Medicinal Chemistry* **2009**, *1*, 777.
(11) Nassar, A.-E. F.; Kamel, A. M.; Clarimont, C. *Drug Discovery Today* **2004**, *9*, 1020.
(12) Hagmann, W. *Journal of medicinal chemistry* **2008**, *51*, 4359.
(13) Romano Di Fabio, C. G., Giuseppe Alvaro, Giorgio Pentassuglia, Domenica A. Pizzi, Daniele Donati,; Tino Rossi, G. G., Mario Mattioli, Zadeo Cimarosti, Carla Marchioro, Stefano Provera, Laura Zonzini,; Dino Montanari, S. M., Philip A. Gerrard, David G. Trist, Emiliangelo Ratti, and Mauro Corsi *Journal of medicinal chemistry* **2009**, *52*, 3238.
(14) M. van Heek, C. F., D. Compton et al. *British Journal of Pharmacology* **2000**, *129*, 1748.
(15) Igel, M. S., T.; Bergmann, K. *J. Clin. Pharmacol.* **2002**, *42*, 835.
(16) Hak Lee, S.; Chung, N.; Kwan, J.; Kim, D.-I.; Ho Kim, W.; Jeong Kim, C.; Seung Kim, H.; Hoon Park, S.; Seog Seo, H.; Gu Shin, D.; Woo Shin, Y.; Shim, W.-J.; Ahn, T. H.; Ho Yun, K.; Yoon, M.-H.; Cha, K.-S.; Choi, S.-W.; Wook Han, S.; Su Hyon, M. *Clinical Therapeutics* **2007**, *29*, 2365.
(17) Saito, Y.; Yamada, N.; Teramoto, T.; Itakura, H.; Hata, Y.; Nakaya, N.; Mabuchi, H.; Tushima, M.; Sasaki, J.; Goto, Y.; Ogawa, N. *Arzneimittelforschung* **2002**, *52*, 251.
(18) Alan, E. W., Michael Dukes, Jean Bowler *Cancer Research* **1991**, *51*, 3867.
(19) Ryan, A. J.; Wedge, S. R. *British journal of cancer* **2005**, *92 Suppl 1*, S6.
(20) Kung, H. F.; Choi, S. R.; Qu, W.; Zhang, W.; Skovronsky, D. *Journal of medicinal chemistry* **2010**, *53*, 933.
(21) Ghorab, M. M.; Ragab, F. A.; Heiba, H. I.; Arafa, R. K.; El-Hossary, E. M. *Medicinal Chemistry Research* **2010**, *20*, 388.
(22) Kathrotiya, H. G.; Patel, M. P. *European journal of medicinal chemistry* **2013**, *63*, 675.
(23) Mistry, S. N.; Valant, C.; Sexton, P. M.; Capuano, B.; Christopoulos, A.; Scammells, P. J. *Journal of medicinal chemistry* **2013**, *56*, 5151.
(24) Kantarjian, H. M.; Giles, F.; Gattermann, N.; Bhalla, K.; Alimena, G.; Palandri, F.; Ossenkoppele, G. J.; Nicolini, F.-E.; O'Brien, S. G.; Litzow, M.; Bhatia, R.; Cervantes, F.; Haque, A.; Shou, Y.; Resta, D. J.; Weitzman, A.; Hochhaus, A.; le Coutre, P. *Blood* **2007**, *110*, 3540.
(25) Kuang, Y.-H.; Shen, T.; Chen, X.; Sodani, K.; Hopper-Borge, E.; Tiwari, A. K.; Lee, J. W. K. K.; Fu, L.-W.; Chen, Z.-S. *Biochemical Pharmacology* **2010**, *79*, 154.

(26) Kobayashi, H.; Ogawa, M.; Alford, R.; Choyke, P. L.; Urano, Y. *Chemical reviews* **2010**, *110*, 2620.
(27) Welsher, K.; Sherlock, S. P.; Dai, H. *Proceedings of the National Academy of Sciences* **2011**, *108*, 8943.
(28) Drexhage, K. H. *Fluorescence Efficiency of Laser Dyes*; National Bureau of Standards, 1976; Vol. 13.
(29) Meimetis, L. G.; Carlson, J. C. T.; Giedt, R. J.; Kohler, R. H.; Weissleder, R. *Angewandte Chemie International Edition* **2014**, *53*, 7531.
(30) Lindqvist, L. L., G. W. *J. Chem. Phys.* **1966**, *44*, 1711.
(31) Fink, D. W. W., C. R. *J. Chem. Phys.* **1970**, *53*.
(32) Urano, Y. K., M.; Kanda, K.; Ueno, T.; Hirose, K.; Nagano, T. *J. Am. Chem. Soc.* **2005**, *127*, 4888.
(33) Sun, W.-C.; Gee, K. R.; Klaubert, D. H.; Haugland, R. P. *The Journal of Organic Chemistry* **1997**, *62*, 6469.
(34) Mitronova, G. B., V.; Bossi, M.; Wurm, C.; Meyer, L.; Medda, R.; Moneron, G.; Bretschneider, S.; Eggeling, C.; Jakobs, S.; Hell, S. *Chemistry A European Journal* **2010**, *16*, 4477.
(35) Frangioni, J. *Current Opinion in Chemical Biology* **2003**, *7*, 626.
(36) Weissleder, R. *Science* **2006**, *312*, 1168.
(37) Loudet, A.; Burgess, K. *Chemical reviews* **2007**, *107*, 4891.
(38) Nanjunda, R.; Owens, E. A.; Mickelson, L.; Dost, T. L.; Stroeva, E. M.; Huynh, H. T.; Germann, M. W.; Henary, M. M.; Wilson, W. D. *Molecules* **2013**, *18*, 13588.
(39) Chernega, O. I.; Levchenko, S. M.; Ryabitskii, A. B.; Gerasov, A. O.; Kachkovskii, O. D.; Yagupolskii, Y. L. *Dyes and Pigments* **2015**, *123*, 176.
(40) Renard, B.-L.; Aubert, Y.; Asseline, U. *Tetrahedron Letters* **2009**, *50*, 1897.
(41) Etzioni, R.; Urban, N.; Ramsey, S.; McIntosh, M.; Schwartz, S.; Reid, B.; Radich, J.; Anderson, G.; Hartwell, L. *Nat Rev Cancer* **2003**, *3*, 243.
(42) Ametamey, S. M.; Honer, M.; Schubiger, P. A. *Chemical reviews* **2008**, *108*, 1501.
(43) Serdons, K.; Terwinghe, C.; Vermaelen, P.; Van Laere, K.; Kung, H.; Mortelmans, L.; Bormans, G.; Verbruggen, A. *Journal of medicinal chemistry* **2009**, *52*, 1428.
(44) Choi, S. R.; Golding, G.; Zhuang, Z.; Zhang, W.; Lim, N.; Hefti, F.; Benedum, T. E.; Kilbourn, M. R.; Skovronsky, D.; Kung, H. F. *Journal of Nuclear Medicine* **2009**, *50*, 1887.
(45) Kepe, V.; Moghbel, M. C.; Långström, B.; Zaidi, H.; Vinters, H. V.; Huang, S.-C.; Satyamurthy, N.; Doudet, D.; Mishani, E.; Cohen, R. M.; Høilund-Carlsen, P. F.; Alavi, A.; Barrio, J. R. *Journal of Alzheimer's disease : JAD* **2013**, *36*, 613.
(46) Zhang, W.; Oya, S.; Kung, M. P.; Hou, C.; Maier, D. L.; Kung, H. F. *Nuclear medicine and biology* **2005**, *32*, 799.
(47) Grierson, J. R.; Link, J. M.; Mathis, C. A.; Rasey, J. S.; Krohn, K. A. *Journal of Nuclear Medicine* **1989**, *30*, 343.
(48) Yamamoto, F.; Aoki, M.; Furusawa, Y.; Ando, K.; Kuwabara, Y.; Masuda, K.; Sasaki, S.; Maeda, M. *Biological and Pharmaceutical Bulletin* **2002**, *25*, 616.
(49) Alauddin, M. M.; Conti, P. S.; Fissekis, J. D. *Journal of Labelled Compounds and Radiopharmaceuticals* **2002**, *45*, 583.

(50) Hendricks, J. A.; Keliher, E. J.; Wan, D.; Hilderbrand, S. A.; Weissleder, R.; Mazitschek, R. *Angewandte Chemie* **2012**, *51*, 4603.
(51) Huang, X.; Gillies, R. J.; Tian, H. *Journal of labelled compounds & radiopharmaceuticals* **2015**, *58*, 156.
(52) Sromek, A. W.; Zhang, S.; Akurathi, V.; Packard, A. B.; Li, W.; Alagille, D.; Morley, T. J.; Baldwin, R.; Tamagnan, G.; Neumeyer, J. L. *Journal of labelled compounds & radiopharmaceuticals* **2014**, *57*, 725.
(53) Lemaire, C.; Damhaut, P.; Lauricella, B.; Mosdzianowski, C.; Morelle, J. L.; Monclus, M.; Van Naemen, J.; Mulleneers, E.; Aerts, J.; Plenevaux, A.; Brihaye, C.; Luxen, A. *Journal of Labelled Compounds and Radiopharmaceuticals* **2002**, *45*, 435.
(54) Priem, T.; Bouteiller, C.; Camporese, D.; Brune, X.; Hardouin, J.; Romieu, A.; Renard, P. Y. *Organic & biomolecular chemistry* **2013**, *11*, 469.
(55) Yokoyama, J.; Fujimaki, M.; Ohba, S.; Anzai, T.; Yoshii, R.; Ito, S.; Kojima, M.; Ikeda, K. *OncoTargets and therapy* **2013**, *6*, 325.
(56) C.-H. Liang, W.-Y. D., J.-P. Ren, F.-M. Zhou, Y. Hu, H.-J. Mao, D.-M. Han *Eur Rev Med Pharmacol Sci* **2014**, *18*, 3638.
(57) Santhanam, P. O., C. *Endocrine Practices* **2014**, *20*.
(58) Owens, E. A.; Hyun, H.; Tawney, J. G.; Choi, H. S.; Henary, M. *Journal of medicinal chemistry* **2015**, *58*, 4348.
(59) Owens, E. A.; Hyun, H.; Dost, T. L.; Lee, J. H.; Park, G.; Pham, D. H.; Park, M. H.; Choi, H. S.; Henary, M. *Journal of medicinal chemistry* **2016**, *59*, 5311.
(60) Allen, C. F. H.; Wilson, C. V. *Journal of the American Chemical Society* **1943**, *65*, 611.
(61) Henary, M.; Levitz, A. *Dyes and Pigments* **2013**, *99*, 1107.
(62) Onoe, S.; Temma, T.; Kanazaki, K.; Ono, M.; Saji, H. *BIOMEDO* **2015**, *20*, 096006.
(63) Owens, E. A.; Hyun, H.; Dost, T. L.; Lee, J. H.; Park, G.; Pham, D. H.; Park, M. H.; Choi, H. S.; Henary, M. *Journal of Medicinal Chemistry* **2016**.
(64) Kuang, D.; Uchida, S.; Humphry-Baker, R.; Zakeeruddin, S. M.; Grätzel, M. *Angewandte Chemie International Edition* **2008**, *47*, 1923.
(65) Wang, Z.-S.; Koumura, N.; Cui, Y.; Takahashi, M.; Sekiguchi, H.; Mori, A.; Kubo, T.; Furube, A.; Hara, K. *Chemistry of Materials* **2008**, *20*, 3993.
(66) Guo, M.; Huang, J.; Deng, Y.; Shen, H.; Ma, Y.; Zhang, M.; Zhu, A.; Li, Y.; Hui, H.; Wang, Y.; Yang, X.; Zhang, Z.; Chen, H. *Advanced Functional Materials* **2015**, *25*, 58.
(67) Luo, S.; Tan, X.; Fang, S.; Wang, Y.; Liu, T.; Wang, X.; Yuan, Y.; Sun, H.; Qi, Q.; Shi, C. *Advanced Functional Materials* **2016**, *26*, 2975.
(68) Frangioni, J. V. *Current Opinion in Chemical Biology* **2003**, *7*, 626.
(69) Sauve, G.; Kamat, P. V.; Thomas, K. G.; Thomas, K. J.; Das, S.; George, M. V. *The Journal of Physical Chemistry* **1996**, *100*, 2117.
(70) Mojzych, M.; Henary, M. In *Heterocyclic Polymethine Dyes: Synthesis, Properties and Applications*; Strekowski, L., Ed.; Springer Berlin Heidelberg: Berlin, Heidelberg, 2008, p 1.
(71) Etter, M. C.; Kress, R. B.; Bernstein, J.; Cash, D. J. *Journal of the American Chemical Society* **1984**, *106*, 6921.

2 SYNTHESIS AND CHARACTERIZATION OF PENTAMETHINE CARBOCYANINE FLUOROPHORES

2.1 Introduction: Intraoperative Imaging

After initial preoperative scans, MRI, PET, SPECT, ect, are taken to visualize the area of interest, there still remains hours between when the patient goes into surgery (if this course of action is required). In the time between these two activities, the body shifts and the surgical field differs from what the initial scans show, if only slightly. Currently, the method for determining if any diseased tissue remains is to send samples for biopsy until showing only healthy cells. This process remains sufficient when dealing with larger organs or tissues, or tissues known to regenerate like the liver, however when dealing with small sensitive glands such as the thyroid or adrenal gland damaging any parts of these delicate glands can cause major post-operative complications.[55] Visualizing healthy cells in conjunction with diseased cells can help to reduce these complications and one such solution would be the use of organic dyes and reduce the reliance of the naked eye visualization and experience. The damaging on these tissues, as they regulate the body's hormone levels and maintain the overall homeostasis of the body can result in post-operative recovery, varying hormone conditions and even morbidity. A more specific complication of this type of surgery is hypocalcaemia; it is a condition where a lack of calcium is present in the body, is one of the two largest complications after thyroid and neck surgeries. It is widely accepted that the intricate surgeries involving the endocrine system and some of its organs have yet to be perfected.[56,57] The cyanine dye class represents a promising candidate for the reasons stated above. The implementation of these dyes would have no noticable interference with surgeon's current

process. The dyes would be injected preoperatively, track to the area of interest (design), and visualized with the use of a series of cameras and NIR lights. Figure 25 gives a schematic of how this apparatus may look like with a mouse being the surgical field. Then, hours after the surgery is complete, the dyes would be cleared from the body naturally with no toxicity or other concerns to the patient.

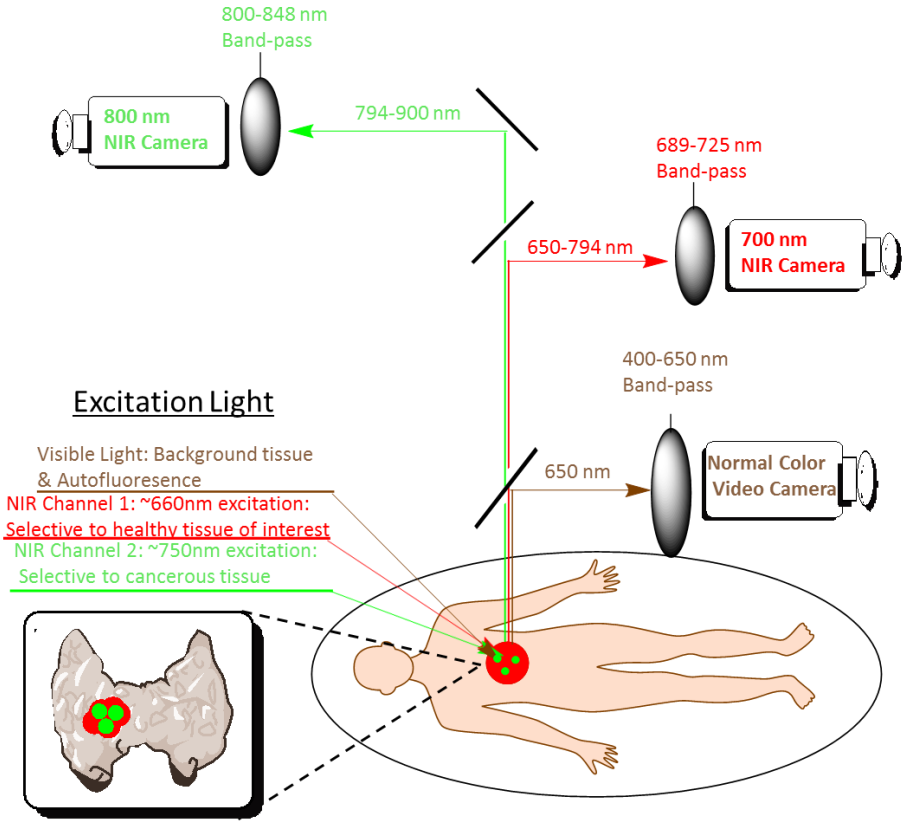

Figure 25. An illustration of a system of NIR cameras visualizing dyes to be used intraoperatively.

Excitation lights of three wavelengths illuminate the surgical field which contains the dyes: (**a, brown**) background tissue with no dye absorption or bioluminescence, (**b, red**) dye targeting healthy endocrine cells and (**c, green**) dye targeting diseased tissue. With the use of a camera

system, the images can be overlaid and portrayed for a surgeon to see exactly what he or she is removing, without having to rely solely on preoperative scans, biopsies, or experience. The combination of these techniques, preoperative and intraoperative imaging, could lead to more accurate surgical procedures with less postoperative complications.

2.2 Rationale

The rationale for the projects presented in this thesis begins with the continuing modifications of a scaffold developed by our group[58,7] and found to image certain endocrine system tissues. Initially, over 200 pentamethine carbocyanine dyes were screened and lead molecules were determined. Our previous developments[58,7] explored hydrophobicity and electron withdrawing groups on the dyes to test their uptake in the endocrine organs. This current study is an expansion of our findings and continues to explore the electronic effects of EWG on the indolenium end units and features the idea to incorporate fluorine atoms in the dye scaffold. Other halogenated atoms such as chlorine and bromine atoms were also incorporated with the dye scaffold as a comparison. The synthetic route and means to purify the compounds was generally known after many modifications and publications from our lab's previous work.[7, 47-49] After the fluorinated symmetrical pentamethine carbocyanine dyes were synthesized and tested for the endocrine uptake, it was found that there was uptake in the targeted tissues and glands: compounds with chlorine and bromine at the 5-position on the indolenine showed high uptake in the salivary glands, fluorine exhibited uptake in the thyroid and parathyroid glands, and the trifluoromethyl compounds showed uptake in the pituitary gland. Dyes of this nature that target the endocrine system without the use of targeting ligands are the first of their kind. Detailed information of the

synthesis and animal data is described in detail as shown in our recent publication in the Journal of Medicinal Chemistry. The reprint found on page 53.

It is possible that altering the number of fluorine atoms might have an effect on the optical properties and usefulness of the dyes. Therefore in chapter two, asymmetric analogs featuring only one fluorine atom were synthesized and purified. The optical properties and quantum yield of these agents were performed and sent to Beth Israel Deaconess Medical Center for biodistribution studies to confirm the endocrine tissue uptake in mouse models. The data confirmed that the optical properties were not ideal for biological use. Then a third set of compounds described feature pentanoic acid groups stemming from the nitrogen on the heterocycle end unit. These dyes, along with being pH sensitive, hold value to both medicinal chemistry and renewable energy chemistry. The carboxylic acid groups can act as a chelator for titanium oxide plates in a dye-sensitized solar cell system or as a linker from a dye to a ligand to be used *in vivo*. The study on this set of carboxylated pentamethine carbocyanine dyes is to observe their optical properties for effectiveness for *in vivo* studies, both for the attachment of ligands, or solely for their structure inherent targeting qualities.

2.3 Synthesis and Optical Property Determination of Halogenated Pentamethine Dyes

As mentioned, this work is featured in a manuscript published in 2016 in the *Journal of Medicinal Chemistry* under the title Near-Infrared Illumination of Native3 Tissues for Image-Guided Surgery: *doi*: 10.1021/acs.jmedchem.6b00038. Contributions are a continuation of synthetic work performed as part of my undergraduate research project. This part of the thesis will only include my contributions to the publication, however a full version of the manuscript will be provided in the appendix. The synthetic portion of compounds **14-25** have been previously

reported, however **26-28** and all of the optical property studies was performed during my Masters tenure.

2.3.1 Synthesis of Pentamethine Fluorophores

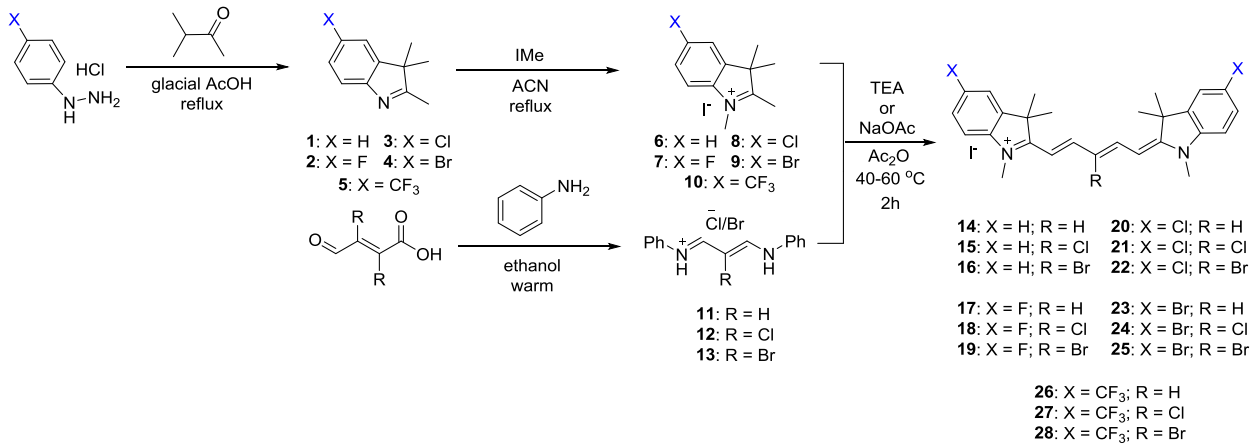

*Scheme 2. Synthesis of 700 nm Emitting Pentamethine Cyanines Featuring Neutral (X = H) and Electron-Withdrawing (X = F, Cl, Br, CF3) Moieties, compounds **14-28**.* [59]

The final dyes **14-28** were synthesized starting with para-substituted halogenated phenyl hydrazines. The hydrazines were reacted with 3-methyl-2-butanone in acetic acid heated under reflux for 72 h to afford the 5-halogenated indolenines **1-5**. This reaction proceeds through a 3, 3-sigmatropic rearrangement reaction to form the heterocycle.[60] After a basic workup where the products were extracted using dichloromethane (DCM) and sodium bicarbonate to neutralize the acetic acid, the indolenines were then reacted with iodomethane in acetonitrile at reflux for 24 h. This led to the formation of indolenine salts **6-10** through an S_N2 reaction mechanism. . No workup was needed and the crude material was used in the next step of the reaction. Reacting salts **6-10** with 'linkers' **11-13** in a 2:1 molar ratio in acetic anhydride at 60 ^oC for 45 min, the formation of dyes **14-28** occurred. The formation of the fluorophores were monitored using regular phase thin

layer chromatography with a mobile phase of 99:1 DCM: methanol as well as by UV-Vis. The reaction mixtures were allowed to cool, dissolved in DCM and then washed six times with water. The water was dried using sodium sulfate and the organic layer was then gravity filtered and the solvent was evaporated off. The crystals were washed then with diethyl ether and dried by vacuum overnight. The purification of the dyes was achieved by simple recrystallization using diethyl ether from dichloromethane. Pure product yields of 37-78% were achieved. Characterization of the final dyes included ^{1}H NMR, ^{13}C NMR, ^{19}F NMR, liquid chromatography mass spectrometry, and melting point determination will be included in the experimental section on page 80.

2.3.2 Optical Properties

The optical property studies, shown in Table 1, were determined experimentally in several solvents to determine the in vivo success for the fluorophores. We can see that the compounds with hydrogen, fluorine, chlorine, and bromide groups (**14**–**25**) exhibit sharp and NIR absorbance bands with very high molar absorptivity all being >100,000 M^{-1} cm^{-1} which suggests that these fluorophores will satisfactorily absorb NIR wavelengths in vivo and will be compatible with the intraoperative imaging system. The trifluoromethyl substituted compounds are very poor at absorbing light at their wavelength of maximum absorbance, as indicated by their low molar absorptivity values in Table 1. This is attributed to the high-electron-withdrawing characteristics of the trifluoromethyl groups which lowers the overall probability of electron movement across the methine bridge connecting the aza-heterocycles. The in vivo success of these compounds also depends of the quantum yield and more importantly the molecular brightness (determined as the product of extinction coefficient and quantum yield) of the compounds in serum; therefore, we examined the quantum yield of these fluorophores in fetal bovine serum (FBS). Compounds **14**–

28 exhibit high quantum yield values in serum which is very appealing. All of the synthesized compounds have sufficiently high molecular brightness values in serum, with many compounds exhibiting molecular brightness values of >20,000. We observed an overall trend for the majority of compounds that as the size of the central halogen increases, the molecular brightness decreases.

Table 2. Optical Properties of 700 nm Emitting NIR Fluorophores, ***14-28****.*[a]

ID	λ_{abs} (nm)				Extinction Coefficient (ε, $M^{-1}cm^{-1}$)				λ_{em} (nm)		Stokes Shift		QY (Φ, %)		MB (ε x Φ)	
	DMSO	EtOH	PBS	FBS	DMSO	EtOH	PBS	FBS	EtOH	FBS	EtOH	FBS	EtOH	FBS	EtOH	FBS
14	647	645	640	649	212,500	248,200	218,800	184,500	660	662	15	13	32.7	31.0	81,161	57,195
15	645	644	642	638	235,300	207,800	171,000	168,800	659	665	15	27	29.2	28.8	60,677	48,614
16	645	641	638	634	257,330	253,200	204,400	211,700	657	660	16	26	30.1	43.6	76,213	92,301
17	645	641	638	649	216,700	225,800	196,500	164,400	663	662	22	13	31.6	35.2	71,352	58,868
18	646	643	638	638	210,900	233,700	193,400	193,400	658	660	15	22	16.5	15.3	38,561	29,590
19	642	641	635	644	173,200	210,500	170,900	145,800	658	658	17	14	16.3	11.9	34,312	17,350
20	652	649	645	660	183,400	204,200	174,200	136,000	658	669	19	9	41.5	57.5	84,743	78,200
21	653	652	647	658	192,800	207,800	140,200	136,000	664	666	14	8	18.3	28.5	38,027	38,760
22	650	648	643	655	233,100	250,600	185,000	153,700	665	663	17	12	15.4	17.4	38,592	26,744
23	653	650	653	662	181,200	174,500	144,800	141,100	670	671	20	9	42.4	57.0	73,988	80,427
24	655	653	660	648	140,200	189,600	121,500	119,700	667	671	14	23	20.8	23.0	39,437	27,531
25	643	641	635	644	169,000	169,600	166,900	159,600	657	663	16	21	15.5	11.8	26,288	18,833
26	642	638	636	648	41,200	45,200	28,700	30,600	656	654	18	6	58.7	89.2	26,532	27,295
27	644	640	638	649	72,000	114,900	56,300	19,500	656	655	16	6	20.5	47.4	23,555	9,243
28	641	638	635	644	32,400	49,700	19,600	8,400	653	651	15	7	21.1	29.0	10,487	2,436

[a]All measurements were performed in DMSO, ethanol (EtOH), phosphate buffer solution (PBS), and fetal bovine serum (FBS), at pH = 7.4, 37 °C. λ_{abs}, wavelength of maximum absorbance, λ_{em}, wavelength of maximum emission; QY, quantum yield; and MB, molecular brightness

Photostability studies were performed on a select number of contrast agents to observe their performance when continuously irradiated and can be seen in Figure 26. The selected compounds featuring a hydrogen atom at the *meso* position of the polymethine bridge showed little decomposition after being exposed to light for 48 h, however, when chlorine or bromine replace

the hydrogen, there is noticeable degradation of up to 35% of the original absorbance. Only a minimal 4% absorbance was lost for each of the first compounds in each set; furthermore, these data help conclude that these compounds would be applicable for long-duration surgical resections with the ability to absorb and fluoresce NIR-light for high-contrast imaging with a half-life of >48h for the entire set studied. The studies were compared to the same concentration of dyes kept in dark containers, but the same distance from the lamp to determine if thermal degradation contributed as well. We found an absence in measurable degradation for the samples kept in the dark which leads us to conclude that heat from the lamp imparts a negligible effect and the absorbance decrease comes from irradiation.

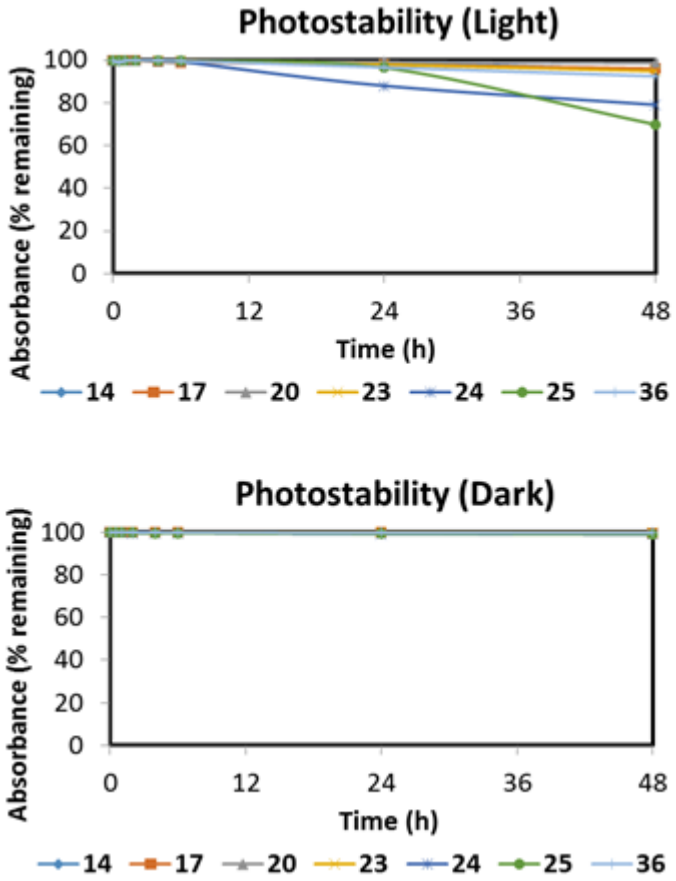

Figure 26. Photodegradation profile in light and dark conditions of a select subset of NIR fluorescent contrast agents. The absorbance values for the individual fluorophores were measured (at the wavelength of maximum absorption) at different intervals to determine the percentage of absorption remaining.

2.3.3 Physicochemical Properties

Performing calculations on the HOMO/LUMO electron levels can give a unique perspective of molecules. When analyzing the minimized three-dimensional structures, we see that the *meso*-halogenation perturbs the *trans*-pseudoalkene angles and the elongated structure of the fluorophore which actually shortens the overall length and perturbs the conjugated bridge by requiring the compound to bend to accommodate this central substitution. This is an interesting

finding since upon first glance, it seems that adding larger groups to the middle of the compound would result in an elongation of the compound simply because it would force the neighboring hydrogen atoms apart. Another potential explanation for the decrease in molecular brightness is the heavy atom effect that can effectively stabilize the triplet state, allowing for a higher probability for competing decay processes of the excited state (i.e., phosphorescence or energy transfer) compared to the nonhalogenated fluorophores.

	Physicochemical Properties							
ID	**MW (g/mol)**	**LogD[a] (pH = 7.4)**	**TPSA**	**H-bond acceptors**	**Length (A)**	**Volume (Å^3)**	**Dipole (debye)**	**Polarizability**
14	383.548	3.56	6.25	1	18.665	445.51	1.95	76.14
15	417.994	3.79	6.25	1	18.530	458.45	0.89	77.21
16	462.445	3.96	6.25	1	18.453	462.96	0.79	77.55
17	419.529	3.84	6.25	2	18.684	455.28	4.23	76.95
18	453.974	4.08	6.25	3	18.536	468.22	3.32	78.02
19	498.425	4.24	6.25	3	18.475	472.73	3.26	78.36
20	452.439	4.77	6.25	2	18.674	472.01	3.55	78.30
21	486.884	5.00	6.25	3	18.539	484.95	2.58	79.37
22	531.335	5.17	6.25	3	18.464	489.45	2.52	79.71
23	541.341	5.09	6.25	2	18.665	481.25	3.74	79.05
24	575.786	5.33	6.25	3	18.517	494.19	2.79	80.12
25	620.237	5.50	6.25	3	18.340	498.70	2.73	80.40
26	519.544	5.31	6.25	6	20.188	511.26	8.04	81.47
27	553.989	5.55	6.25	7	19.547	524.14	7.58	82.54
28	598.440	5.70	6.25	7	19.406	528.65	7.62	82.88

[a]Log *D* = partition coefficient at pH 7.4, TPSA = total polar surface area, while molecular parameters (length, volume dipole, and polarizability) were calculated using Spartan Wavefunction (V10) DFT starting with the minimized structural conformation of the lowest energy.

Based on the high performance optically and physicochemical values such as cLogD, the fluorophores **14-28** were then sent to collaborators at Beth Isreal Deaconess Medical Center at Harvard University for animal studies. During the *in vivo* studies, it was found that compounds

17-19 displayed high uptake in the thyroid glands, compounds **20-25** showed uptake in the salivary glands, and compounds **26-28** had uptake in the pituitary gland. All of these compunds showed good uptake in various endocrine system tissues with good optical properties and show great promise for further studies for intraoperative imaging. These studies can be seen in full in the paper attached in the appendix.[59]

2.3.4 Conclusions

This study was successful in synthesizing a set of near-infrared fluorophores and determining their optical properties. The combination of the design of the compounds and the viability of their optical efficiencies lead to their use in *in vivo* animal studies. The dyes were successfully synthesized in good yields, up to 78%, and their optical properties in four solvents were determined. Based on their optical properties, *in vivo* studies were performed (appendix) and it was found that these dyes were valuable in the visualization of various endocrine tissues using a series of NIR cameras.

2.3.5 Experimental Details

2.3.5.1 Synthesis of Pentamethine Cyanine Analogs

The chemical reagents used in the synthesis of these compounds were obtained from Acros Organics, Alfa Aesar, and Matrix Scientific. The reactions were followed using silica gel 60 F_{254} thin-layer chromatography plates (Merck EMD Millipore, Darmstadt, Germany). Open column chromatography was utilized for the purification of all final compounds using 60–200 μm, 60A, classic column silica gel (Dynamic Adsorbents, Norcross, GA). The ^{1}H NMR and ^{13}C NMR spectra were obtained using high-quality Kontes NMR tubes (Kimble Chase, Vineland, NJ) rated to 500 MHz and were recorded on a Bruker Avance (400 MHz) spectrometer using DMSO-d_6 or

MeOD-d_4 containing tetramethylsilane (TMS) as an internal calibration standard set to 0.0 ppm. UV–vis/NIR absorption spectra were recorded on a Varian Cary 50 spectrophotometer. High-resolution accurate mass spectra (HRMS) were obtained either at the Georgia State University Mass Spectrometry Facility using a Waters Q-TOF micro (ESI-Q-TOF) mass spectrometer or utilizing a Waters Micromass LCT TOF ES+ Premier mass spectrometer. Liquid chromatography utilized a Waters 2487 single wavelength absorption detector with wavelengths set between 640 and 700 nm depending on the particular photophysical properties. The column used in LC was a Waters Delta-Pak 5 μM 100A 3.9 × 150 mm reversed-phase C_{18} column. Evaporative light-scattering detection analyzes trace impurities that cannot be observed by alternate methods; a SEDEX 75 ELSD was utilized in tandem with liquid chromatography. The integral under the curve was determined for both the LC and ELSD spectra and was used to confirm the purity (>95%) of the synthesized contrast agents.

2.3.5.2 Optical and Physicochemical Property Analyses

All optical measurements were performed in various solvents, including ethanol, dimethyl sulfoxide (DMSO), phosphate buffered saline (PBS, pH 7.4), and at 37 °C in 100% FBS buffered with 50 mM HEPES, pH 7.4. Absorbance and fluorescence emission spectra of the series of NIR fluorophores were measured using Varian Cary 50 absorbance spectrophotometer (190–1100 nm) and Shimadzu RF-5301PC spectrofluorometer (350–1000 nm). For fluorescence quantum yield (QY) measurements, rhodamine 800 in absolute ethanol (QY = 28%) was used as a calibration standard, under conditions of matched absorbance at 620 nm. In silico calculations of physicochemical distribution coefficient (log *D* at pH 7.4) was calculated using Marvin and JChem

calculator plugins (ChemAxon, Budapest, Hungary). Electrostatic maps were calculated using Spartan DFT calculations at the B3LYP level.

2.3.5.3 Photostability Analysis

The photostability experiments were performed to determine the photobleaching threshold of the fluorophores. We determined the photobleaching rate by measuring the decrease in absorbance at the wavelength of maximum absorption over a 48h time period. The light condition involved a glass cell containing individual contrast agent (0.01 mm in methanol) that was affixed 250 mm away from a 15W F15T8 broad spectrum bulb being irradiated using a portable lamp at room temperature. The dark control was also examined to exclude chemical decomposition phenomena. The absorbance values were measured at various time points and then plotted versus time to obtain the photostability graphs in light and dark.

2.3.5.4 Liquid Chromatography-Mass Spectrometry Analysis

The purity of all compounds was measured using liquid chromatography–mass spectrometry (LC-MS) on a Waters system consisting of a 1525 binary HPLC pump with a manual 7725i Rheodyne injector, a 996 photodiode array (PDA) detector, and a 2475 multiwavelength fluorescence detector. The column eluent was divided in 2 using a flow splitter (Upchurch Scientific). A portion of the eluent flowed into an ELSD (Richards Scientific) while the rest flowed into a Micromass LCT ESI-TOF spectrometer (Waters) equipped with a Symmetry (R) C18 (4.6 × 150 mm, 5 μm) reverse-phase HPLC column. For mass spectrometry, the mobile phase was solvent A = 0.1% formic acid in water and solvent B = CH_3CN with 95% A for 5 min and a linear gradient from 5% to 40% CH_3CN (from A to B for 30 min) at a flow rate of 1 mL/min, capillary voltage was −3317 V, and sample cone voltage was −50 V.

2.3.5.5 Synthesis and Characterization of NIR Fluorophores

To obtain the final dyes **14–28**, the precursor salts **6–10** (2 mol equiv) were added to a clean, dry round-bottom flask. The compounds were stirred in 10 mL of acetic anhydride, and either sodium acetate (3 mol equiv) was added along with 1 mol equiv of individual malondialdehyde linker **11–13**. The reaction was allowed to stir at 40–60 °C for 2 h. The reactions were monitored closely using regular phase thin-layer chromatography with a mobile phase of DCM/MeOH (99:1) as well as UV–vis-NIR spectrophotometer in quartz cuvettes with methanol as a solvent to visualize the absorption band at ∼650 nm against that of the starting materials ∼400 nm. Upon completion of the reaction, the mixtures were allowed to cool, and the solvent was evaporated. The residue was extracted using DCM and was washed with DI water (3 × 70 mL). The resulting organic layer was dried under magnesium sulfate, gravity filtered, and evaporated to afford crystals that were washed with diethyl ether (2 × 50 mL) and hexanes (50 mL) to yield crystals that were dried under vacuum overnight. The pure product was obtained after dissolving in methanol and precipitating with ether several times, or the compounds were isolated using flash column chromatography and 5% methanol in DCM as the eluting solvent. After purification, the compounds were obtained in the designated yields and were fully characterized.

1,3,3-Trimethyl-2-((1E,3E,5E)-5-(1,3,3-trimethylindolin-2-ylidene)penta-1,3-dien-1-yl)-3H-indol-1-ium iodide (**14**)**:** Yield 64%, MP >260 ^{o}C ; ^{1}H NMR (400 MHz, MeOD-d_4) **δ**: 1.71 (s, 12H), 3.63 (s, 6H), 6.28 (d, J = 16.0 Hz, 2H), 6.65 (t, J = 12.0 Hz, 1H), 7.24 (t, J = 8.0 Hz, 2H), 7.29 (d, J = 8.0 Hz, 2H), 7.39 (t, J = 8.0 Hz, 2H), 7.48 (d, J = 8.0 Hz, 2H), 8.25 (t, J = 12.0 Hz, 2H); ^{13}C NMR (100 MHz, MeOD-d_4) **δ** 27.90, 31.71, 50.50, 104.44, 111.83, 123.31, 126.20, 129.71, 142.56, 144.29, 155.52, 175.28. TOF HRMS m/z $[M]^+$ calculated for $[C_{27}H_{31}N_2]^+$ 383.2487, found 383.2474.

2-((1E,3Z,5E)-3-Chloro-5-(1,3,3-trimethylindolin-2-ylidene)penta-1,3-dien-1-yl)-1,3,3-trimethyl-3H-indol-1-ium iodide (**15**)**:** Yield 64%, M.P. 230-232 °C, ^{1}H NMR (400 MHz, MeOD-d_4) **δ** 1.76 (s, 12H), 3.71 (s, 6H), 6.435 (d, *J* = 12 Hz, 2H), 7.32 (t, *J* = 8 Hz, 2H), 7.39 (d, *J* = 8 Hz, 2H), 7.45 (t, *J* = 8 Hz, 2H), 7.54 (d, *J* = 8 Hz, 2H), 8.345 (d, *J* = 12 Hz, 2H). ^{13}C NMR (100 MHz, MeOD-d_4) **δ** 25.03, 29.53, 48.55, 98.93, 110.02, 121.00, 121.86, 124.55, 127.43, 140.42, 141.67, 146.72, 174.28. TOF HRMS m/z $[M]^+$ calculated for $[C_{27}H_{30}N_2Cl]^+$ 417.2098 found 417.2107.

2-((1E,3Z,5E)-3-Bromo-5-(1,3,3-trimethylindolin-2-ylidene)penta-1,3-dien-1-yl)-1,3,3-trimethyl-3H-indol-1-ium iodide (**16**)**:** Yield 61%, M.P. 230-232 ºC ; ^{1}H NMR (400 MHz, $CDCl_3$-d_1) **δ** 1.91 (s, 12H), 3.82 (s, 6H), 6.36 (d, *J* = 8 Hz, 2H), 7.16 (d, *J* = 8.0 Hz, 2H, 7.26-7.31 (m, 4H), 7.39-7.44 (m, 4H) 8.93 (d, *J* = 12 Hz, 2H). ^{13}C NMR (100 MHz, DMSO-d_6) **δ** 27.04, 31.98, 49.85, 102.61, 112.19, 115.98, 122.94, 125.97, 128.93, 141.78, 143.02, 149.64, 175.14. TOF HRMS m/z $[M]^+$ calculated for $[C_{27}H_{30}N_2Br]^+$ 461.1592 found 461.1585.

5-Fluoro-2-((1E,3E,5E)-5-(5-fluoro-1,3,3-trimethylindolin-2-ylidene)penta-1,3-dien-1-yl)-1,3,3-trimethyl-3H-indol-1-ium iodide (**17**): Yield 78%, MP >260 ºC, ^{1}H-NMR(400 MHz, DMSO-d_6) **δ** 1.68 (s, 12H), 3.59 (s, 6H), 6.23 (d, *J* = 12.0 Hz, 2H), 6.52 (s, 1H), 7.24 (s, 2H), 7.39 (s, 2H), 7.62 (s, 2H), 8.29 (s, 2H). ^{13}C-NMR (100 MHz, DMSO-d_6) δ: 27.27, 31.85, 49.54, 103.64, 103.76, 110.82, 111.07, 112.43, 112.49, 112.59, 112.66, 115.15, 125.54, 139.55, 143.60, 143.69, 154.27, 154.29, 159.32, 161.72, 173.64. TOF HR-MS ESI m/z $[M]^+$ calculated for $[C_{27}H_{29}F_2N_2]^+$ 419.2299, found 419.2296.

2-((1E,3Z,5E)-3-Chloro-5-(5-fluoro-1,3,3-trimethylindolin-2-ylidene)penta-1,3-dien-1-yl)-5-fluoro-1,3,3-trimethyl-3H-indol-1-ium (**18**): Yield 37%, MP >260 ºC, ^{1}H-NMR(400 MHz, DMSO-d_6) **δ**: 1.72 (s, 12H), 3.67 (s, 6H), 6.26 (d, *J* = 14 Hz, 2H), 7.29,7.31 (t, *J* = 6.8 Hz, 8.8 Hz, 2H), 7.52-7.54 (m, 2H), 7.70 (d, *J* = 6 Hz, 2H), 8.41 (d, *J* = 14 Hz, 2H). ^{19}F NMR (375 MHz, DMSO- d_6) **δ**: -116.67 (s, 2F). TOF HR-MS ESI m/z $[M]^+$ calculated for $[C_{27}H_{29}F_2ClN_2]^+$ 453.1909 found 453.1914.

2-((1E,3Z,5E)-3-Bromo-5-(5-fluoro-1,3,3-trimethylindolin-2-ylidene)penta-1,3-dien-1-yl)-5-fluoro-1,3,3-trimethyl-3H-indol-1-ium (**19**) Yield 52%, ^{1}H-NMR(400 MHz, DMSO-d_6) **δ**: 1.72 (s, 12H), 3.67 (s, 6H), 6.26 (d, *J* = 13.2 Hz, 2H), 7.32 (t, *J* = 8.8 Hz, 2H) , 7.55-7.52 (m, 2H),

7.70 (d, *J* = 7.6, 2H), 8.46 (d, *J* = 13.6, 2H). ^{19}F NMR (375 MHz, DMSO- d_6) **δ**: -116.67 (s, 2F). TOF HR-MS ESI m/z $[M]^+$ calculated $[C_{27}H_{29}F_2N_2Br]^+$ was 497.1404 found 497.1394.

5-Chloro-2-((1E,3E,5E)-5-(5-chloro-1,3,3-trimethylindolin-2-ylidene)penta-1,3-dien-1-yl)-1,3,3-trimethyl-3H-indol-1-ium iodide (**20**): Yield 59%, MP >260 ºC, ^{1}H-NMR(400 MHz, DMSO-d_6) **δ**: 1.69 (s, 12H), 3.59 (s, 6H), 6.27 (d, *J* = 14 Hz, 2H), 6.551 (t, *J* = 12.4, 12.0 Hz, 1H), 7.39 (d, *J* = 8.8 Hz, 2H), 7.46 (d, *J* = 8.4 Hz, 2H), 7.80 (s, 2H), 8.32 (t, *J* = 13.2 Hz, 2H). ^{13}C-NMR (100 MHz, DMSO-d_6) **δ**: 27.30, 31.84, 49.51, 104.09, 112.87, 123.29, 126.16, 128.67, 129.50, 142.23, 143.54, 154.72, 173.65. TOF HR-MS ESI m/z $[M]^+$ calculated for $[C_{27}H_{29}Cl_2N_2]^+$ 451.1708, found 451.1722.

5-Chloro-2-((1E,3Z,5E)-3-chloro-5-(5-chloro-1,3,3-trimethylindolin-2-ylidene)penta-1,3-dien-1-yl)-1,3,3-trimethyl-3H-indol-1-ium (**21**): Yield 53%, MP >260 ºC, ^{1}H-NMR(400 MHz, DMSO-d_6) **δ**: 1.72 (s, 12H), 3.67 (s, 6H), 6.26 (d, *J* = 14 Hz, 2H), 7.52 (m, 4H), 7.89 (s, 2H), 8.43 (d, *J* = 13.6, 2H). ^{13}C-NMR (100 MHz, DMSO-d_6) **δ**: 26.81, 32.15, 49.98, 100.72, 113.62, 123.06, 123.49, 128.80, 130.31, 142.02, 143.83, 147.96, 174.97. TOF HR-MS ESI m/z $[M]^+$ calculated for $[C_{27}H_{29}Cl_3N_2]^+$ 485.1318 found 485.1317.

2-((1E,3Z,5E)-3-Bromo-5-(5-chloro-1,3,3-trimethylindolin-2-ylidene)penta-1,3-dien-1-yl)-5-chloro-1,3,3-trimethyl-3H-indol-1-ium iodide (**22**) Yield 69%, MP 252-254 ºC ^{1}H-NMR(400 MHz, DMSO-d_6) **δ**: 1.73 (s, 12H), 3.67 (s, 6H), 6.28 (d, *J* = 13.2 Hz, 2H), 7.52 (m, 4H), 7.89 (s, 2H), 8.47 (d, *J* = 13.2 Hz, 2H). ^{13}C-NMR (100 MHz, DMSO-d_6) **δ**: 26.79, 32.16, 50.03, 102.96, 113.65, 116.40, 123.51, 128.82, 130.35, 141.99, 143.83, 149.98, 175.15. TOF HR-MS ESI m/z $[M]^+$ calculated $[C_{27}H_{28}BrN_2Cl_2]^+$ was 529.0813 found 529.0810.

5-Bromo-2-((1E,3E,5E)-5-(5-bromo-1,3,3-trimethylindolin-2-ylidene)penta-1,3-dien-1-yl)-1,3,3-trimethyl-3H-indol-1-ium iodide (**23**): Yield 62%, MP >260 ºC, ^{1}H-NMR(400 MHz, DMSO-d_6) δ: 1.69 (s, 12H), 3.58 (s, 6H), 6.27 (d, *J* = 14 Hz, 2H), 6.56 (t, *J* = 12.4, 12 Hz, 1H), 7.35 (d, *J* = 8.4 Hz, 2H), 7.59 (d, *J* = 8.4, 2H), 7.93 (s, 2H), 8.33 (t, *J* = 13.2 Hz, 2H). ^{13}C-NMR (100 MHz, DMSO-d_6) **δ** 27.25, 31.71, 49.48, 104.07, 113.33, 117.45, 126.09, 131.51, 142.63, 143.85, 154.86, 173.45. TOF HR-MS ESI m/z $[M]^+$ calculated for $[C_{27}H_{29}Br_2N_2]^+$ 539.0697, found 539.0695.

5-Bromo-2-((1E,3Z,5E)-5-(5-bromo-1,3,3-trimethylindolin-2-ylidene)-3-chloropenta-1,3-dien-1-yl)-1,3,3-trimethyl-3H-indol-1-ium (**24**): Yield 72%, MP >260 ºC, ^{1}H-NMR(400 MHz,

DMSO-d_6) **δ**: 1.72 (s, 12H), 3.67 (s, 6H), 6.28 (d, *J* = 12.0 Hz, 2H), 7.47 (d, *J* = 8.0 Hz, 2H), 7.63 (d, *J* = 8.0 Hz, 2H), 8.01 (s, 2H), 8.43 (d, *J* = 12.0 Hz, 2H). ^{13}C-NMR (100 MHz, DMSO-d_6) **δ**: 26.81, 32.17, 49.96, 100.69, 114.05, 118.37, 123.13, 126.26, 131.63, 142.40, 144.11, 147.96, 174.78. TOF HR-MS ESI m/z $[M]^+$ calculated for $[C_{27}H_{28}Br_2N_2Cl]^+$ 573.0308, found 573.0316.

5-Bromo-2-((1E,3Z,5E)-3-bromo-5-(5-bromo-1,3,3-trimethylindolin-2-ylidene)penta-1,3-dien-1-yl)-1,3,3-trimethyl-3H-indol-1-ium iodide (**25**): Yield 46%, MP 231-232 ^{o}C, ^{1}H-NMR(400 MHz, DMSO-d_6) δ: 1.72 (s, 12H), 3.66 (s, 6H), 6.28 (d, *J* = 13.2 Hz, 2H), 7.47 (d, *J* = 8.0 Hz, 2H), 6.64 (d, *J* = 8.4 Hz, 2H), 8.01 (s, 2H), 8.48 (d, *J* = 13.6 Hz, 2H). ^{13}C-NMR (100 MHz, DMSO-d_6) δ: 26.79, 32.11, 50.03, 102.97, 114.07, 116.47, 118.42, 126.27, 131.65, 142.40, 144.13, 150.03, 175.01. TOF HR-MS ESI m/z $[M]^+$ calculated $[C_{27}H_{28}Br_3N_2]^+$ was 616.9803, found 616.9814.

1,3,3-Trimethyl-5-(trifluoromethyl)-2-((1E,3E)-5-((E)-1,3,3-trimethyl-5-(trifluoromethyl)indolin-2-ylidene)penta-1,3-dien-1-yl)-3H-indol-1-ium iodide (**26**): Yield 55%, MP 218-221°C, ^{1}H NMR (400 MHz, $CDCl_3$): **δ** 1.81 (s, 12H), 3.79 (s, 6H), 6.53 (d, *J* = 13.6 Hz, 2H), 7.11 (t, *J* = 13.6 Hz, 1H), 7.21(d, *J* = 8.4 Hz, 2H), 7.60 (s, 2H), 7.70 (d, *J* = 7.6 Hz, 2H), 8.02 (t, *J* = 13.6, 2H). ^{19}FNMR: (375 MHz, DMSO-d_6): **δ** 62.00. TOF HRMS m/z $[M]^+$ calculated for $[C_{29}H_{29}N_2F_6]^+$ 519.2297, found 519.2393.

2-((1E,3Z)-3-Chloro-5-((E)-1,3,3-trimethyl-5-(trifluoromethyl)indolin-2-ylidene)penta-1,3-dien-1-yl)-1,3,3-trimethyl-5-(trifluoromethyl)-3H-indol-1-ium iodide (**27**): Yield 71%, MP 226-228 °C, ^{1}H NMR (400 MHz, $CDCl_3$): **δ** 1.91 (s, 12H), 3.87 (s, 6H), 6.47 (d, *J* = 13.6 Hz, 2 H), 7.30 (s, 2H), 7.65 (m, 4H), 8.90 (d, *J* = 10.4 Hz, 2H). ^{19}F NMR (375 MHz, DMSO-d_6): **δ** 62.05. TOF HRMS m/z $[M]^+$ calculated for $[C_{29}H_{28}N_2F_6Cl]^+$ 553.1840, found 553.1996.

2-((1E,3Z)-3-Bromo-5-((E)-1,3,3-trimethyl-5-(trifluoromethyl)indolin-2-ylidene)penta-1,3-dien-1-yl)-1,3,3-trimethyl-5-(trifluoromethyl)-3H-indol-1-ium iodide (**28**): Yield 71%, MP 226-228 °C, ^{1}H NMR (400 MHz, $CDCl_3$): **δ** 1.91 (s, 12H), 3.87 (s, 6H), 6.46 (bs, 2H), 7.30 (s, 2H), 7.69 (m, 4H), 8.91 (d, *J* =, 7.2 Hz, 2H). ^{19}F NMR (375 MHz, DMSO-d_6), **δ**: 62.01. TOF HRMS m/z $[M]^+$ calculated for $[C_{29}H_{28}N_2F_6Br]^+$ 597.1335, found 597.1597.

Journal of Medicinal Chemistry

Article

pubs.acs.org/jmc

Near-Infrared Illumination of Native Tissues for Image-Guided Surgery

Eric A. Owens,[†,#] Hoon Hyun,[‡,§,#] Tyler L. Dost,[†,#] Jeong Heon Lee,[‡] GwangLi Park,[‡] Dang Huan Pham,[§] Min Ho Park,[∥] Hak Soo Choi,[*,‡] and Maged Henary[*,†]

[†]Center for Diagnostics and Therapeutics, Center for Biotechnology and Drug Design, Department of Chemistry, Georgia State University, Petit Science Center, 100 Piedmont Ave SE, Atlanta, Georgia 30303, United States

[‡]Gordon Center for Medical Imaging, Division of Nuclear Medicine and Molecular Imaging, Department of Radiology, Massachusetts General Hospital and Harvard Medical School, Boston, Massachusetts 02114, United States

[§]Department of Biomedical Sciences and [∥]Department of Surgery, Chonnam National University Medical School, Gwangju 501-746, South Korea

Supporting Information

ABSTRACT: Our initial efforts to prepare tissue-specific near-infrared (NIR) fluorescent compounds generated successful correlation between physicochemical properties and global uptake in major organs after systemic circulation and biodistribution. Herein, we focus on the effects on biodistribution based on modulating electronic influencing moieties from donating to withdrawing moieties at both the heterocyclic site and through *meso*-substitution of pentamethine cyanine fluorophores. These selected modifications harnessed innate biodistribution pathways through the structure-inherent targeting, resulting in effective imaging of the adrenal glands, pituitary gland, lymph nodes, pancreas, and thyroid and salivary glands. These native-tissue contrast agents will arm surgeons with a powerful and versatile arsenal for intraoperative NIR imaging in real time.

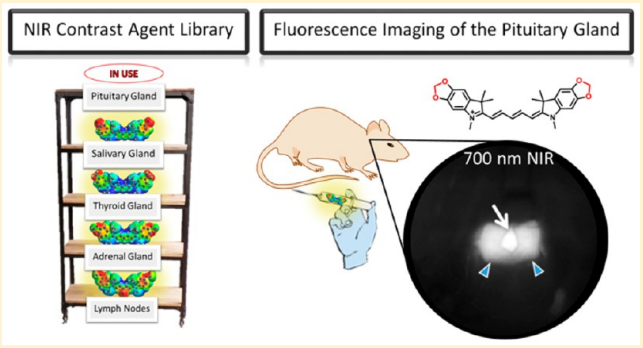

INTRODUCTION

During endocrine surgeries and intricate surgical resections, surgeons mostly rely on their naked eye and experience during often-lengthy procedures to avoid sensitive glands and tissues.[1−3] Neglecting to carefully navigate the surgical field can lead to poor patient prognosis even morbidity.[4−11] Endocrine and exocrine tissues regulate the body's hormone levels, and any perturbation, especially transection, can jeopardize the patient's ability to recover after surgery and maintain proper hormone levels.[12−15] The important task of avoiding sensitive tissues is often difficult as these small and imperative glands are often obscured by blood and surrounding tissues. Surgeons require an imaging modality that can allow them to visualize these tissues during cancer resection surgeries to improve the surgical success rate, lower overall fatalities, and advance patient prognoses.

Near-infrared (NIR) fluorescence-guided resection of cancerous tissues has demonstrated significant promise with increasing advancements being reported over the recent years.[15−27] Unfortunately, research efforts have been overwhelmingly concentrated on developing cancer-specific NIR-fluorophores with optimal optical, physicochemical, and targeting properties. This only satisfies one-half of the main objective: the ability to simultaneously image the surgical field with both a disease-targeted fluorophore and a native-tissue-targeted fluorophore of distinct wavelengths that can both be simultaneously and separately detected for direct dual-target imaging in real time.

Significant advancements have been made to develop NIR-fluorescent compounds that target sensitive endogenous tissue and help surgeons avoid these hormonal glands in real time without changing the overall look of the surgical field. The class of NIR-fluorescent cyanine dyes has shown excellent promise in the area of NIR-fluorescence image-guided surgery for in vivo tumor targeting. Cyanine chromophores are broadly defined by having two nitrogen-containing heterocycles that are connected through an electron-deficient polymethine bridge with a delocalized monocation conjugated between both nitrogen atoms. The wavelengths associated with these compounds are heavily dependent on the length of the polymethine bridge and the terminal heterocyclic moieties. Polymethine cyanines are chemically stable NIR-fluorescent compounds, and we have investigated the pentamethine class of compounds previously[16,20] and herein for laying the groundwork for endogenous tissue targeting. The heptamethine cyanine class (~800 nm

Received: January 8, 2016
Published: April 21, 2016

DOI: 10.1021/acs.jmedchem.6b00038
J. Med. Chem. 2016, 59, 5311−5323

Scheme 1. Synthesis of 700 nm Emitting Pentamethine Cyanines Featuring Neutral (X = H) and Electron-Withdrawing (X = F, Cl, Br, CF_3) Moieties

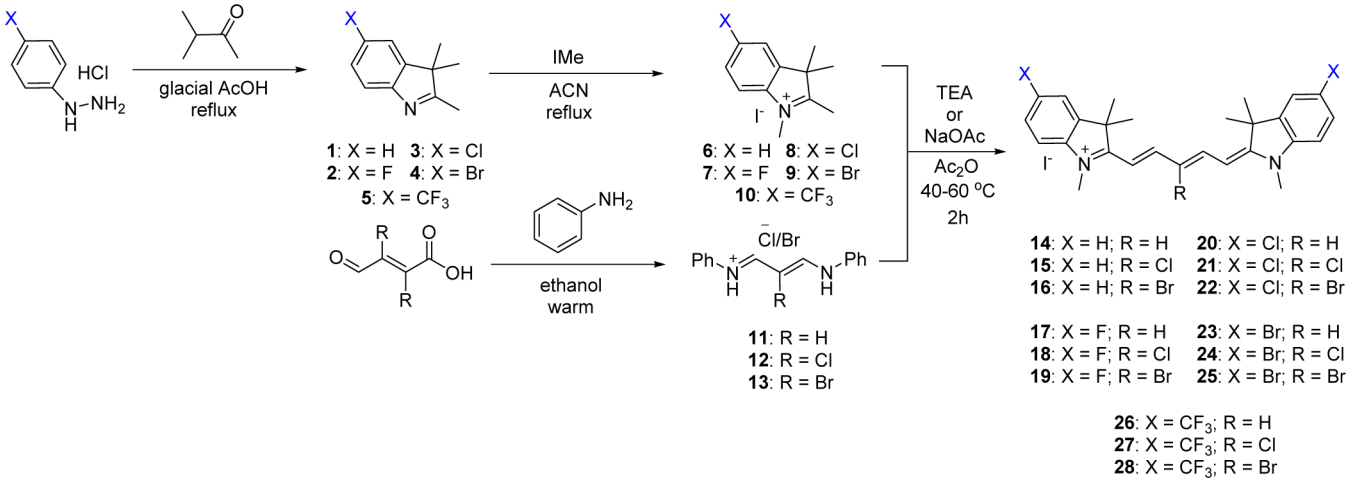

Scheme 2. Synthesis of 700 nm Emitting Pentamethine Cyanines Featuring Electron-Donating Methoxy Groups

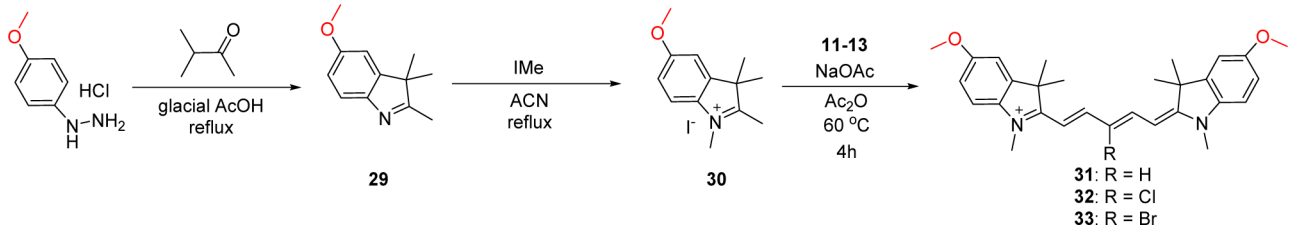

fluorescence) has been more extensively explored for disease targeting through the development of zwitterionic decorated heptamethine cyanines linked with a propinoic acid and conjugated with a small cyclic peptide (cRGD-ZW800–1).[10,21,22] The longer NIR wavelengths (i.e., 800 nm) are more easily detected against the background and usually reserved to detect occult cancerous metastasis due to the minimal autofluorescence. We plan to further exploit the 700 nm channel (pentamethine cyanines) for native tissue imaging for dual channel intraoperative imaging.

Toward achieving this goal, we have continued to harness the structure-inherent tissue affinity to determine the innate biodistribution and targeting by modulating overall molecular characteristics such as hydrophobicity (determined through log *D* calculations), total polar surface area, molecular size/weight, and the electronic contributions (electron-donating/-withdrawing characteristics).[15,24,26] The compounds synthesized and analyzed herein vary by their heterocyclic moieties (electron donating or withdrawing) and various halogenation at the central carbon atom of the polymethine chain which alters the net dipole, volume, polarization, and even the overall shape of the compounds. We expect these selected modifications to offer biological perturbation toward understanding the molecular characteristics for targeting specific tissues. Correlating these molecular descriptors with in vivo biodistribution is expected to result in a clinically significant paradigm in the quest of translating NIR-targeted contrast agents into the clinic, and every analyzed compound offers another evidentiary piece to the puzzle.

RESULTS AND DISCUSSION

Synthesis of Pentamethine Fluorophores. Since it has been previously reported that halogenated hydrocarbons localize in higher concentration within endocrine and exocrine glands compared to their nonhalogenated counterparts,[16] we decided to probe the effect of halogenation on pentamethine cyanines for endocrine and exocrine tissue targeting. For a direct comparison, we synthesized electron-donating counterparts that could offer insight into how potential electronic factors present in the compounds may influence biodistribution. We selected methoxy and methylene-dioxy heterocyclic groups for a direct comparison to the halogenated counterparts and fully expected perturbation in the biological distribution profile, but we could not predict the results of these modifications. Understanding the effects that altering physicochemical properties imparts on the distribution adds important fundamental knowledge about future targeting ability for this and many other classes of imaging agents.

We have developed several optimized synthetic routes for maximizing the structural diversity in the pentamethine cyanine pharmacophore. The compounds with neutral effects and electron-withdrawing groups are synthesized starting with the corresponding phenyl hydrazine salts being refluxed in the presence of 3-methyl-2-butanone in acidic conditions. This reaction furnishes the indolenines **2**–**5** in excellent yield. We then alkylated the obtained oil using iodomethane in acetonitrile, which yields the cationic salt **6**–**10** bearing an acidic methylene proton. We also separately react aniline with a warm ethanolic solution of either mucochloric or mucobromic acid to obtain the pentamethine precursor **12** or **13**, with **11** being commercially obtained. These two compounds are individually combined in the presence of acetic anhydride

DOI: 10.1021/acs.jmedchem.6b00038
J. Med. Chem. 2016, 59, 5311–5323

Scheme 3. Synthesis of 700 nm Emitting Pentamethine Cyanines Featuring Electron-Donating Methylene Dioxy Substitution on the Phenyl Rings

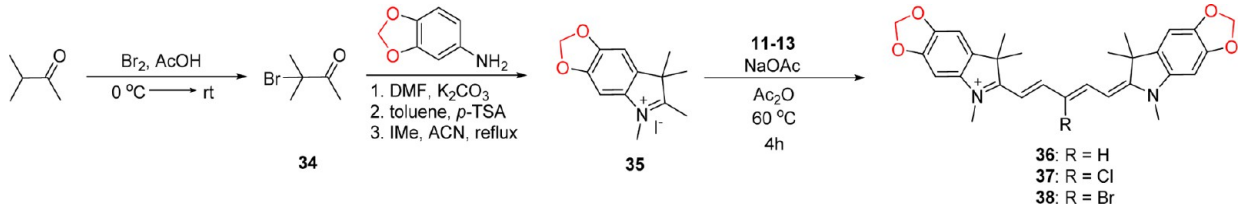

Table 1. Optical Properties of 700 nm Emitting NIR Fluorophores[a]

		λ_{abs} (nm)			extinction coefficient (ε, $M^{-1}cm^{-1}$)				λ_{em} (nm)		Stokes shift		QY (Φ, %)		MB ($\varepsilon \times \Phi$)	
ID	DMSO	EtOH	PBS	FBS	DMSO	EtOH	PBS	FBS	EtOH	FBS	EtOH	FBS	EtOH	FBS	EtOH	FBS
14	647	645	640	649	212,500	248,200	218,800	184,500	660	662	15	13	32.7	31.0	81,161	57,195
15	645	644	642	638	235,300	207,800	171,000	168,800	659	665	15	27	29.2	28.8	60,677	48,614
16	645	641	638	634	257,330	253,200	204,400	211,700	657	660	16	26	30.1	43.6	76,213	92,301
17	645	641	638	649	216,700	225,800	196,500	164,400	663	662	22	13	31.6	35.2	71,352	58,868
18	646	643	638	638	210,900	233,700	193,400	193,400	658	660	15	22	16.5	15.3	38,561	29,590
19	642	641	635	644	173,200	210,500	170,900	145,800	658	658	17	14	16.3	11.9	34,312	17,350
20	652	649	645	660	183,400	204,200	174,200	136,000	658	669	19	9	41.5	57.5	84,743	78,200
21	653	652	647	658	192,800	207,800	140,200	136,000	664	666	14	8	18.3	28.5	38,027	38,760
22	650	648	643	655	233,100	250,600	185,000	153,700	665	663	17	12	15.4	17.4	38,592	26,744
23	653	650	653	662	181,200	174,500	144,800	141,100	670	671	20	9	42.4	57.0	73,988	80,427
24	655	653	660	648	140,200	189,600	121,500	119,700	667	671	14	23	20.8	23.0	39,437	27,531
25	643	641	635	644	169,000	169,600	166,900	159,600	657	663	16	21	15.5	11.8	26,288	18,833
26	642	638	636	648	41,200	45,200	28,700	30,600	656	654	18	6	58.7	89.2	26,532	27,295
27	644	640	638	649	72,000	114,900	56,300	19,500	656	655	16	6	20.5	47.4	23,555	9243
28	641	638	635	644	32,400	49,700	19,600	8400	653	651	15	7	21.1	29.0	10,487	2,436
31	671	668	658	674	152,300	205,000	133,600	135,000	696	696	28	22	9.6	11.9	19,680	16,070
32	672	671	658	676	148,100	210,000	135,900	162,000	694	692	23	16	3.9	9.7	8190	15,710
33	669	669	655	676	94,200	154,000	82,100	109,000	689	688	20	12	5.1	9.7	7218	10,570
36	691	690	680	698	107,200	108,100	89,200	85,900	705	716	15	18	4.7	6.5	5081	5584
37	689	690	678	693	147,200	156,600	127,100	117,800	716	712	26	19	3.0	4.2	4698	4948
38	687	687	675	691	154,900	165,800	135,700	125,000	715	716	28	25	2.9	3.1	4808	3875

[a]All measurments were performed in DMSO, ethanol (EtOH), PBS, and FBS, pH = 7.4 at 37 °C. Abbreviations: λ_{abs}, wavelength of maximum absorbance; λ_{em}, wavelength of maximum emission; QY, quantum yield; and MB, molecular brightness.

and either triethylamine (fluorine-containing compounds) or sodium acetate and are heated to afford the brilliant blue pentamethine fluorophores Schemes 1 and 2.

The electron-donating containing methoxy-substituted compounds are prepared through an identical synthetic route; however, the final step requires a longer reaction time at a slightly elevated temperature, due to the methoxy group electron-donating effects which increases the pK_a of the methylene proton resulting in reduced reactivity of the methylene carbon. We also designed a complementary set of compounds bearing heterocyclic-donating groups features the methylene dioxy ring shown in compounds **36**–**38**. These compounds are prepared using an alternate synthetic strategy beginning with the acidic bromination of 3-methyl-2-butanone followed by S_N1 replacement of the tertiary bromine by the methylene dioxyaniline compound. Upon heating in the presence of acid catalyst, *para*-toluenesulfonic acid, the compound forms the cyclic methylene dioxy 2,3,3-trimethylindolenine ring through a largely unexplored Bischler–Möhlau method that can be alkylated using aforementioned conditions for the formation of compound **35**. The final methylene dioxy compounds **36**–**38** were synthesized using similar chemistry as the methoxy group (Scheme 3).

Optical and Physicochemical Properties. The optical properties, shown in Table 1, were performed in several solvents to determine the in vivo success for the fluorophores. We can see that the compounds with hydrogen, chlorine, bromide, and methoxy groups (**14**–**25**, **31**–**33**) exhibit sharp and NIR absorbance bands with very high molar absorptivity all being >100,000 M^{-1} cm^{-1} which suggests that these fluorophores will satisfactorily absorb NIR wavelengths in vivo and will be compatible with the intraoperative imaging system. As expected, the methylenedioxy compounds exhibited slightly lower molar absorptivity due to a broadening of the absorption profile which results from a more widely dispersed energy sublevels. Similarly, the trifluoromethyl substituted compounds are very poor at absorbing light at their wavelength of maximum absorbance, as indicated by their low molar absorptivity values in Table 1. We attribute this to the high-electron-withdrawing characteristics of the trifluoromethyl groups which lowers the overall probability of electron movement across the methine bridge connecting the aza-heterocycles. The in vivo success of these compounds also depends of the quantum yield and more importantly the molecular brightness (determined as the product of extinction coefficient and quantum yield) of the compounds in serum; therefore, we examined the quantum yield of these

DOI: 10.1021/acs.jmedchem.6b00038
J. Med. Chem. 2016, 59, 5311–5323

fluorophores in fetal bovine serum (FBS). Compounds **14**−**28**, **31**−**33** exhibit high quantum yield values in serum which is very appealing. All of the synthesized compounds have sufficiently high molecular brightness values in serum, with many compounds exhibiting molecular brightness values of >20,000. We observed an overall trend for the majority of compounds that as the size of the central halogen increases, the molecular brightness decreases. When analyzing the minimized three-dimensional structures, we see that the *meso*-halogenation perturbs the *trans*-pseudoalkene angles and the elongated structure of the fluorophore which actually shortens the overall length and perturbs the conjugated bridge by requiring the compound to bend to accommodate this central substitution. This is an interesting finding since upon first glance, it seems that adding larger groups to the middle of the compound would result in an elongation of the compound simply because it would force the neighboring hydrogen atoms apart. Another potential explanation for the decrease in molecular brightness is the heavy atom effect that can effectively stabilize the triplet state, allowing for a higher probability for competing decay processes of the excited state (i.e., phosphorescence or energy transfer) compared to the nonhalogenated fluorophores.

Photostability studies were performed on a select number of contrast agents to observe their performance when continuously irradiated and can be seen in Figure 1. The selected

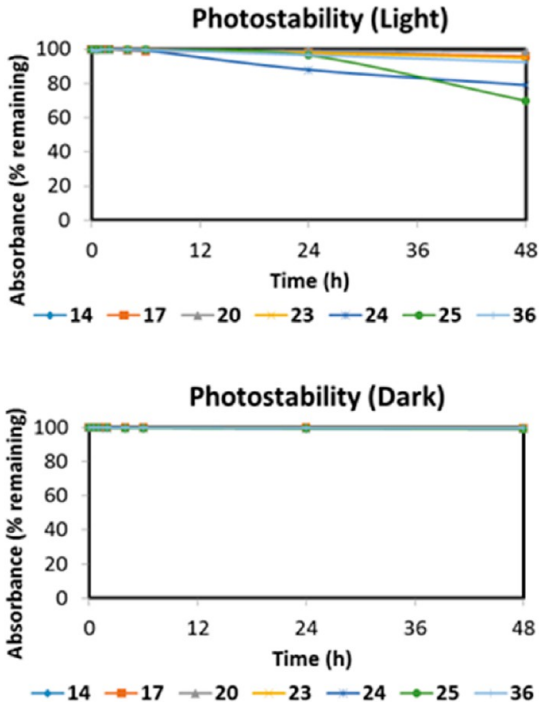

Figure 1. Photodegradation profile in light and dark conditions of a select subset of NIR fluorescent contrast agents. The absorbance values for the individual fluorophores were measured (at the wavelength of maximum absorption) at different intervals to determine the percent absorption remaining.

compounds featuring a hydrogen atom at the *meso* position of the polymethine bridge showed little decomposition after being exposed to light for 48 h, however, when chlorine or bromine replace the hydrogen, there is noticeable degradation of up to 35% of the original absorbance. Only a minimal 4% absorbance was lost for each of the first compounds in each set; furthermore, these data help conclude that these compounds would be applicable for long-duration surgical resections with the ability to absorb and fluoresce NIR-light for high-contrast imaging with a half-life of >48h for the entire set studied. The studies were compared to the same concentration of dyes kept in dark containers, but the same distance from the lamp to determine if thermal degradation contributed as well. We found an absence in measurable degradation for the samples kept in the dark which leads us to conclude that heat from the lamp imparts a negligible effect and the absorbance decrease comes from irradiation.

Structure-Inherent Targeting Ability of NIR Fluorophores. As native tissue targeting remains predominantly understudied, we focused our attention to the salivary, thyroid, pituitary, adrenal glands, lymph nodes, and pancreas. As these tissues facilitate the regulation of human hormone levels, they are important for long-term health and should be carefully avoided during surgical resection in surrounding areas.

After in vivo studies, we found compounds that exhibited high SBR in targeted tissues (high is designated as a ratio of target signal to surrounding tissue being >2.0). Without surface or subcellular receptors readily available for the particular native tissues, it has been difficult to infer mechanistic insight of how these fluorophores localize within their respective tissues. However, we have found several key structural components that help facilitate structure-inherent biodistribution and localization in important tissues, including the salivary, thyroid, pituitary, adrenal glands, lymph nodes, and pancreas.

In surgical resections such as thyroidectomies, it is crucial to remove the entire thyroid gland while maintaining complete integrity of the parathyroid gland. Selective thyroid gland imaging is paramount in the ability to avoid partial thyroid resection or accidental parathyroid transection which can cause several abnormal human conditions such as hypocalcemia.

The common clinical indications of salivary gland imaging are pain and swelling. Imaging is useful in identifying the masses of salivary glands and also in differentiating them from the masses/pathologies of adjacent cervical spaces. In proven cases of salivary gland tumors, imaging helps in delineating the extent of the lesion and invasion of adjacent cervical spaces. Cancerous tissues in this area can grow quickly, and surgical resection of the diseased tissue is needed while sparing excision of the exocrine salivary glands themselves.

Toward finding the thyroid and salivary glands targeting by using NIR fluorophores, we evaluated the imaging capability of these compounds in thyroid and salivary glands. Table 3 shows the thyroid and salivary glands targeting for the entire set of compounds. The targeting of these two tissues seemed to parallel each other, suggesting a biological connection between these two tissues, though despite an extensive literature review, an explanation for this remains unclear. Among the entire set of prepared compounds, we found that central halogenation reduced the targeting efficacy into these glands. Surprisingly, the parent set of compounds (**14**−**16**) all targeted the salivary gland with superior SBR. From our data, we can see overall that the salivary glands are sensitive to the central halogenation but remain tolerant to the heterocyclic halogen incorporation. Compounds **20**−**25** exhibit the halogen trend we observed. With the heterocyclic halogen substitution, the salivary gland targeting remains high; however, when the central halogen is incorporated within the same compounds, we have a severely diminished targeted ability (i.e., from compound **20** with SBR of >5 to compounds **21** and **22** with SBR of 1−2). Specifically compounds **17**−**25** shown in Figures 2 and 3 exemplify this

DOI: 10.1021/acs.jmedchem.6b00038
J. Med. Chem. 2016, 59, 5311−5323

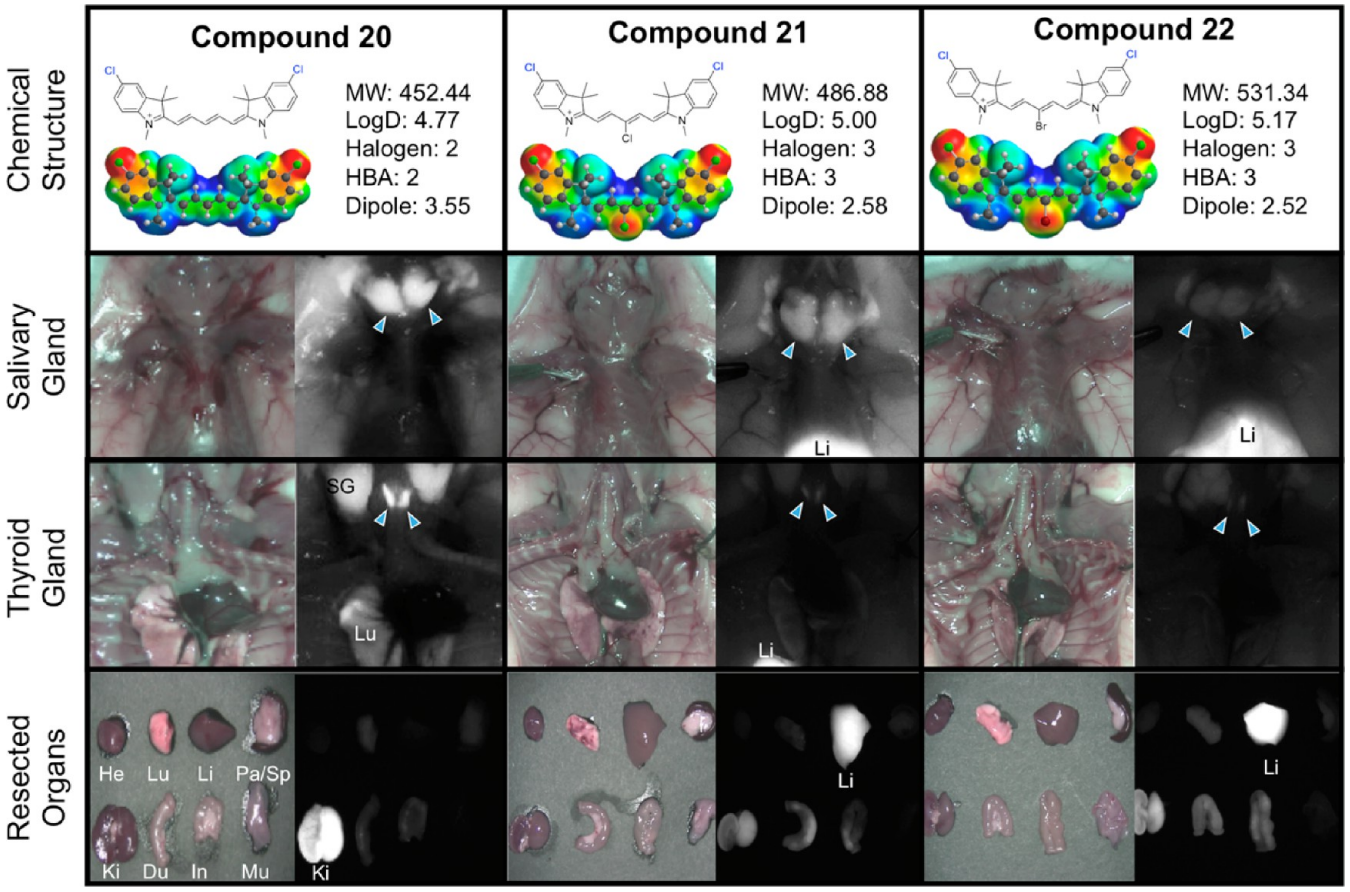

Figure 2. Compounds **20**–**22**, targeting to salivary glands and thyroid glands, and biodistribution of resected organs in CD-1 mice. Ten nmol of each fluorophore was injected intravenously into 25 g CD-1 mice 4 h prior to imaging and resection. Abbreviations used are Du, duodenum; He, heart; In, intestine; Ki, kidneys; Li, liver; Lu, lungs; Mu, muscle; Pa, pancreas; SG, salivary gland, Sp, spleen. Arrows indicate the targeted gland.

trend. Compounds **17**, **20**, and **23** do not feature halogens at the central carbon of the polymethine chain and exhibit the most effective thyroid and salivary gland localization. As the halogen incorporation increases, the thyroid and salivary gland localization is forfeited in deference to nonspecific accumulation and high liver uptake due to hepatobiliary clearance arising from the increase in hydrophobicity.

As one of the important endocrine glands, the pituitary gland (dubbed the master gland) is responsible for controlling the hormonal release of signaling chemicals throughout the body. Transecting this precious gland during surgery causes lasting side effects from hormone dysregulation with imbalances perpetuating during the lifetime of the patent. Tumors associated with the pituitary gland can interfere with signaling the release of many hormones such as thyroid-stimulating hormone which directly influences metabolic activity, energy levels, growth hormones, and the nervous system. Efforts to remove pituitary gland tumors must critically and clearly image the native tissue to prevent accidental damage. We found excellent pituitary gland targeting with the trifluoromethyl compounds **26**–**28** (Figure 4). The trifluoromethyl substitutions increase the dipole of the compound considerably (Table 2) which we anticipated to elicit a drastic biological response compared to the alternate halogenated counterparts. Indeed, the vast change in electronic dipole from 1 to 4 debye (other compounds) to >7.5 debye in the trifluoromethyl substituted compounds (which also corresponds to an increase in polarizability) lowered the target recognition to some endocrine tissues; however, the thyroid gland targeting remained elevated when the central position was halogen-free.

Lymph nodes are widely distributed and are responsible for immune system function and can indicate an abnormal physiological condition. For example, an increase in size may indicate leukemia due to increased trafficking of lymphocytes from the blood into the lymph nodes. Additionally, thorough examination of the lymph nodes is crucial for the staging of cancer as tumor metastases normally first localize in sentinel lymph nodes. For surgical avoidance and the frequent necessity to biopsy, a NIR imaging technique to visualize this tissue is highly important. In the developed set of compounds, we noticed effective targeting of the lymph node by the methoxy derivatives **31**–**33** which is surprising in the context of the methylene dioxy compounds **36**–**38** exhibiting low lymph node targeting. Interestingly we see an inverse effect of the previous set of compounds where the *meso* halogenation increases the imaging signal as compared to the surrounding tissue in the lymph node with **32** and **33** having a SBR of >5 as indicated by the +++ in Table 3. Figure 5 shows two successful examples of nodal imaging in the inguinal and lumbar nodes with compound **33** exhibiting excellent targeting characteristics.

The adrenal glands, located above the kidney, produce essential and nonessential hormones that primarily control the body's metabolism, blood pressure, and stress response. In Figure 6, we observed that the methylene dioxy compounds **36**–**38** exhibited adrenal gland targeting characteristics (++, SBR 3–5) that also seemed to be tolerant to the addition of

DOI: 10.1021/acs.jmedchem.6b00038
J. Med. Chem. 2016, 59, 5311–5323

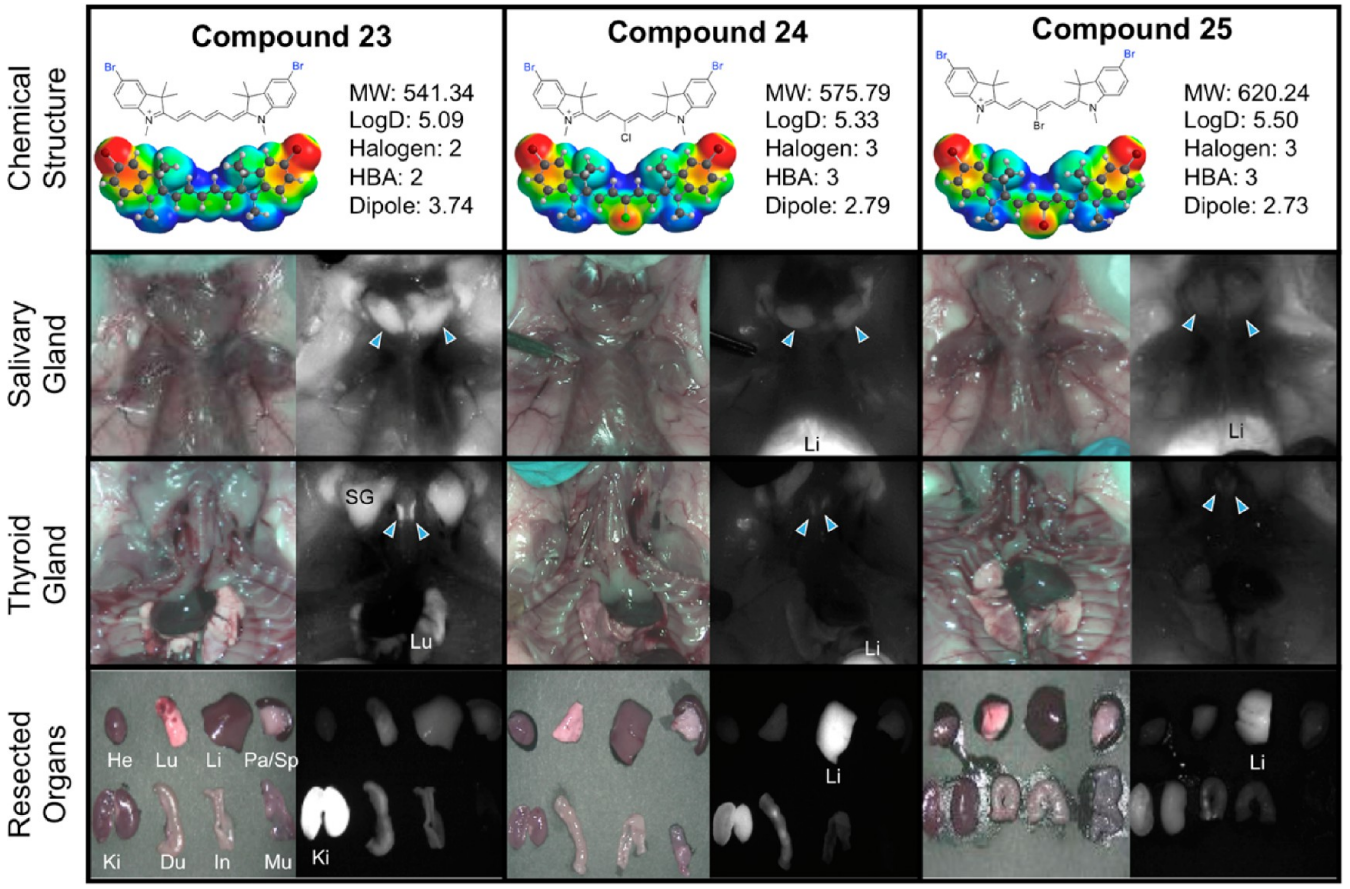

Figure 3. Compounds **23**–**25**, targeting to salivary glands and thyroid glands, and biodistribution of resected organs in CD-1 mice. Ten nmol of each fluorophore was injected intravenously into 25 g CD-1 mice 4 h prior to imaging and resection. Abbreviations used are Du, duodenum; He, heart; In, intestine; Ki, kidneys; Li, liver; Lu, lungs; Mu, muscle; Pa, pancreas; SG, salivary gland, Sp, spleen. Arrowheads indicate the targeted gland.

meso-halogens. It seems that the log *D* values predominantly govern the localization of these compounds as the five compounds (**31**, **32**, **36**–**38**) with the lowest log *D* were the most effective at targeting this tissue, with the methylene dioxy compounds **36**–**38** prevailing as the best contrast agents for the adrenal gland across the series. This finding is also true in their pancreas targeting ability, as all three compounds within this set exhibit excellent SBR in pancreatic tissue. Interestingly, the small change from methoxy **31**–**33** to the locked ring structure of **36**–**38** alters the targeting ability of the compound (i.e., comparing **33** and **38**). This finding also corroborates our previous results that pancreatic targeting requires low comparative log *D* values. Indeed the highest pancreas targeting characteristics are from compounds exhibiting comparatively low log *D* values (i.e., compounds **36**–**38**, log *D* 2.80–3.21). Additionally, the central halogenation seems to lower pancreas-targeting substantially, except for the methylene dioxy set of compounds. It is very interesting that independent halogenation (either central or terminal heterocycles) does not seem to greatly perturb the pancreatic tissue uptake, except for when the trifluoromethyl group is incorporated. Halogenating both positions, however, has a detrimental effect on the compound-pancreas localization. For example, compounds **15**, **16**, **17**, **20**, and **23** are all effective at pancreas targeting, and only have halogens at either the heterocycles or bridge. Compounds **18**, **19**, **21**, **22**, **24**, and **25** with all sites halogenated exhibit reduced pancreas uptake. We attribute this effect to an increase in overall hydrophobicity imparted by too many halogens on the core structure. Additionally, structures with higher molecular weight in addition to greater hydrophobic character seem to be poor at pancreatic localization.

Preliminary Cytotoxicity of NIR fluorophores. To confirm cell cytotoxicity of the tissue-specific fluorophores, NIH/3T3 mouse fibroblast cells were incubated with the selected NIR fluorophores, respectively, for 1 h at 37 °C and gently washed with DMEM. Then, the viability of fibroblasts was assessed by the alamarBlue assay. The assay system incorporates an oxidation–reduction (REDOX) indicator that both fluorescence and changes color in response to chemical reduction of growth medium resulting from cell growth. As shown in Figure 7, over 75% of the cells were viable when treated with NIR fluorophores at concentrations of 2 μM and 10 μM. Therefore, notable cell death was not observed even with the high concentration of the NIR fluorophores. These results confirm that tissue-specific NIR fluorophores do not show obvious cytotoxic effects.

■ CONCLUSIONS

Toward satisfying the clinical need for native tissue targeted contrast agents in real-time NIR image-guided surgery, we present compounds that are effective at imaging the salivary, thyroid, pituitary, adrenal glands, lymph nodes, and pancreas. We are confident that this work will lay the foundation for development of native tissue contrast agents for clinical use.

DOI: 10.1021/acs.jmedchem.6b00038
J. Med. Chem. 2016, 59, 5311–5323

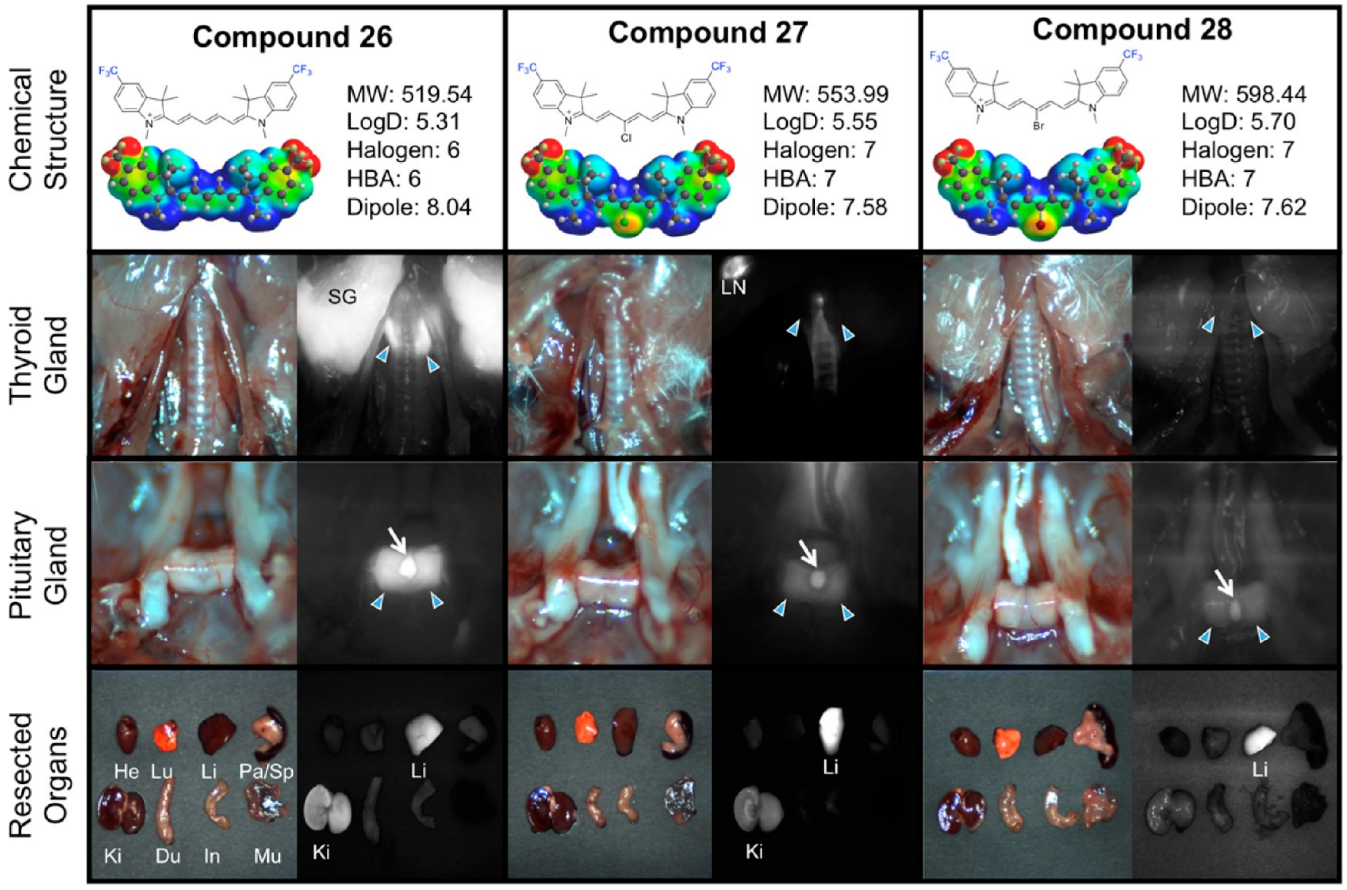

Figure 4. Compounds **26**–**28**, targeting to thyroid glands and pituitary gland, and biodistribution of resected organs in CD-1 mice. Ten nmol of each fluorophore was injected intravenously into 25 g CD-1 mice 4 h prior to imaging and resection. Abbreviations used are Du, duodenum; He, heart; In, intestine; Ki, kidneys; Li, liver; LN, lymph node; Lu, lungs; Mu, muscle; Pa, pancreas; SG, salivary gland, Sp, spleen. Arrows indicate the targeted gland. For pituitary glands, arrowheads indicate the anterior portion and arrows for posterior pituitary.

EXPERIMENTAL DETAILS

Synthesis of Pentamethine Cyanine Analogs. The chemical reagents used in the synthesis of these compounds were obtained from Acros Organics, Alfa Aesar, and Matrix Scientific. The reactions were followed using silica gel 60 F_{254} thin-layer chromatography plates (Merck EMD Millipore, Darmstadt, Germany). Open column chromatography was utilized for the purification of all final compounds using 60–200 μm, 60A, classic column silica gel (Dynamic Adsorbents, Norcross, GA). The ^{1}H NMR and ^{13}C NMR spectra were obtained using high-quality Kontes NMR tubes (Kimble Chase, Vineland, NJ) rated to 500 MHz and were recorded on a Bruker Avance (400 MHz) spectrometer using DMSO-d_6 or MeOD-d_4 containing tetramethylsilane (TMS) as an internal calibration standard set to 0.0 ppm. UV–vis/NIR absorption spectra were recorded on a Varian Cary 50 spectrophotometer. High-resolution accurate mass spectra (HRMS) were obtained either at the Georgia State University Mass Spectrometry Facility using a Waters Q-TOF micro (ESI-Q-TOF) mass spectrometer or utilizing a Waters Micromass LCT TOF ES+ Premier mass spectrometer. Liquid chromatography utilized a Waters 2487 single wavelength absorption detector with wavelengths set between 640 and 700 nm depending on the particular photophysical properties. The column used in LC was a Waters Delta-Pak 5 μM 100A 3.9 × 150 mm reversed-phase C_{18} column. Evaporative light-scattering detection analyzes trace impurities that cannot be observed by alternate methods; a SEDEX 75 ELSD was utilized in tandem with liquid chromatography. The integral under the curve was determined for both the LC and ELSD spectra and was used to confirm the purity (>95%) of the synthesized contrast agents.

Optical and Physicochemical Property Analyses. All optical measurements were performed in various solvents, including ethanol, dimethyl sulfoxide (DMSO), phosphate buffered saline (PBS, pH 7.4), and at 37 °C in 100% FBS buffered with 50 mM HEPES, pH 7.4. Absorbance and fluorescence emission spectra of the series of NIR fluorophores were measured using Varian Cary 50 absorbance spectrophotometer (190–1100 nm) and Shimadzu RF-5301PC spectrofluorometer (350–1000 nm). For fluorescence quantum yield (QY) measurements, rhodamine 800 in absolute ethanol (QY = 28%) was used as a calibration standard, under conditions of matched absorbance at 620 nm. In silico calculations of physicochemical distribution coefficient (log D at pH 7.4) was calculated using Marvin and JChem calculator plugins (ChemAxon, Budapest, Hungary). Electrostatic maps were calculated using Spartan DFT calculations at the B3LYP level.

Photostability Analysis. The photostability experiments were performed to determine the photobleaching threshold of the fluorophores. We determined the photobleaching rate by measuring the decrease in absorbance at the wavelength of maximum absorption over a 48h time period. The light condition involved a glass cell containing individual contrast agent (0.01 mm in methanol) that was affixed 250 mm away from a 15W F15T8 broad spectrum bulb being irradiated using a portable lamp at room temperature. The dark control was also examined to exclude chemical decomposition phenomena. The absorbance values were measured at various time points and then plotted versus time to obtain the photostability graphs in light and dark.

Liquid Chromatography–Mass Spectrometry Analysis. The purity of all compounds was measured using liquid chromatography–mass spectrometry (LC-MS) on a Waters system consisting of a 1525 binary HPLC pump with a manual 7725i Rheodyne injector, a 996 photodiode array (PDA) detector, and a 2475 multiwavelength

DOI: 10.1021/acs.jmedchem.6b00038
J. Med. Chem. 2016, 59, 5311–5323

Table 2. in Silico Physicochemical Properties of 700 nm Emitting NIR Fluorophores (log *D*, TPSA, and H-bond acceptors) Calculated Using Marvin and JChem Calculator Plugins[a]

	physicochemical properties							
ID	MW (g/mol)	log *D* (pH = 7.4)	TPSA	H-bond acceptors	length (A)	volume (Å^3)	dipole (debye)	polarizability
14	383.548	3.56	6.25	1	18.665	445.51	1.95	76.14
15	417.994	3.79	6.25	1	18.530	458.45	0.89	77.21
16	462.445	3.96	6.25	1	18.453	462.96	0.79	77.55
17	419.529	3.84	6.25	2	18.684	455.28	4.23	76.95
18	453.974	4.08	6.25	3	18.536	468.22	3.32	78.02
19	498.425	4.24	6.25	3	18.475	472.73	3.26	78.36
20	452.439	4.77	6.25	2	18.674	472.01	3.55	78.30
21	486.884	5.00	6.25	3	18.539	484.95	2.58	79.37
22	531.335	5.17	6.25	3	18.464	489.45	2.52	79.71
23	541.341	5.09	6.25	2	18.665	481.25	3.74	79.05
24	575.786	5.33	6.25	3	18.517	494.19	2.79	80.12
25	620.237	5.50	6.25	3	18.340	498.70	2.73	80.40
26	519.544	5.31	6.25	6	20.188	511.26	8.04	81.47
27	553.989	5.55	6.25	7	19.547	524.14	7.58	82.54
28	598.440	5.70	6.25	7	19.406	528.65	7.62	82.88
31	443.600	3.24	24.71	2	20.631	500.23	4.10	80.61
32	478.045	3.48	24.71	3	20.527	513.28	3.04	81.68
33	522.496	3.64	24.71	3	20.142	517.72	2.89	82.02
36	471.577	2.80	43.17	4	21.203	496.69	2.69	80.33
37	506.019	3.04	43.17	5	20.847	509.64	1.77	81.39
38	550.473	3.21	43.17	5	20.680	514.15	1.72	81.74

[a]Log *D* = partition coefficient at pH 7.4, TPSA = total polar surface area, while molecular parameters (length, volume dipole, and polarizability) were calculated using Spartan Wavefunction (V10) DFT starting with the minimized structural conformation of the lowest energy.

Table 3. Targeting Properties and Biodistribution of 700 nm Emitting NIR Fluorophores for Specific Organs/Tissues at 4 h Post-Injection[a]

	targeted tissues						biodistribution					
ID	AG	Pa	PG	SG	TG	LN	Li	Ki	He	Lu	Sp	Bo
14	−	+++	++	+++	++	++	−	+++	+	−	−	++
15	−	+++	+	+++	+	+	+	+++	−	−	−	+
16	+	++	−	+++	+	+	+	+++	−	−	−	+
17	−	+++	++	+++	+++	++	−	+++	−	+	−	+
18	+	++	+	++	++	++	++	+++	−	+	−	−
19	−	+	−	+	+	−	++	+++	−	+	−	−
20	++	+++	+++	+++	+++	+++	−	+++	+	++	−	++
21	+	+	+	++	+	−	+++	++	−	−	−	−
22	+	+	−	+	+	−	+++	++	−	+	−	−
23	+	+++	+++	+++	+++	+++	++	+++	+	++	−	++
24	+	+	+	++	+	+	+++	++	−	+	−	+
25	+	+	−	+	+	−	+++	++	−	+	−	−
26	−	++	+++	++	++	−	+++	++	−	−	−	−
27	−	+	+	+	−	++	+++	++	−	−	−	−
28	+	+	−	+	−	−	+++	+	−	−	−	−
31	++	+++	++	+++	++	++	+	+++	+	+	−	+
32	++	++	++	++	++	+++	+++	+++	−	−	−	−
33	+	+	++	++	+	+++	+++	+++	−	+	+	−
36	++	+++	+++	++	+	+	++	+++	+	+	−	−
37	++	+++	++	++	++	+	+++	++	−	−	−	−
38	++	+++	++	++	++	+	+++	++	−	−	−	−

[a]Abbreviations used are AG, adrenal gland; Pa, pancreas; PG, pituitary gland; TG, thyroid gland; SG, salivary gland; Li, liver; Ki, kidneys; He, heart; Lu, lungs; Sp, spleen; Bo, bone; LN, lymph node. The SBR of each organ/tissue relative to the abdominal wall was quantified and labeled as − , 1−2; + , 2−3; ++, 3−5; and +++, >5.

fluorescence detector. The column eluent was divided in 2 using a flow splitter (Upchurch Scientific). A portion of the eluent flowed into an ELSD (Richards Scientific) while the rest flowed into a Micromass LCT ESI-TOF spectrometer (Waters) equipped with a Symmetry (R) C18 (4.6 × 150 mm, 5 μm) reverse-phase HPLC column. For mass spectrometry, the mobile phase was solvent A = 0.1% formic acid in water and solvent B = CH_3CN with 95% A for 5 min and a linear gradient from 5% to 40% CH_3CN (from A to B for 30 min) at a flow

DOI: 10.1021/acs.jmedchem.6b00038
J. Med. Chem. 2016, 59, 5311−5323

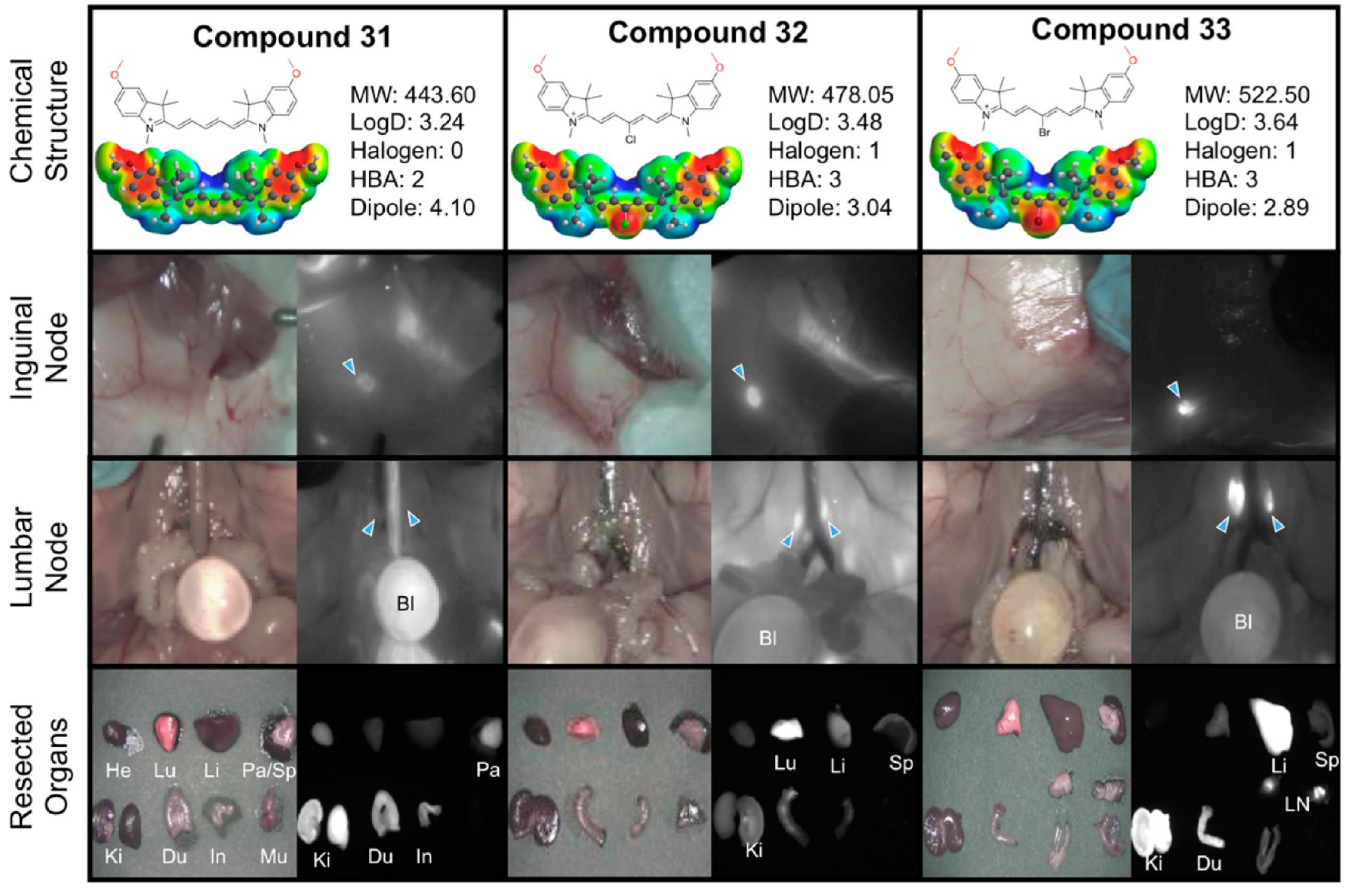

Figure 5. Compounds **31**–**33**, targeting to inguinal and lumbar lymph nodes, and biodistribution of resected organs in CD-1 mice. Ten nmol of each fluorophore was injected intravenously into 25 g CD-1 mice 4 h prior to imaging and resection. Abbreviations used are Bl, bladder; Du, duodenum; He, heart; In, intestine; Ki, kidneys; Li, liver; LN, lymph node; Lu, lungs; Mu, muscle; Pa, pancreas; Sp, spleen. Arrows indicate the targeted gland.

rate of 1 mL/min, capillary voltage was −3317 V, and sample cone voltage was −50 V.

Cell Viability Assay. The cell toxicity and proliferation were assessed by alamarBlue (Thermo Scientific) assay. The NIH/3T3 fibroblasts were seeded onto 96-well plates (1×10^4 cells per well). To test cytotoxicity depending on the fluorophore type and concentration, cells were treated with 2 and 10 μM of each NIR fluorophore ($n = 6$) for 1 h and cultured at 24 h post-treatment. At each assay time point, the incubation cell media was replaced with 100 μL of fresh media. Ten μL of alamarBlue solution was directly added to 100 μL each well and incubated for 4 h at 37 °C in a humidified 5% CO_2 incubator. Finally, the 96-well plates were placed into a microplate reader (Spark 10M, TECAN, Switzerland) for measuring the absorption intensity at 570 nm and fluorescence intensity at 590 nm. The data were presented by dividing by dye-untreated control group. The statistical significance was determined by one-way analysis of variance (ANOVA).

Animal Models and Biodistribution. Animals were housed in an AAALAC-certified facility and were studied under the supervision of BIDMC's IACUC in accordance with the approved institutional protocol no. 057-2014. Male CD-1 mice (20–30 g, 6–8 weeks, Charles River Laboratories, Wilmington, MA) were anesthetized with 100 mg/kg ketamine and 10 mg/kg xylazine intraperitoneally (Webster Veterinary, Fort Devens, MA). For intraoperative imaging and biodistribution, the imaging system equipped with a custom filter set (Chroma Technology Corporation, Brattleboro, VT) composed of a 650 ± 22 nm excitation filter, a 680 nm dichroic mirror, and an 710 ± 25 nm emission filter was used at a fluence rate of 4 mW/cm^2, with white light (400–650 nm) at 40,000 lx. Color and NIR fluorescence images were acquired simultaneously with custom software at rates up to 15 Hz over a 15 cm diameter field of view. The imaging system was positioned at a distance of 18 in. from the surgical field. For each experiment, camera exposure time and image normalization were held constant.

Quantitative Analysis. At each time point, the fluorescence and background intensity of a region of interest (ROI) over each tissue was quantified using custom imaging software and ImageJ software (NIH, Bethesda, MD) version 1.45q. The signal-to-background ratio (SBR) was calculated as SBR = fluorescence/background, where background is the signal intensity of neighboring tissues such as muscle or skin obtained over the period of imaging time. All NIR fluorescence images for a particular fluorophore were normalized identically for all conditions of an experiment. At least three animals were analyzed at each time point. Statistical analysis was carried out using the unpaired Student's *t*-test or one-way ANOVA. Results were presented as mean ± SD, and curve fitting was performed using Prism version 4.0a software (GraphPad, San Diego, CA).

Synthesis and Characterization of NIR Fluorophores. To obtain the final dyes **14**–**28**, **31**–**33**, and **36**–**38**, the precursor salts **6**–**10**, **30**, and **35** (2 mol equiv) were added to a clean, dry round-bottom flask. The compounds were stirred in 10 mL of acetic anhydride, and either sodium acetate or triethyl amine (3 mol equiv) was added along with 1 mol equiv of individual malondialdehyde linker **11**–**13**. The reaction was allowed to stir at 40–60 °C for 2 h. The reactions were monitored closely using regular phase thin-layer chromatography with a mobile phase of DCM/MeOH (99:1) as well as UV–vis-NIR spectrophotometer in quartz cuvettes with methanol as a solvent to visualize the absorption band at ∼650 nm against that of the starting materials ∼400 nm. Upon completion of the reaction, the mixtures were allowed to cool, and the solvent was evaporated. The residue was extracted using DCM and was washed with DI water

DOI: 10.1021/acs.jmedchem.6b00038
J. Med. Chem. 2016, 59, 5311–5323

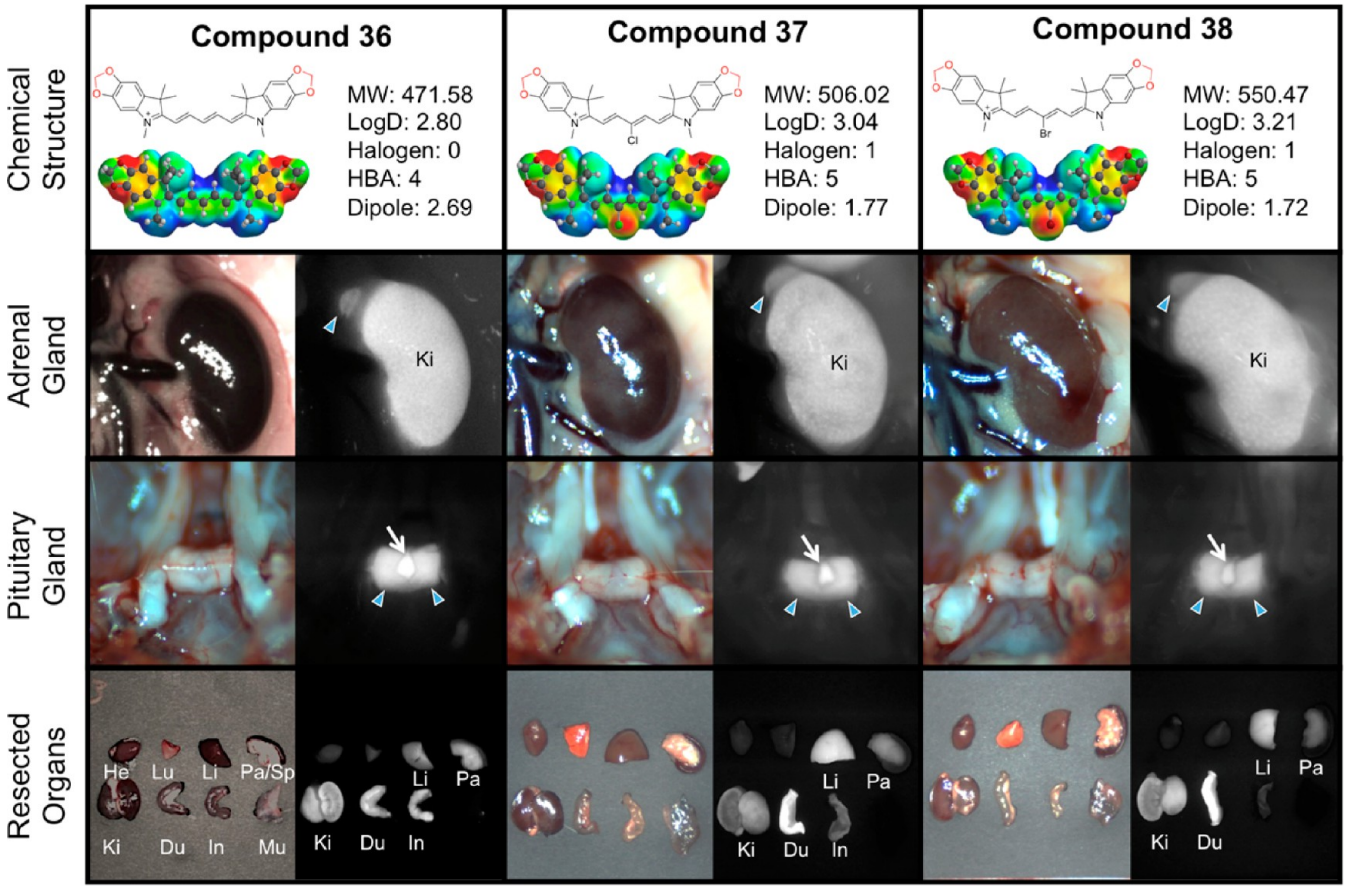

Figure 6. Compounds **36**–**38**, targeting to adrenal glands and pituitary gland, and biodistribution of resected organs in CD-1 mice. Ten nmol of each fluorophore was injected intravenously into 25 g CD-1 mice 4 h prior to imaging and resection. Abbreviations used are Du, duodenum; He, heart; In, intestine; Ki, kidneys; Li, liver; Lu, lungs; Mu, muscle; Pa, pancreas; SG, salivary gland, Sp, spleen. Arrows indicate the targeted gland. For pituitary glands, arrowheads indicate the anterior portion and arrows for posterior pituitary.

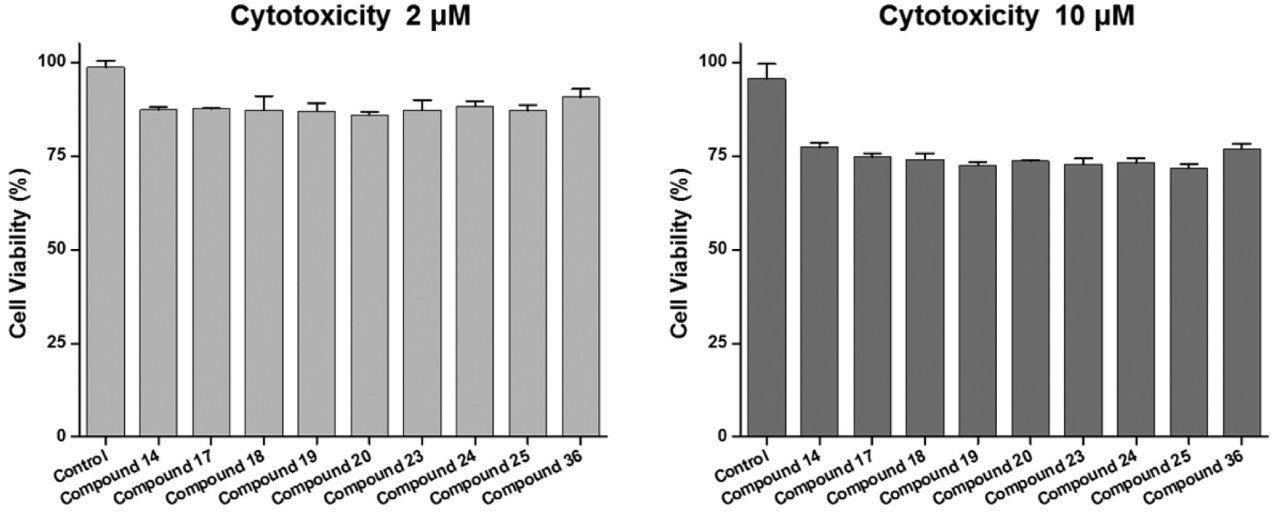

Figure 7. Cell viability assay of selected NIR fluorophores using NIH/3T3 fibroblasts. Cell viability was plotted 1 day post-treatment of compounds at a concentration of 2 μM (left) or 10 μM (right), compared to untreated control as measured by the alamarBlue assay. Data are representative of N = 6 independent experiments per condition (mean ± SD).

(3 × 70 mL). The resulting organic layer was dried under magnesium sulfate, gravity filtered, and evaporated to afford crystals that were washed with diethyl ether (2 × 50 mL) and hexanes (50 mL) to yield crystals that were dried under vacuum overnight. The pure product was obtained after dissolving in methanol and precipitating with ether several times, or the compounds were isolated using flash column chromatography and 5% methanol in DCM as the eluting solvent. After purification, the compounds were obtained in the designated yields and were fully characterized.

*1,3,3-Trimethyl-2-((1E,3E,5E)-5-(1,3,3-trimethylindolin-2-ylidene)-penta-1,3-dien-1-yl)-3H-indol-1-ium Iodide (**14**).* Yield 64%, mp > 260 °C; ^{1}H NMR (400 MHz, MeOD-d_4) δ: 1.71 (s, 12H), 3.63 (s,

DOI: 10.1021/acs.jmedchem.6b00038
J. Med. Chem. 2016, 59, 5311–5323

6H), 6.28 (d, J = 16.0 Hz, 2H), 6.65 (t, J = 12.0 Hz, 1H), 7.24 (t, J = 8.0 Hz, 2H), 7.29 (d, J = 8.0 Hz, 2H), 7.39 (t, J = 8.0 Hz, 2H), 7.48 (d, J = 8.0 Hz, 2H), 8.25 (t, J = 12.0 Hz, 2H); ^{13}C NMR (100 MHz, MeOD-d_4) δ 27.90, 31.71, 50.50, 104.44, 111.83, 123.31, 126.20, 129.71, 142.56, 144.29, 155.52, 175.28. TOF HRMS m/z $[M]^+$ calcd for $[C_{27}H_{31}N_2]^+$ 383.2487, found 383.2474.

*2-((1E,3Z,5E)-3-Chloro-5-(1,3,3-trimethylindolin-2-ylidene)penta-1,3-dien-1-yl)-1,3,3-trimethyl-3H-indol-1-ium Iodide (**15**).* Yield 64%, mp 230−232 °C; ^{1}H NMR (400 MHz, MeOD-d_4) δ 1.76 (s, 12H), 3.71 (s, 6H), 6.435 (d, J = 12 Hz, 2H), 7.32 (t, J = 8 Hz, 2H), 7.39 (d, J = 8 Hz, 2H), 7.45 (t, J = 8 Hz, 2H), 7.54 (d, J = 8 Hz, 2H), 8.345 (d, J = 12 Hz, 2H). ^{13}C NMR (100 MHz, MeOD-d_4) δ 25.03, 29.53, 48.55, 98.93, 110.02, 121.00, 121.86, 124.55, 127.43, 140.42, 141.67, 146.72, 174.28. TOF HRMS m/z $[M]^+$ calcd for $[C_{27}H_{30}N_2Cl]^+$ 417.2098 found 417.2107.

*2-((1E,3E,5E)-3-Bromo-5-(1,3,3-trimethylindolin-2-ylidene)penta-1,3-dien-1-yl)-1,3,3-trimethyl-3H-indol-1-ium Iodide (**16**).* Yield 61%, mp 230−232 °C ; ^{1}H NMR (400 MHz, $CDCl_3$-d_1) δ 1.91 (s, 12H), 3.82 (s, 6H), 6.36 (d, J = 8 Hz, 2H), 7.16 (d, J = 8.0 Hz, 2H, 7.26−7.31 (m, 4H), 7.39−7.44 (m, 4H) 8.93 (d, J = 12 Hz, 2H). ^{13}C NMR (100 MHz, DMSO-d_6) δ 27.04, 31.98, 49.85, 102.61, 112.19, 115.98, 122.94, 125.97, 128.93, 141.78, 143.02, 149.64, 175.14. TOF HRMS m/z $[M]^+$ calcd for $[C_{27}H_{30}N_2Br]^+$ 461.1592 found 461.1585.

*5-Fluoro-2-((1E,3E,5E)-5-(5-fluoro-1,3,3-trimethylindolin-2-ylidene)penta-1,3-dien-1-yl)-1,3,3-trimethyl-3H-indol-1-ium Iodide (**17**).* Yield 78%, mp > 260 °C; ^{1}H NMR(400 MHz, DMSO-d_6) δ 1.68 (s, 12H), 3.59 (s, 6H), 6.23 (d, J = 12.0 Hz, 2H), 6.52 (s, 1H), 7.24 (s, 2H), 7.39 (s, 2H), 7.62 (s, 2H), 8.29 (s, 2H). ^{13}C NMR (100 MHz, DMSO-d_6) δ: 27.27, 31.85, 49.54, 103.64, 103.76, 110.82, 111.07, 112.43, 112.49, 112.59, 112.66, 115.15, 125.54, 139.55, 143.60, 143.69, 154.27, 154.29, 159.32, 161.72, 173.64. TOF HR-MS ESI m/z $[M]^+$ calcd for $[C_{27}H_{29}F_2N_2]^+$ 419.2299, found 419.2296.

*2-((1E,3E,5E)-3-Chloro-5-(5-fluoro-1,3,3-trimethylindolin-2-ylidene)penta-1,3-dien-1-yl)-5-fluoro-1,3,3-trimethyl-3H-indol-1-ium (**18**).* Yield 37%, mp > 260 °C; ^{1}H NMR(400 MHz, DMSO-d_6) δ: 1.72 (s, 12H), 3.67 (s, 6H), 6.26 (d, J = 14 Hz, 2H), 7.29,7.31 (t, J = 6.8 Hz, 8.8 Hz, 2H), 7.52−7.54 (m, 2H), 7.70 (d, J = 6 Hz, 2H), 8.41 (d, J = 14 Hz, 2H). ^{19}F NMR (375 MHz, DMSO-d_6) δ: −116.67 (s, 2F). TOF HR-MS ESI m/z $[M]^+$ calcd for $[C_{27}H_{29}F_2ClN_2]^+$ 453.1909 found 453.1914.

*2-((1E,3E,5E)-3-Bromo-5-(5-fluoro-1,3,3-trimethylindolin-2-ylidene)penta-1,3-dien-1-yl)-5-fluoro-1,3,3-trimethyl-3H-indol-1-ium (**19**).* Yield 52%, ^{1}H NMR(400 MHz, DMSO-d_6) δ: 1.72 (s, 12H), 3.67 (s, 6H), 6.26 (d, J = 13.2 Hz, 2H), 7.32 (t, J = 8.8 Hz, 2H), 7.55−7.52 (m, 2H), 7.70 (d, J = 7.6, 2H), 8.46 (d, J = 13.6, 2H). ^{19}F NMR (375 MHz, DMSO-d_6) δ: −116.67 (s, 2F). TOF HR-MS ESI m/z $[M]^+$ calcd $[C_{27}H_{29}F_2N_2Br]^+$ was 497.1404 found 497.1394.

*5-Chloro-2-((1E,3E,5E)-5-(5-chloro-1,3,3-trimethylindolin-2-ylidene)penta-1,3-dien-1-yl)-1,3,3-trimethyl-3H-indol-1-ium Iodide (**20**).* Yield 59%, mp > 260 °C; ^{1}H NMR(400 MHz, DMSO-d_6) δ: 1.69 (s, 12H), 3.59 (s, 6H), 6.27 (d, J = 14 Hz, 2H), 6.551 (t, J = 12.4, 12.0 Hz, 1H), 7.39 (d, J = 8.8 Hz, 2H), 7.46 (d, J = 8.4 Hz, 2H), 7.80 (s, 2H), 8.32 (t, J = 13.2 Hz, 2H). ^{13}C NMR (100 MHz, DMSO-d_6) δ: 27.30, 31.84, 49.51, 104.09, 112.87, 123.29, 126.16, 128.67, 129.50, 142.23, 143.54, 154.72, 173.65. TOF HR-MS ESI m/z $[M]^+$ calcd for $[C_{27}H_{29}Cl_2N_2]^+$ 451.1708, found 451.1722.

*5-Chloro-2-((1E,3E,5E)-3-chloro-5-(5-chloro-1,3,3-trimethylindolin-2-ylidene)penta-1,3-dien-1-yl)-1,3,3-trimethyl-3H-indol-1-ium (**21**).* Yield 53%, mp > 260 °C; ^{1}H NMR(400 MHz, DMSO-d_6) δ: 1.72 (s, 12H), 3.67 (s, 6H), 6.26 (d, J = 14 Hz, 2H), 7.52 (m, 4H), 7.89 (s, 2H), 8.43 (d, J = 13.6, 2H). ^{13}C NMR (100 MHz, DMSO-d_6) δ: 26.81, 32.15, 49.98, 100.72, 113.62, 123.06, 123.49, 128.80, 130.31, 142.02, 143.83, 147.96, 174.97. TOF HR-MS ESI m/z $[M]^+$ calcd for $[C_{27}H_{29}Cl_3N_2]^+$ 485.1318 found 485.1317.

*2-((1E,3E,5E)-3-Bromo-5-(5-chloro-1,3,3-trimethylindolin-2-ylidene)penta-1,3-dien-1-yl)-5-chloro-1,3,3-trimethyl-3H-indol-1-ium Iodide (**22**).* Yield 69%, mp 252−254 °C ^{1}H NMR(400 MHz, DMSO-d_6) δ: 1.73 (s, 12H), 3.67 (s, 6H), 6.28 (d, J = 13.2 Hz, 2H), 7.52 (m, 4H), 7.89 (s, 2H), 8.47 (d, J = 13.2 Hz, 2H). ^{13}C NMR (100 MHz, DMSO-d_6) δ: 26.79, 32.16, 50.03, 102.96, 113.65, 116.40, 123.51, 128.82, 130.35, 141.99, 143.83, 149.98, 175.15. TOF HR-MS ESI m/z $[M]^+$ calcd $[C_{27}H_{28}BrN_2Cl_2]^+$ was 529.0813 found 529.0810.

*5-Bromo-2-((1E,3E,5E)-5-(5-bromo-1,3,3-trimethylindolin-2-ylidene)penta-1,3-dien-1-yl)-1,3,3-trimethyl-3H-indol-1-ium Iodide (**23**).* Yield 62%, mp > 260 °C; ^{1}H NMR(400 MHz, DMSO-d_6) δ: 1.69 (s, 12H), 3.58 (s, 6H), 6.27 (d, J = 14 Hz, 2H), 6.56 (t, J = 12.4, 12 Hz, 1H), 7.35 (d, J = 8.4 Hz, 2H), 7.59 (d, J = 8.4, 2H), 7.93 (s, 2H), 8.33 (t, J = 13.2 Hz, 2H). ^{13}C NMR (100 MHz, DMSO-d_6) δ 27.25, 31.71, 49.48, 104.07, 113.33, 117.45, 126.09, 131.51, 142.63, 143.85, 154.86, 173.45. TOF HR-MS ESI m/z $[M]^+$ calcd for $[C_{27}H_{29}Br_2N_2]^+$ 539.0697, found 539.0695.

*5-Bromo-2-((1E,3E,5E)-5-(5-bromo-1,3,3-trimethylindolin-2-ylidene)-3-chloropenta-1,3-dien-1-yl)-1,3,3-trimethyl-3H-indol-1-ium (**24**).* Yield 72%, mp > 260 °C; ^{1}H NMR(400 MHz, DMSO-d_6) δ: 1.72 (s, 12H), 3.67 (s, 6H), 6.28 (d, J = 12.0 Hz, 2H), 7.47 (d, J = 8.0 Hz, 2H), 7.63 (d, J = 8.0 Hz, 2H), 8.01 (s, 2H), 8.43 (d, J = 12.0 Hz, 2H). ^{13}C NMR (100 MHz, DMSO-d_6) δ: 26.81, 32.17, 49.96, 100.69, 114.05, 118.37, 123.13, 126.26, 131.63, 142.40, 144.11, 147.96, 174.78. TOF HR-MS ESI m/z $[M]^+$ calcd for $[C_{27}H_{28}Br_2N_2Cl]^+$ 573.0308, found 573.0316.

*5-Bromo-2-((1E,3E,5E)-3-bromo-5-(5-bromo-1,3,3-trimethylindolin-2-ylidene)penta-1,3-dien-1-yl)-1,3,3-trimethyl-3H-indol-1-ium Iodide (**25**).* Yield 46%, mp 231−232 °C; ^{1}H NMR(400 MHz, DMSO-d_6) δ: 1.72 (s, 12H), 3.66 (s, 6H), 6.28 (d, J = 13.2 Hz, 2H), 7.47 (d, J = 8.0 Hz, 2H), 6.64 (d, J = 8.4 Hz, 2H), 8.01 (s, 2H), 8.48 (d, J = 13.6 Hz, 2H). ^{13}C NMR (100 MHz, DMSO-d_6) δ: 26.79, 32.11, 50.03, 102.97, 114.07, 116.47, 118.42, 126.27, 131.65, 142.40, 144.13, 150.03, 175.01. TOF HR-MS ESI m/z $[M]^+$ calcd $[C_{27}H_{28}Br_3N_2]^+$ was 616.9803, found 616.9814.

*1,3,3-Trimethyl-5-(trifluoromethyl)-2-((1E,3E)-5-((E)-1,3,3-trimethyl-5-(trifluoromethyl)indolin-2-ylidene)penta-1,3-dien-1-yl)-3H-indol-1-ium Iodide (**26**).* Yield 55%, mp 218−221 °C; ^{1}H NMR (400 MHz, $CDCl_3$): δ 1.81 (s, 12H), 3.79 (s, 6H), 6.53 (d, J = 13.6 Hz, 2H), 7.11 (t, J = 13.6 Hz, 1H), 7.21(d, J = 8.4 Hz, 2H), 7.60 (s, 2H), 7.70 (d, J = 7.6 Hz, 2H), 8.02 (t, J = 13.6, 2H). ^{19}FNMR: (375 MHz, DMSO-d_6): δ 62.00. TOF HRMS m/z $[M]^+$ calcd for $[C_{29}H_{29}N_2F_6]^+$ 519.2297, found 519.2393.

*2-((1E,3Z)-3-Chloro-5-((E)-1,3,3-trimethyl-5-(trifluoromethyl)-indolin-2-ylidene)penta-1,3-dien-1-yl)-1,3,3-trimethyl-5-(trifluoromethyl)-3H-indol-1-ium Iodide (**27**).* Yield 71%, mp 226−228 °C; ^{1}H NMR (400 MHz, $CDCl_3$): δ 1.91 (s, 12H), 3.87 (s, 6H), 6.47 (d, J = 13.6 Hz, 2 H), 7.30 (s, 2H), 7.65 (m, 4H), 8.90 (d, J = 10.4 Hz, 2H). ^{19}F NMR (375 MHz, DMSO-d_6): δ 62.05. TOF HRMS m/z $[M]^+$ calcd for $[C_{29}H_{28}N_2F_6Cl]^+$ 553.1840, found 553.1996.

*2-((1E,3Z)-3-Bromo-5-((E)-1,3,3-trimethyl-5-(trifluoromethyl)-indolin-2-ylidene)penta-1,3-dien-1-yl)-1,3,3-trimethyl-5-(trifluoromethyl)-3H-indol-1-ium Iodide (**28**).* Yield 71%, mp 226−228 °C; ^{1}H NMR (400 MHz, $CDCl_3$): δ 1.91 (s, 12H), 3.87 (s, 6H), 6.46 (bs, 2H), 7.30 (s, 2H), 7.69 (m, 4H), 8.91 (d, J = , 7.2 Hz, 2H). ^{19}F NMR (375 MHz, DMSO-d_6), δ: 62.01. TOF HRMS m/z $[M]^+$ calcd for $[C_{29}H_{28}N_2F_6Br]^+$ 597.1335, found 597.1597.

*5-Methoxy-2,3,3-trimethyl-3H-indole (**29**).* Yield 78%, reddish brown oil; ^{1}H NMR (400 MHz, DMSO-d_6) δ 1.17 (s, 6H), 2.16 (s, 3H), 3.68 (s, 3H), 6.74 (m, 2H), 7.38 (s,1H).

*5-Methoxy-1,2,3,3-tetramethyl-3H-indol-1-ium Iodide (**30**).* ^{1}H NMR (400 MHz, DMSO-d_6) δ 1.51 (s, 6H), 2.71 (s, 3H), 3.86 (s, 3H), 3.94 (s, 3H), 7.14 (d, J = 8.0 Hz, 1H), 7.47 (s, 1H), 7.81 (d, J = 8.0 Hz, 1H).

*5-Methoxy-2-((1E,3E,5E)-5-(5-methoxy-1,3,3-trimethylindolin-2-ylidene)penta-1,3-dien-1-yl)-1,3,3-trimethyl-3H-indol-1-ium Iodide (**31**).* Yield 75%, mp 228−230 °C; ^{1}H NMR (400 MHz, DMSO-d_6): δ 1.66 (s, 12H), 3.56 (s, 3H), 3.81 (s, 6H), 6.17 (d, J = 12 Hz, 2H), 6.46 (t, J = 12 Hz, 1H), 6.95 (d, J = 8 Hz, 2H), 7.30−7.28 (m, 4H), 8.23 (t, J = 12 Hz, 2H). ^{13}C NMR (100 MHz, DMSO-d_6): δ 26.48, 30.62, 48.45, 55.29, 102.06, 108.43, 111.02, 112.84, 123.73, 135.80, 142.15, 151.94, 156.98, 171.55. TOF HRMS m/z $[M]^+$ calcd for $[C_{29}H_{35}N_2O_2]^+$ 443.2699, found 443.2692.

*2-((1E,3E,5E)-3-Chloro-5-(5-methoxy-1,3,3-trimethylindolin-2-ylidene)penta-1,3-dien-1-yl)-5-methoxy-1,3,3-trimethyl-3H-indol-1-ium Iodide (**32**).* Yield 80%, mp 235−237 °C; ^{1}H NMR (400 MHz, MeOD-d_4) δ 1.73 (s, 12H), 3.67 (s, 6H), 3.85 (s, 6H), 6.34 (d, J = 12

DOI: 10.1021/acs.jmedchem.6b00038
J. Med. Chem. 2016, 59, 5311−5323

Hz, 2H), 6.99 (d, J = 8.0 Hz, 2H), 7.14 (s, 2H), 7.29 (d, J = 8.0 Hz, 2H), 8.23 (d, J = 12 Hz, 2H). ^{13}C NMR (100 MHz, DMSO-d_6) δ 27.05, 31.96, 49.88, 56.33, 99.74, 109.36, 112.76, 114.07, 121.81, 136.50, 143.49, 146.18, 158.51, 173.76. TOF HRMS m/z $[M]^+$ calcd for $[C_{29}H_{34}N_2O_2Cl]^+$ 477.2309; found 477.2327.

*2-((1E,3E,5E)-3-Bromo-5-(5-methoxy-1,3,3-trimethylindolin-2-ylidene)penta-1,3-dien-1-yl)-5-methoxy-1,3,3-trimethyl-3H-indol-1-ium Iodide (**33**).* Yield 55%, mp 214−216 °C; ^{1}H NMR (400 MHz, DMSO-d_6): δ 1.69 (s, 12H), 3.63 (s, 6H), 3.81 (s, 6H), 6.18 (d, J = 12 Hz, 2H), 6.97 (d, J = 8.0 Hz, 2H), 7.35 (s, 2H), 7.40 (d, J = 8 Hz, 2H), 8.38 (d, J = 12 Hz, 2H). ^{13}C NMR (100 MHz, DMSO-d_6): δ 26.20, 31.16, 49.13, 55.53, 101.20, 108.56, 112.00, 113.28, 114.41, 135.67, 142.68, 147.32, 157.72, 173.09. TOF HRMS m/z $[M]^+$ calcd for $[C_{29}H_{34}N_2O_2Br]^+$ 521.1804 found 521.1801.

*5,7,7-Trimethyl-6-((1E,3E,5Z)-5-(5,7,7-trimethyl-5H-[1,3]dioxolo[4,5-f]indol-6(7H)-ylidene)penta-1,3-dien-1-yl)-7H-[1,3]dioxolo[4,5-f]indol-5-ium Iodide (**36**).* Yield 38%, ^{1}H NMR (400 MHz, DMSO-d_6) δ: 1.63 (s, 12H), 3.54 (s, 6H), 6.06 (s, 4H), 6.18 (d, J = 16.0 Hz, 2H), 6.46 (t, J = 16.0 Hz, 1H), 7.13 (s, 2H), 7.28 (s, 2H), 8.16 (t, J = 15 Hz, 2H). ^{13}C NMR (100 MHz, DMSO-d_6) δ: 27.59, 31.89, 49.29, 94.35, 102.18, 103.40, 104.03, 125.11, 134.93, 137.52, 145.55, 148.02, 152.68, 173.32. TOF HRMS m/z $[M]^+$ calcd for $[C_{29}H_{31}O_4N_2]^+$ 471.2278 found 471.2268.

*6-((1E,3E,5E)-3-Chloro-5-(5,7,7-trimethyl-5,7-dihydro-6H-[1,3]dioxolo[4,5-f]indol-6-ylidene)penta-1,3-dien-1-yl)-5,7,7-trimethyl-7H-[1,3]dioxolo[4,5-f]indol-5-ium (**37**).* Yield 39%, ^{1}H NMR (400 MHz, DMSO-d_6) δ: 1.66 (s, 12H), 3.63 (s, 6H), 6.10 (s, 4H), 6.21 (d, J = 13.6 Hz, 2H), 7.29 (s, 2H), 7.38 (s, 2H), 8.30 (d, J = 13.6 Hz, 2H). ^{13}C NMR (100 MHz, DMSO-d_6) δ: 27.10, 32.20, 49.70, 94.92, 100.10, 102.34, 104.12, 135.49, 137.25, 146.04, 146.12, 148.10, 174.41. TOF HRMS m/z $[M]^+$ calcd for $[C_{29}H_{30}N_2O_4Cl]^+$ 505.1894 found 505.1871.

*6-((1E,3E,5E)-3-Bromo-5-(5,7,7-trimethyl-5,7-dihydro-6H-[1,3]dioxolo[4,5-f]indol-6-ylidene)penta-1,3-dien-1-yl)-5,7,7-trimethyl-7H-[1,3]dioxolo[4,5-f]indol-5-ium (**38**).* Yield 27%, ^{1}H NMR (400 MHz, DMSO-d_6) δ: 1.66 (s, 12H), 3.62 (s, 6H), 6.10 (s, 4H), 6.21 (d, J = 13.6 Hz, 2H), 7.29 (s, 2H), 7.39 (s, 2H), 8.36 (d, J = 13.6 Hz, 2H). ^{13}C NMR (100 MHz, DMSO-d_6) δ: 27.08, 32.20, 49.76, 94.94, 102.34, 104.14, 113.95, 135.50, 137.22, 146.16, 146.16, 148.02, 174.59. TOF HRMS m/z $[M]^+$ calcd for $[C_{29}H_{30}N_2O_4Br]^+$ 549.1389 found 549.1368.

■ ASSOCIATED CONTENT

Supporting Information

The Supporting Information is available free of charge on the ACS Publications website at DOI: 10.1021/acs.jmedchem.6b00038.

instrumentation, general methods, synthetic procedures, and NMR and MS spectra (PDF)

SMILES information (CSV)

■ AUTHOR INFORMATION

Corresponding Authors

*Phone: 404-413-5566. E-mail: mhenary1@gsu.edu. Fax: 404-413-5505

*Phone: 617-726-5784. E-mail: hchoi12@mgh.harvard.edu. Fax: 617-643-2604.

Author Contributions

#These authors contributed equally.

Notes

The authors declare no competing financial interest.

■ ACKNOWLEDGMENTS

This study was supported by a Georgia State University dissertation grant to E.A.O. M.H. wishes to thank the Brains and Behavior Grant, the Health Innovation Grant and the Georgia Research Alliance Grant for their financial support. H.S.C. thanks the NIH/NIBIB grant #R01-EB-011523 for their support. E.A.O. was supported through a predoctoral fellowship from the Center for Diagnostics and Therapeutics (CDT). H.H. was financially supported by Chonnam National University (2015). Thank you Andrew Levitz and Nicholas Bruschi for helping with the synthesis.

■ ABBREVIATIONS USED

NIR, near-infrared; log D, distribution coefficient; SBR, signal-to-noise ratio; DMEM, Dulbecco's modified eagle's medium; ANOVA, analysis of variance

■ REFERENCES

(1) Yokoyama, J.; Fujimaki, M.; Ohba, S.; Anzai, T.; Yoshii, R.; Ito, S.; Kojima, M.; Ikeda, K. A feasibility study of NIR fluorescent image-guided surgery in head and neck cancer based on the assessment of optimum surgical time as revealed through dynamic imaging. *OncoTargets Ther.* **2013**, *6*, 325−330.

(2) Ris, F.; Hompes, R.; Cunningham, C.; Lindsey, I.; Guy, R.; Jones, O.; George, B.; Cahill, R. A.; Mortensen, N. J. Near-infrared (NIR) perfusion angiography in minimally invasive colorectal surgery. *Surg. Endosc.* **2014**, *28*, 2221−2226.

(3) Li, C.; Cao, L.; Zhang, Y.; Yi, P.; Wang, M.; Tan, B.; Deng, Z.; Wu, D.; Wang, Q. Preoperative detection and intraoperative visualization of brain tumors for more precise surgery: a new dual-modality MRI and NIR nanoprobe. *Small* **2015**, *11*, 4517−4525.

(4) Zhu, N.; Huang, C. Y.; Mondal, S.; Gao, S.; Huang, C.; Gruev, V.; Achilefu, S.; Liang, R. Compact wearable dual-mode imaging system for real-time fluorescence image-guided surgery. *J. Biomed. Opt.* **2015**, *20*, 96010.

(5) Chan, H. H.; Siewerdsen, J. H.; Vescan, A.; Daly, M. J.; Prisman, E.; Irish, J. C. 3D rapid prototyping for otolaryngology-head and neck surgery: applications in image-guidance, surgical simulation and patient-specific modeling. *PLoS One* **2015**, *10*, e0136370.

(6) Zheng, J.; Muhanna, N.; De Souza, R.; Wada, H.; Chan, H.; Akens, M. K.; Anayama, T.; Yasufuku, K.; Serra, S.; Irish, J.; Allen, C.; Jaffray, D. A multimodal nano agent for image-guided cancer surgery. *Biomaterials* **2015**, *67*, 160−168.

(7) Ramakrishnan, V. R.; Kingdom, T. T. Does image-guided surgery reduce complications? *Otolaryngol. Clin. North Am.* **2015**, *48*, 851−859.

(8) Al-Qudah, M. Image-guided sinus surgery in sinonasal pathologies with skull base/orbital erosion. *J. Craniofac. Surg.* **2015**, *26*, 1606−1608.

(9) Xi, L.; Jiang, H. Image-guided surgery using multimodality strategy and molecular probes. *Wiley Interdiscip. Rev. Nanomed. Nanobiotechnol.* **2016**, *8*, 46−60.

(10) Njiojob, C. N.; Owens, E. A.; Narayana, L.; Hyun, H.; Choi, H. S.; Henary, M. Tailored near-infrared contrast agents for image guided surgery. *J. Med. Chem.* **2015**, *58*, 2845−2854.

(11) Hill, T. K.; Abdulahad, A.; Kelkar, S. S.; Marini, F. C.; Long, T. E.; Provenzale, J. M.; Mohs, A. M. Indocyanine green-loaded nanoparticles for image-guided tumor surgery. *Bioconjugate Chem.* **2015**, *26*, 294−303.

(12) Liang, C. H.; Di, W. Y.; Ren, J. P.; Zhou, F. M.; Hu, Y.; Mao, H. J.; Han, D. M. Imaging, clinical and pathological features of salivary gland adenolymphoma. *Eur. Rev. Med. Pharmacol. Sci.* **2014**, *18*, 3638−3644.

(13) Santhanam, P.; Oakley, C. Pet imaging of the adrenal gland-utility and pitfalls. *Endocr. Pract.* **2014**, *20*, 375−377.

(14) Sumi, M.; Van Cauteren, M.; Sumi, T.; Obara, M.; Ichikawa, Y.; Nakamura, T. Salivary gland tumors: use of intravoxel incoherent motion MR imaging for assessment of diffusion and perfusion for the differentiation of benign from malignant tumors. *Radiology* **2012**, *263*, 770−777.

DOI: 10.1021/acs.jmedchem.6b00038
J. Med. Chem. 2016, 59, 5311−5323

(15) Hyun, H.; Park, M. H.; Owens, E. A.; Wada, H.; Henary, M.; Handgraaf, H. J.; Vahrmeijer, A. L.; Frangioni, J. V.; Choi, H. S. Structure-inherent targeting of near-infrared fluorophores for parathyroid and thyroid gland imaging. *Nat. Med.* **2015**, *21*, 192−197.
(16) Owens, E. A.; Hyun, H.; Tawney, J. G.; Choi, H. S.; Henary, M. Correlating molecular character of NIR imaging agents with tissue-specific uptake. *J. Med. Chem.* **2015**, *58*, 4348−4356.
(17) Owens, E. A.; Lee, S.; Choi, J.; Henary, M.; Choi, H. S. NIR fluorescent small molecules for intraoperative imaging. *Wiley Interdiscip. Rev. Nanomed. Nanobiotechnol.* **2015**, *7*, 828−838.
(18) Wada, H.; Hyun, H.; Vargas, C.; Gravier, J.; Park, G.; Gioux, S.; Frangioni, J. V.; Henary, M.; Choi, H. S. Pancreas-targeted NIR fluorophores for dual-channel image-guided abdominal surgery. *Theranostics* **2015**, *5*, 1−11.
(19) Salim, M. M.; Owens, E. A.; Gao, T.; Lee, J. H.; Hyun, H.; Choi, H. S.; Henary, M. Hydroxylated near-infrared BODIPY fluorophores as intracellular pH sensors. *Analyst* **2014**, *139*, 4862−4873.
(20) Park, M. H.; Hyun, H.; Ashitate, Y.; Wada, H.; Park, G.; Lee, J. H.; Njiojob, C.; Henary, M.; Frangioni, J. V.; Choi, H. S. Prototype nerve-specific near-infrared fluorophores. *Theranostics* **2014**, *4*, 823−833.
(21) Choi, H. S.; Nasr, K.; Alyabyev, S.; Feith, D.; Lee, J. H.; Kim, S. H.; Ashitate, Y.; Hyun, H.; Patonay, G.; Strekowski, L.; Henary, M.; Frangioni, J. V. Synthesis and in vivo fate of zwitterionic near-infrared fluorophores. *Angew. Chem., Int. Ed.* **2011**, *50*, 6258−6263.
(22) Choi, H. S.; Gibbs, S. L.; Lee, J. H.; Kim, S. H.; Ashitate, Y.; Liu, F.; Hyun, H.; Park, G.; Xie, Y.; Bae, S.; Henary, M.; Frangioni, J. V. Targeted zwitterionic near-infrared fluorophores for improved optical imaging. *Nat. Biotechnol.* **2013**, *31*, 148−153.
(23) Ashitate, Y.; Kim, S. H.; Tanaka, E.; Henary, M.; Choi, H. S.; Frangioni, J. V.; Flaumenhaft, R. Two-wavelength near-infrared fluorescence for the quantitation of drug antiplatelet effects in large animal model systems. *J. Vasc. Surg.* **2012**, *56*, 171−180.
(24) Hyun, H.; Owens, E. A.; Wada, H.; Levitz, A.; Park, G.; Park, M. H.; Frangioni, J. V.; Henary, M.; Choi, H. S. Cartilage-specific near-infrared fluorophores for biomedical imaging. *Angew. Chem., Int. Ed.* **2015**, *54*, 8648−8652.
(25) Wada, H.; Hyun, H.; Vargas, C.; Genega, E. M.; Gravier, J.; Gioux, S.; Frangioni, J. V.; Choi, H. S. Sentinel Lymph Node Mapping of Liver. *Ann. Surg. Oncol.* **2015**, *22*, 1147−1155.
(26) Hyun, H.; Wada, H.; Bao, K.; Gravier, J.; Yadav, Y.; Laramie, M.; Henary, M.; Frangioni, J. V.; Choi, H. S. Phosphonated near-infrared fluorophores for biomedical imaging of bone. *Angew. Chem., Int. Ed.* **2014**, *53*, 10668−10672.
(27) Ashitate, Y.; Hyun, H.; Kim, S. H.; Lee, J. H.; Henary, M.; Frangioni, J. V.; Choi, H. S. Simultaneous mapping of pan and sentinel lymph nodes for real-time image-guided surgery. *Theranostics* **2014**, *4*, 693−700.

DOI: 10.1021/acs.jmedchem.6b00038
J. Med. Chem. 2016, 59, 5311−5323

2.4 Synthesis and Optical Properties of Asymmetric Pentamethine Cyanine Dyes

Based on the results in the previous section, fluorophores that feature varying numbers of fluorine atoms were synthesized and studied to determine viability for endocrine tissue imaging. This was done by designing asymmetric pentamethine carbocyanine dyes with fluorine atoms and trifluoromethyl groups at the 5-position on the indolenine heterocycles. After research into the synthetic route,[61] it was discovered that modified reaction conditions would have to be developed. After purification of the dyes, optical property studies in two solvents were performed and the data was analyzed before animal data was sent for.

2.4.1 Introduction

As the utility of polymethine cyanine dyes grows spanning several fields, tracers and *in vivo* optical imaging labels,[62, 7,63] solar cells,[64, 65] and medicinal compounds,[66,67] the understanding between the chemical structure of these molecules and their optical performances must keep up for the improving development of the dyes. This family of dyes has been extensively researched due to its reasonable ease of synthetic modification, highly favorable optical properties for *in vivo* application, and low toxicity in the body.[68] The cyanine dye class of dye consists of two nitrogen containing heterocycles with an elongated positively charged polymethine bridge. These compounds differ from other classes of dyes, such as BODIPY, fluorescein, ect., by the range at which the compounds optically operate in: the near-infrared region. This region lies between 650 nm and 900 nm and is very beneficial for *in vivo* imaging as there is a good signal to background ratio compared to auto fluorescence body tissue and the dyes. They are beneficial for solar cell utilization due to their third-order optical nonlinearity and fast response time.[69] Based on currently available literature, most of the cyanine dyes being published and studied are symmetrical.[70] The

symmetric synthetic route is simple and better understood than the asymmetric one. Asymmetric routes have been explored using a variety of heterocycles for monomethine and trimethine dyes, but when analyzing routes for pentamethine dyes, fewer literature examples exist.[61] The synthetic route for symmetric cyanine dyes is quite robust and proceeds with little solvent for a several hundred milligram scale reaction as well as low heat and relatively little work up. The reactions are relatively clean and if properly stoichiometrically measured, two molar equivalents of indolium added to one molar equivalent of malonaldehyde bis-phenyl amine hydrochloride "linker", the reaction gives relatively high yield and favorable optical and *in vivo* properties, almost eliminating the need to study their asymmetric counterparts. Asymmetric dyes have rarely been studied and their optical properties seem to be unreported in literature. In this study, we synthesized and optically characterized several asymmetric pentamethine cyanine to and compare their properties with that of the previously published symmetrical analogs. The symmetric analogs were published previously by our lab and studied in mouse models for the imaging of the endocrine system.[63]

2.5 Results and Discussion

2.5.1 Synthesis

Scheme 5 shows the synthetic route to obtain new asymmetric dyes. Commercially available phenyl hydrazines **1**, **4** and **5** were added to clean, dry round bottom flasks in acetic acid and 3-methyl-2-butanone and heated to reflux for 72 h. After a basic workup using sodium bicarbonate, the resulting indoles **2**, **6**, and **7** were stirred in minimal (>8 mL) acetonitrile with methyl iodide in a sealed tube for 24 h. To synthesize the dyes **10 a-f**, compound **3** and 1 molar equivalent of sodium acetate were allowed to react at room temperature for 10 min before substituted malonaldehyde bis-phenyl amines were added to the reaction and heated to 30 ^{o}C. The

second indole terminal unit, **8** or **9**, and another equivalent of base were added upon observing a peak at ~650 nm on a UV-Vis spectrum. This was subsequently heated to reflux and allowed to react until completion. All reactions were monitored via TLC using dichloromethane/methanol (1%) as eluent. The dyes were extracted using DCM and washed 5 times with DI water. The organic layer was dried using magnesium sulfate, filtered and the solvent was evaporated off before the crystals were dried under vacuum for 24 h. The dyes were purified by washing the crystals with 25 mL of diethyl ether and 25 mL of hexanes before drying again under vacuum. The route to obtain the symmetrical dyes is published by Henary *et. al.* in 2016. [63]

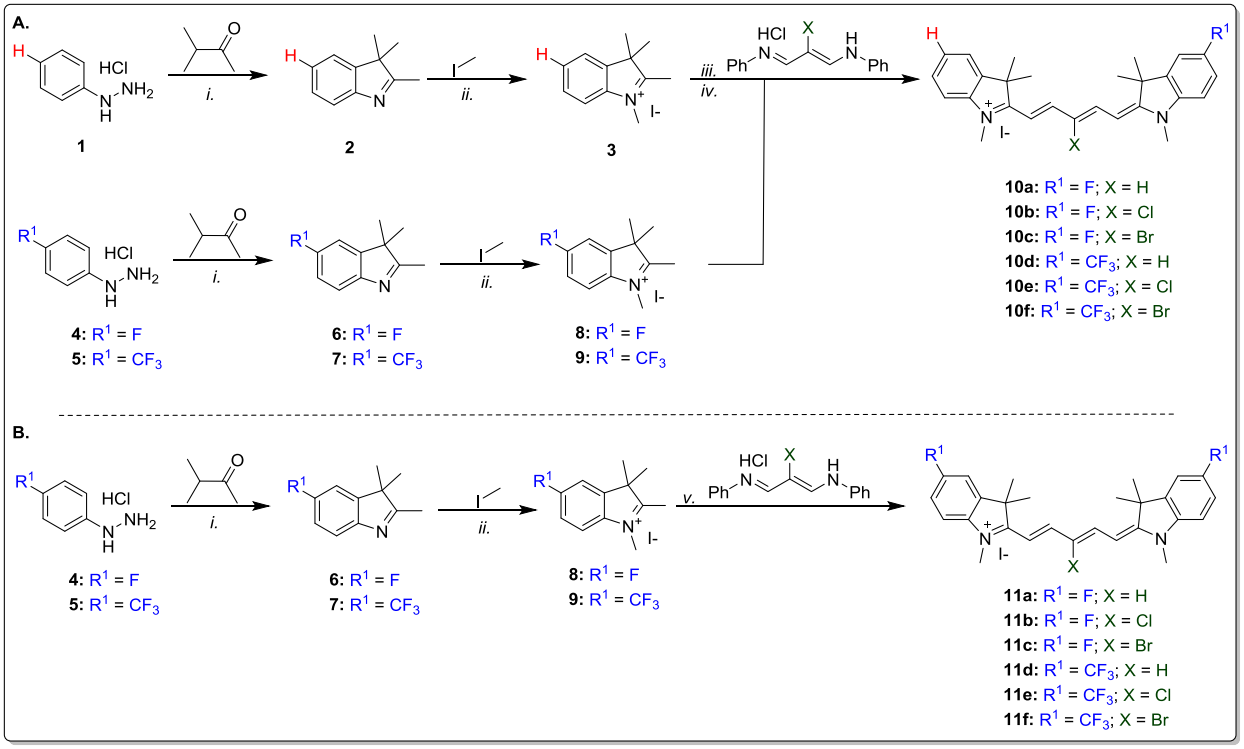

Scheme 3. Synthetic routes taken to obtain symmetrical (A.) and unsymmetrical pentamethine cyanine dyes (B.). i. acetic acid (25mL), reflux, 72hr; ii. acetonitrile, reflux, 24hr; iii. sodium acetate, acetic anhydride, RT, 20min; iv. sodium acetate, acetic anhydride, 60 °C, 20 min; sodium acetate, acetic anhydride, 60 °C, 30 min.

2.5.2 Optical Properties Study

The optical properties of the symmetric versions of these dyes (**11 a-f**) have been previously published by our group in 2015 and 2016.[7,63] Table 1 highlights the differences between the asymmetric fluorophores (**10 a-c**) and fluorinated symmetrical fluorophores (**11 a-c**). Firstly, when analyzing the fluorinated asymmetric dyes, we notice 2.7, 3.9, and 3.9-fold decrease in extinction coefficient respectively, compared to the corresponding symmetric dyes with H, Cl, and Br at the gamma-carbon. We attribute this to the uneven distribution of electrons across the conjugated system. When the compounds have symmetric electronic effects stemming from both sides of the "push-π-pull" system, a very high molar attenuation coefficient is observed. However, when one side features a highly electron withdrawing group, such as fluorine atom or a trifluoromethyl group, we hypothesize that the withdrawing effect localizes the electrons at the nitrogen on the corresponding indole more than the equal sharing across the system seen in symmetric dyes, dimming the absorption attenuation. Looking at the overall trends in the novel asymmetric compounds compared to the symmetrical dyes, the molar attenuation coefficient shows an unusual trend when analyzing them in the two solvents. In ethanol, an organic polar protic solvent, the value decreases as the molecular weight increases with hydrogen, chlorine, and bromine being added at the meso position on the polymethine bridge. However when looking at the pattern in aqueous solvent, phosphate buffer, we observe the opposite to this trend but only in the asymmetric fluorophores. Again looking at an organic solvent, the quantum yield values when comparing the two sets of dyes are not that dissimilar and follow a similar pattern, decreasing with increasing halogen size, however, when analyzing the molecular brightness values (MB = ε x Φ), the unsymmetrical dyes do not seem to be ideal candidates for *in vivo* imaging studies. The

extinction coefficients remain very low in comparison to the symmetrical dyes and we expect then a low signal to background ratio (SBR). As previously published by our group,[7,63] the symmetric dyes have application in the imaging of endocrine system tissues and the signal to background ratio is very high. Predictably with the lower molecular brightness values exhibited by the asymmetric dyes, this value would be significantly lower (~35-80%) than the least bright symmetrical analog. In aqueous media, the quantum yield of the compounds seems somewhat pliable to gamma carbon substitution as the chlorine atom on the bridge increases the quantum yield. The bromine atom, a much larger atom, lowers the quantum yield again, presumably due to the heavy atom affect.

The asymmetric trifluoromethyl compounds (**10 d-f**) mimic the patterns of the symmetrical analogs (**11 d-f**). The quantum yield values are highest with the unsubstituted gamma carbon on the bridge with the chlorine-substituted molecule having the lowest, in ethanol. The molecular brightness trends downwards still moving from lowest molecular weight to highest as expected due to the heavy atom effect. There is an interesting observation in regards to the absorbance and emission maxima: there is a 6 nm greater red shift observed in the asymmetric pentamethine cyanine dyes to the symmetric equivalents. This is due to the energy of the symmetric vs asymmetric compounds. The calculated HOMO and LUMO energies, seen in Table 7, are more negative, about 0.2 eV, in the symmetrical fluorophores than the asymmetric, and although the energy gap between the two stay pretty consistent when transitioning from one comparable molecule to the other, these energy differences contributes to the difference in wavelength maxima of both the absorption and fluorescence spectra. As for efficacy for *in vivo* imaging purposes of these asymmetric dyes, their molecular brightness' discourages us from using them for animal

studies; because the molecular brightness of the dyes is so low, the SBR of the dyes would also be very low and the quantum yield values makes these dyes poor candidates for these studies. Whereas there is a significant drop-off in molar attenuation in the mono fluoro-substituted dyes, **10 a-f**, the only dye that shows this major decrease is the gamma chloro-substituted molecule **10 b** (2.8 fold). The major difference with this set is the quantum yield values, again which we hypothesize to be from the asymmetric nature of the compounds and the unequal resonance sharing through the molecule dye to the highly electron withdrawing nature of the trifluoromethyl group.

*Table 3. A comparison of symmetrical and unsymmetrical pentamethine cyanine dyes **11 a-c** and **10 a-c**. The novel dyes optical properties were performed in polar protic and aqueous solvents*

ID	λ_{abs} (nm)		Extinction Coefficient (e, $M^{-1}cm^{-1}$)		λ_{em} (nm)		Stokes Shift		QY (Φ, F, %)		MB (e x F)	
	EtOH	**PBS**	**EtOH**	**PBS**	**EtOH**	**PBS**	**EtOH**	**PBS**	**EtOH**	**PBS**	**EtOH**	**PBS**
11a	641	638	225,800	196,500	663	662	22	24	31.6	35.2	71,352	69,168
11b	643	638	233,700	193,400	658	660	15	22	16.5	15.9	38,561	30,750
11c	641	635	210,500	170,900	658	658	17	23	16.3	11.9	34,312	20,337
10a	641	637	83,900	47,300	661	657	20	20	31.0	17.5	26,009	8,278
10b	643	637	67,600	54,000	657	655	20	18	14.7	20.3	9,937	10,962
10c	640	634	54,200	60,700	655	655	15	21	13.2	8.2	7,154	4,977

When the compound is symmetrical, we expect equal push-π-pull throughout the molecule, however when we substitute only one of the 5-H with trifluoro-methyl, this group is pulling the electrons to one side of the molecule more than an even sharing. One way to determine this would be to measure the bond lengths of each bond throughout the conjugated system through to the trifluoro-methyl and the 5-H by x-ray crystallography.[71] All these values and comparisons can be seen in tables 3 and 4. Table 3 highlights the symmetrical fluorine substituted dyes (**11 a-c**) and their asymmetric counterparts (**10 a-c**), while table 4 compares the trifluoromethyl substituted symmetrical compounds (**11 d-f**) and the asymmetric dyes (**10 d-f**).

*Table 4. A comparison of symmetrical and asymmetric pentamethine cyanine dyes **11 d-f** and **10 d-f**. The novel dyes optical properties were performed in polar protic and aqueous solvents.*

ID	λ_{abs} (nm)		Extinction Coefficient (e, $M^{-1}cm^{-1}$)		λ_{em} (nm)		Stokes Shift		QY (Φ, F, %)		MB (e x F)	
	EtOH	**PBS**	**EtOH**	**PBS**	**EtOH**	**PBS**	**EtOH**	**PBS**	**EtOH**	**PBS**	**EtOH**	**PBS**
11d	638	636	45,200	27,700	656	657	18	21	58.7	50.3	26,532	13,933
11e	640	638	114,900	56,300	656	655	18	17	20.5	19.8	23,555	11,147
11f	638	635	49,700	19,500	653	651	15	18	21.1	29.0	10,487	5,655
10d	644	640	42,300	37,800	668	663	24	23	17.7	8.5	7,487	3,213
10e	640	637	52,200	98,000	664	655	24	18	5.9	2.6	3,080	2,548
10f	638	633	34,500	62,200	657	653	19	20	6.1	1.2	2,105	746.4

2.5.3 Physicochemical

Because of the low extinction coeffiencioents of compounds **10 a-f**, it was deemed necessary to perform physicochemical calculations to learn more about the factors that could contribute to these properties. Calculations of physicochemical properties were performed, seen in table 5, to shed some light theoretically about the experimental values obtained through spectroscopic experiments (Table 5).

Table 5. The HOMO/LUMO levels and energy calculated using Spartan '14.

ID	HOMO (eV)	LUMO (eV)	Gap (eV)	Energy
10a	-7.66	-5.51	2.15	-1256.06304
10b	-7.74	-5.65	2.09	-1715.65644
10c	-7.76	-5.66	2.10	-3829.34039
10d	-7.83	-5.61	2.22	-1493.87495
10e	-7.92	-5.79	2.13	-1953.45877
10f	-7.94	-5.80	2.14	-4067.19095
11a	-7.67	-5.52	2.15	-1355.34811
11b	-7.76	-5.7	2.06	-1814.93379
11c	-7.75	-5.64	2.11	-3928.57750
11d	-8.04	-5.8	2.24	-1830.90760
11e	-8.13	-5.98	2.15	-2290.49132
11f	-8.12	-5.92	2.20	-4404.17635

It may seem odd when analyzing the absorbance maxima values for the asymmetric and symmetric dyes that the gamma substituted chlorine compounds have the highest wavelength and

that they do not follow a particular pattern. However when looking at the theoretical HOMO/LUMO gaps, it is seen that these compounds have the lower gap, which corresponds to a higher wavelength since the energy difference and wavelength are inversely proportional according to the energy equation $E = hc/\lambda$. This is consistent through the symmetric and asymmetric fluorophores.

With the asymmetric fluorine compounds, **10 a-c**, there are very few differences in the theoretical electron clouds shown in Figure 27. However, when looking at the trifluoromethyl groups, there are far greater electron withdrawing inductive and resonance effects by the group on the overall molecule. This is visualized by the pear shaped nature of the electron cloud on the HOMO visualization in Figure 27. The electron cloud about the central carbon exhibit a shape that indicates that the trifluoromethyl group is pulling the electrons towards one end of the molecule more than the other. With the symmetrical compounds, **11 a-f**, the clouds that are calculated through Spartan '14 show a symmetrical shape which indicates that, as hypothesized, the electrons will move freely across the conjugated system. But since there is a strong pull from one side of the molecule in **10 d-f**, there is weird shaping of the clouds and it is hypothesized that this unevenness of the conjugation may be a cause for the lower molar absorbance by the molecules.

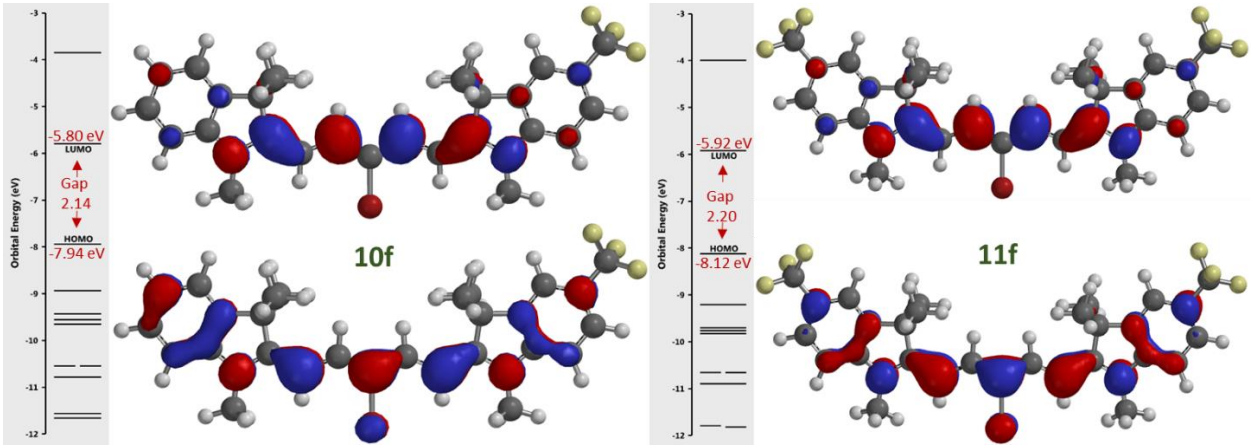

*Figure 27. HOMO/LUMO calculations of compounds **10f** and **11f**. Both the energy gap and the energy levels differ significantly between the symmetric and asymmetric compounds.*

2.5.4 Conclusion

After performing optical property studies and photophysical calculations, a brighter light has been shed on the synthesis and optical efficiencies of a select set of pentamethine cyanine dyes with the potential for application in *in vivo* imaging. In addition to requiring a more complicated synthetic route and purification method, the asymmetric dyes presented displayed significantly lower molar attenuation coefficients, and comparable quantum yield values in organic solvents, which leads to being overall less bright than their symmetrical counterparts. Although this study is not necessarily indicative of all pentamethine cyanine dyes, the hypothesis can be made that having a highly electron withdrawing group at the 5-position of one of the heterocyclic end units may not enhance optical properties for *in vivo* applications due to the heavy withdrawing nature of the fluorine functional groups at this position and its resonance effect on the molecule itself. Future studies will include electron donating atoms at this position as well has complimenting an electron donor atom with an electron withdrawing atom to observe the effects of a, in theory, more activated push-π-pull system. Through these studies, it can be concluded that asymmetric

carbocyanine dyes featuring highly electron withdrawing groups on this specific heterocycle are not worth studying for the use as *in vivo* contrast agents.

2.5.5 Experimental Details

2.5.5.1 Synthesis of Pentamethine Cyanine Analogs

The chemical reagents used in the synthesis of these compounds were obtained from Acros Organics, Alfa Aesar, Matrix Scientific, and Sigma-Aldrich. The reactions were followed using silica gel 60 F_{254} thin-layer chromatography plates (Merck EMD Millipore, Darmstadt, Germany). Open column chromatography was utilized for the purification of all final compounds using 60–200 μm, 60A, classic column silica gel (Dynamic Adsorbents, Norcross, GA). The ^{1}H NMR and ^{13}C NMR spectra were obtained using high-quality Kontes NMR tubes (Kimble Chase, Vineland, NJ) rated to 500 MHz and were recorded on a Bruker Avance (400 MHz) spectrometer using DMSO-d_6 or MeOD-d_4 containing tetramethylsilane (TMS) as an internal calibration standard set to 0.0 ppm. UV–vis/NIR absorption spectra were recorded on a Varian Cary 50 spectrophotometer.

2.5.5.2 Optical Physicochemical Property Analyses

All optical measurements were performed in various solvents, including ethanol and phosphate buffered saline (PBS, pH 7.4), and at 37 °C in 100% FBS buffered with 50 mM HEPES, pH 7.4. Absorbance and fluorescence emission spectra of the series of NIR fluorophores were measured using Varian Cary 50 absorbance spectrophotometer (190–1100 nm) and Shimadzu RF-5301PC spectrofluorometer (350–1000 nm). For fluorescence quantum yield (QY) measurements, rhodamine 800 in absolute ethanol (QY = 28%) was used as a calibration standard, under conditions of matched absorbance at 620 nm. In silico calculations of physicochemical distribution coefficient (log *D* at pH 7.4) was calculated using Marvin and JChem calculator plugins

(ChemAxon, Budapest, Hungary). Electrostatic maps were calculated using Spartan DFT calculations at the B3LYP level.

2.5.5.3 Photostability Analysis

The photostability experiments were performed to determine the photobleaching threshold of the fluorophores. We determined the photobleaching rate by measuring the decrease in absorbance at the wavelength of maximum absorption over a 48 h time period. The light condition involved a glass cell containing individual contrast agent (0.01 mm in methanol) that was affixed 250 mm away from a 15W F15T8 broad spectrum bulb being irradiated using a portable lamp at room temperature. The dark control was also examined to exclude chemical decomposition phenomena. The absorbance values were measured at various time points and then plotted versus time to obtain the photostability graphs in light and dark.

2.5.5.4 Synthesis and Characterization of NIR Fluorophores

Dyes **11a-f** were previously reported by Henary *et al*.[1b] Phenyl hydrazines **1**, **4** and **5** were commercially obtained. They were added to 3 mol. equivalents of 3-methyl-2-butanone in 35 mL of acetic acid and let to react at reflux for 72 h. The resulting indoles (**2**, **6** and **7**), after basic workup with sodium bicarbonate, were reacted with 1.1 mol. equivalent of iodomethane at reflux for 24 h to result in indolenine salts **3**, **8** and **9**. To obtain the final dyes **10 a-f**, compound **3** was added to a clean, dry round-bottom flask. It was stirred in 5 mL of acetic anhydride, and 1 mol. equivalent of sodium acetate along with 1 mol. equivalents of individual malondaldehyde linker. The reaction was allowed to stir at RT for 15 min, wherein the reaction was monitored closely by UV-Vis for the disappearance of the starting material peak (~400 nm) and the production of the half dye (~550 nm). Once all of the starting material was consumed, the other end unit, either **8** or

9, is added to the reaction with another equivalent of base and 5 mL acetic anhydride. The reaction is then let to complete at 60 ^{o}C for 20 minutes. The reactions were monitored closely using regular phase thin-layer chromatography with a mobile phase of DCM/MeOH (99:1) as well as UV–vis-NIR spectrophotometer in quartz cuvettes with methanol as a solvent to visualize the dye absorption band at ~650 nm. Upon completion of the reaction, the reaction mixtures were allowed to cool, and the solvent was evaporated. The residue was extracted using DCM and was washed with DI water (3 × 70 mL). The resulting organic layer was dried under magnesium sulfate, gravity filtered, and evaporated to afford crystals that were washed with diethyl ether (2 × 50 mL) and hexanes (50 mL) to yield crystals that were dried under vacuum overnight. The pure product was obtained after dissolving in methanol and precipitating with ether several times, or the compounds were isolated using flash column chromatography and a gradient of 100% DCM to 5% methanol in DCM was used as the eluting solvent. After purification, the compounds were obtained in the designated yields and were fully characterized.

5-fluoro-1,3,3-trimethyl-2-((1E,3E)-5-((E)-1,3,3-trimethylindolin-2-ylidene)penta-1,3-dien-1-yl)-3H-indol-1-ium iodide (**10a**). Yield 36%, mp > 260 ^{o}C; ^{1}H NMR (400 MHz, DMSO-d_6) **σ**: 1.938 (s, 12h), 3.876 (d, *J* = 6.4 Hz, 6H), 6.478 (m, *J* = 14 Hz, 6 Hz, 13.6 Hz, 2H), 7.018 (t, *J* = 12.4 Hz, 11.6 Hz, 1H), 7.262 (s, 1H), 7.299 (d, *J* = 7.6 Hz, 2H), 7.458 (m, *J* = 7.2 Hz, 7.2 Hz, 10 Hz, 2H), 7.559 (t, *J* = 8.8 Hz, 8 Hz, 2H), 8.403 (m, *J* = 12.4 Hz, 12.4 Hz, 12.4 Hz, 2H). ^{13}C NMR (100 MHz, DMSO-d_6) **σ**: 28.00, 32.48, 32.74, 49.46, 76.74, 77.06, 77.38, 103.89, 104.16, 110.15, 110.40, 110.49, 111.19, 111.27, 115.10, 115.35, 122.24, 125.27, 126.59, 128.62, 138.84, 141.08, 142.70, 153.61, 154.09, 159.52, 173.06, 173.75.

2-((1E,3Z)-3-chloro-5-((E)-1,3,3-trimethylindolin-2-ylidene)penta-1,3-dien-1-yl)-5-fluoro-1,3,3-trimethyl-3H-indol-1-ium iodide (**10b**). Yield 31%, mp > 260 ºC; ^{1}H NMR (400 MHz, DMSO-d_6) **σ**: 1.722 (s, 12H), 3.675 (d, *J* = 5.6 Hz, 6H), 6.277 (t, *J* = 14.4 Hz, 15.6 Hz, 2H), 7.319 (d, *J* = 7.6 Hz, 2H), 7.499 (m, *J* = 19.6 Hz, 7.22 Hz, 3H), 7.686 (s, 2H), 8.425 (t, *J* = 12 Hz, 9.2 Hz, 2H). ^{13}C NMR (100 MHz, DMSO-d_6) **σ**: 26.88, 32.00, 49.79, 100.35, 110.94, 111.20, 112.16, 113.35, 115.37, 115.62, 122.59.22.92, 125.98, 128.93, 139.35, 141.77, 143.04, 143.95, 144.03, 147.53, 147.65, 159.76, 162.17, 147.95, 175.02.

2-((1E,3Z)-3-bromo-5-((E)-1,3,3-trimethylindolin-2-ylidene)penta-1,3-dien-1-yl)-5-fluoro-1,3,3-trimethyl-3H-indol-1-ium iodide (**10c**). Yield 16%, mp > 260 ºC; ^{1}H NMR (400 MHz, DMSO-d_6) **σ**: 1.724 (s, 12H), 3.676 (s, 6H), 6.277 (t, *J* = 14 Hz, 15.6 Hz, 2H), 7.321 (d, *J* = 7.6 Hz, 2H), 7.468 (d, *J* = 6.8 Hz, 1H), 7.527 (s, 2H), 7.698 (s, 2H), 8.479 (d, *J* = 11.2 Hz, 2H). ^{13}C NMR (100 MHz, DMSO-d_6) **σ**: 21.54, 26.84, 32.03, 49.87, 55.42, 102.59, 110.98, 112.22, 113.39, 115.37, 119.42, 122.95, 126.00, 128.91, 129.09, 129.75, 139.31, 141.79, 143.00, 143.94, 149.52, 159.78, 162.18, 172.46, 175.13.

1,3,3-trimethyl-5-(trifluoromethyl)-2-((1E,3E)-5-((E)-1,3,3-trimethylindolin-2-ylidene)penta-1,3-dien-1-yl)-3H-indol-1-ium iodide (**10d**). Yield 29%, mp > 260 ºC; ^{1}H NMR (400 MHz, DMSO-d_6) **σ**: 1.714 (s, 12H), 3.622 (q, 3.622, *J* = 26.4, 46.4 Hz, 6H), 6.210 (q, *J* = 13.6, 25.2, 13.6 Hz, 1H, 6.560 (m, *J* = 14.4, 13.6, 8.8, 12, 12.4 Hz, 2H), 7.495 (m, 6H), 7.593 (s, 1H), 8.326 (m, *J* = 13.6 Hz, 2H); ^{13}C NMR (100 MHz, DMSO-d_6) **σ**:

2-((1E,3Z)-3-chloro-5-((E)-1,3,3-trimethylindolin-2-ylidene)penta-1,3-dien-1-yl)-1,3,3-trimethyl-5-(trifluoromethyl)-3H-indol-1-ium iodide (**10e**). Yield 18%, mp > 260 ºC; ^{1}H NMR (400 MHz, DMSO-d_6) **σ**: 1.776 (d, *J* = 10 Hz, 12H), 3.729 (t, *J* = 24, 45.2 Hz, 6H), 6.441 (d, *J* =

13.6 Hz, 2H), 7.324 (t, *J* = 7.2, 7.2 Hz, 1H), 7.430 (q, *J* = 14, 9.2, 8, 7.2 Hz, 3H), 7.536 (m, *J* = 4.4, 5.2, 7.6 Hz, 2H), 7.815 (s, 1H), 8.388 (d, *J* = 13.6 Hz, 2H). ^{13}C NMR (100 MHz, DMSO-d_6)

2-((1E,3Z)-3-bromo-5-((E)-1,3,3-trimethylindolin-2-ylidene)penta-1,3-dien-1-yl)-1,3,3-trimethyl-5-(trifluoromethyl)-3H-indol-1-ium iodide (**10f**). Yield 11%, mp > 260 ºC; ^{1}H NMR (400 MHz, DMSO-d¬6) σ: 1.741 (s, 12H), 3.688 (m, *J* = 24.4 Hz, 40.4 Hz, 6H), 6.318 (m, *J* = 13.2 Hz, 20 Hz, 12.8 Hz, 54.4 Hz, 6.4 Hz, 35.6 Hz, 2H), 7.524 (m, *J* = 7.2 Hz, 26.8 Hz, 9.6 Hz, 9.2 Hz, 7.6 Hz, 6.4 Hz, 7.2 Hz, 7.6 Hz, 16.4 Hz, 8 Hz, 15.6 Hz, 7.2 Hz, 13.6 Hz, 7.6 Hz, 19.2 Hz, 7.6 Hz, 7H), 8.525 (m, *J* = 8.8 Hz, 4.8Hz, 7.6 Hz, 13.2 Hz, 2H). ^{13}C NMR (100 MHz, DMSO-d_6)

2.6 Synthesis and Optical Properties of Near-Infrared Pentamethine Dyes with N-Substituted Pentanoic Acid Groups

The studies performed in the following section revolved around pentanoic acid groups. The use of these groups on imaging agents such as cyanine dyes can present researchers with unique opportunities to utilize the fluorescent nature of the dyes. The acid group can act as a handle for other ligands: for tissue targeting, for drug delivery, or for metal chelating. Therefore, studies on the fluorophores themselves should be performed to evaluate the imaging agents effectiveness as fluorophores regardless of its ligand handles. The dyes were synthesized, characterized and then optical properties were done to discover the optical efficacy of the pentamethine cyanine dyes. After the optical studies were performed, physicochemical properties were calculated to find out more about the compounds.

2.6.1 Synthesis and Purification of Pentamethine Dyes

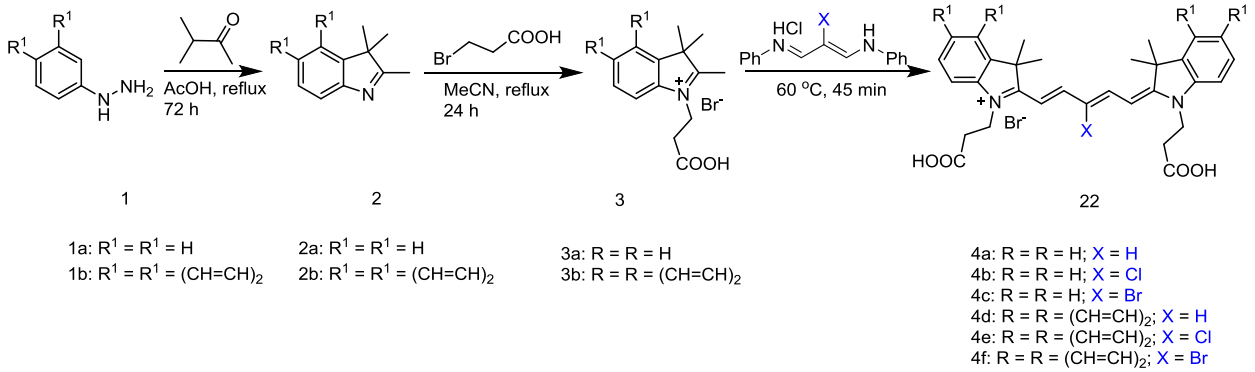

*Scheme 4. The synthetic route used to obtain compounds **4 a-f** from the starting material phenyl hydrazines **1**.*

The final dyes were synthesized starting with para-substituted halogenated phenyl hydrazines. The hydrazines were reacted with 3-methyl-2-butanone in acetic acid at reflux for 72 h to afford indole **2a** or benz[e] indole **2b**. This reaction proceeds through a 3, 3-sigmatropic rearrangement reaction to form the heterocycle. After a basic workup where the products were extracted using dichloromethane (DCM) and sodium bicarbonate to neutralize the acetic acid, the indolenines were then reacted with 3-bromopentanoic acid in acetonitrile at reflux for 24 hours. This led to the formation of indolenine salts **3a-b** through an S_N2 reaction mechanism. No workup was needed and the crude material was used in the next step of the reaction. Reacting salts **3a-b** with unsubstituted or halogenated malonaldehyde bisphenyl amines in a 2:1 molar ratio in acetic anhydride at 60 ^oC for 45 min, the formation of dyes **4a-f** occurred. The formation of the fluorophores were monitored using regular phase thin layer chromatography with a mobile phase of 100% DCM as well as by UV-Vis. The reaction mixtures were allowed to cool, dissolved in DCM and then washed six times with 1M HCL. The water was dried using sodium sulfate and the

organic layer was then gravity filtered and the solvent was evaporated off. The purification of the dyes started with a regular phase open tubular column. After using a mobile phase of 97:3 DCM: methanol, it was found through H^1 NMR and mass spectrometry that there was formation of the mono-ester as well as the di-ester along with the di-acid. Due to the added acidity from the silica column, the methanol was able to convert some of the acid groups to methyl esters. A different method of purification had to be used since the groups were converting on the column due to the methanol but the dye would not move on the column without the methanol.

Since column chromatography could not be used to purify the compounds, and fast recrystallization did not show improved purity, another route had to be explored. A slow recrystallization method called solvent vapor transfer was used. The compound was dissolved in DCM and placed in a small vial; then, the vial was placed in a larger jar with diethyl ether and the lid was secured. The jar was then left untouched for 10 days while the vapors exchange and the crystals grow slowly over the 10 days as opposed to quickly. After the crystallization, the crystals were dried and the H^1 NMR showed that the crystallization had separated the dye from its impurities. This method was useful over all six compounds. The H^1 NMR spectra showed that there was a COOH peak around 11.5 ppm and that there was no the singlet peak integrating to three that was present after column chromatography.

2.6.2 Optical Properties and Physicochemical Calculations

The optical properties of the compounds **4a-f** were measured in ethanol as an organic medium and phosphate buffer as an aqueous one and can be seen in Table 6. The extinction coefficients of the compounds **4a-f** are below 100,000 1/M x cm, usually a marker for researchers to judge fluorophores as viable for *in vivo* studies. The reason for the low extinction coefficient

values is unknown based on the analysis of the structures however when looking at the physicochemical calculations obtained from the minimized structures, a few hypotheses can be made. One of these hypotheses relates to the dimerization that occurs by the carboxylic acids; because of this dimerization, the compound is stretched and the electrons have further to go between carbons on the 'bridge'. The Stokes shift values allow for a clear distinction between excitation light and fluoresced light. The quantum yield values show a unique trend. For compounds **4a-c**, there is an increase in quantum yield values as the halogen on the bridge in ethanol, however the opposite trend occurs in PBS. As the hydrophobicity of the molecules increases when chlorine or bromine are added to the molecule, the aqueous medium is not allowing for efficient absorption to fluorescence to occur while the organic solvent is more tolerant of the hydrophobicity increase. The quantum yield values decreasing is observed for compounds **4d-f** as well, however since the molecules are more hydrophobic due to the greater hydrophobicity of the benz[e] indole compared to the unsubstituted indolenine heterocycle.

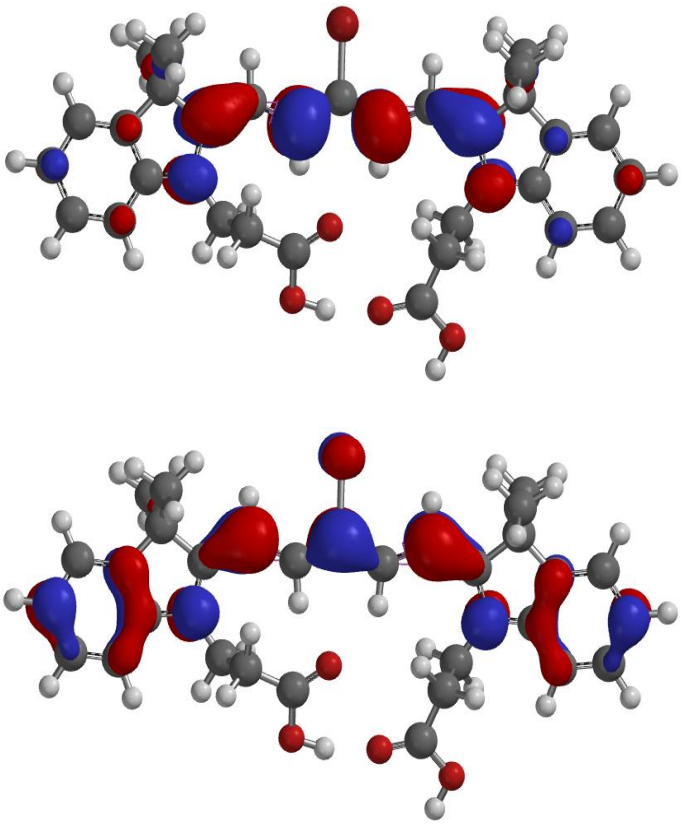

*Figure 28. The HOMO (top) LUMO (bottom) visualizations of compounds **4c**.*

Another unique observation seen from the physicochemical properties is how the atoms on the bridge point. Usually, the gamma hydrogen is pointed down, away from the dimethyl groups, the beta hydrogens point up, and the alpha protons point down . However, after minimization, the hydrogens can be seen to be pointing in the opposite direction. This may be another consequence of the COOH dimerization. Because the propionic acid groups come together under the bridge, there is less room 'under' the molecule. When looking at compound **4c**, it is clear that the bromine molecule is pointing up; this can be seen in figure 28. Usually, the dimethyl groups clog up that space and there is no room for the gamma substituted atom to point up, but due to the bending and puckering up of the molecule, there is now room for this atom to exist pointing upwards.

*Table 6. The optical property data collected from compounds **4a-f** in two solvents.*

ID	λ_{abs} (nm)		Extinction Coefficient (e, $M^{-1}cm^{-1}$)		λ_{em} (nm)		Stokes Shift		QY (F, %)		MB (e x F)	
	EtOH	PBS	EtOH	PBS	EtOH	PBS	EtOH	PBS	EtOH	PBS	EtOH	PBS
4a	646	643	60,700	56,300	668	659	22	16	23	72.3	13,961	40,705
4b	645	644	32,200	30,300	663	657	18	13	67.5	42.2	21,735	12,787
4c	646	644	24,500	18,000	662	655	18	11	78.5	22.5	19,233	4,050
4d	685	680	78,400	50,700	708	697	23	17	42.3	43.4	33,163	22,004
4e	684	680	93,100	79,500	702	695	18	15	21	20.7	19,551	16,457
4f	684	681	95,400	81,000	702	695	18	14	19.9	16.2	19,985	13,122

2.6.3 Conclusions

Compounds **4a-f** were successfully synthesized and purified using an unorthodox method compared to what is usually performed for this family of dyes. The dyes were characterized and their optical properties were studied in preparation for *in vivo* imaging. The dyes need to be studied further for biodistribution and more in depth H^1 NMR studies to fully understand the extent of the

dimerization of the acid groups. The dyes can serve as useful handles for other ligands as well as for biodistribution studies. Their optical properties suggest that these dyes could be useful for *in vivo* imaging of tissues. The dyes were sent to be studied by our collaborators at Beth Isreal Deaconess Medical Center on rat models. These studies will show if there is any structure inherent properties afforded from the pentanoic acid groups.

2.6.4 Experimental Details

2.6.4.1 Synthesis of Pentamethine Cyanine Analogs

The chemical reagents used in the synthesis of these compounds were obtained from Acros Organics, Alfa Aesar, Matrix Scientific, and Sigma-Aldrich. The reactions were followed using silica gel 60 F_{254} thin-layer chromatography plates (Merck EMD Millipore, Darmstadt, Germany). Open column chromatography was utilized for the purification of all final compounds using 60–200 μm, 60A, classic column silica gel (Dynamic Adsorbents, Norcross, GA). The ^{1}H NMR and ^{13}C NMR spectra were obtained using high-quality Kontes NMR tubes (Kimble Chase, Vineland, NJ) rated to 500 MHz and were recorded on a Bruker Avance (400 MHz) spectrometer using DMSO-d_6 or MeOD-d_4 containing tetramethylsilane (TMS) as an internal calibration standard set to 0.0 ppm. UV–vis/NIR absorption spectra were recorded on a Varian Cary 50 spectrophotometer.

2.6.4.2 Optical Physicochemical Property Analyses

All optical measurements were performed in various solvents, including ethanol and phosphate buffered saline (PBS, pH 7.4), and at 37 °C in 100% FBS buffered with 50 mM HEPES, pH 7.4. Absorbance and fluorescence emission spectra of the series of NIR fluorophores were measured using Varian Cary 50 absorbance spectrophotometer (190–1100 nm) and Shimadzu RF-5301PC spectrofluorometer (350–1000 nm). For fluorescence quantum yield (QY) measurements,

rhodamine 800 in absolute ethanol (QY = 28%) was used as a calibration standard, under conditions of matched absorbance at 620 nm. In silico calculations of physicochemical distribution coefficient (log *D* at pH 7.4) was calculated using Marvin and JChem calculator plugins (ChemAxon, Budapest, Hungary). Electrostatic maps were calculated using Spartan DFT calculations at the B3LYP level.

2.6.4.3 Synthesis and Characterization of NIR Fluorophores

Phenyl hydrazines **1a-b** were commercially obtained. They were added to 3 mol. equivalents of 3-methyl-2-butanone in 35 mL of acetic acid and let to react at reflux for 72 h. The resulting indoles (**2a-b**), after basic workup with sodium bicarbonate, were reacted with 1.1 mol. equivalent of iodomethane at reflux for 24 h to result in indolenine salts **3a-b**. To obtain the final dyes **4 a-f**, compound **3** was added to a clean, dry round-bottom flask. Two mol. equivalents was stirred in 5 mL of acetic anhydride, and 4 mol. equivalent of sodium acetate along with 1 mol. equivalents of individual malondaldehyde linker. The reaction was allowed to stir at RT for 15 min. If the reaction proceeded longer than that, the product peak at ~650 nm would decrease on UV-Vis. The reactions were monitored closely using regular phase thin-layer chromatography with a mobile phase of DCM/MeOH (99:1). Upon completion of the reaction, the reaction mixtures were allowed to cool, and the solvent was evaporated. The residue was extracted using DCM and was washed with 1M AcOH (3 × 70 mL). The resulting organic layer was dried under magnesium sulfate, gravity filtered, and evaporated to afford crystals that were washed with diethyl ether (2 × 50 mL) and hexanes (50 mL) to yield crystals that were dried under vacuum overnight. The dyes were purified using solvent transfer crystallography. The dyes were dissolved in DCM in a small vial and placed in a larger vial with the bottom covered in diethyl ether. The vials were sealed and

the solvents were allowed to exchange over a 10 day period. After the time was done, the solvent was decanted and the pure crystals were dried under vacuum. After purification, the compounds were obtained in the designated yields and were fully characterized.

1-(2-carboxyethyl)-2-((1E,3E)-5-((E)-1-(2-carboxyethyl)-3,3-dimethylindolin-2-ylidene)penta-1,3-dien-1-yl)-3,3-dimethyl-3H-indol-1-ium iodide (**4a**). Yield 18%, mp > 260 ºC; ^{1}H NMR (400 MHz, MeOD-d_4) **σ**: 1.741 (s, 12h), 2.720 (t, *J* = 6.8, 7.2 Hz, 4H), 4.388 (t, *J* = 6.8, 7.6 Hz, 4H), 6.406 (d, *J* = 13.6 Hz, 2H), 6.662 (t, *J* = 13.2, 12.4 Hz, 1H), 7.271 (t, *J* = 6.8, 7.6 Hz, 2H), 7.402 (m, *J* = 7.6, 8, 7.2, 4.6 Hz, 4H), 7.505 (d, *J* = 7.2 Hz, 2H), 8.269 (t, *J* = 12.8 Hz, 2H). ^{13}C NMR (100 MHz, DMSO-d_6) **σ**: 27.61, 31.77, 33.29, 49.35, 52.16, 103.58, 103.98, 104.42, 111.34, 111.83, 119.72, 122.87, 125.35, 126.46, 128.78, 129.06, 141.67, 142.13, 154.71, 171.34.

1-(2-carboxyethyl)-2-((1E,3Z)-5-((E)-1-(2-carboxyethyl)-3,3-dimethylindolin-2-ylidene)-3-chloropenta-1,3-dien-1-yl)-3,3-dimethyl-3H-indol-1-ium (**4b**). Yield 20%, mp > 260 ºC; ^{1}H NMR (400 MHz, DMSO-d_6) **σ**: 1.692 (s, 12h), 2.752 (d, *J* = 26.4 Hz, 4H), 4.717 (s, 4H), 6.357 (d, *J* = 12.4 Hz, 2H), 7.290 (s, 4H), 7.654 (s, 2H), 8.497 (s, 2H). ^{13}C NMR (100 MHz, DMSO-d_6) **σ**: 27.29, 31.98, 49.96, 52.56, 100.64, 112.36, 123.17, 126.14, 129.04, 132.10, 141.80, 148.40, 171.16, 174.96.

2-((1E,3Z)-3-bromo-5-((E)-1-(2-carboxyethyl)-3,3-dimethylindolin-2-ylidene)penta-1,3-dien-1-yl)-1-(2-carboxyethyl)-3,3-dimethyl-3H-indol-1-ium bromide (**4c**). Yield 21%, mp > 260 ºC; ^{1}H NMR (400 MHz, DMSO-d_6) **σ**: 1.687 (s, 12h), 2.772 (d, *J* = 3.6 Hz, 4H), 4.419 (s, 4H), 6.439 (d, *J* = 8.4 Hz, 2H), 7.320 (m, 8H), 8.529 (d, *J* = 12.4, 2H).

3-(2-carboxyethyl)-2-((1E,3E,5E)-5-(3-(2-carboxyethyl)-1,1-dimethyl-1,3-dihydro-2H-benzo[e]indol-2-ylidene)penta-1,3-dien-1-yl)-1,1-dimethyl-1H-benzo[e]indol-3-ium bromide

(**4d**). Yield 12%, mp > 260 ^{o}C; ^{1}H NMR (400 MHz, DMSO-d_6) **σ**: 1.861 (s, 4H) 1.959 (s, 12h), 4.452 (s, 4H), 6.402 (d, *J* = 13.6Hz, 2H), 7.540 (s, 2H), 7.691 (s, 2H), 7.699 (s, 4H), 8.244, (s, 2H), 8.595 (s, 2H).

3-(2-carboxyethyl)-2-((1E,3Z,5E)-5-(3-(2-carboxyethyl)-1,1-dimethyl-1,3-dihydro-2H-benzo[e]indol-2-ylidene)-3-chloropenta-1,3-dien-1-yl)-1,1-dimethyl-1H-benzo[e]indol-3-ium bromide (**4e**). Yield 14%, mp > 260 ^{o}C; ^{1}H NMR (400 MHz, DMSO-d_6) **σ**: 1.967 (s, 12H) 2.798 (s, 4H), 4.529 (s, 4H), 6.460 (s, 2H), 7.538 (s, 2H), 7.685 (s, 2H), 7.696 (s, 4H), 7.834, (s, 2H), 8.084 (s, 4H), 8.188 (s, 2H), 8.632 (s, 2H).

2-((1E,3Z,5E)-3-bromo-5-(3-(2-carboxyethyl)-1,1-dimethyl-1,3-dihydro-2H-benzo[e]indol-2-ylidene)penta-1,3-dien-1-yl)-3-(2-carboxyethyl)-1,1-dimethyl-1H-benzo[e]indol-3-ium bromide (**4f**). Yield 15%, mp > 260 ^{o}C; ^{1}H NMR (400 MHz, DMSO-d_6) **σ**: 1.861 (s, 4H) 1.959 (s, 12H), 4.452 (s, 4H), 6.436 (d, *J* = 13.6Hz, 2H), 7.536 (s, 2H), 7.756 (s, 2H), 8.079 (s, 4H), 8.244, (s, 2H), 8.626 (s, 2H).

2.6.5 References

1. (a) Onoe, S.; Temma, T.; Kanazaki, K.; Ono, M.; Saji, H., Development of photostabilized asymmetrical cyanine dyes for in vivo photoacoustic imaging of tumors. *BIOMEDO* **2015,** *20* (9), 096006-096006; (b) Owens, E. A.; Hyun, H.; Dost, T. L.; Lee, J. H.; Park, G.; Pham, D. H.; Park, M. H.; Choi, H. S.; Henary, M., Near-Infrared Illumination of Native Tissues for Image-Guided Surgery. *Journal of Medicinal Chemistry* **2016**.
2. (a) Kuang, D.; Uchida, S.; Humphry-Baker, R.; Zakeeruddin, S. M.; Grätzel, M., Organic Dye-Sensitized Ionic Liquid Based Solar Cells: Remarkable Enhancement in Performance through Molecular Design of Indoline Sensitizers. *Angewandte Chemie International Edition* **2008,** *47* (10), 1923-1927; (b) Wang, Z.-S.; Koumura, N.; Cui, Y.; Takahashi, M.; Sekiguchi, H.; Mori, A.; Kubo, T.; Furube, A.; Hara, K., Hexylthiophene-Functionalized Carbazole Dyes for Efficient Molecular Photovoltaics: Tuning of Solar-Cell Performance by Structural Modification. *Chemistry of Materials* **2008,** *20* (12), 3993-4003.
3. (a) Guo, M.; Huang, J.; Deng, Y.; Shen, H.; Ma, Y.; Zhang, M.; Zhu, A.; Li, Y.; Hui, H.; Wang, Y.; Yang, X.; Zhang, Z.; Chen, H., Photothermal Therapy: pH-Responsive Cyanine-Grafted Graphene Oxide for Fluorescence Resonance Energy Transfer-Enhanced Photothermal Therapy (Adv. Funct. Mater. 1/2015). *Advanced Functional Materials* **2015,** *25* (1), 58-58; (b) Luo, S.; Tan, X.; Fang, S.; Wang, Y.; Liu, T.; Wang, X.; Yuan, Y.; Sun, H.; Qi, Q.; Shi, C., Cancer Phototherapy: Mitochondria-Targeted Small-Molecule Fluorophores for Dual Modal Cancer Phototherapy (Adv. Funct. Mater. 17/2016). *Advanced Functional Materials* **2016,** *26* (17), 2975-2975.

4. Frangioni, J. V., In vivo near-infrared fluorescence imaging. *Current Opinion in Chemical Biology* **2003,** *7* (5), 626-634.
5. Sauve, G.; Kamat, P. V.; Thomas, K. G.; Thomas, K. J.; Das, S.; George, M. V., Photochemistry of Squaraine Dyes: Excited Triplet State and Redox Properties of Crown Ether Squaraines. *The Journal of Physical Chemistry* **1996,** *100* (6), 2117-2124.
6. Mojzych, M.; Henary, M., Synthesis of Cyanine Dyes. In *Heterocyclic Polymethine Dyes: Synthesis, Properties and Applications*, Strekowski, L., Ed. Springer Berlin Heidelberg: Berlin, Heidelberg, 2008; pp 1-9.
7. Henary, M.; Levitz, A., Synthesis and applications of unsymmetrical carbocyanine dyes. *Dyes and Pigments* **2013,** *99* (3), 1107-1116.
8. Hyun, H.; Park, M. H.; Owens, E. A.; Wada, H.; Henary, M.; Handgraaf, H. J. M.; Vahrmeijer, A. L.; Frangioni, J. V.; Choi, H. S., Structure-inherent targeting of near-infrared fluorophores for parathyroid and thyroid gland imaging. *Nat Med* **2015,** *21* (2), 192-197.
9. Etter, M. C.; Kress, R. B.; Bernstein, J.; Cash, D. J., Solid-state chemistry and structures of a new class of mixed dyes. Cyanine-oxonol. *Journal of the American Chemical Society* **1984,** *106* (23), 6921-6927.

APPENDICES

Chapter 1

Appendix A.1 ^{1}H NMR Spectra

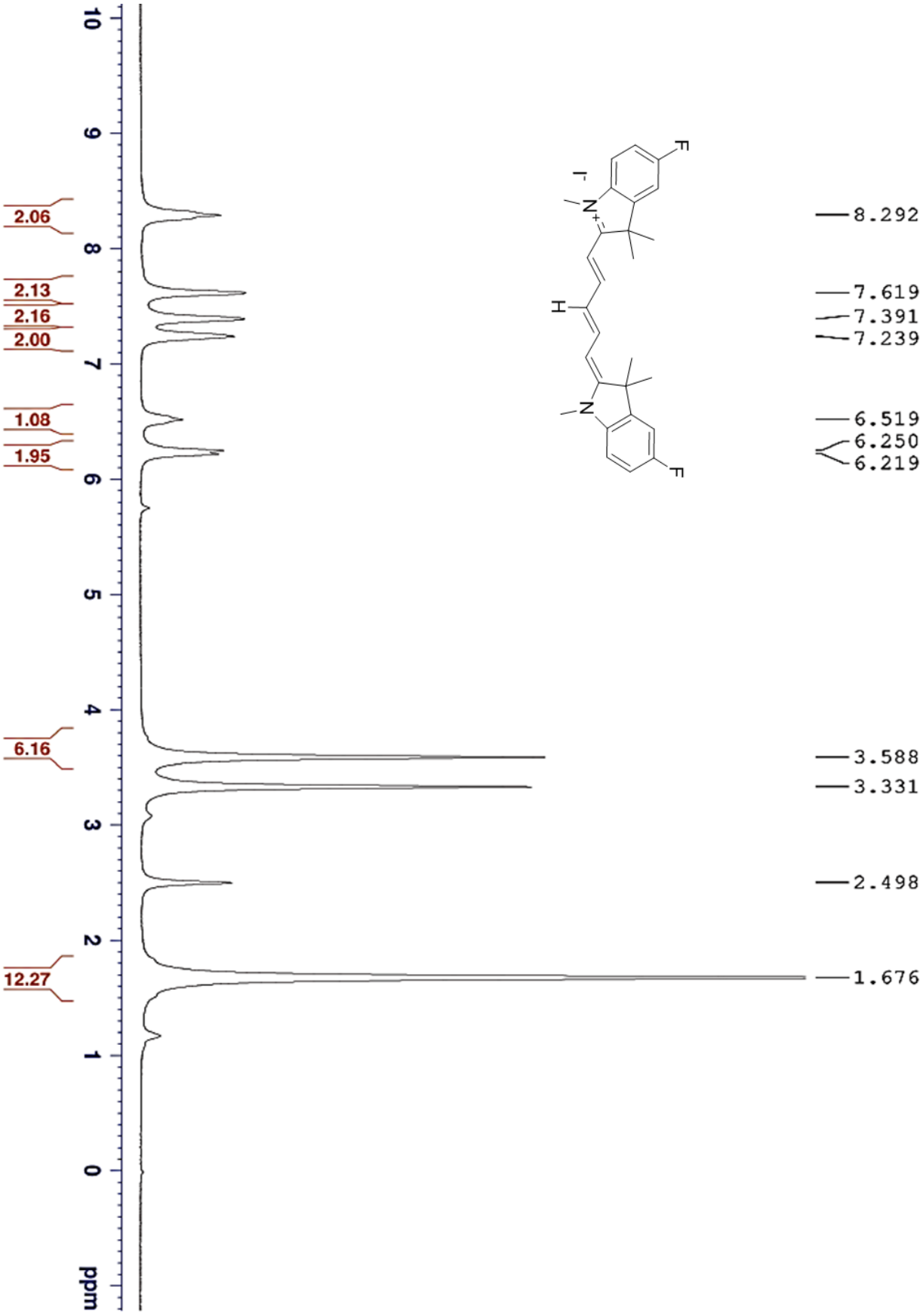
2.06
2.13
2.16
2.00
1.08
1.95
6.16
12.27
ppm
8.292
7.619
7.391
7.239
6.519
6.250
6.219
3.588
3.331
2.498
1.676

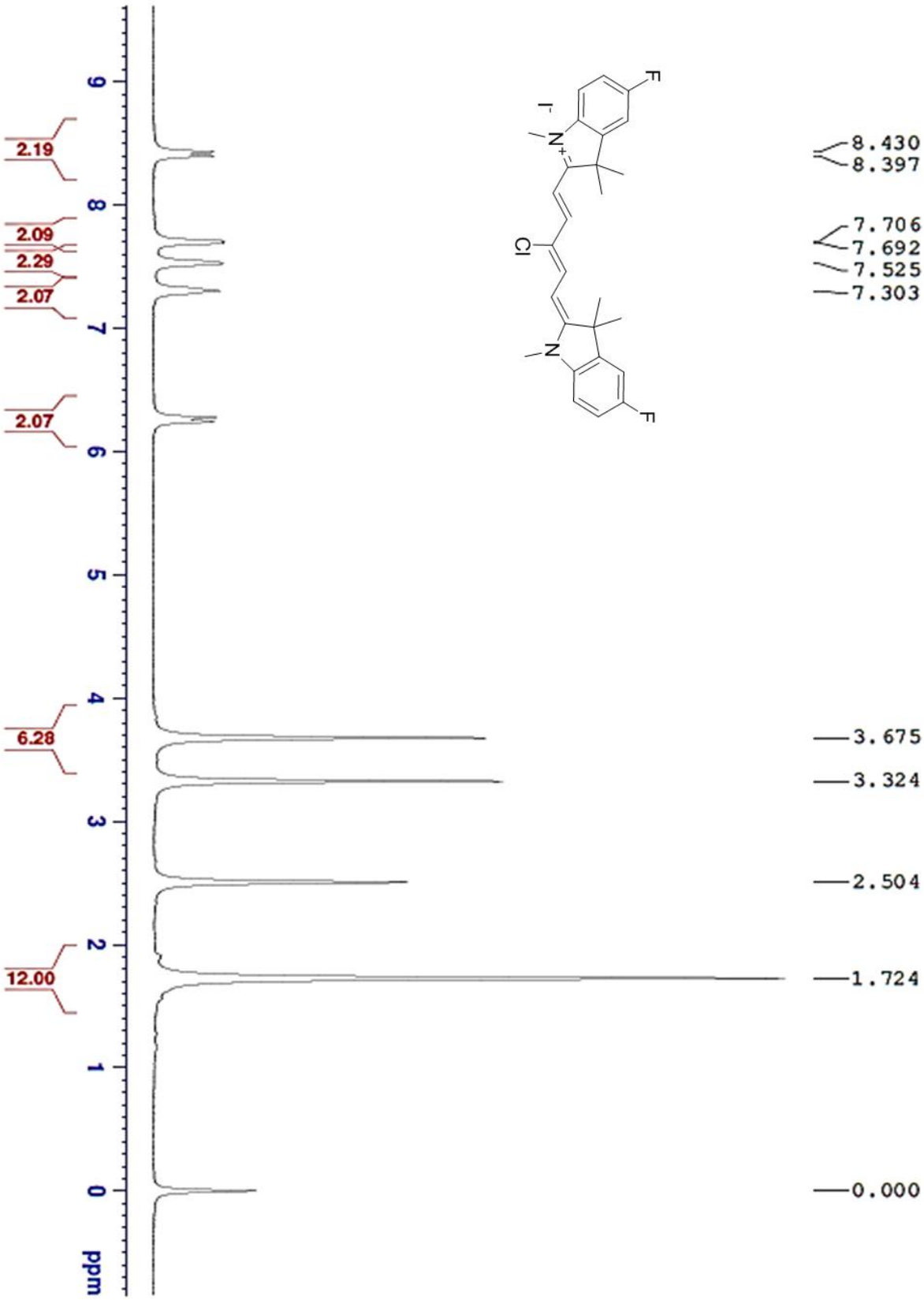
2.19
2.09
2.29
2.07
2.07
6.28
12.00
9
8
7
6
5
4
3
2
1
0
ppm
I⁻
N⁺
Cl
F
F
N
8.430
8.397
7.706
7.692
7.525
7.303
3.675
3.324
2.504
1.724
0.000

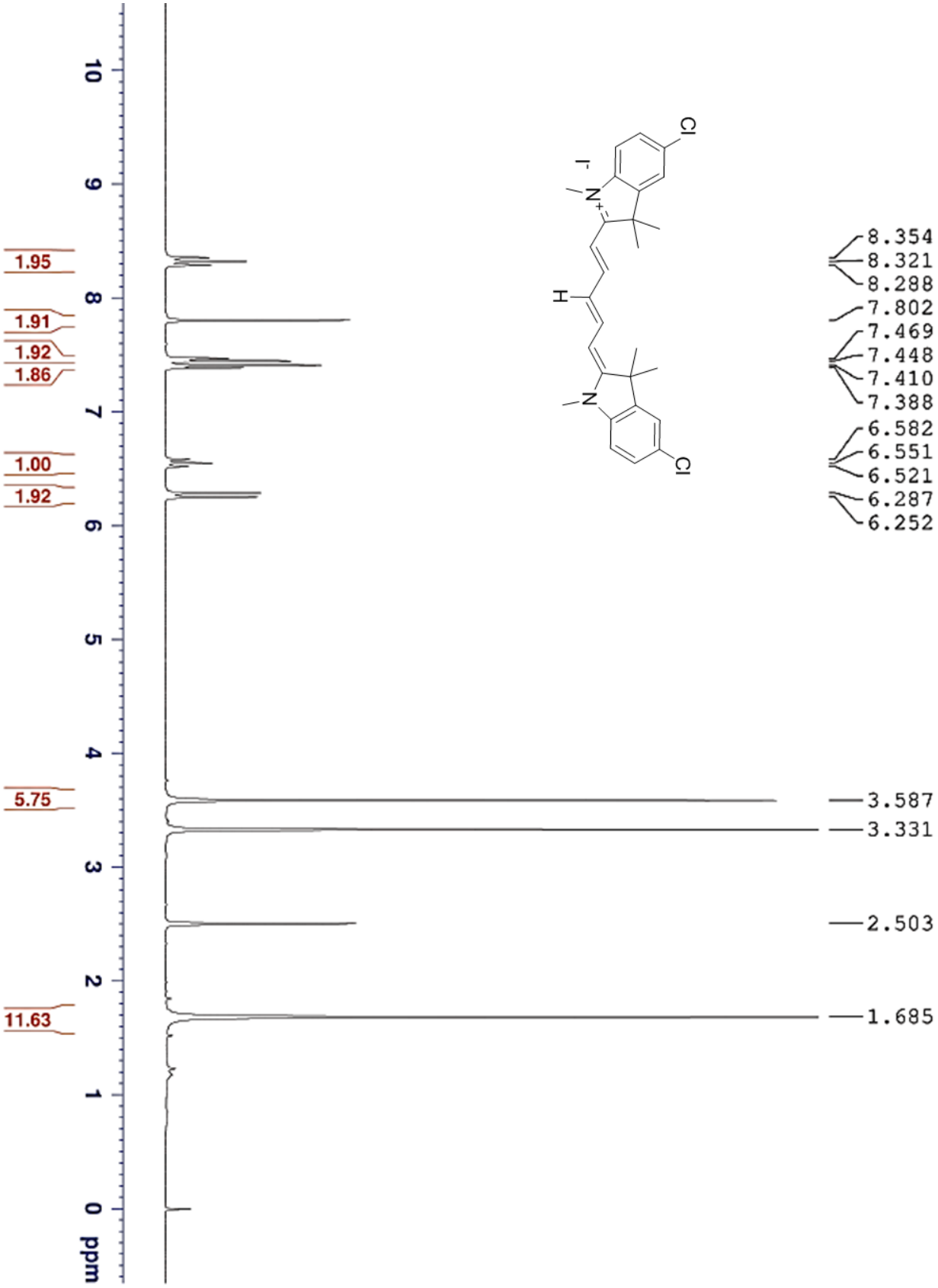
8.354
8.321
8.288
7.802
7.469
7.448
7.410
7.388
6.582
6.551
6.521
6.287
6.252
3.587
3.331
2.503
1.685
1.95
1.91
1.92
1.86
1.00
1.92
5.75
11.63
ppm
Cl
I -
H
N
Cl

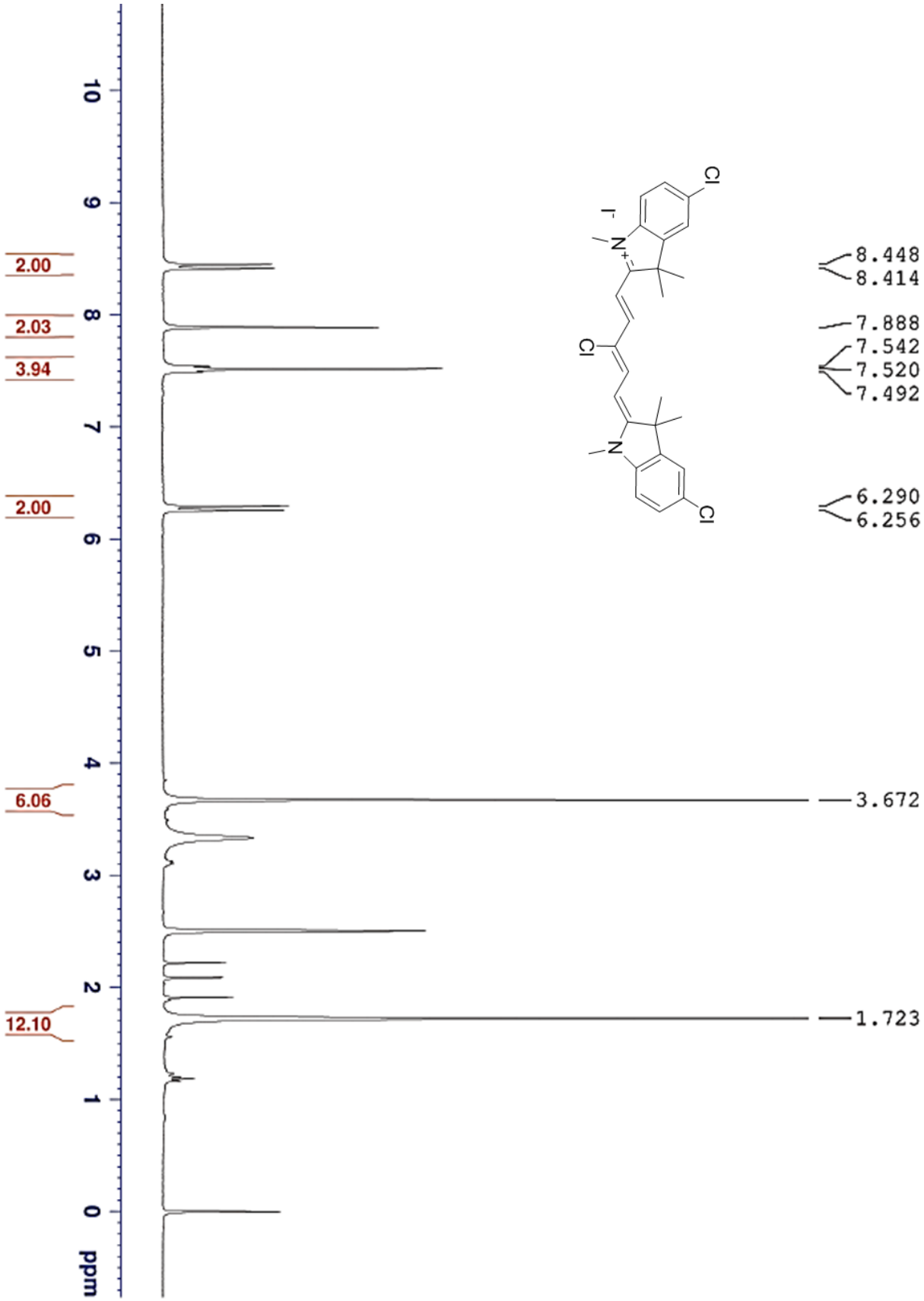
8.448
8.414
7.888
7.542
7.520
7.492
6.290
6.256
3.672
1.723
2.00
2.03
3.94
2.00
6.06
12.10
ppm

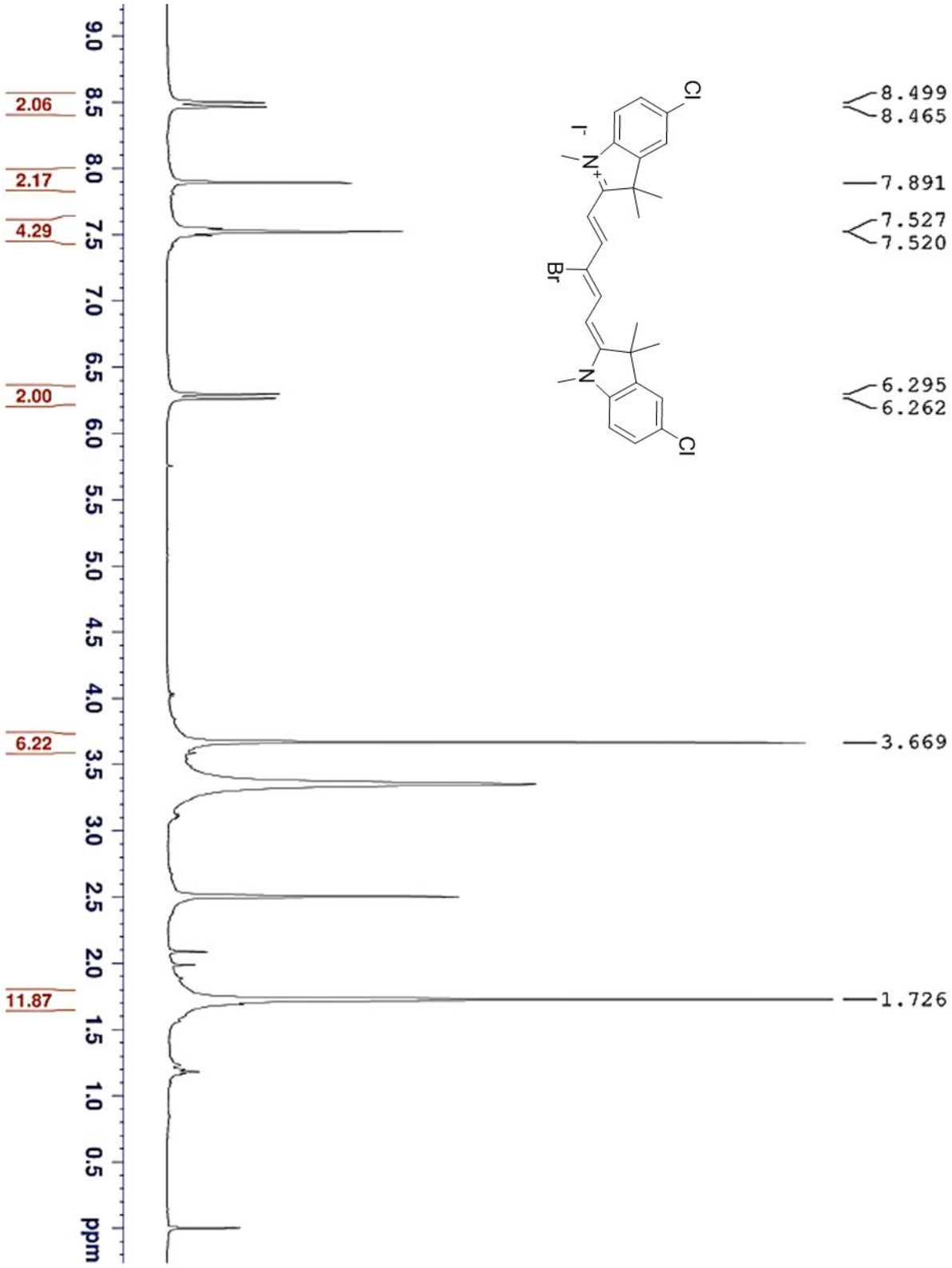
2.06
2.17
4.29
2.00
6.22
11.87
9.0
8.5
8.0
7.5
7.0
6.5
6.0
5.5
5.0
4.5
4.0
3.5
3.0
2.5
2.0
1.5
1.0
0.5
ppm
Cl
I-
N+
Br
N
Cl
8.499
8.465
7.891
7.527
7.520
6.295
6.262
3.669
1.726

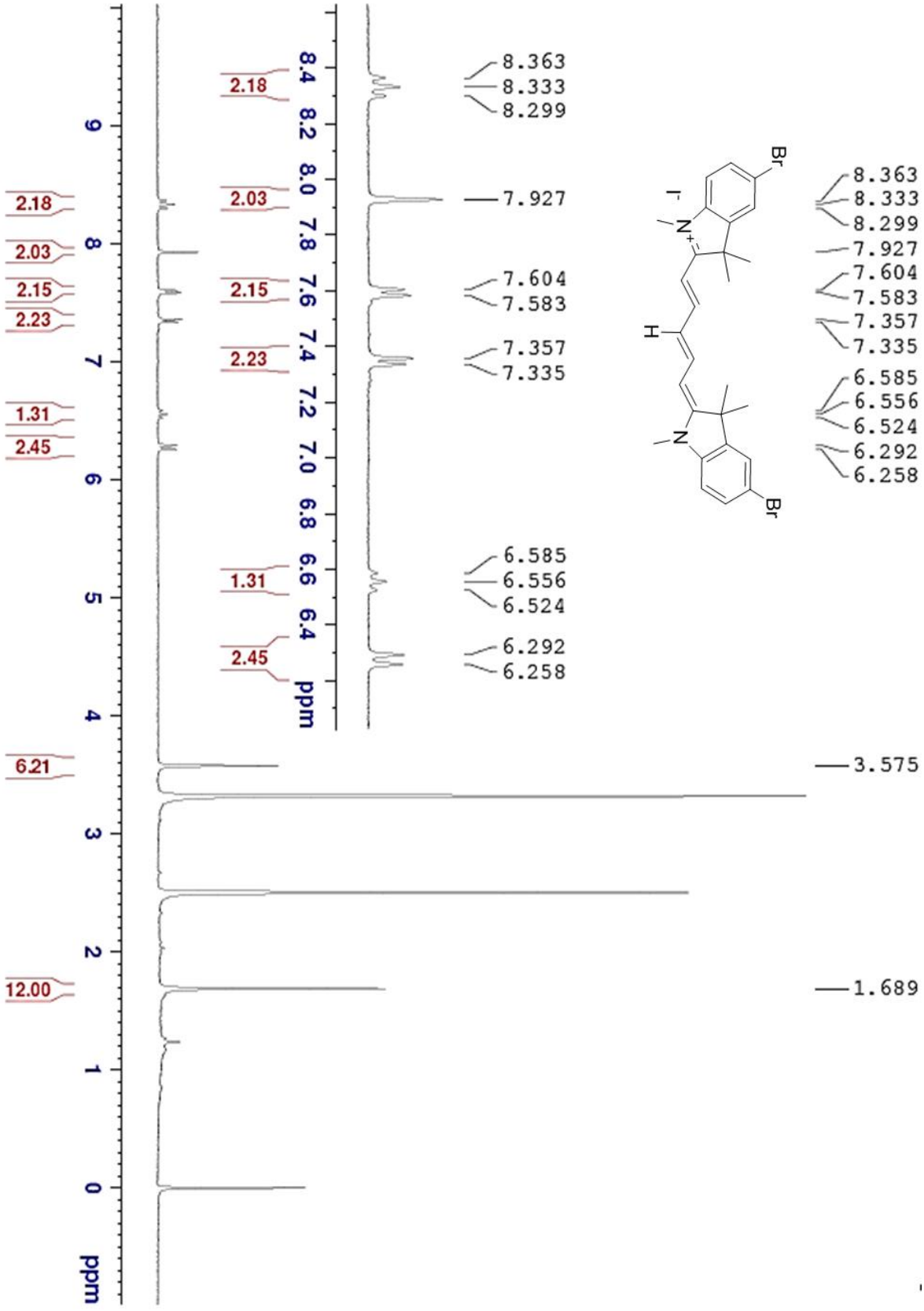
8.363
8.333
8.299
7.927
7.604
7.583
7.357
7.335
6.585
6.556
6.524
6.292
6.258
3.575
1.689
2.18
2.03
2.15
2.23
1.31
2.45
6.21
12.00
ppm
Br
I-
N+
H
N
Br

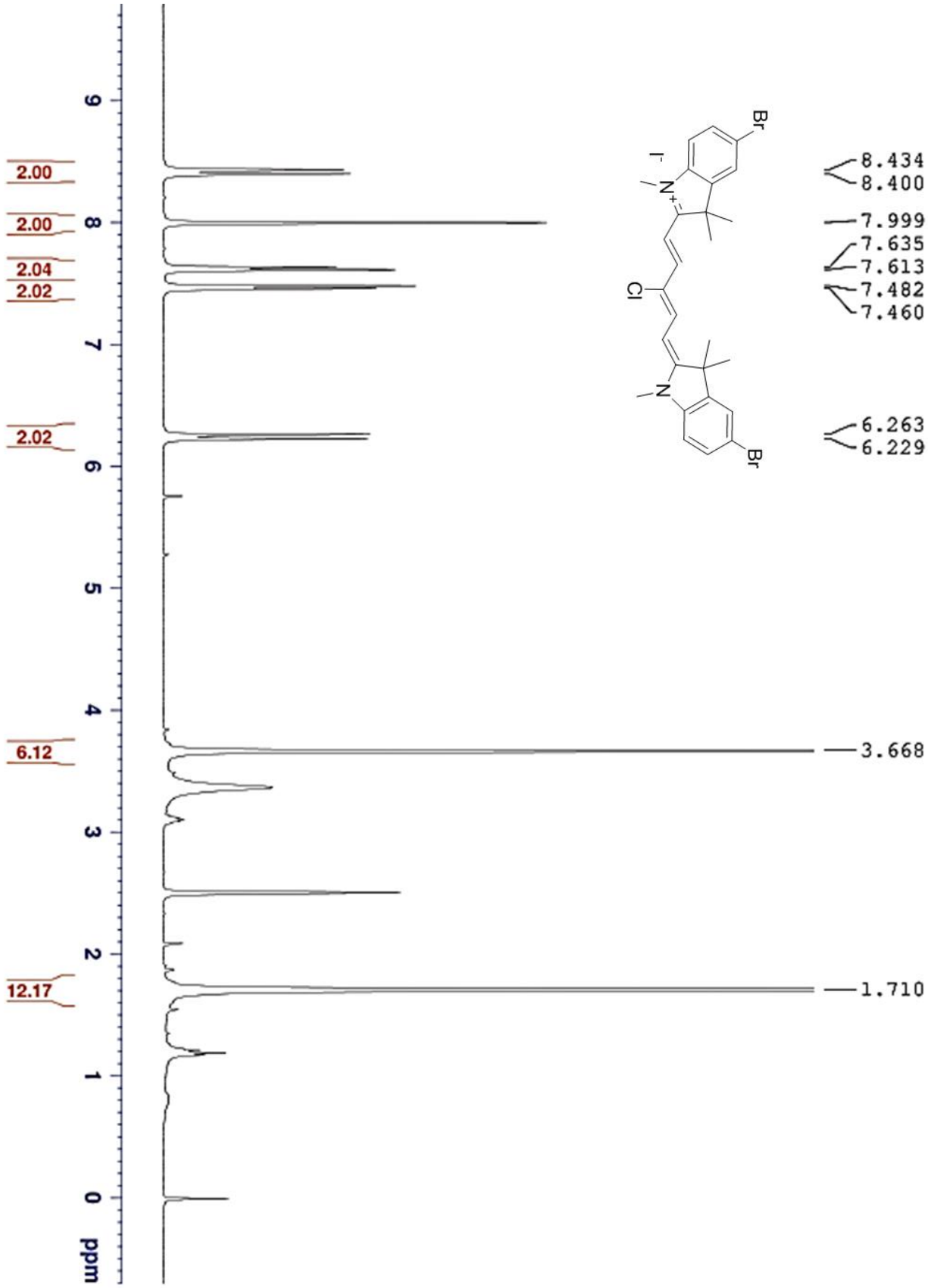
2.00
2.00
2.04
2.02
2.02
6.12
12.17
ppm
9
8
7
6
5
4
3
2
1
0
Br
I-
N+
Cl
N
Br
8.434
8.400
7.999
7.635
7.613
7.482
7.460
6.263
6.229
3.668
1.710

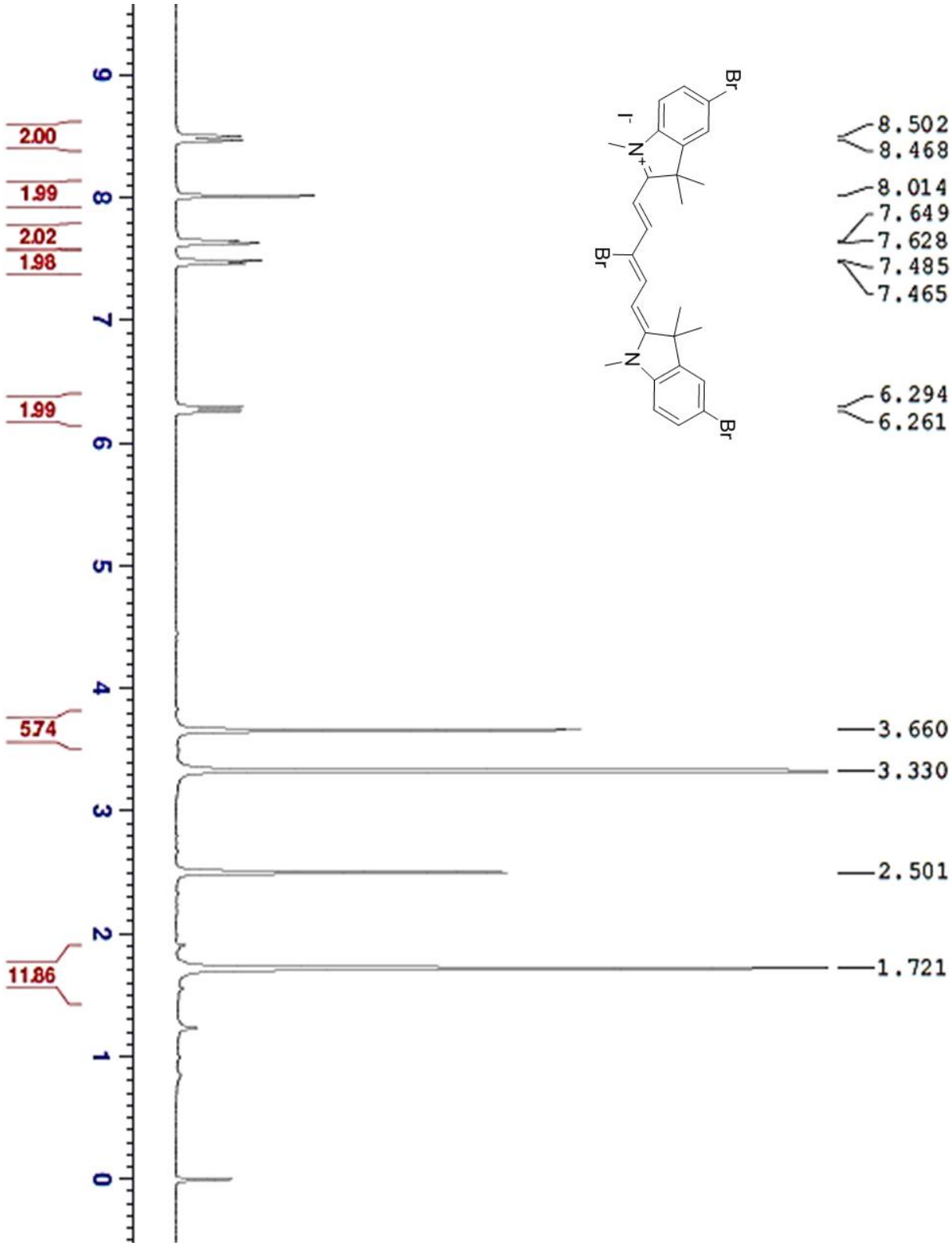
2.00
1.99
2.02
1.98
1.99
5.74
11.86
8.502
8.468
8.014
7.649
7.628
7.485
7.465
6.294
6.261
3.660
3.330
2.501
1.721

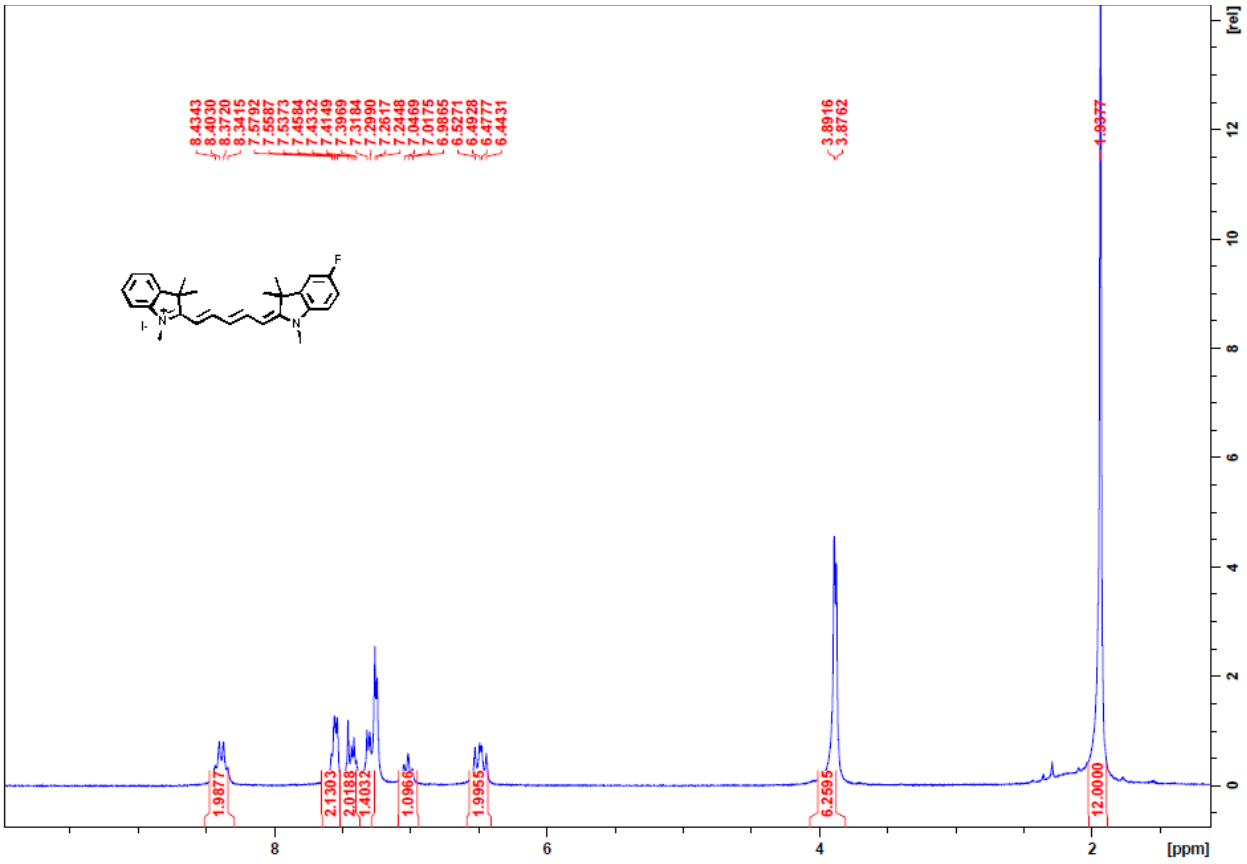
8.4343
8.4030
8.3720
8.3415
7.5792
7.5587
7.5373
7.4584
7.4432
7.4149
7.3969
7.3184
7.2990
7.2617
7.2448
7.0469
7.0175
6.9865
6.5271
6.4928
6.4777
6.4431
3.8916
3.8762
1.9377
F
I-
N+
N
1.9877
2.1303
2.0188
1.4032
1.0966
1.9955
6.2595
12.0000
8
6
4
2
[ppm]
[rel]
0
2
4
6
8
10
12

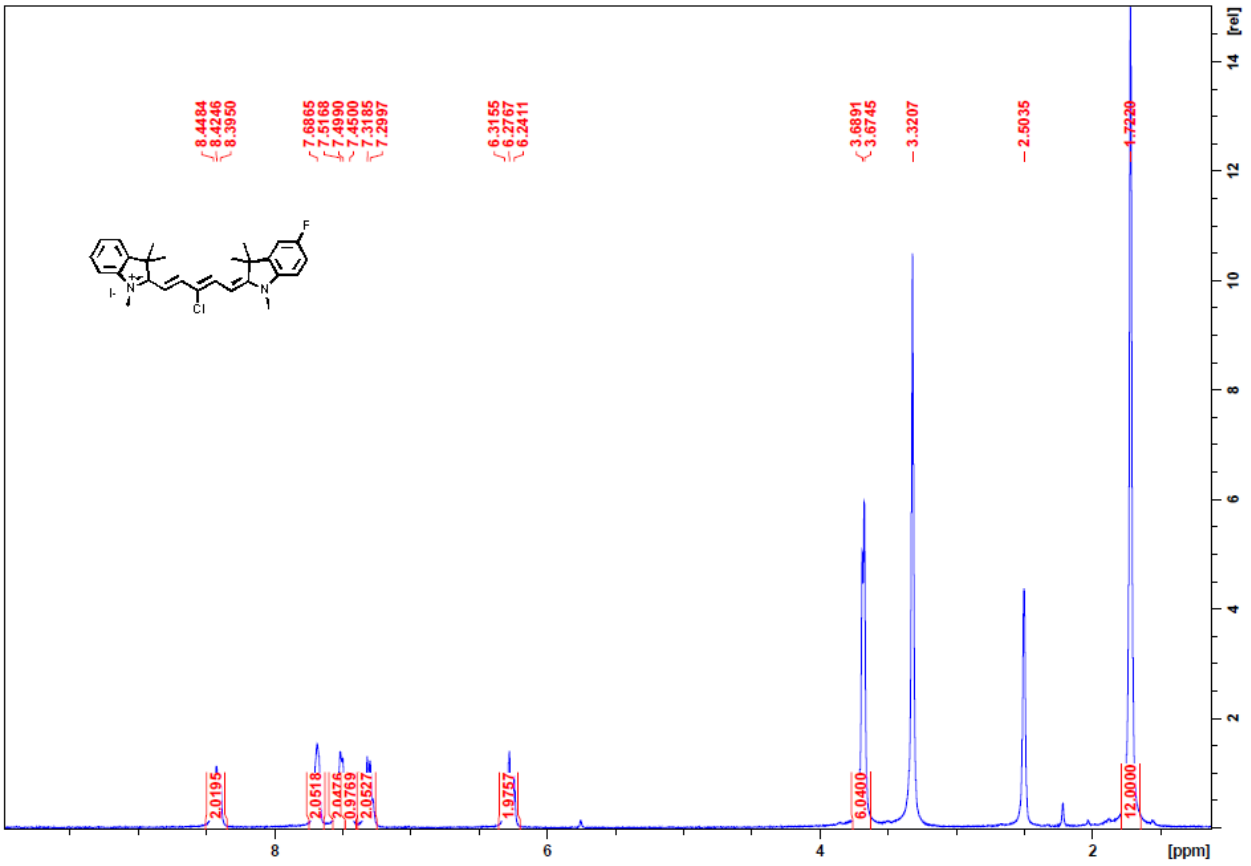
8.4484
8.4246
8.3950
7.6865
7.5168
7.4990
7.4500
7.3185
7.2997
6.3155
6.2767
6.2411
3.6891
3.6745
3.3207
2.5035
1.7220
2.0195
2.0518
2.0476
0.9769
2.0527
1.9757
6.0400
12.0000
F
I-
N+
Cl
N
8
6
4
2
[ppm]
[rel]

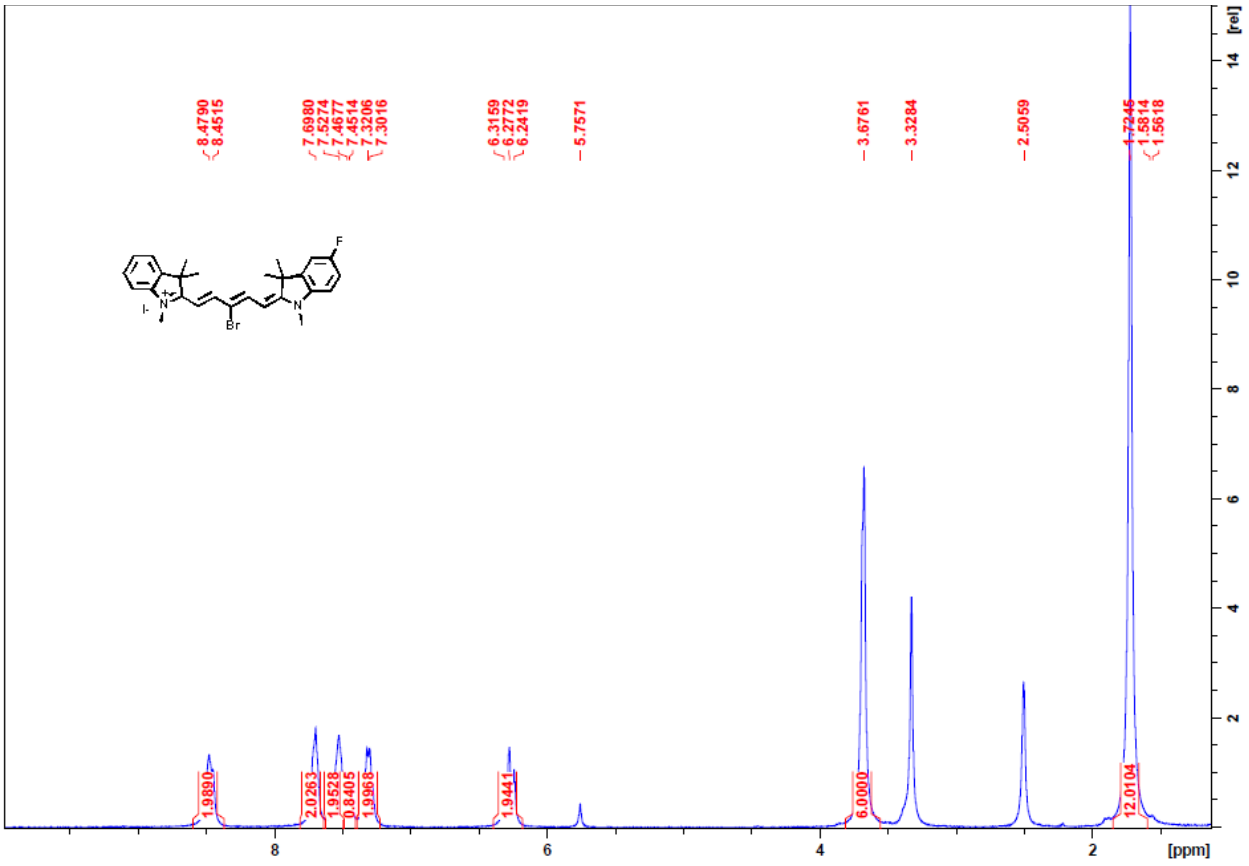
8.4790
8.4515
7.6980
7.5274
7.4677
7.4514
7.3206
7.3016
6.3159
6.2772
6.2419
5.7571
3.6761
3.3284
2.5059
1.7245
1.5814
1.5618
1.9890
2.0263
1.9528
0.8405
1.9965
1.9441
6.0000
12.0104
F
Br
I-
[rel]
[ppm]

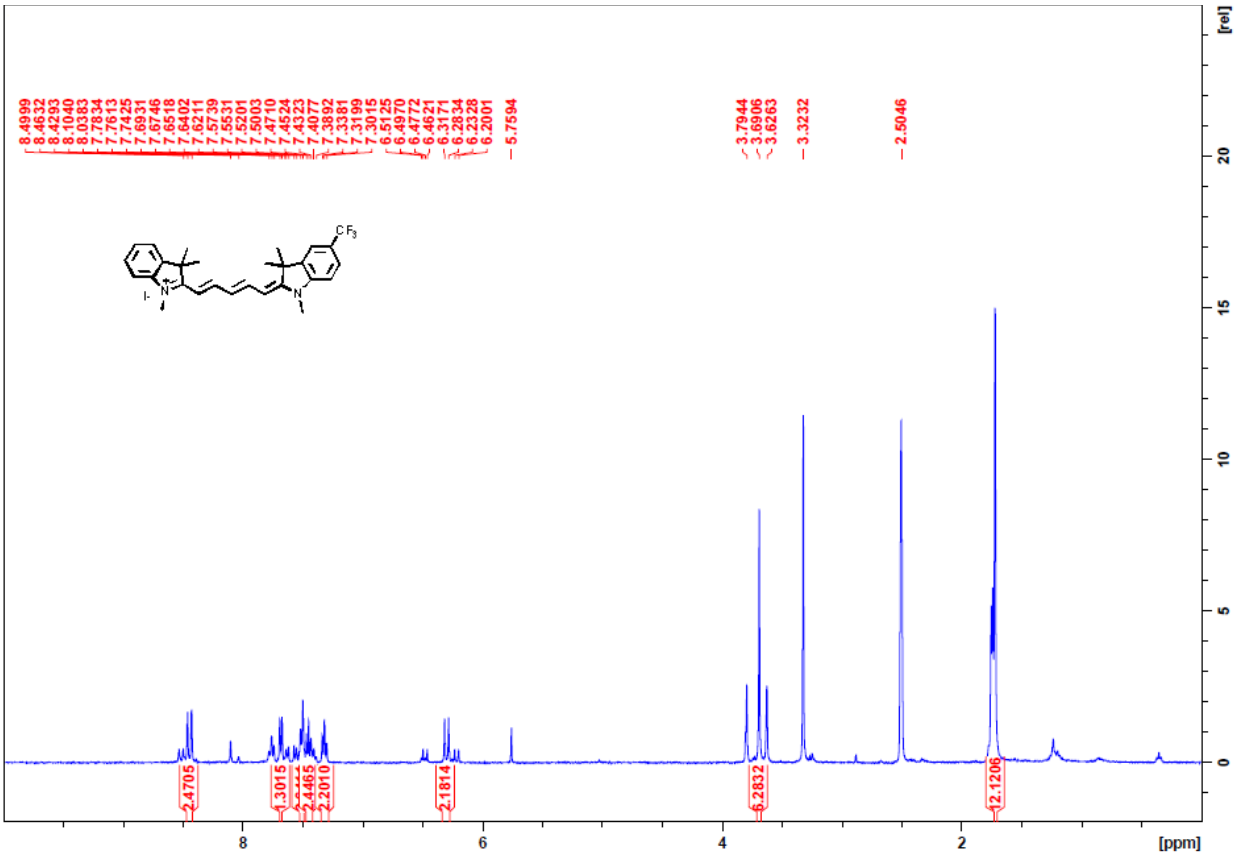
8.4999
8.4632
8.4293
8.1040
8.0383
7.7834
7.7613
7.7425
7.6931
7.6746
7.6518
7.6402
7.6211
7.5739
7.5531
7.5201
7.5003
7.4710
7.4524
7.4323
7.4077
7.3892
7.3381
7.3199
7.3015
6.5125
6.4970
6.4772
6.4621
6.3171
6.2834
6.2328
6.2001
5.7594
3.7944
3.6906
3.6263
3.3232
2.5046
CF3
I-
N+
N
2.4705
1.3015
2.4465
2.2010
2.1814
6.2832
12.1206
8
6
4
2
[ppm]
[rel]
0
5
10
15
20

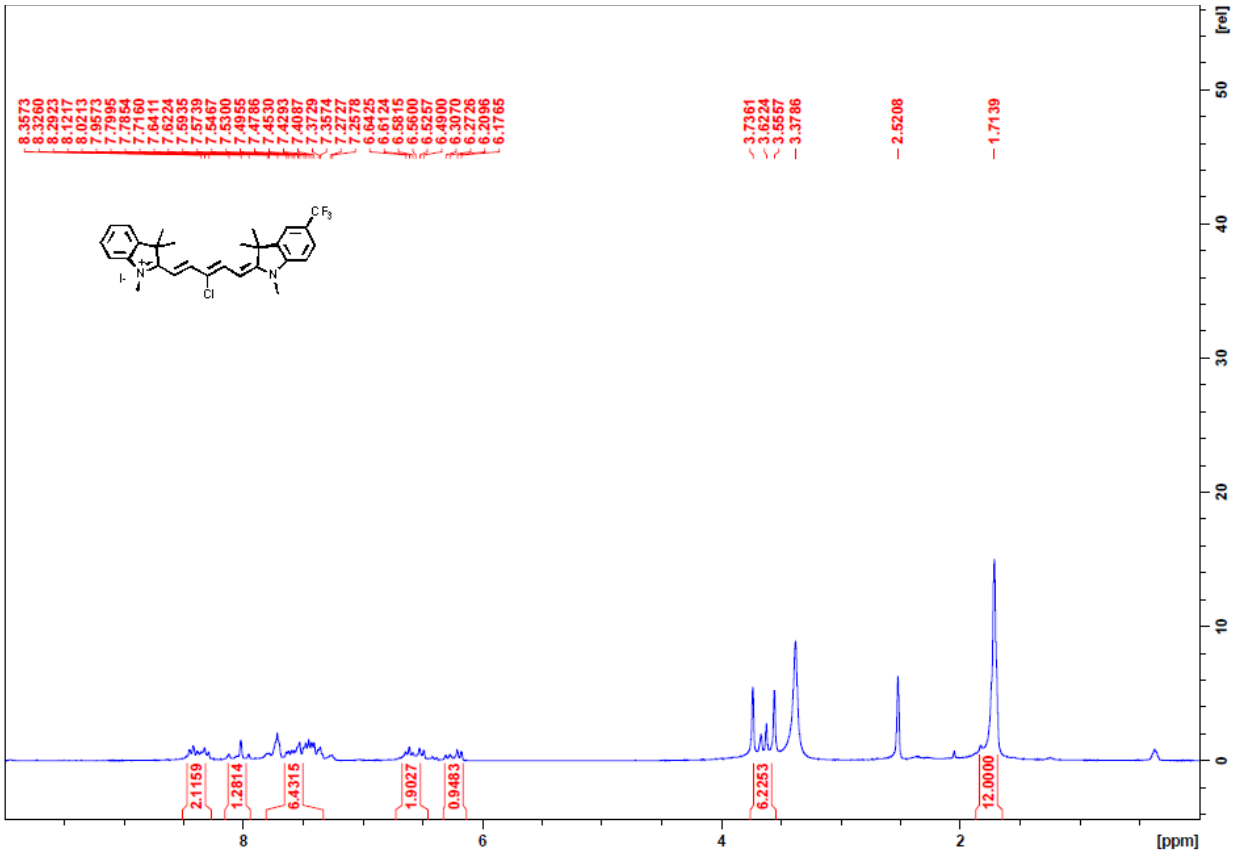
8.3573
8.3260
8.2923
8.1217
8.0213
7.9573
7.7995
7.7854
7.7160
7.6411
7.6224
7.5935
7.5739
7.5467
7.5300
7.4955
7.4786
7.4530
7.4293
7.4087
7.3729
7.3574
7.2727
7.2578
6.6425
6.6124
6.5815
6.5600
6.5257
6.4900
6.3070
6.2726
6.2096
6.1765
3.7361
3.6224
3.5557
3.3786
2.5208
1.7139
CF3
I-
N+
N
Cl
2.1159
1.2814
6.4315
1.9027
0.9483
6.2253
12.0000
8
6
4
2
[ppm]
[rel]
50
40
30
20
10
0

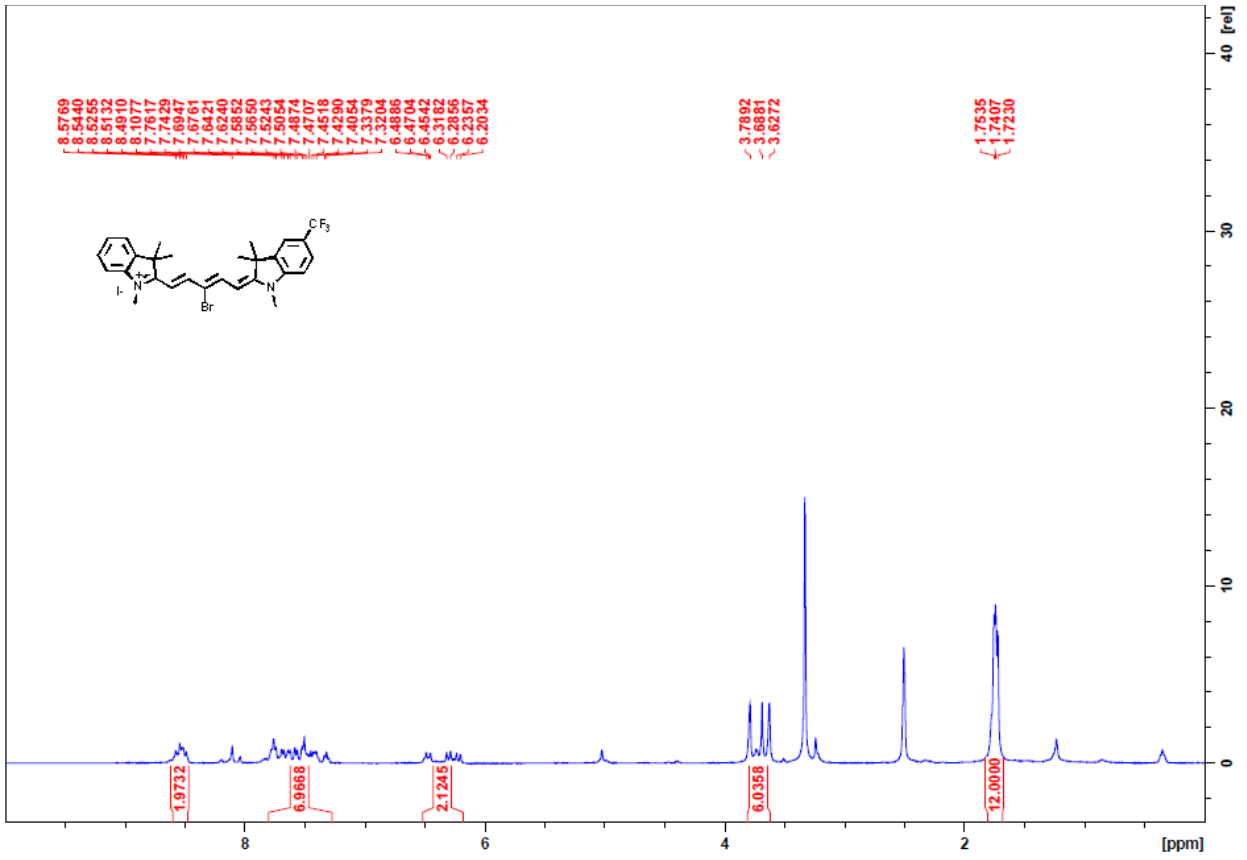
8.5769
8.5440
8.5255
8.5132
8.4910
8.1077
7.7617
7.7429
7.6947
7.6761
7.6421
7.6240
7.5852
7.5650
7.5243
7.5054
7.4874
7.4707
7.4518
7.4290
7.4054
7.3379
7.3204
6.4886
6.4704
6.4542
6.3182
6.2856
6.2357
6.2034
3.7892
3.6881
3.6272
1.7535
1.7407
1.7230
CF3
I-
N+
N
Br
1.9732
6.9668
2.1245
6.0358
12.0000
8
6
4
2
[ppm]
40
30
20
10
0
[rel]

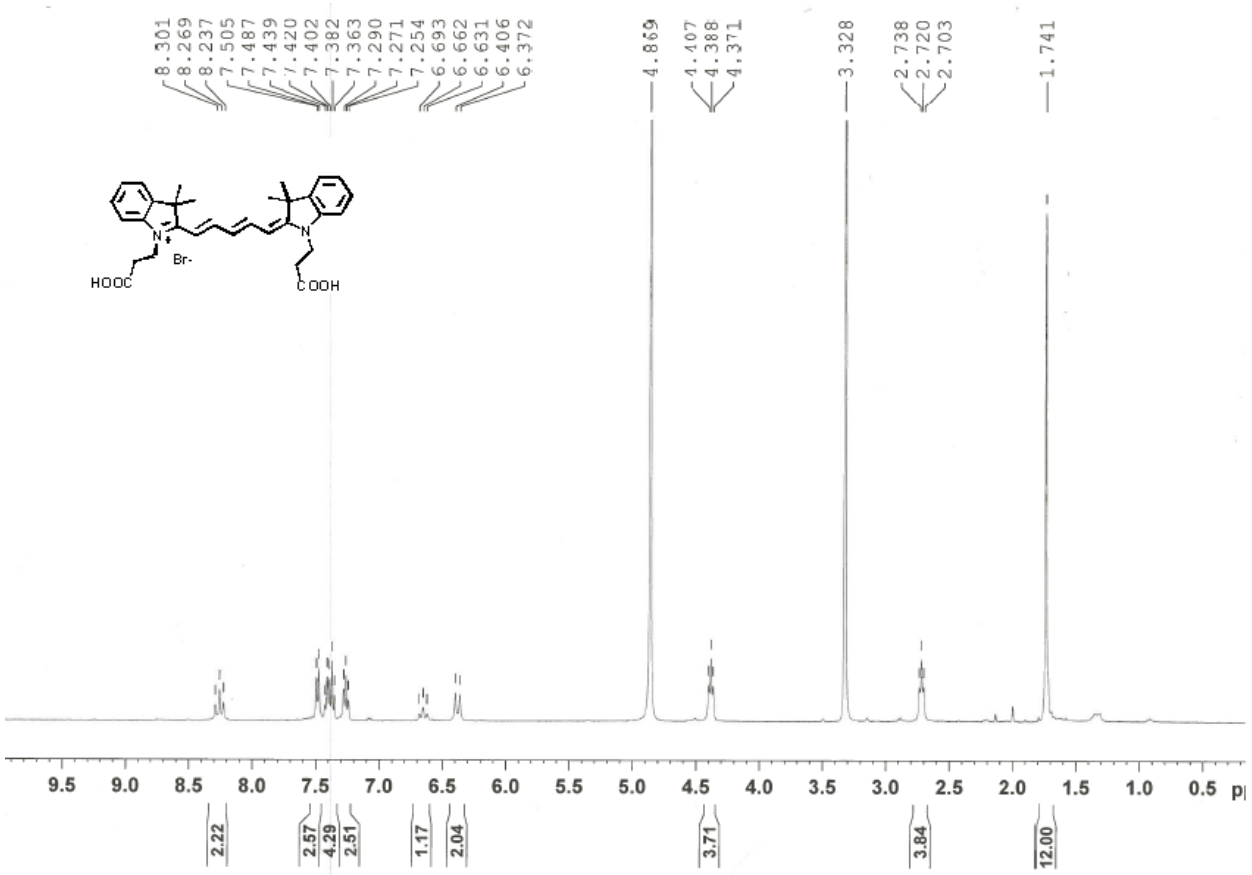
8.301
8.269
8.237
7.505
7.487
7.439
7.420
7.402
7.382
7.363
7.290
7.271
7.254
6.693
6.662
6.631
6.406
6.372
4.869
4.407
4.388
4.371
3.328
2.738
2.720
2.703
1.741
HOOC
Br-
COOH
9.5
9.0
8.5
8.0
7.5
7.0
6.5
6.0
5.5
5.0
4.5
4.0
3.5
3.0
2.5
2.0
1.5
1.0
0.5
2.22
2.57
4.29
2.51
1.17
2.04
3.71
3.84
12.00

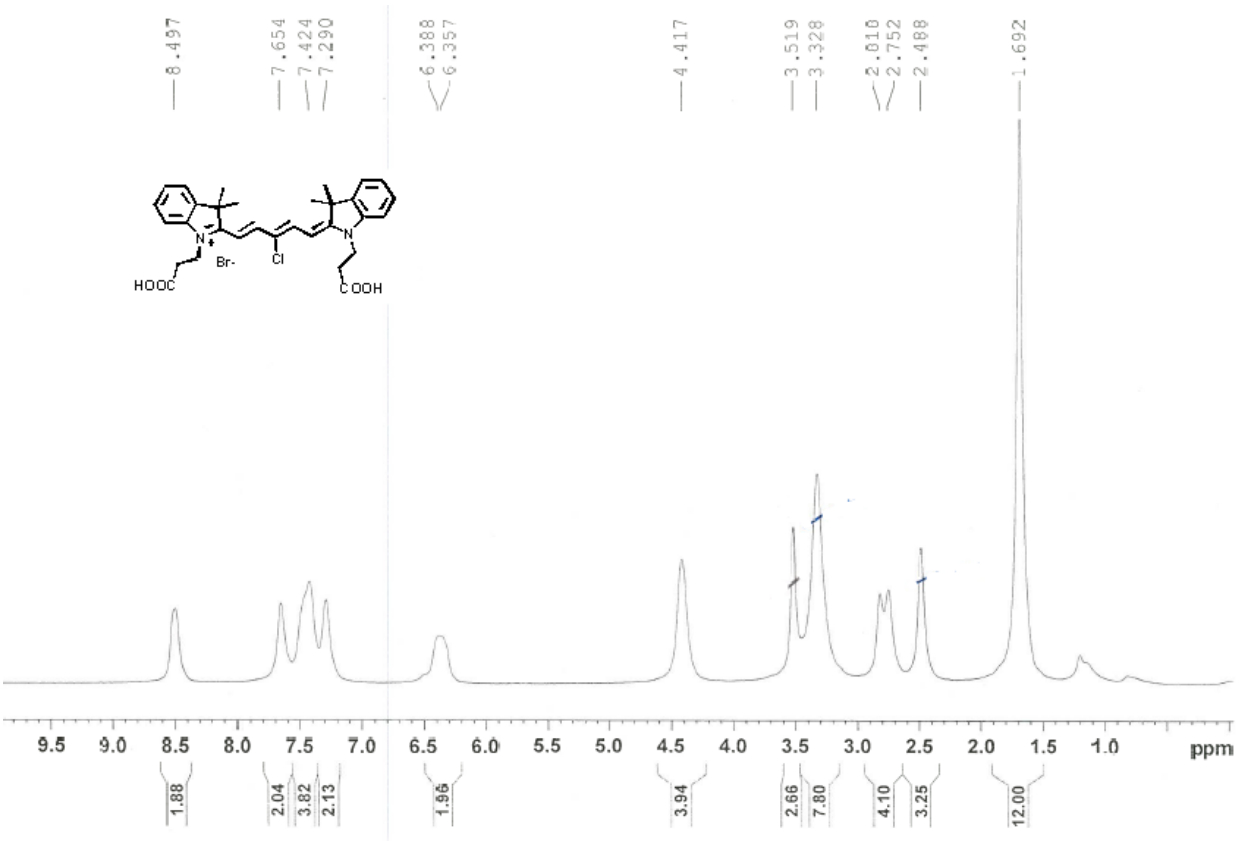
8.497
7.654
7.424
7.290
6.388
6.357
4.417
3.519
3.328
2.810
2.752
2.488
1.692
HOOC
Br-
Cl
COOH
9.5
9.0
8.5
8.0
7.5
7.0
6.5
6.0
5.5
5.0
4.5
4.0
3.5
3.0
2.5
2.0
1.5
1.0
ppm
1.88
2.04
3.82
2.13
1.96
3.94
2.66
7.80
4.10
3.25
12.00

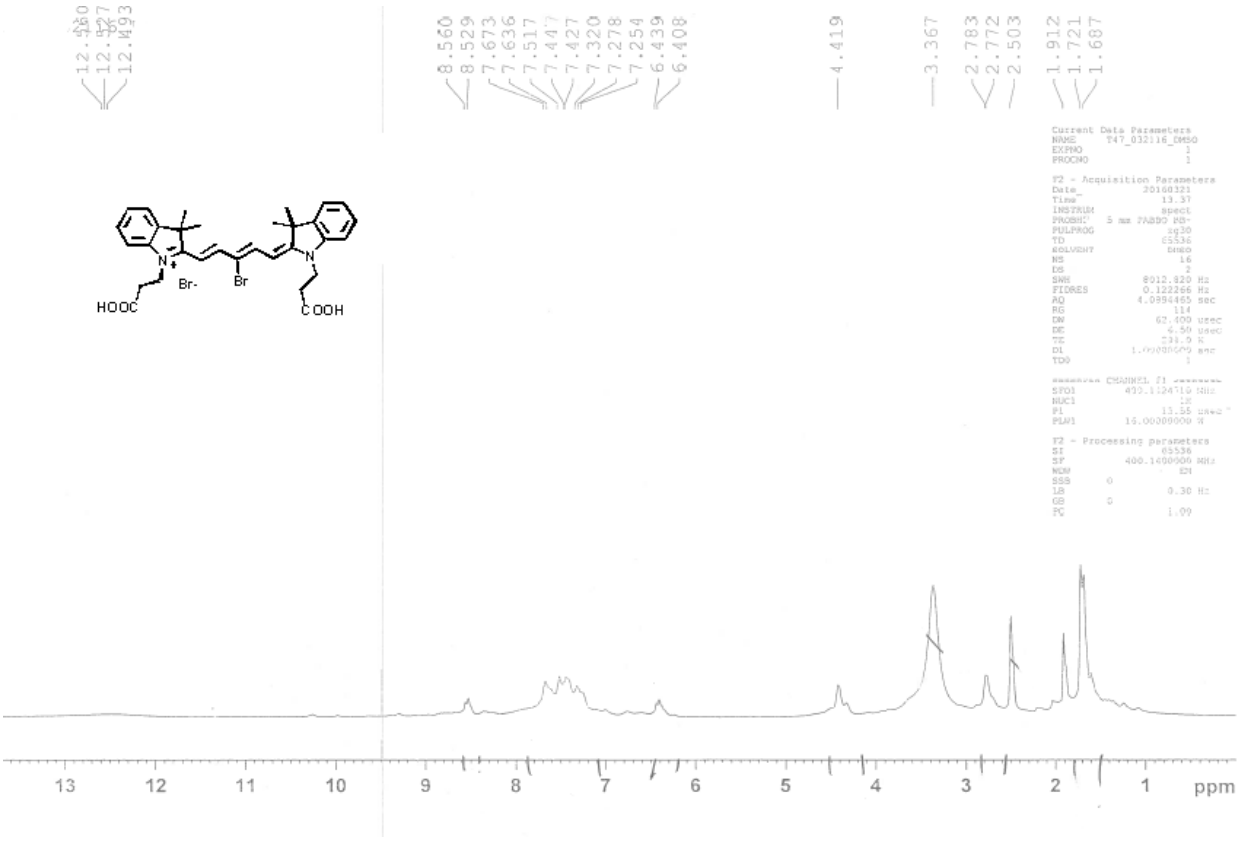
12.493
8.560
8.529
7.673
7.636
7.517
7.447
7.427
7.320
7.278
7.254
6.439
6.408
4.419
3.367
2.783
2.772
2.503
1.912
1.721
1.687
Br-
Br
HOOC
COOH
13
12
11
10
9
8
7
6
5
4
3
2
1
ppm

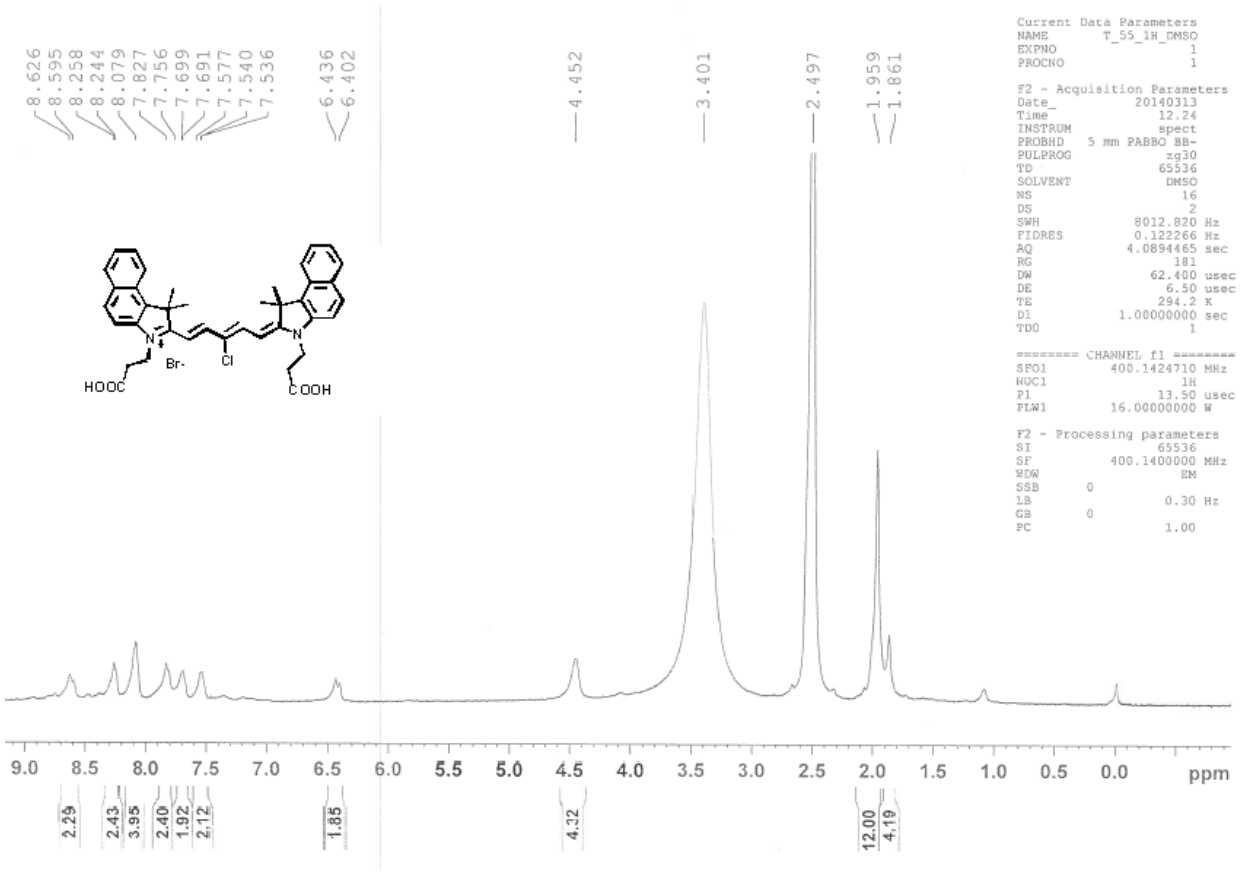
8.626
8.595
8.258
8.244
8.079
7.827
7.756
7.699
7.691
7.577
7.540
7.536
6.436
6.402
4.452
3.401
2.497
1.959
1.861
Br-
Cl
HOOC
COOH
Current Data Parameters
NAME T_55_1H_DMSO
EXPNO 1
PROCNO 1
F2 - Acquisition Parameters
Date_ 20140313
Time 12.24
INSTRUM spect
PROBHD 5 mm PABBO BB-
PULPROG zg30
TD 65536
SOLVENT DMSO
NS 16
DS 2
SWH 8012.820 Hz
FIDRES 0.122266 Hz
AQ 4.0894465 sec
RG 181
DW 62.400 usec
DE 6.50 usec
TE 294.2 K
D1 1.00000000 sec
TD0 1
======== CHANNEL f1 ========
SFO1 400.1424710 MHz
NUC1 1H
P1 13.50 usec
PLW1 16.00000000 W
F2 - Processing parameters
SI 65536
SF 400.1400000 MHz
WDW EM
SSB 0
LB 0.30 Hz
GB 0
PC 1.00
9.0 8.5 8.0 7.5 7.0 6.5 6.0 5.5 5.0 4.5 4.0 3.5 3.0 2.5 2.0 1.5 1.0 0.5 0.0 ppm
2.29
2.43
3.95
2.40
1.92
2.12
1.85
4.32
12.00
4.19

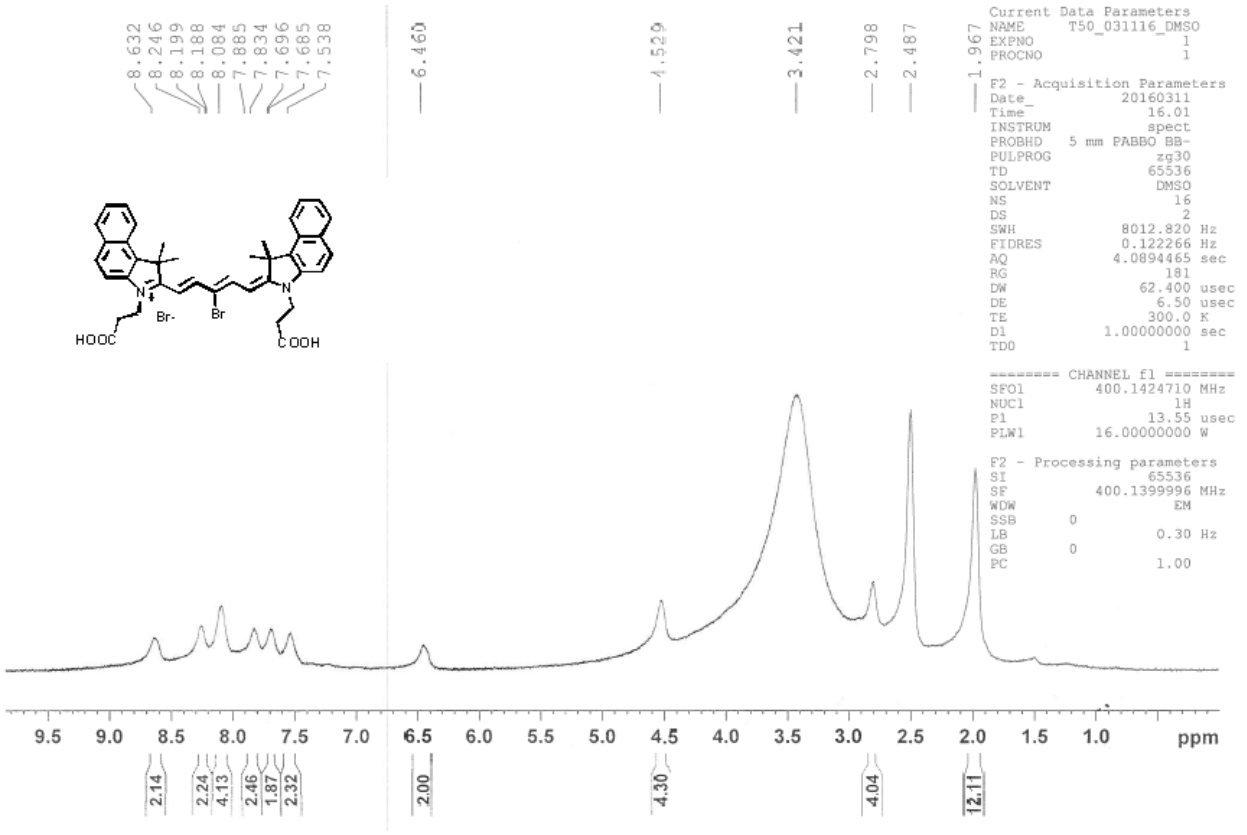
8.632
8.246
8.199
8.188
8.084
7.885
7.834
7.696
7.685
7.538
6.460
4.529
3.421
2.798
2.487
1.967
HOOC
Br-
Br
COOH
Current Data Parameters
NAME T50_031116_DMSO
EXPNO 1
PROCNO 1
F2 - Acquisition Parameters
Date_ 20160311
Time 16.01
INSTRUM spect
PROBHD 5 mm PABBO BB-
PULPROG zg30
TD 65536
SOLVENT DMSO
NS 16
DS 2
SWH 8012.820 Hz
FIDRES 0.122266 Hz
AQ 4.0894465 sec
RG 181
DW 62.400 usec
DE 6.50 usec
TE 300.0 K
D1 1.00000000 sec
TD0 1
======== CHANNEL f1 ========
SFO1 400.1424710 MHz
NUC1 1H
P1 13.55 usec
PLW1 16.00000000 W
F2 - Processing parameters
SI 65536
SF 400.1399996 MHz
WDW EM
SSB 0
LB 0.30 Hz
GB 0
PC 1.00
9.5 9.0 8.5 8.0 7.5 7.0 6.5 6.0 5.5 5.0 4.5 4.0 3.5 3.0 2.5 2.0 1.5 1.0 ppm
2.14
2.24
4.13
2.46
1.87
2.32
2.00
4.30
4.04
12.11

Appendix A.2 ^{13}C NMR Spectra

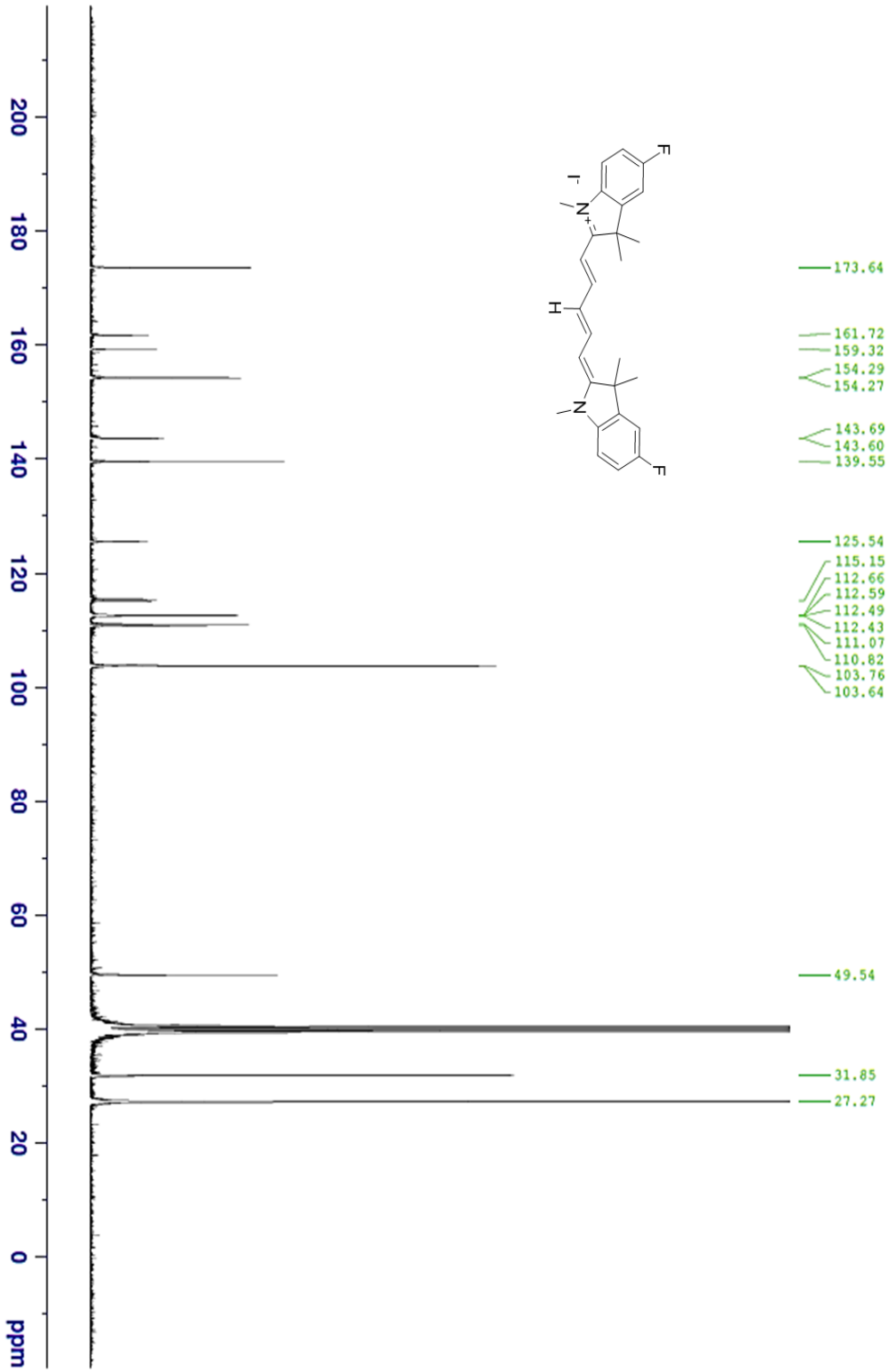
200
180
160
140
120
100
80
60
40
20
0
ppm
F
I-
N+
H
N
F
173.64
161.72
159.32
154.29
154.27
143.69
143.60
139.55
125.54
115.15
112.66
112.59
112.49
112.43
111.07
110.82
103.76
103.64
49.54
31.85
27.27

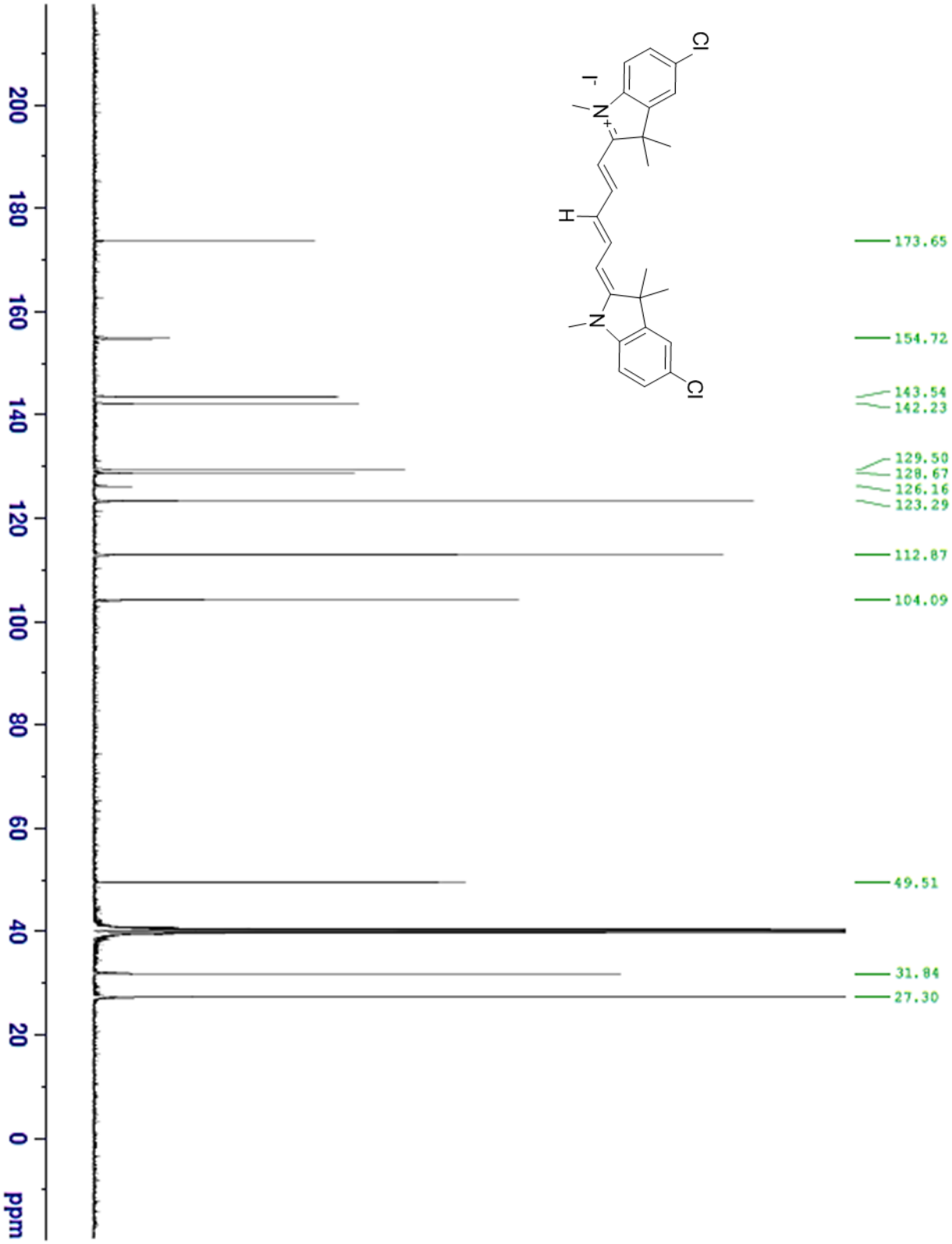
Cl
I⁻
N⁺
H
N
Cl
173.65
154.72
143.54
142.23
129.50
128.67
126.16
123.29
112.87
104.09
49.51
31.84
27.30
200
180
160
140
120
100
80
60
40
20
0
ppm

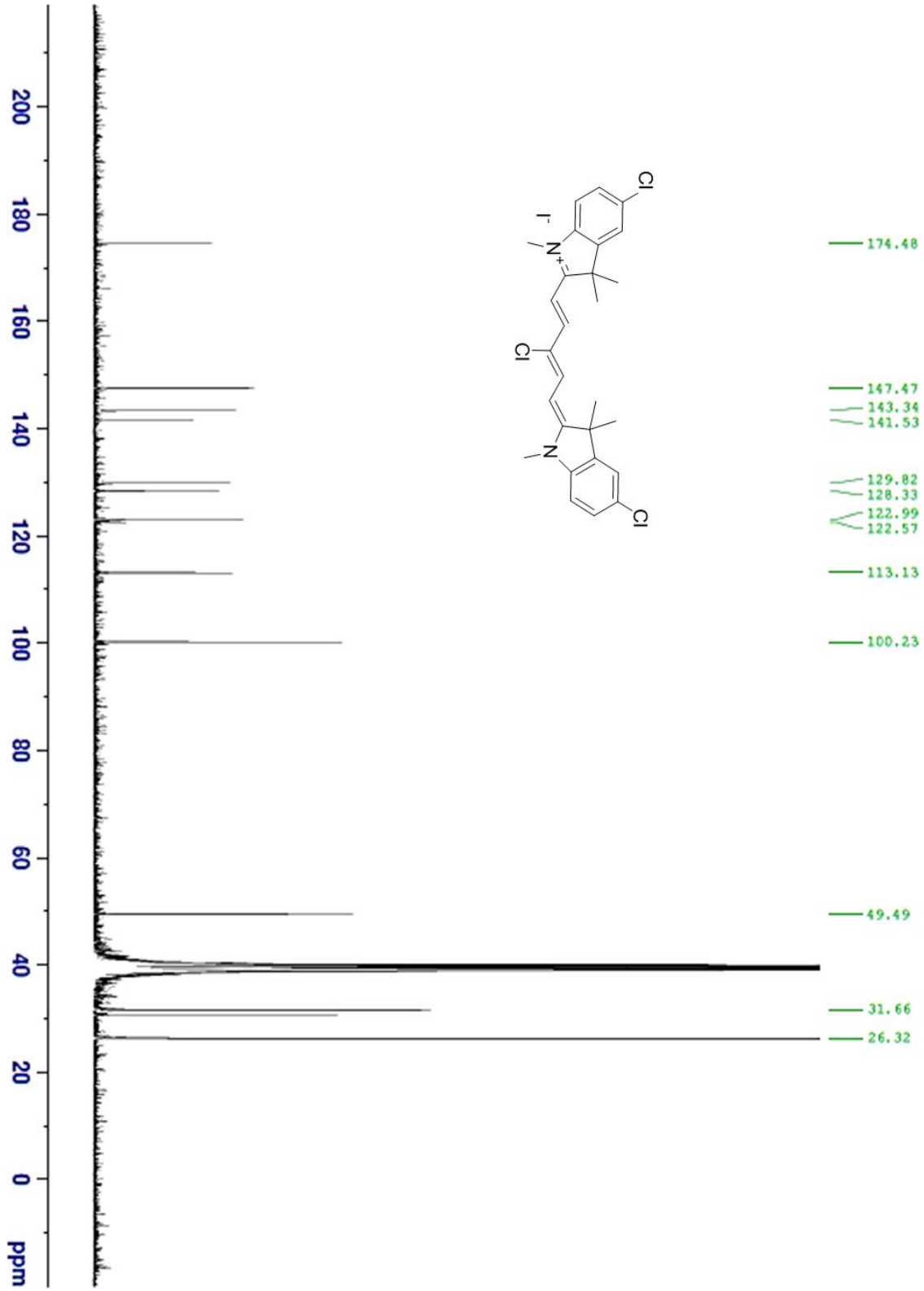
Cl
I⁻
N⁺
Cl
N
Cl
174.48
147.47
143.34
141.53
129.82
128.33
122.99
122.57
113.13
100.23
49.49
31.66
26.32
200
180
160
140
120
100
80
60
40
20
0
ppm

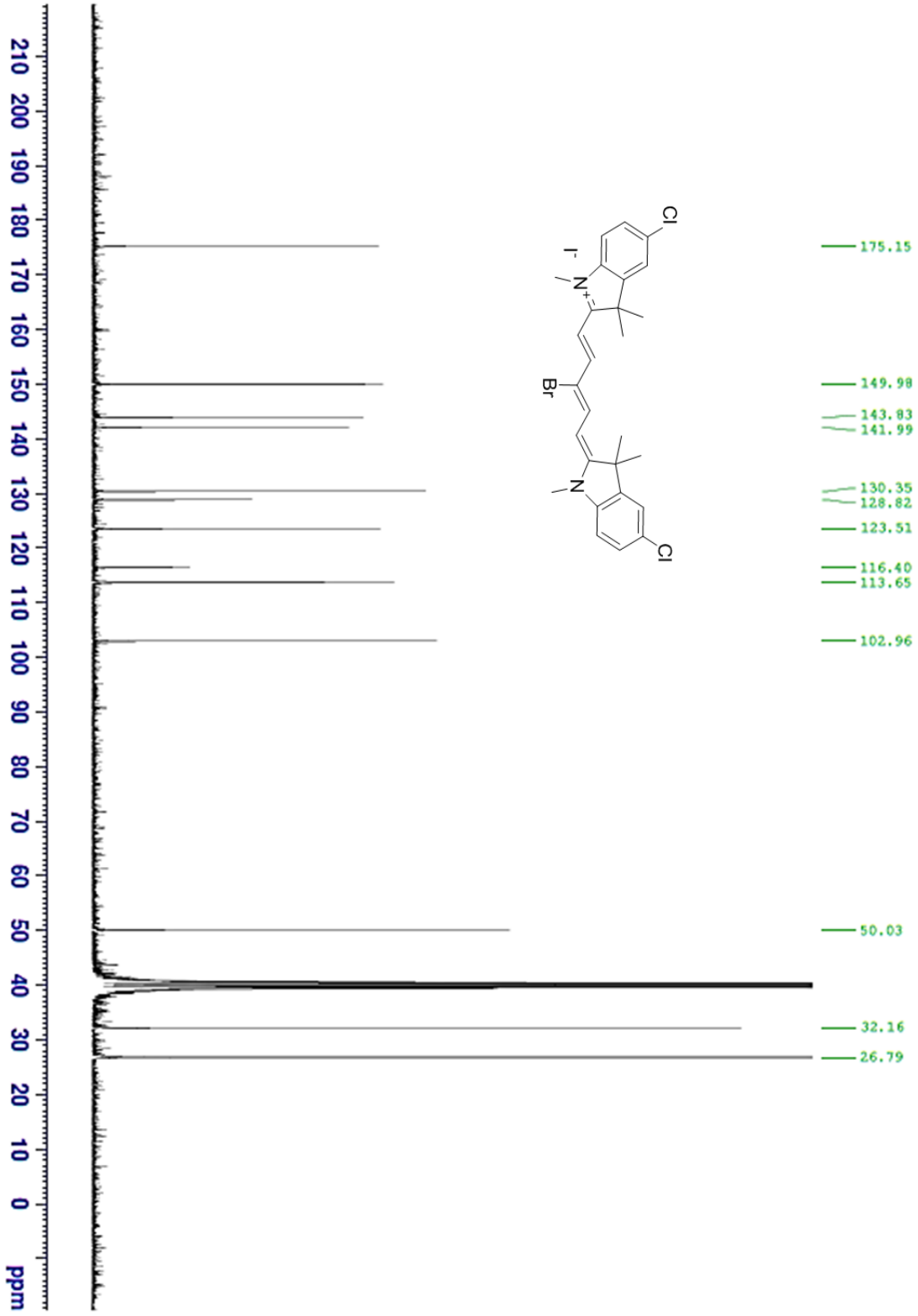
175.15
149.98
143.83
141.99
130.35
128.82
123.51
116.40
113.65
102.96
50.03
32.16
26.79
Cl
I-
N+
Br
N
Cl
210 200 190 180 170 160 150 140 130 120 110 100 90 80 70 60 50 40 30 20 10 0 ppm

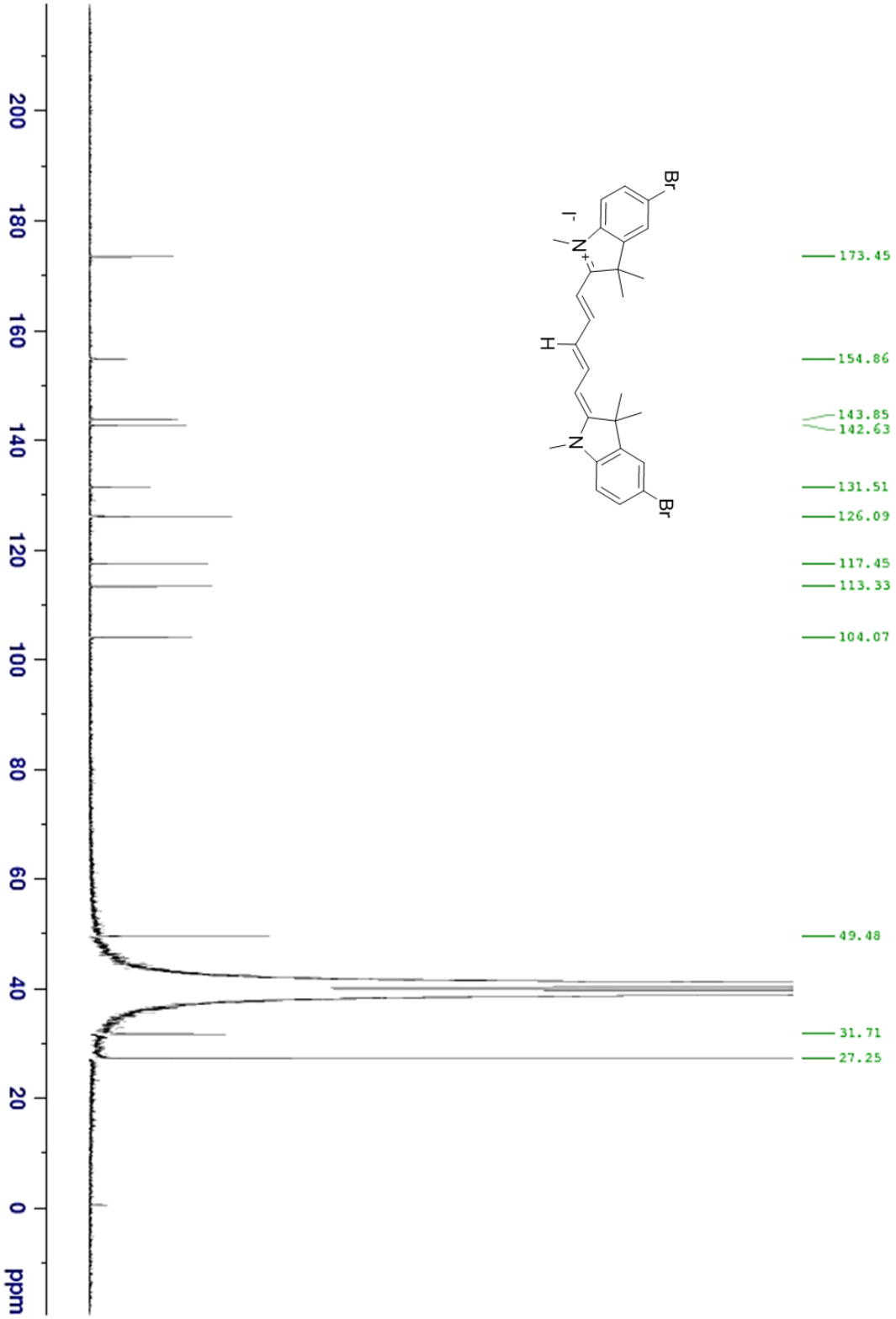
Br
I-
N+
H
N
Br
173.45
154.86
143.85
142.63
131.51
126.09
117.45
113.33
104.07
49.48
31.71
27.25
200
180
160
140
120
100
80
60
40
20
0
ppm

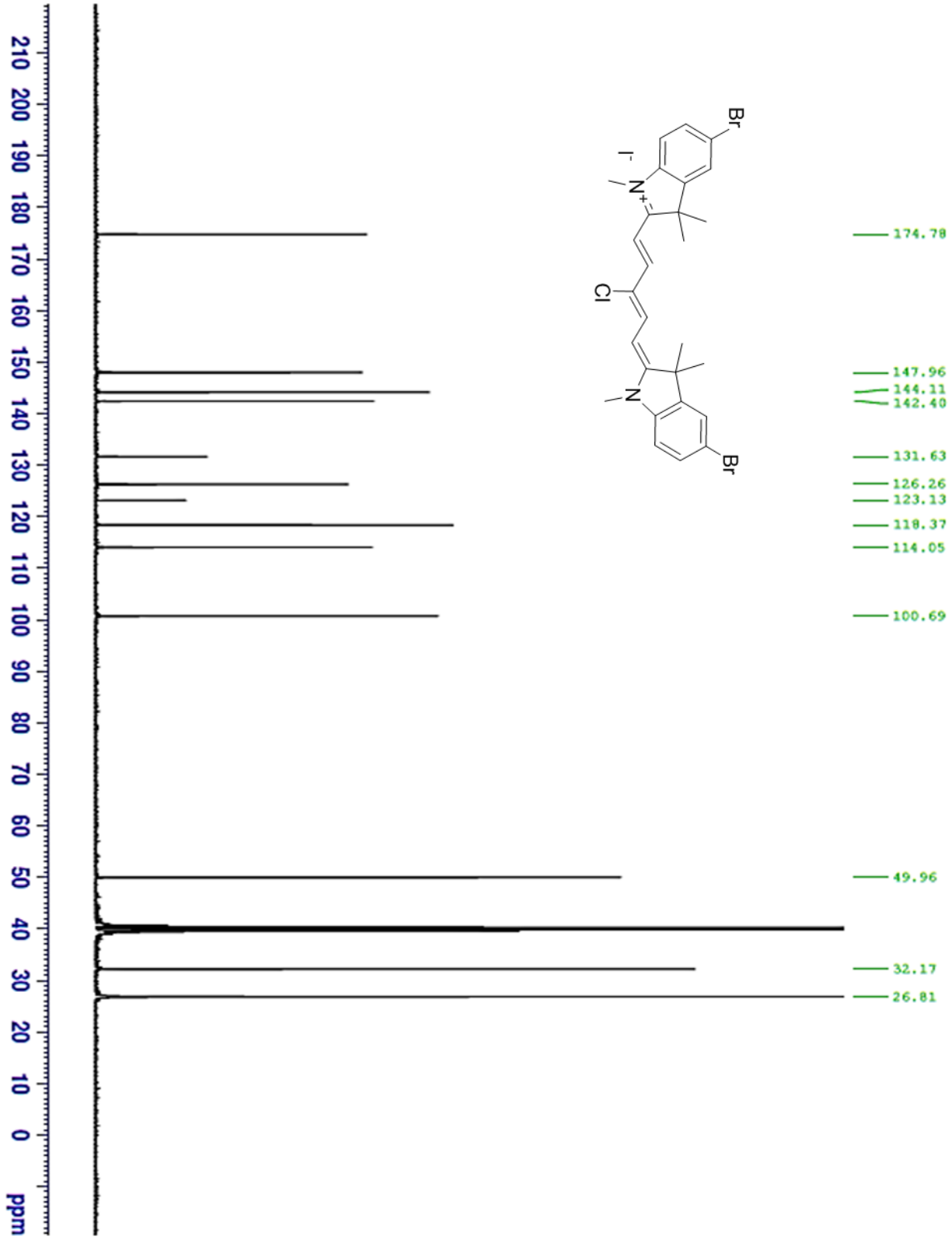
Br
I⁻
N⁺
Cl
N
Br
174.78
147.96
144.11
142.40
131.63
126.26
123.13
118.37
114.05
100.69
49.96
32.17
26.81
210 200 190 180 170 160 150 140 130 120 110 100 90 80 70 60 50 40 30 20 10 0 ppm

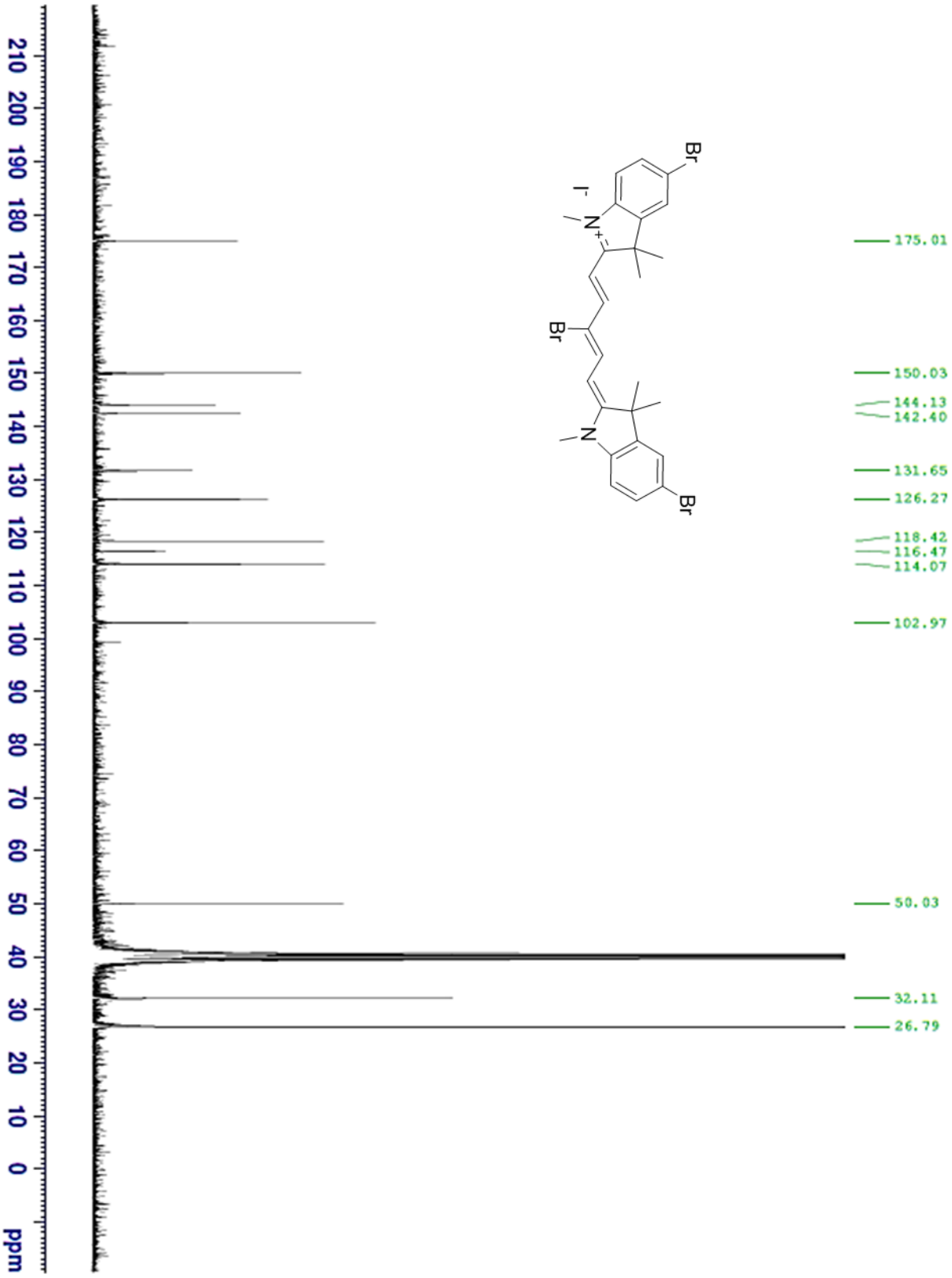
175.01
150.03
144.13
142.40
131.65
126.27
118.42
116.47
114.07
102.97
50.03
32.11
26.79
Br
Br
Br
I-
N+
N
210 200 190 180 170 160 150 140 130 120 110 100 90 80 70 60 50 40 30 20 10 0 ppm

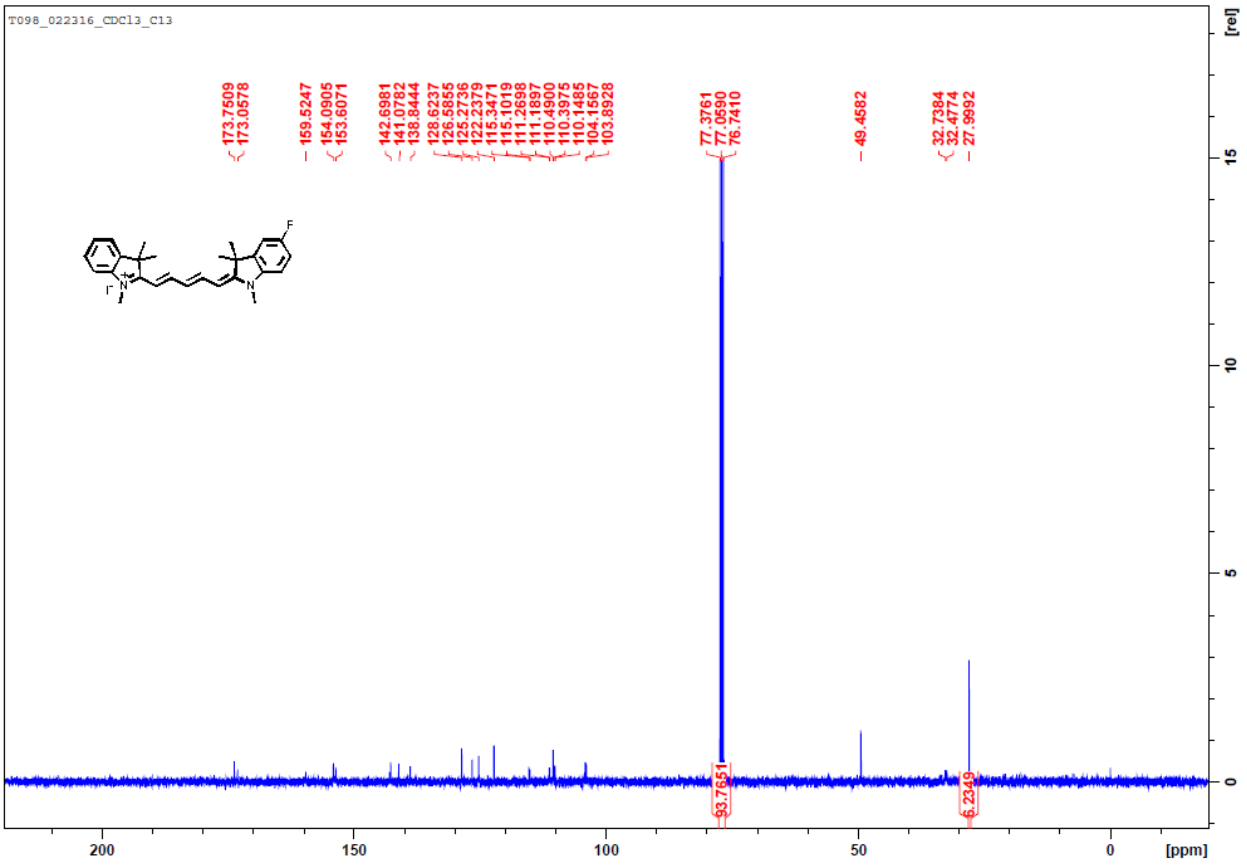
T098_022316_CDCl3_C13
173.7509
173.0578
159.5247
154.0905
153.6071
142.6981
141.0782
138.8444
128.6237
126.5855
125.2736
122.2379
115.3471
115.1019
111.2698
111.1897
110.4900
110.3975
110.1485
104.1567
103.8928
77.3761
77.0590
76.7410
49.4582
32.7384
32.4774
27.9992
F
I⁻
N
93.7651
6.2349
200
150
100
50
0
[ppm]
[rel]
15
10
5
0

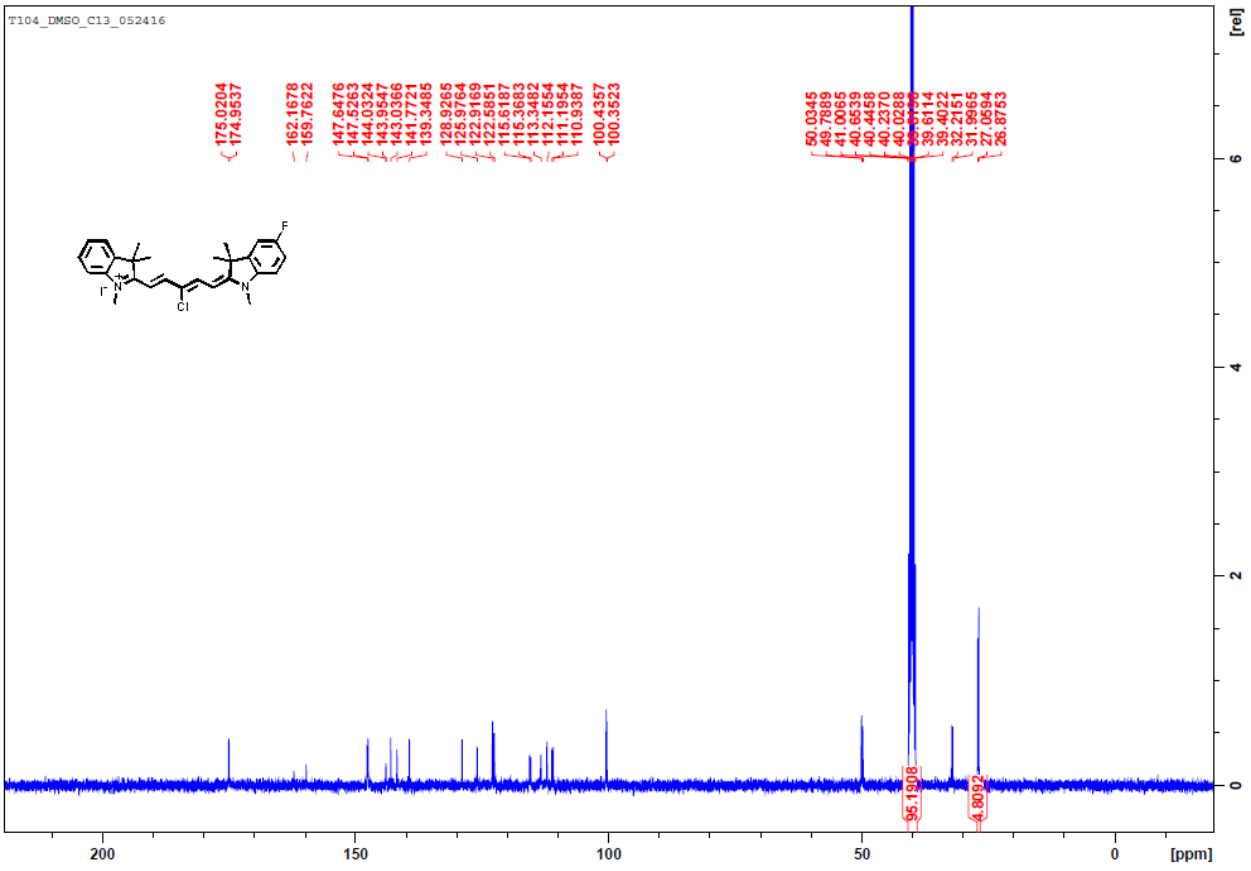
T104_DMSO_C13_052416
175.0204
174.9537
162.1678
159.7622
147.6476
147.5263
144.0324
143.9947
143.0366
141.7721
139.3485
128.9265
125.9764
122.9169
122.5851
115.6187
115.3683
113.3482
112.1554
111.1954
110.9387
100.4357
100.3523
50.0345
49.7889
41.0065
40.6539
40.4458
40.2370
40.0288
39.8199
39.6114
39.4022
32.2151
31.9965
27.0694
26.8753
95.1908
4.8092
[rel]
[ppm]
200
150
100
50
0
2
4
6
F
Cl
N

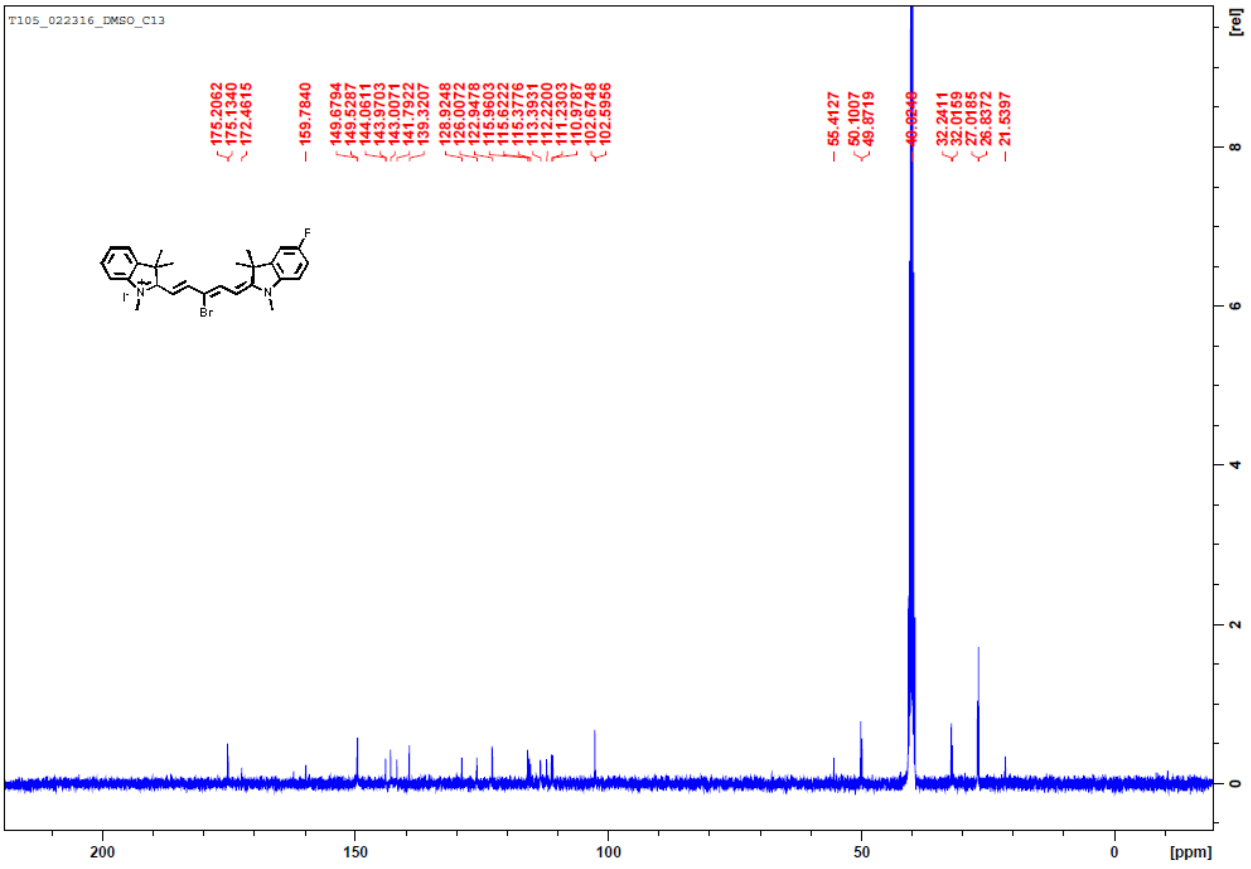
T105_022316_DMSO_C13
175.2062
175.1340
172.4615
159.7840
149.6794
149.5287
144.0611
143.9703
143.0071
141.7922
139.3207
128.9248
126.0072
122.9478
115.9603
115.6222
115.3776
113.3931
112.2200
111.2303
110.9787
102.6748
102.5956
55.4127
50.1007
49.8719
40.0240
32.2411
32.0159
27.0185
26.8372
21.5397
F
Br
I
[rel]
[ppm]
200
150
100
50
0

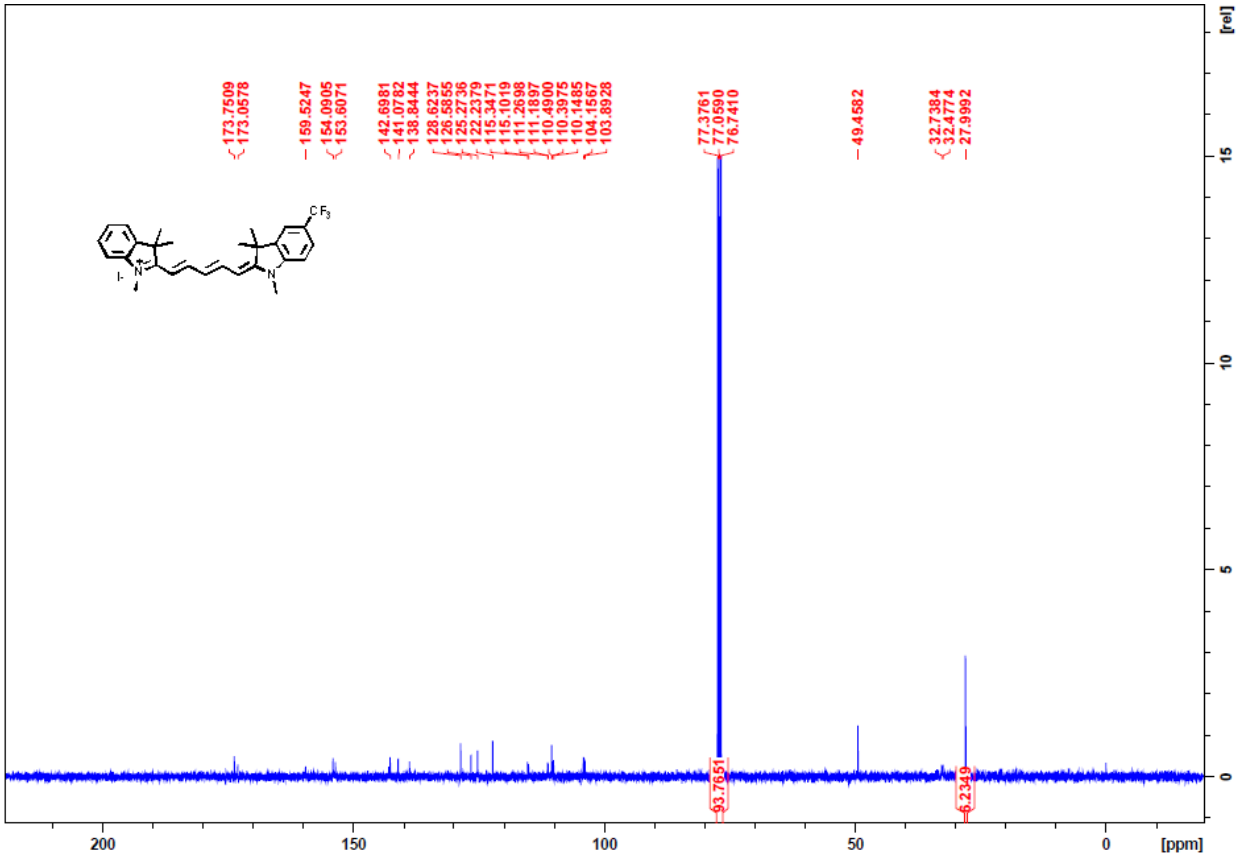
173.7509
173.0578
159.5247
154.0905
153.6071
142.6981
141.0782
138.8444
128.6237
126.5855
125.2736
122.2379
115.3471
115.1019
111.2698
111.1897
110.4990
110.3975
110.1485
104.1567
103.8928
77.3761
77.0590
76.7410
49.4582
32.7384
32.4774
27.9992
93.7651
6.2349
CF3
I-
N+
N
[rel]
15
10
5
0
200
150
100
50
0
[ppm]

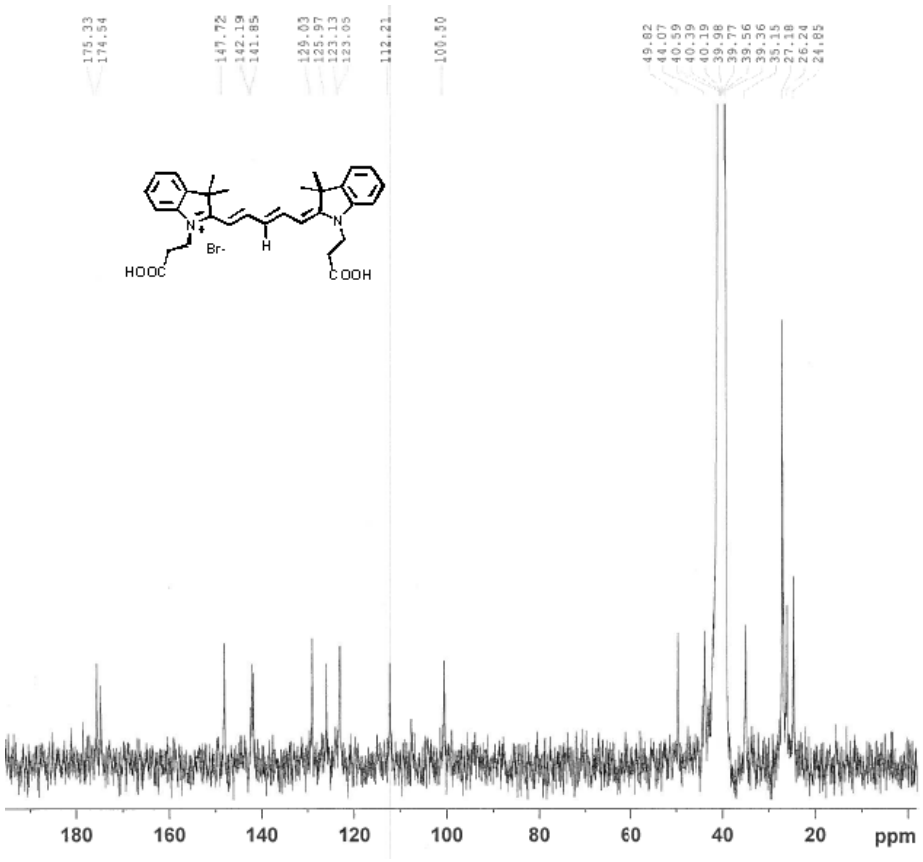


```
Current Data Parameters
NAME        t85 DMSO 13C
EXPNO                  1
PROCNO                 1

F2 - Acquisition Parameters
Date_           20160318
Time              10.13
INSTRUM           spect
PROBHD   5 mm PABBO BB-
PULPROG         zgpg30
TD                65536
SOLVENT            DMSO
NS                   935
DS                     4
SWH           24038.461 Hz
FIDRES         0.366798 Hz
AQ             1.3631488 sec
RG                   203
DW                20.800 usec
DE                 6.50 usec
TE                298.2 K
D1            2.00000000 sec
D11           0.03000000 sec
TD0                    1

======== CHANNEL f1 ========
SFO1        100.6253441 MHz
NUC1                13C
P1                 9.00 usec
PLW1         62.00000000 W

======== CHANNEL f2 ========
SFO2        400.1416006 MHz
NUC2                1H
CPDPRG[2         waltz16
PCPD2             90.00 usec
PLW2         16.00000000 W
PLW12         0.36267000 W
PLW13         0.29376000 W

F2 - Processing parameters
SI                 32768
SF          100.6152830 MHz
WDW                EM
SSB       0
LB                 5.00 Hz
GB        0
PC                 1.40
```

Appendix A.3 ^{19}F NMR Spectra

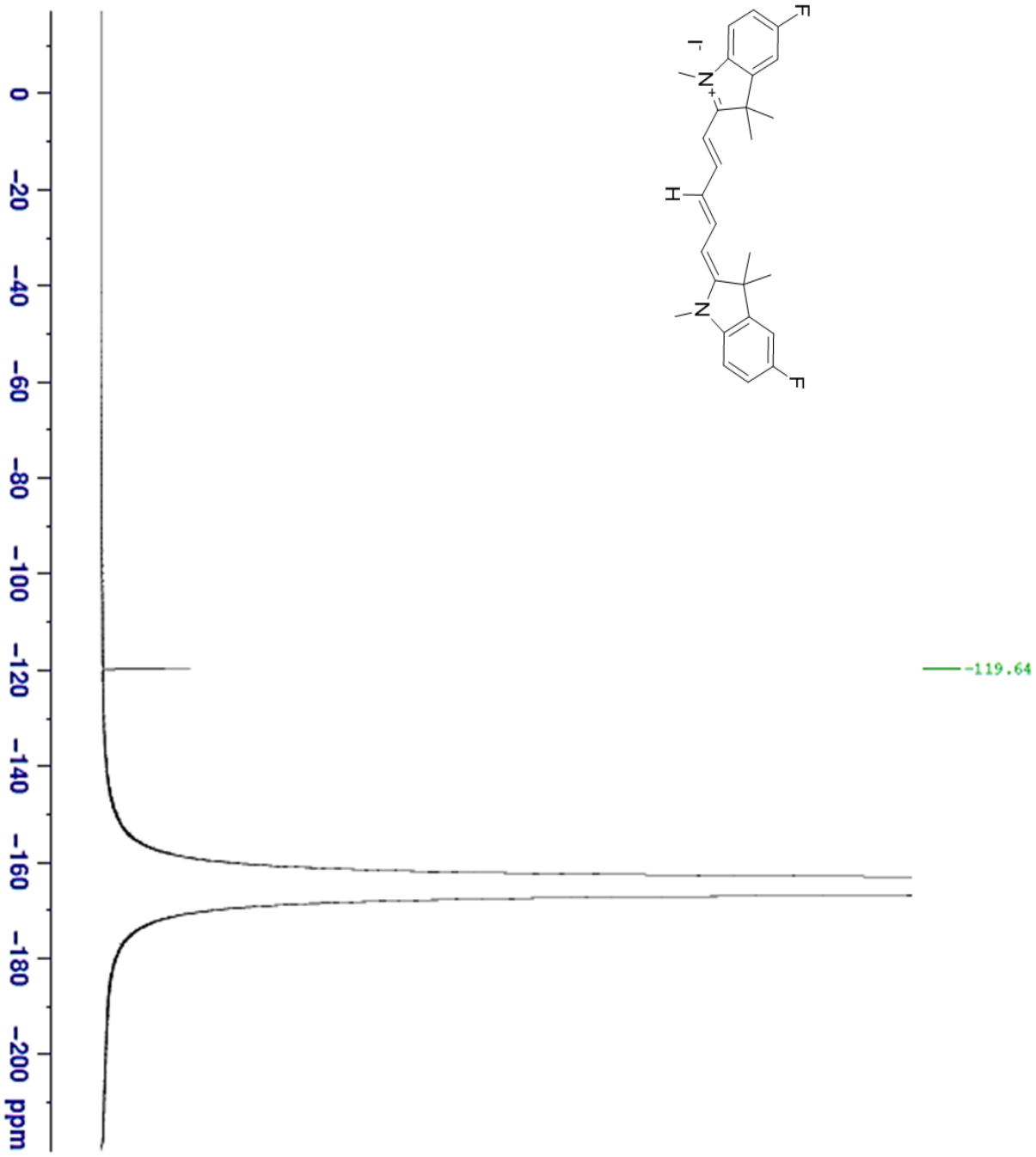

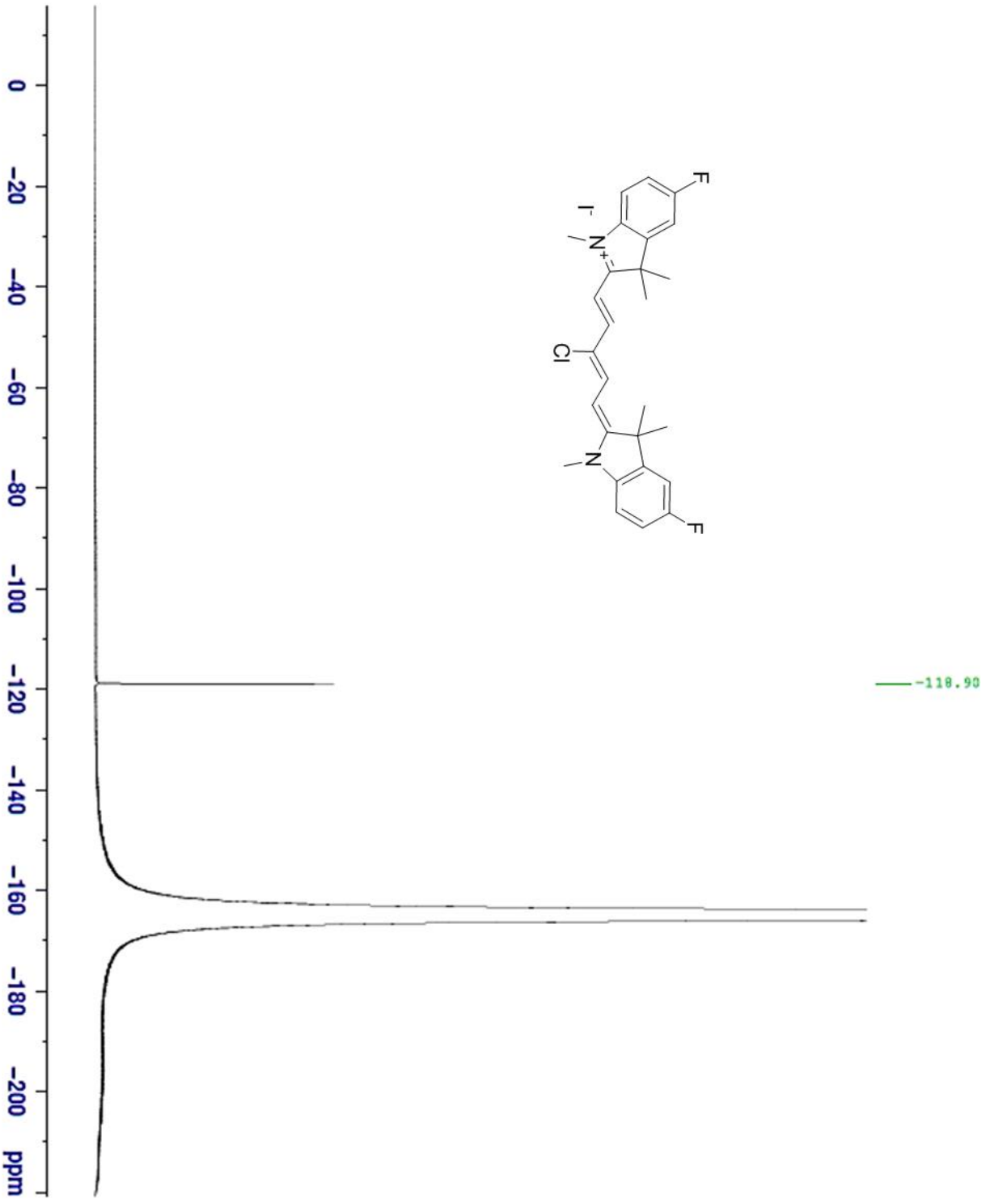
0
-20
-40
-60
-80
-100
-120
-140
-160
-180
-200
ppm
-118.90
F
I⁻
N⁺
Cl
N
F

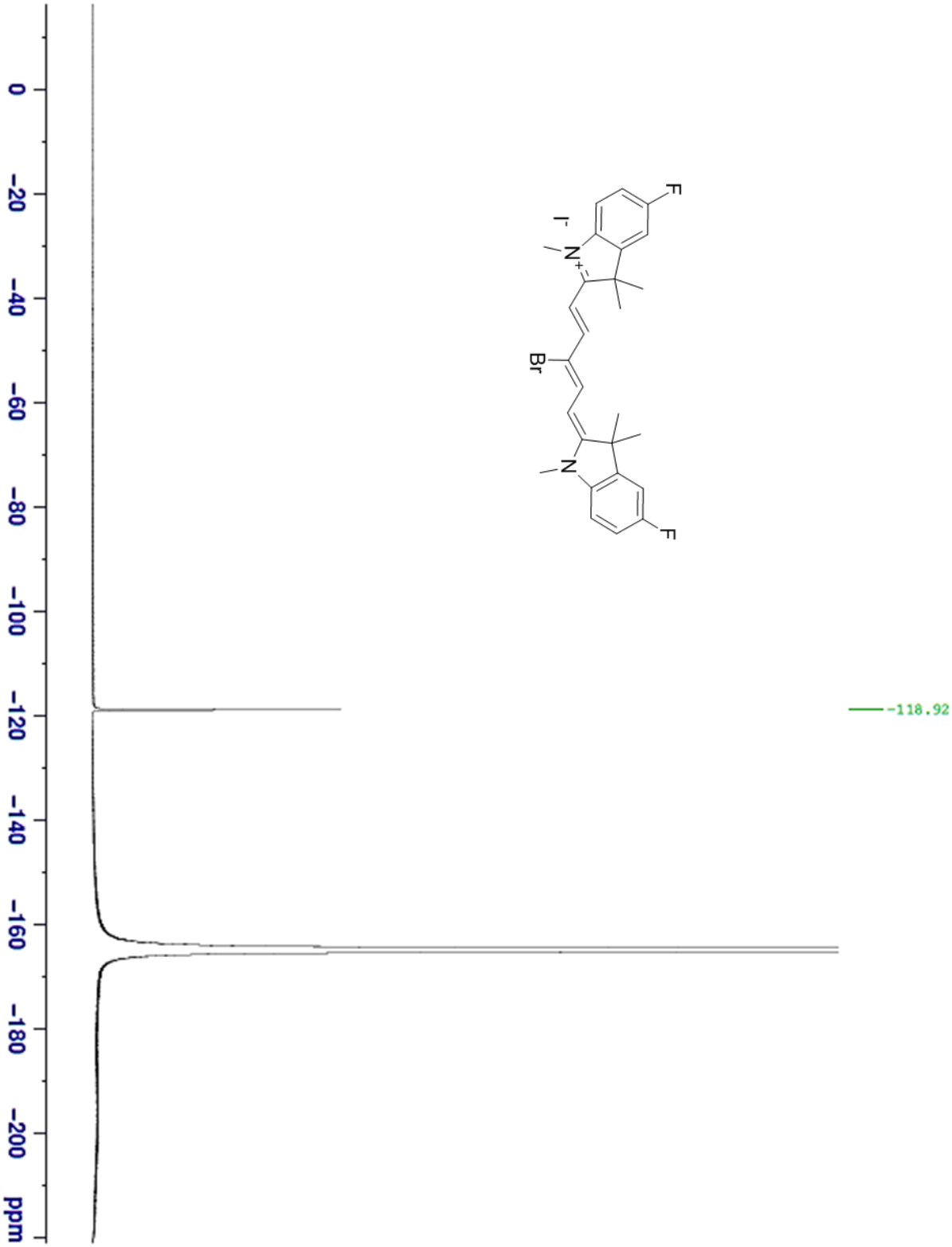
0
-20
-40
-60
-80
-100
-120
-140
-160
-180
-200
ppm
-118.92
F
I-
N+
Br
N
F

Appendix A.3 Mass Spectra

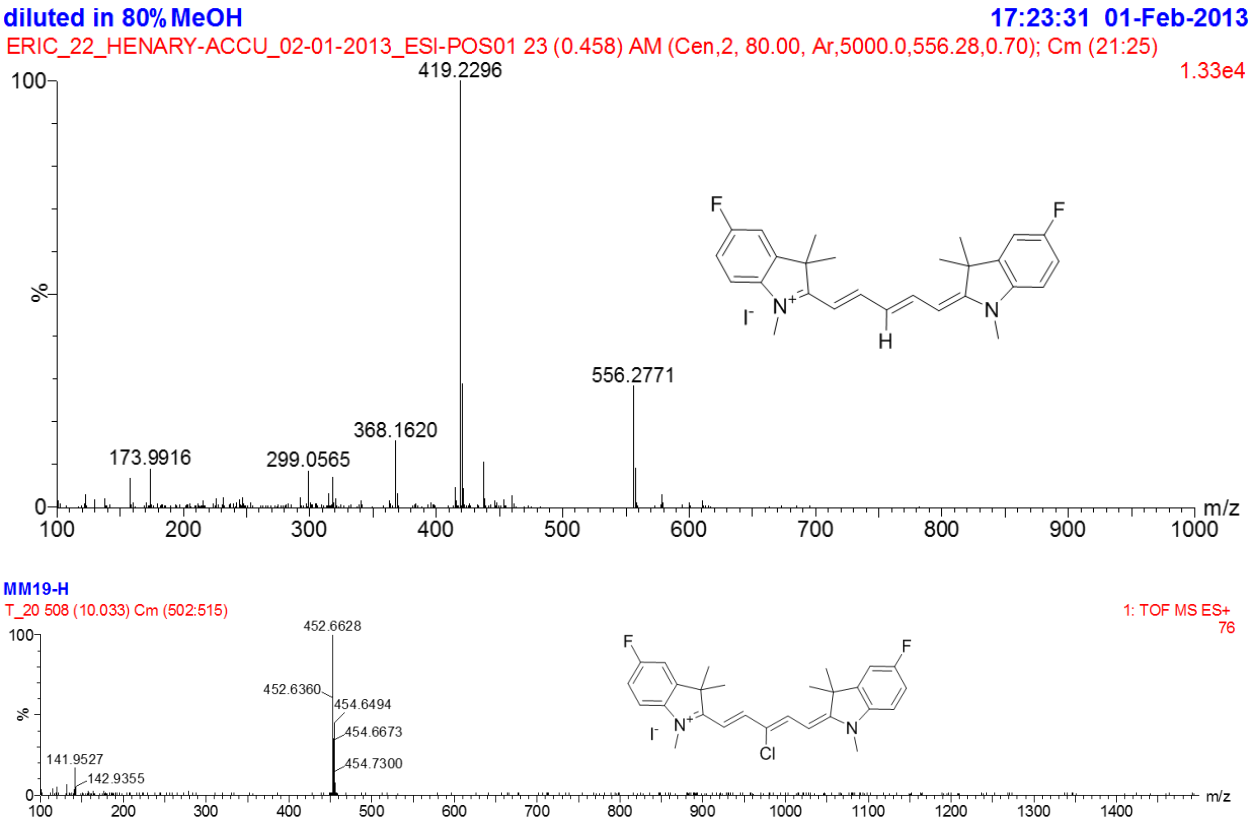

diluted in 80% MeOH **15:58:33 01-Feb-2013**

ERIC_34_HENARY-ACCU_02-01-2013_ESI-POS 45 (0.897) AM (Cen,2, 80.00, Ar,5000.0,556.28,0.70); Sm (SG, 3x3.00); Cm (

9.20e3

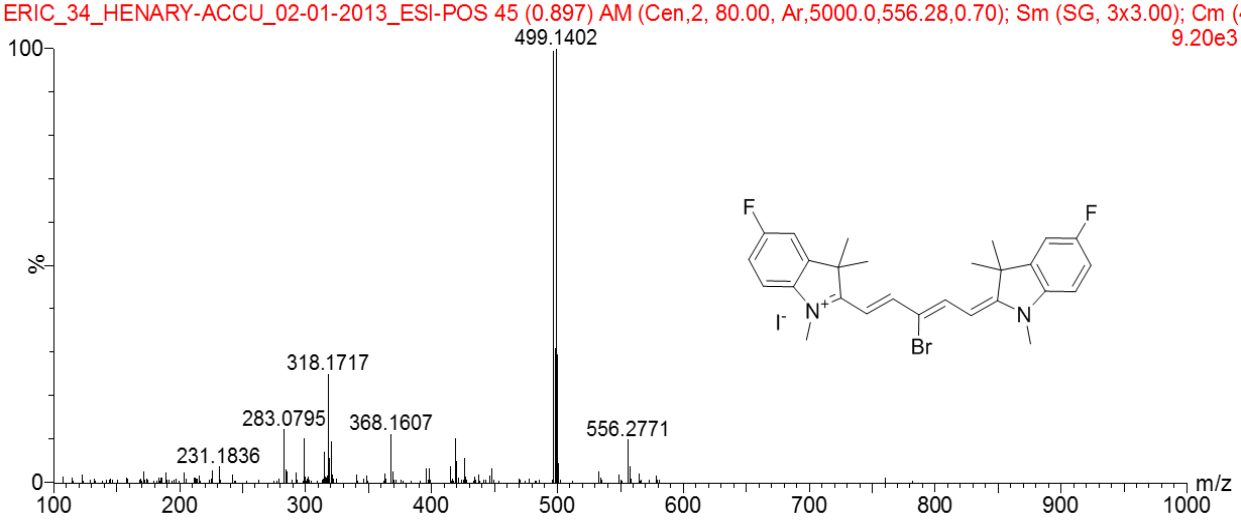

diluted in 80% MeOH **17:14:54 01-Feb-2013**

ERIC_23_HENARY-ACCU_02-01-2013_ESI-POS01 72 (1.429) AM (Cen,2, 80.00, Ar,5000.0,556.28,0.70); Cm (72:78)

9.98e3

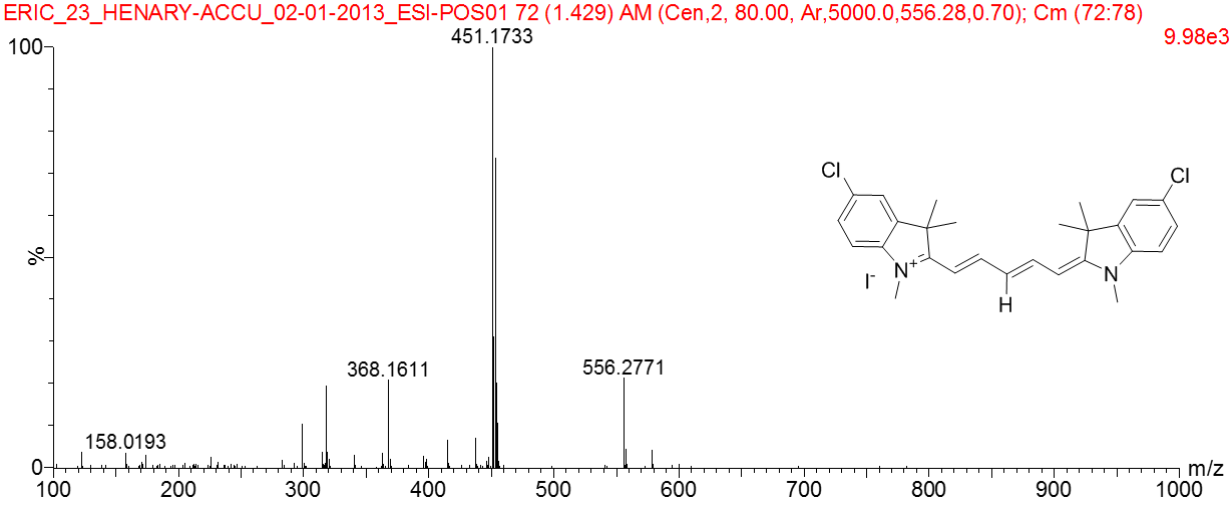

diluted in 80% MeOH **16:44:36 01-Feb-2013**

ERIC_29_HENARY-ACCU_02-01-2013_ESI-POS 120 (2.394) AM (Cen,2, 80.00, Ar,5000.0,556.28,0.70); Cm (117:123)

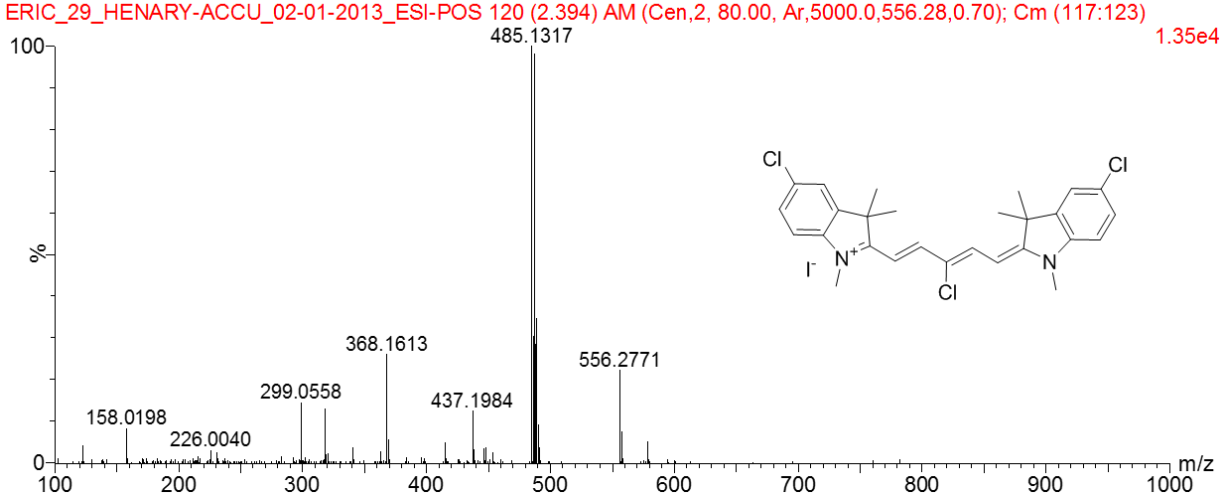

diluted in 80% MeOH **15:36:17 01-Feb-2013**

ERIC_35_HENARY-ACCU_02-01-2013_ESI-POS 113 (2.254) AM (Cen,2, 80.00, Ar,5000.0,556.28,0.70); Sm (SG, 3x3.00); Cm

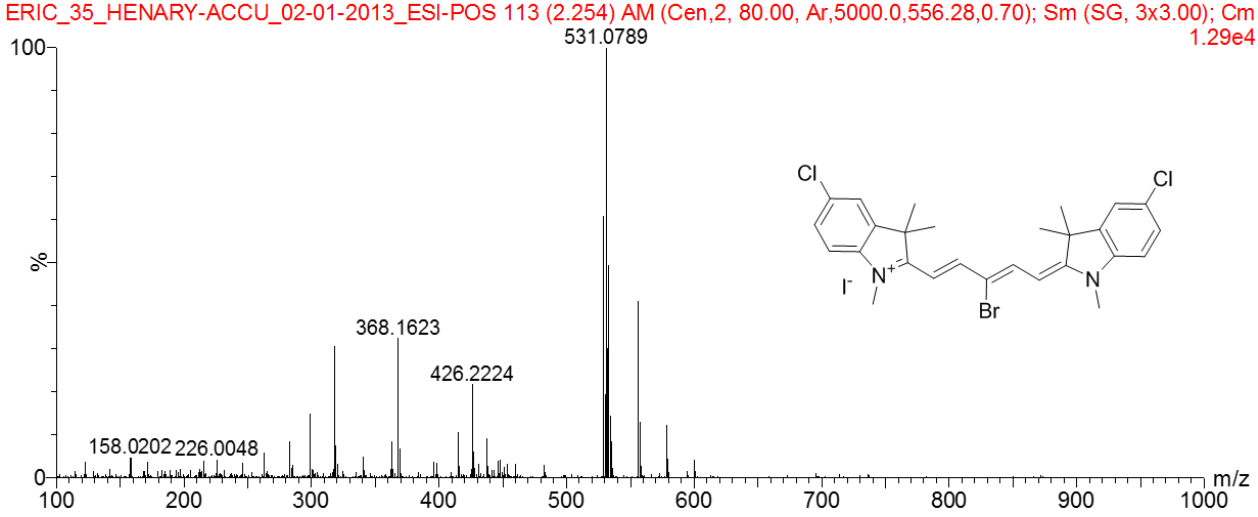

diluted in 80% MeOH **17:10:50 01-Feb-2013**

ERIC_24_HENARY-ACCU_02-01-2013_ESI-POS01 22 (0.437) AM (Cen,2, 80.00, Ar,5000.0,556.28,0.70); Sm (SG, 3x3.00); Cm

1.96e4

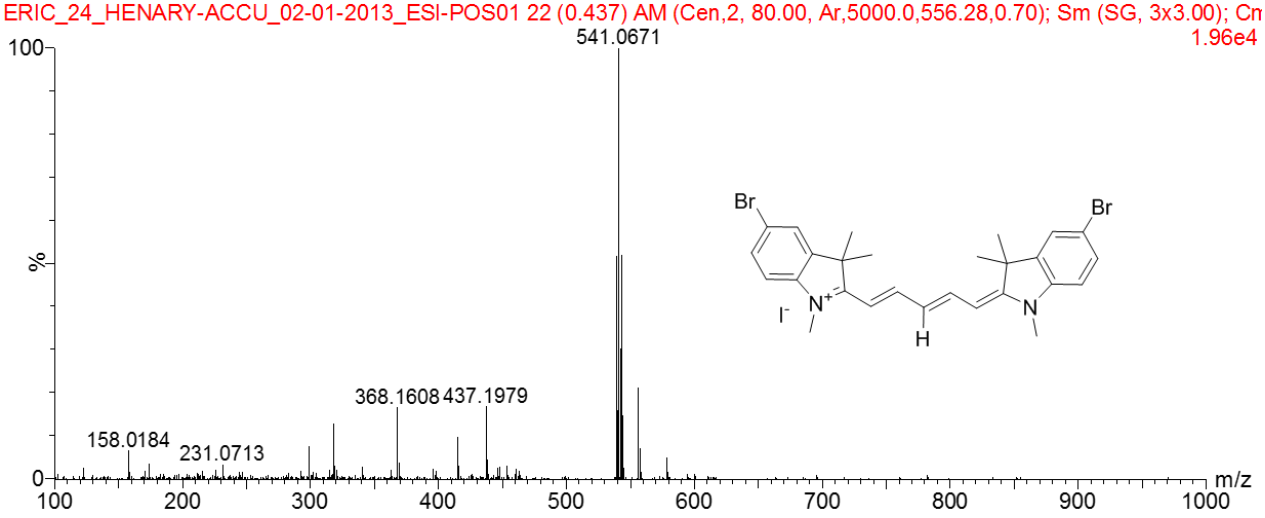

diluted in 80% MeOH **16:40:08 01-Feb-2013**

ERIC_30_HENARY-ACCU_02-01-2013_ESI-POS 39 (0.779) AM (Cen,2, 80.00, Ar,5000.0,556.28,0.70); Sm (SG, 3x3.00); Cm (

1.49e4

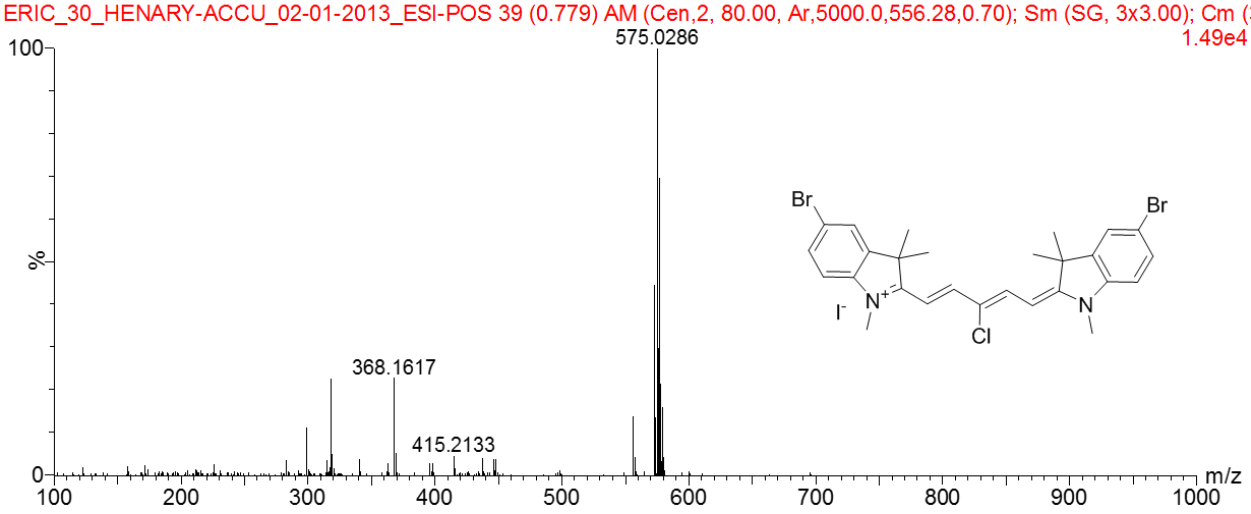

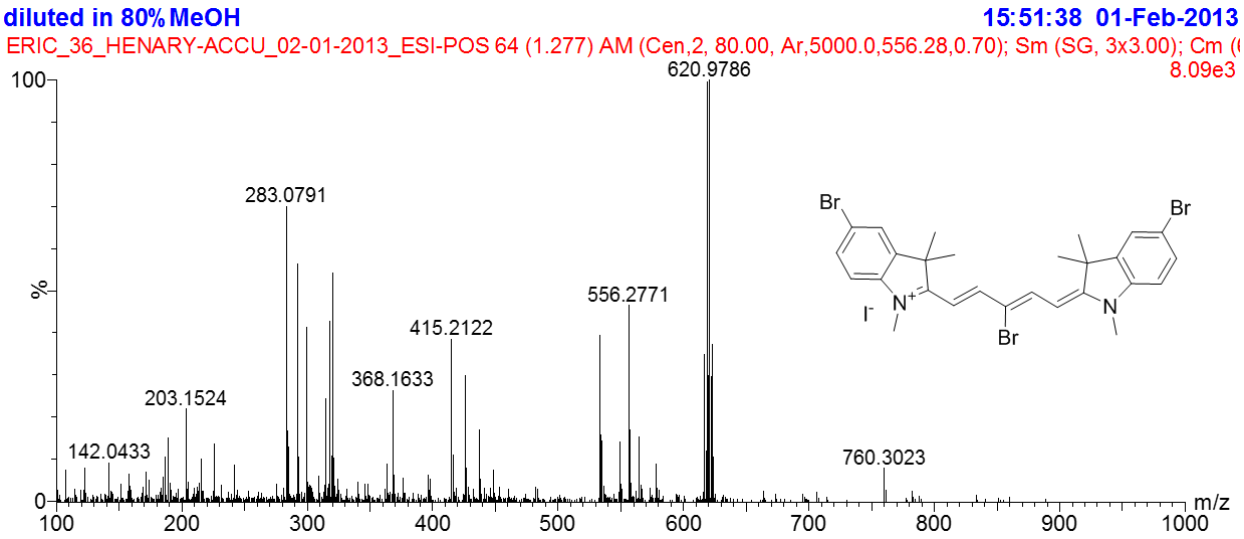

Appendix A.4 Absorbance and Fluorescence Spectra

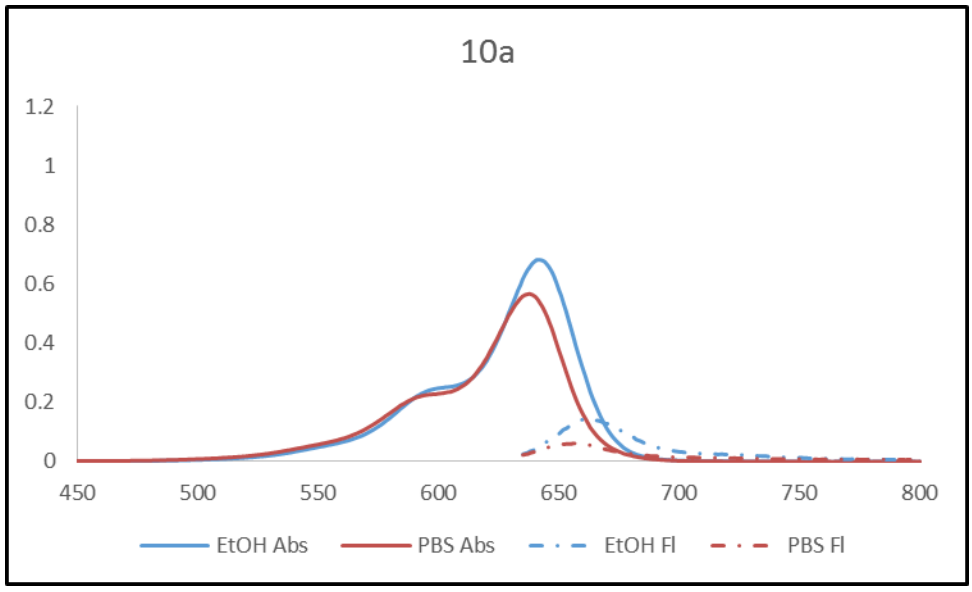

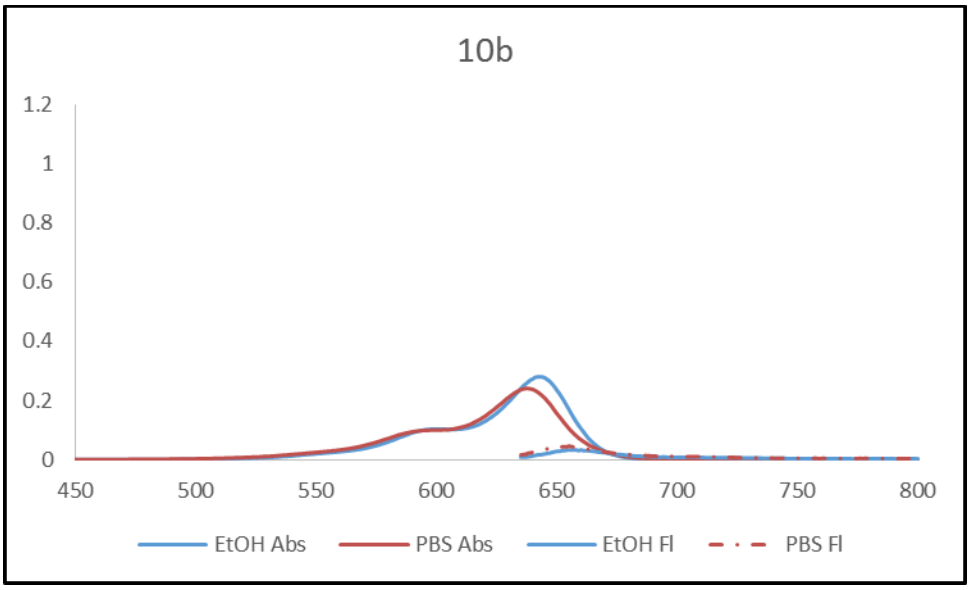
10b
1.2
1
0.8
0.6
0.4
0.2
0
450
500
550
600
650
700
750
800
EtOH Abs
PBS Abs
EtOH Fl
PBS Fl

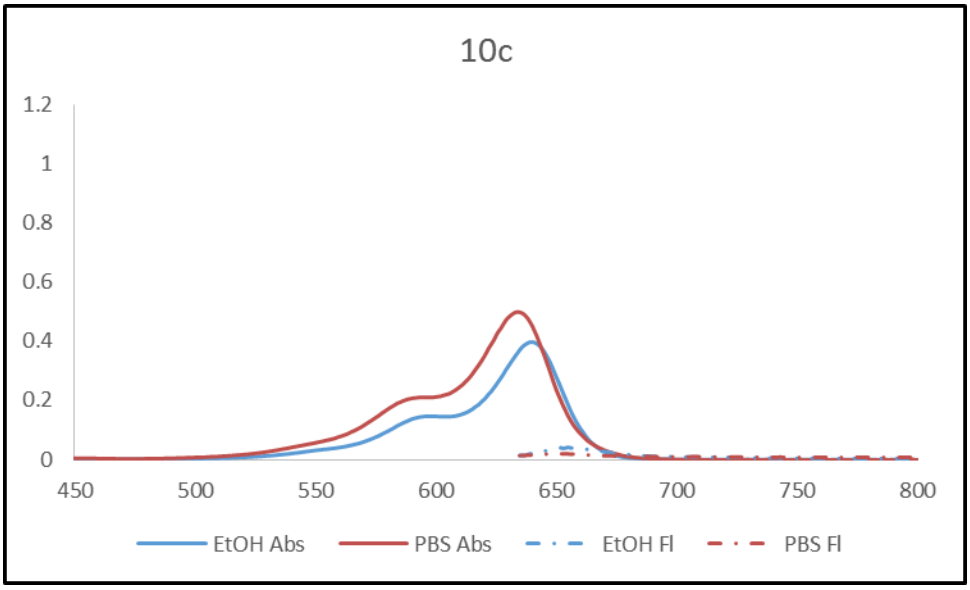
10c
1.2
1
0.8
0.6
0.4
0.2
0
450
500
550
600
650
700
750
800
EtOH Abs
PBS Abs
EtOH Fl
PBS Fl

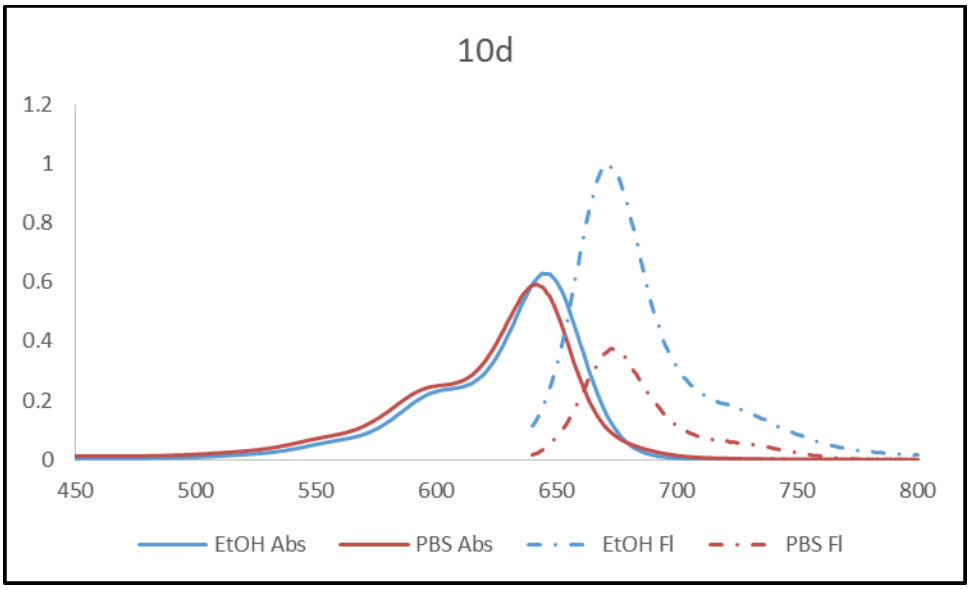
10d
1.2
1
0.8
0.6
0.4
0.2
0
450
500
550
600
650
700
750
800
EtOH Abs
PBS Abs
EtOH Fl
PBS Fl

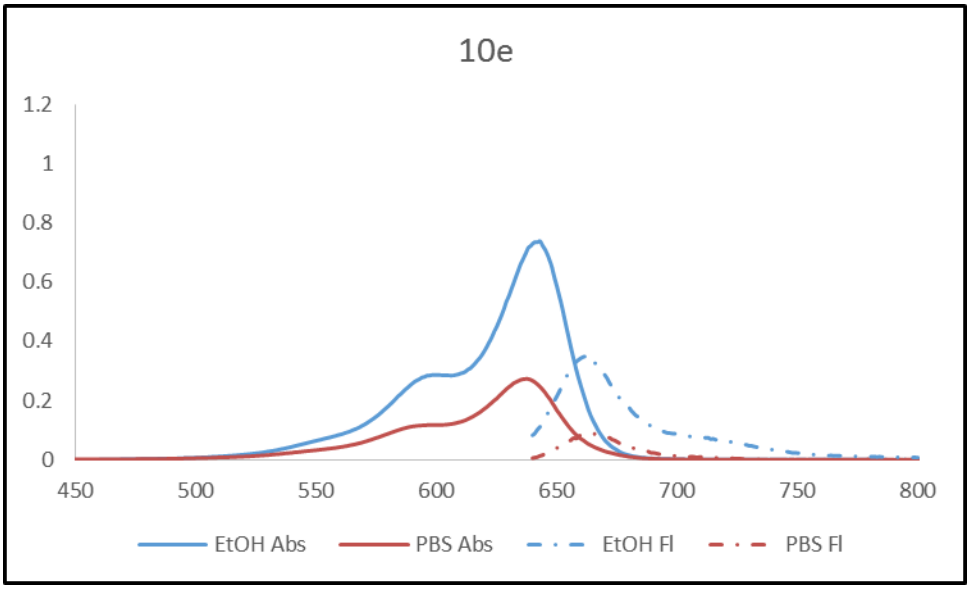
10e
1.2
1
0.8
0.6
0.4
0.2
0
450
500
550
600
650
700
750
800
EtOH Abs
PBS Abs
EtOH Fl
PBS Fl

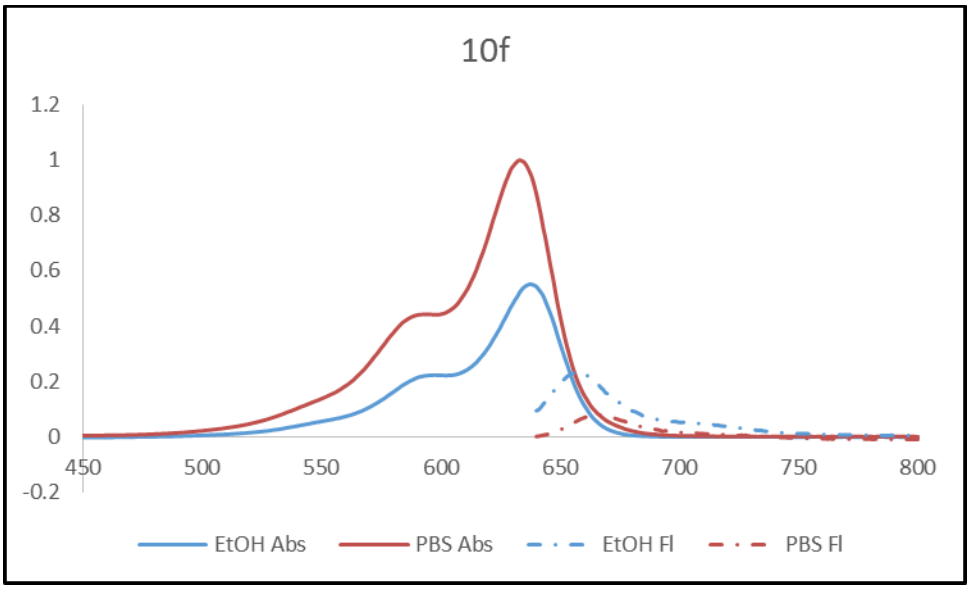

Appendix B.4 Physicochemical Properties

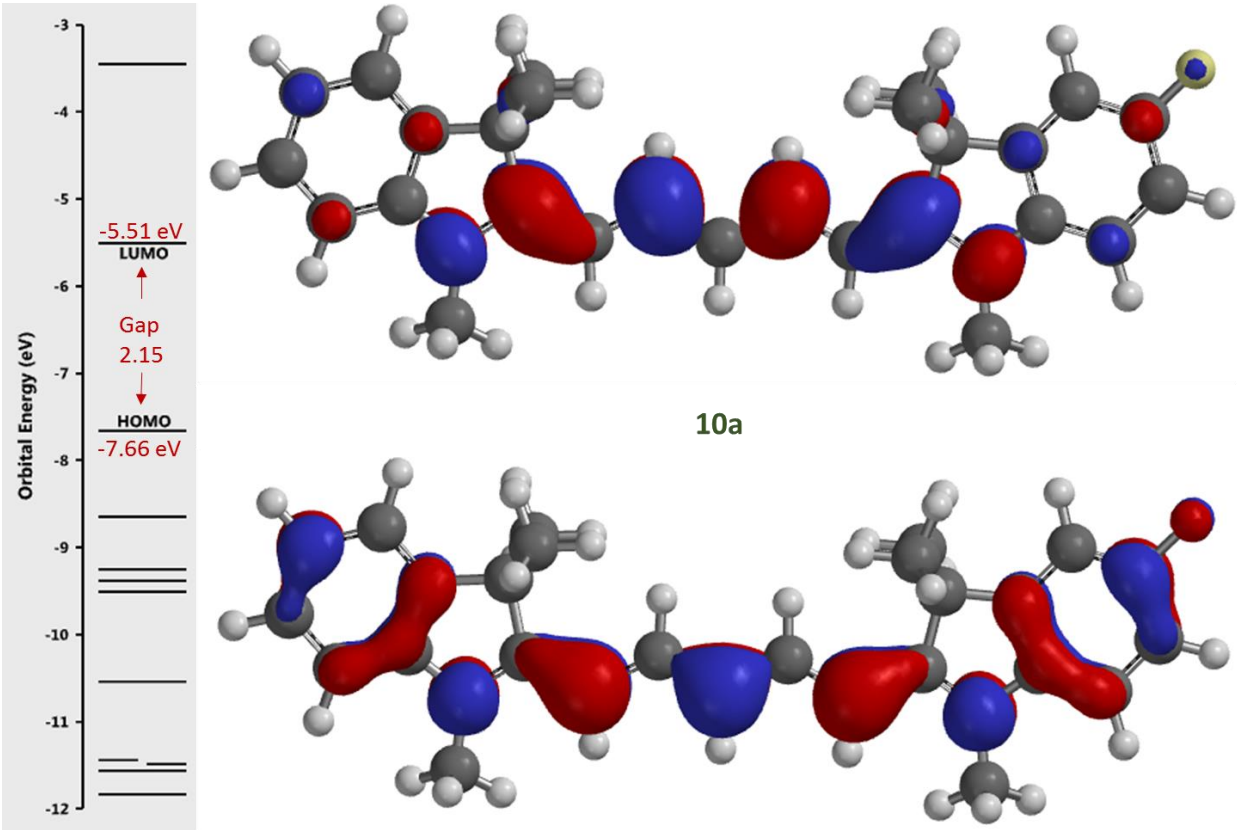

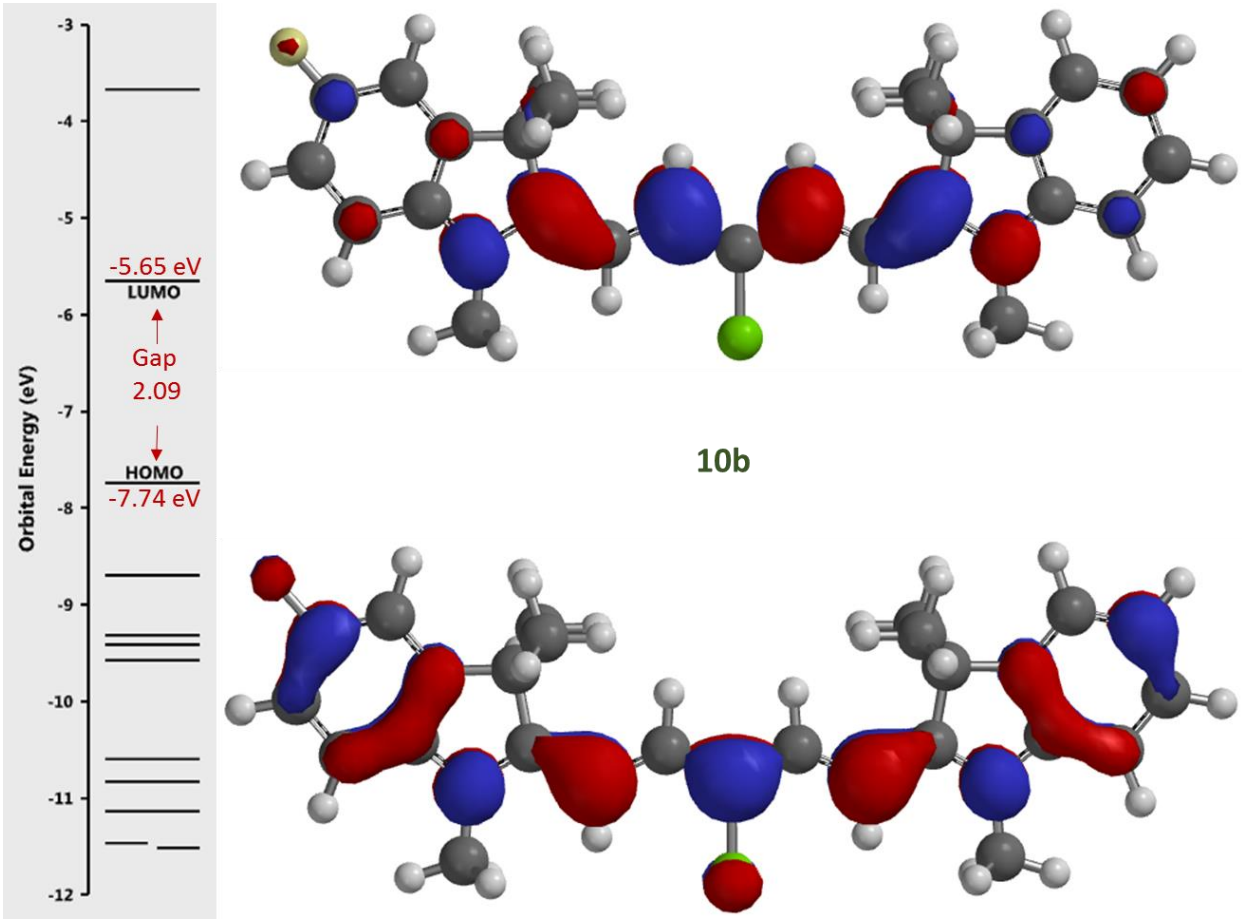
Orbital Energy (eV)
-3
-4
-5
-6
-7
-8
-9
-10
-11
-12
-5.65 eV
LUMO
Gap
2.09
HOMO
-7.74 eV
10b

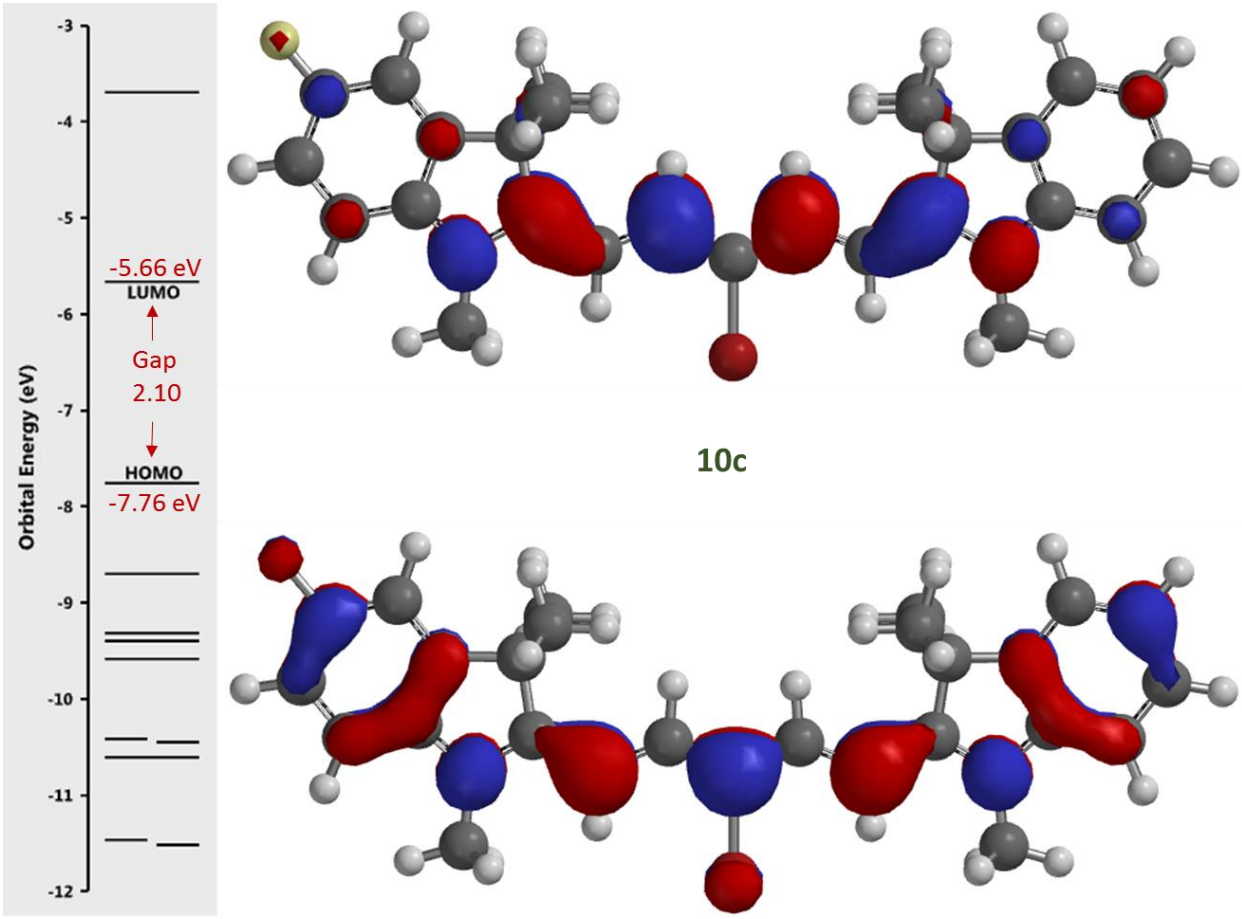
Orbital Energy (eV)
-3
-4
-5
-6
-7
-8
-9
-10
-11
-12
-5.66 eV
LUMO
Gap
2.10
HOMO
-7.76 eV
10c

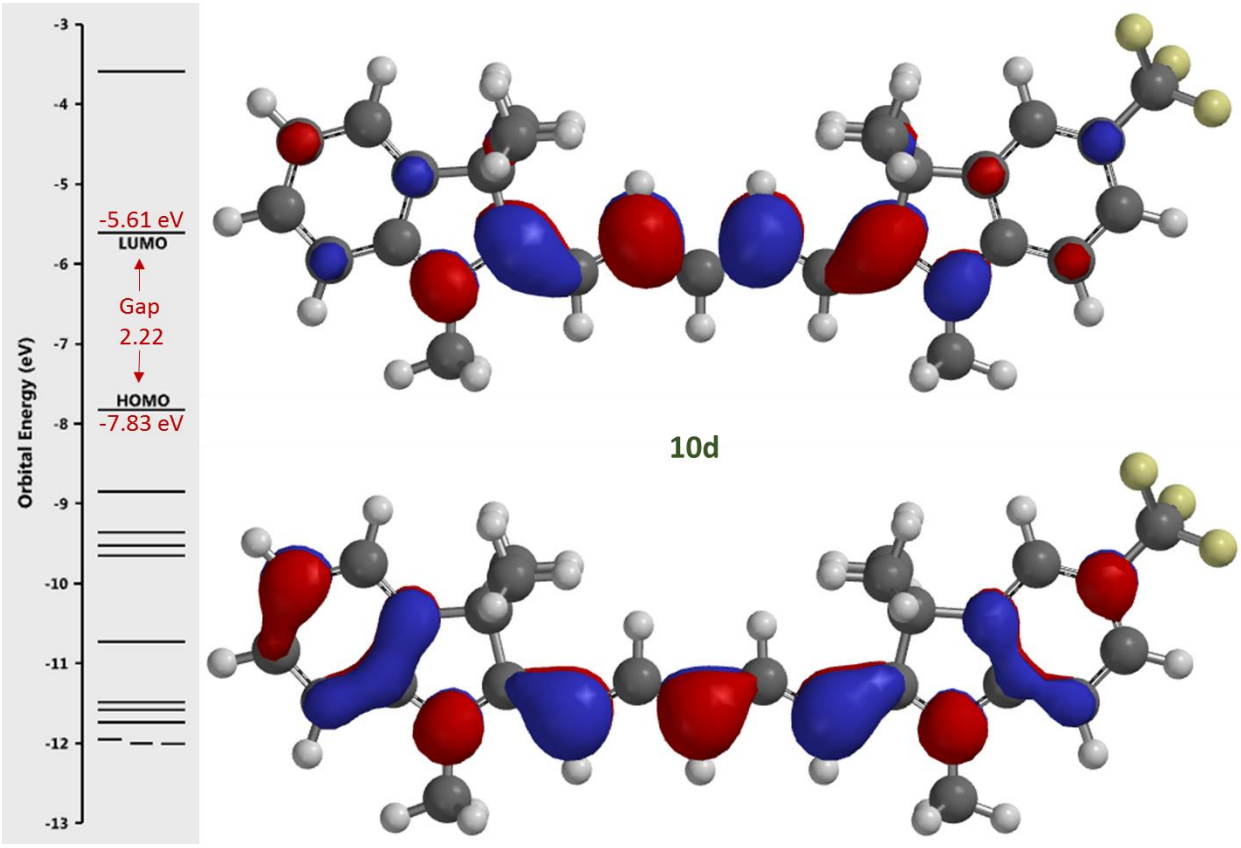
Orbital Energy (eV)
-3
-4
-5
-6
-7
-8
-9
-10
-11
-12
-13
-5.61 eV
LUMO
Gap
2.22
HOMO
-7.83 eV
10d

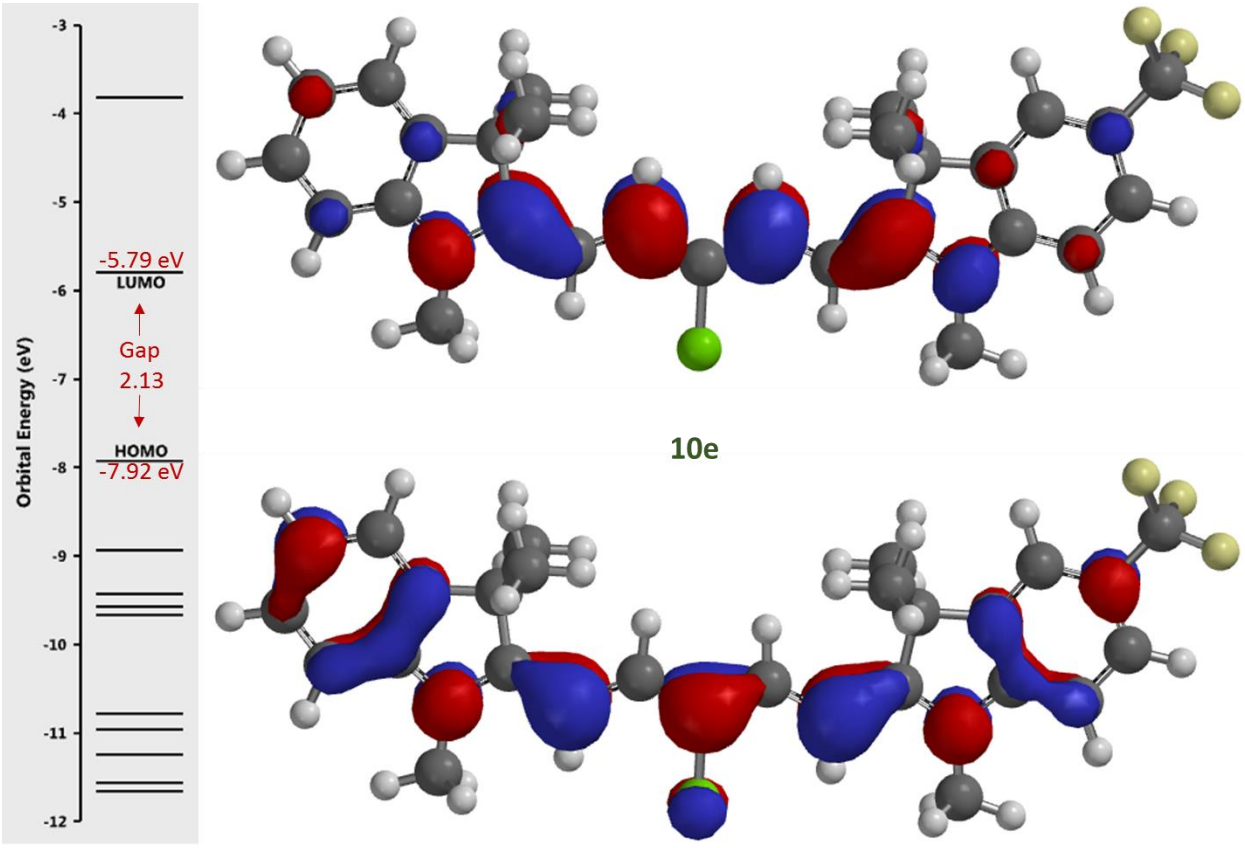
Orbital Energy (eV)
-3
-4
-5
-6
-7
-8
-9
-10
-11
-12
-5.79 eV
LUMO
Gap
2.13
HOMO
-7.92 eV
10e

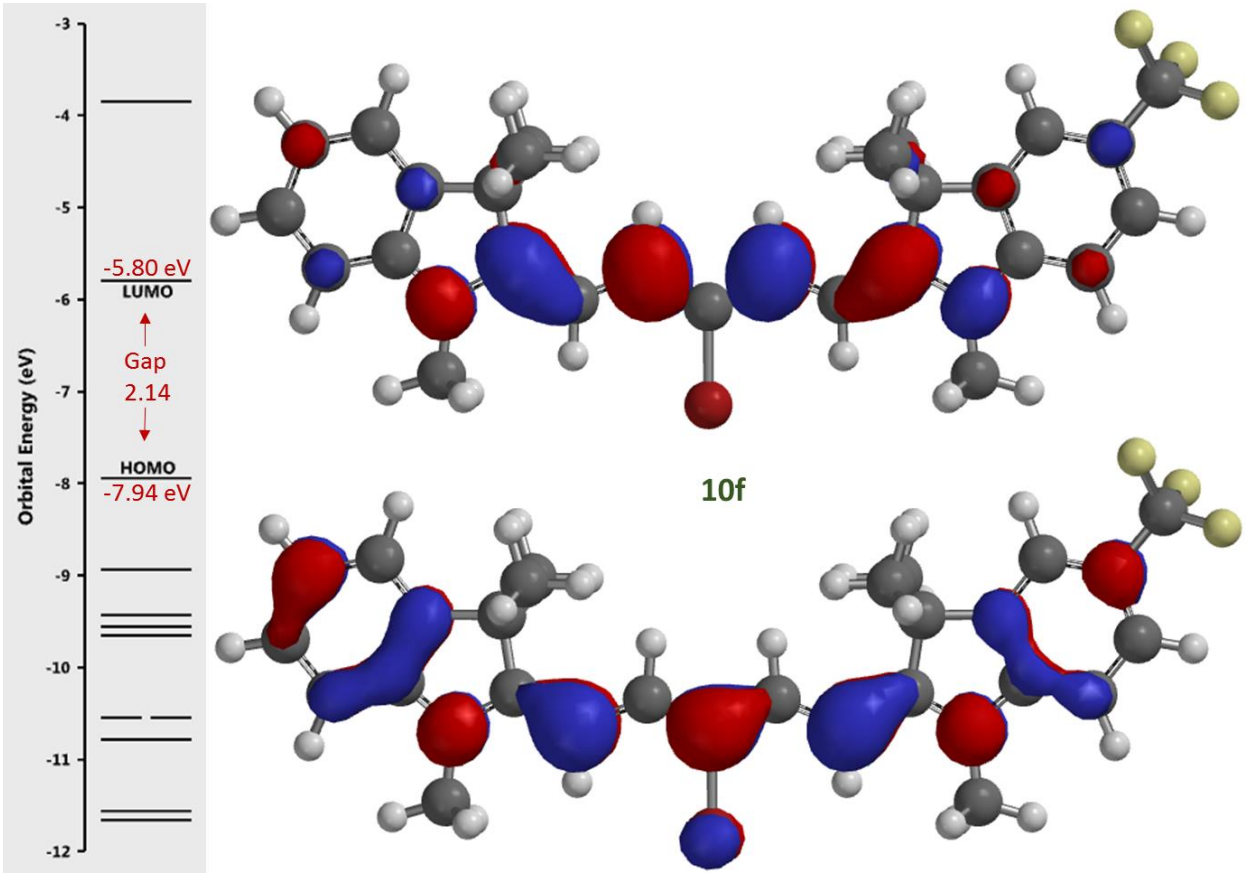
Orbital Energy (eV)
-3
-4
-5
-6
-7
-8
-9
-10
-11
-12
-5.80 eV
LUMO
Gap
2.14
HOMO
-7.94 eV
10f

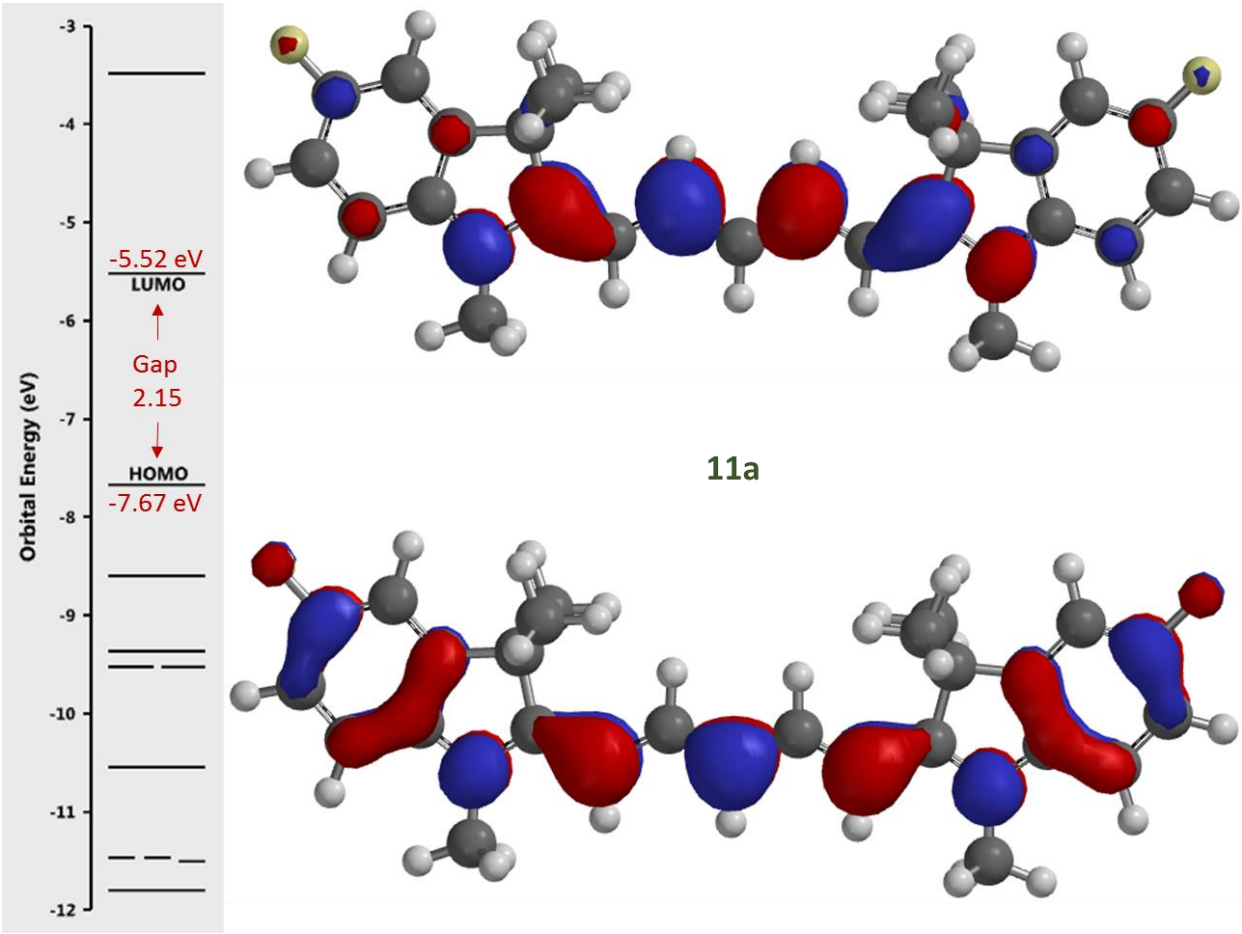
Orbital Energy (eV)
-3
-4
-5
-6
-7
-8
-9
-10
-11
-12
-5.52 eV
LUMO
Gap
2.15
HOMO
-7.67 eV

11a

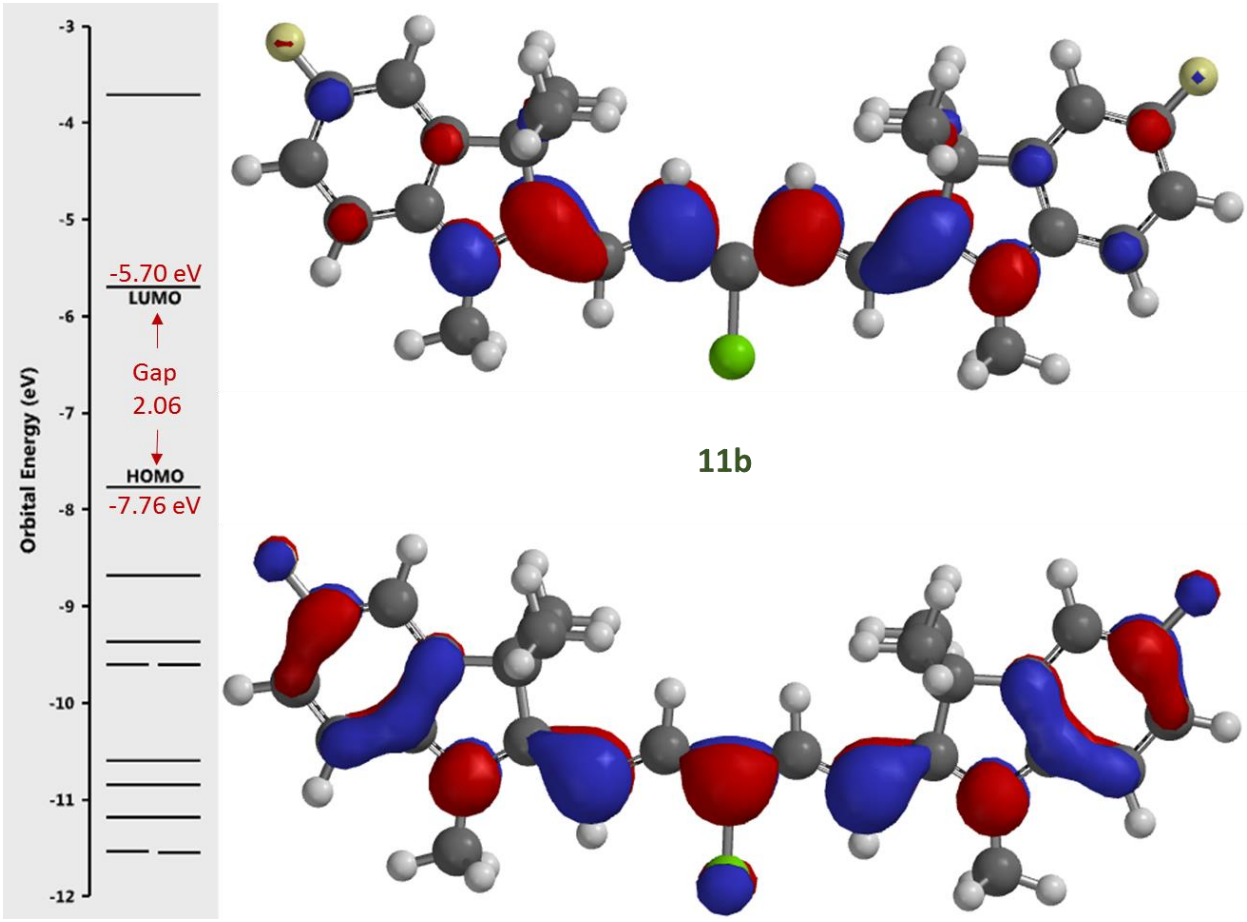
Orbital Energy (eV)
-3
-4
-5
-6
-7
-8
-9
-10
-11
-12
-5.70 eV
LUMO
Gap
2.06
HOMO
-7.76 eV

11b

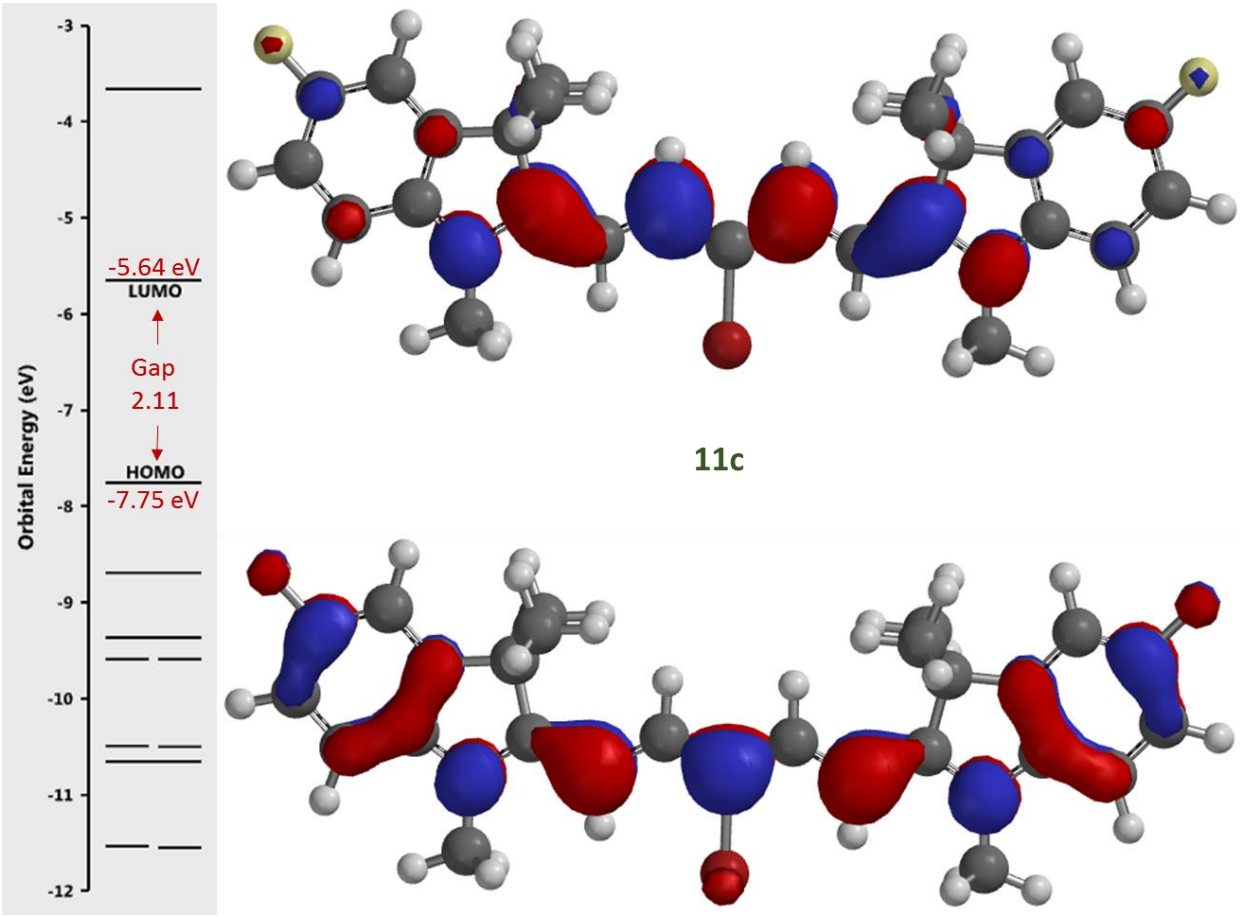
Orbital Energy (eV)
-3
-4
-5
-6
-7
-8
-9
-10
-11
-12
-5.64 eV
LUMO
Gap
2.11
HOMO
-7.75 eV
11c

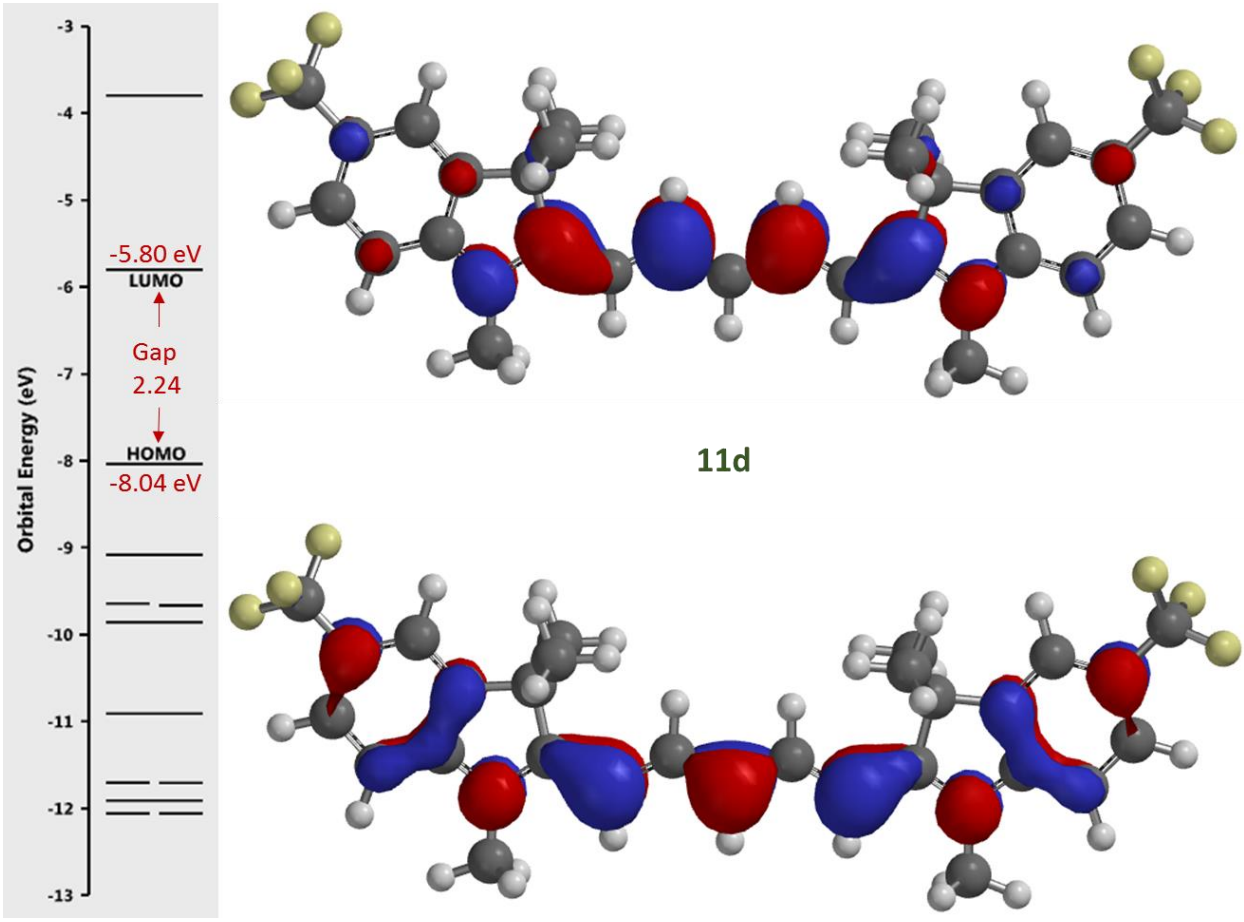
Orbital Energy (eV)
-3
-4
-5
-6
-7
-8
-9
-10
-11
-12
-13
-5.80 eV
LUMO
Gap
2.24
HOMO
-8.04 eV
11d

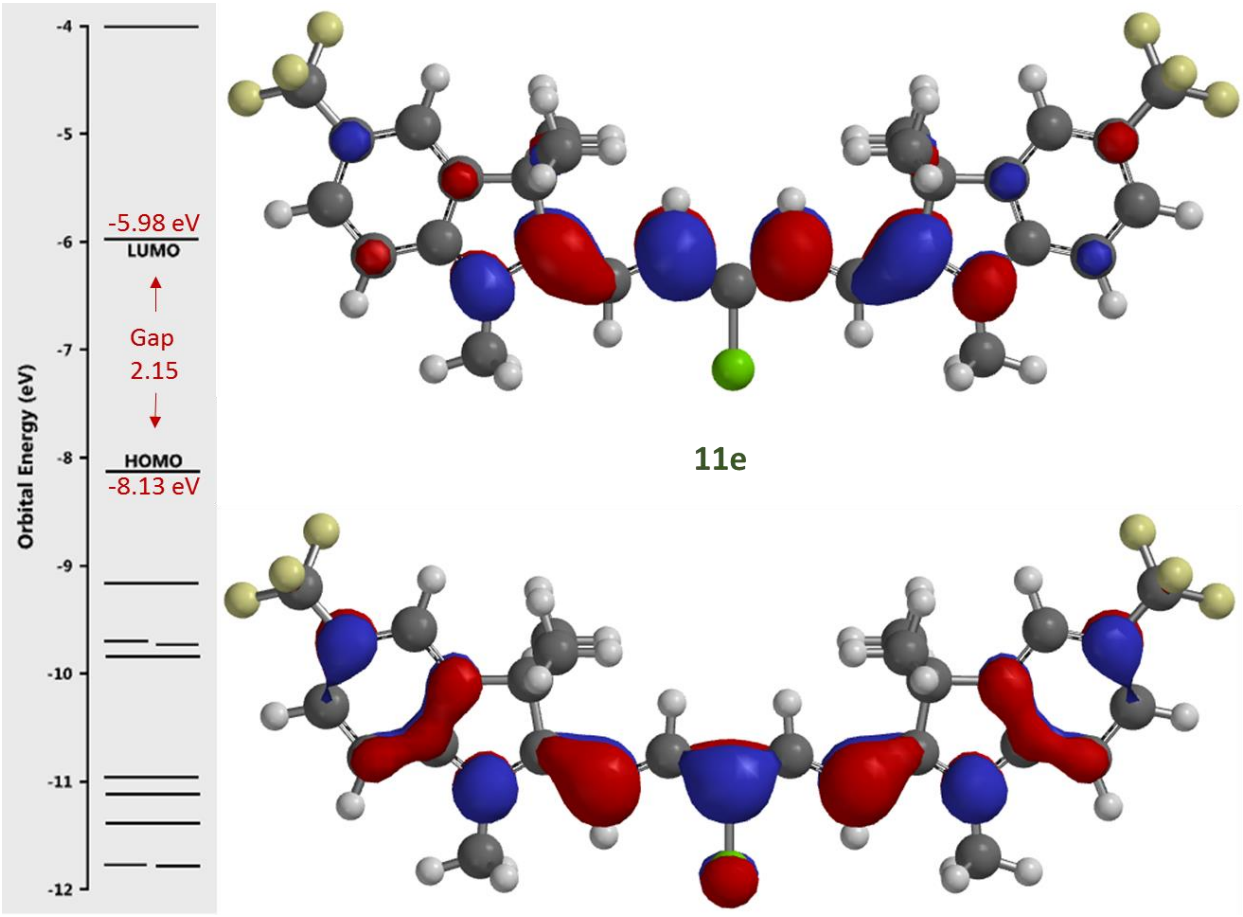
Orbital Energy (eV)
-4
-5
-6
-7
-8
-9
-10
-11
-12
-5.98 eV
LUMO
Gap
2.15
HOMO
-8.13 eV
11e

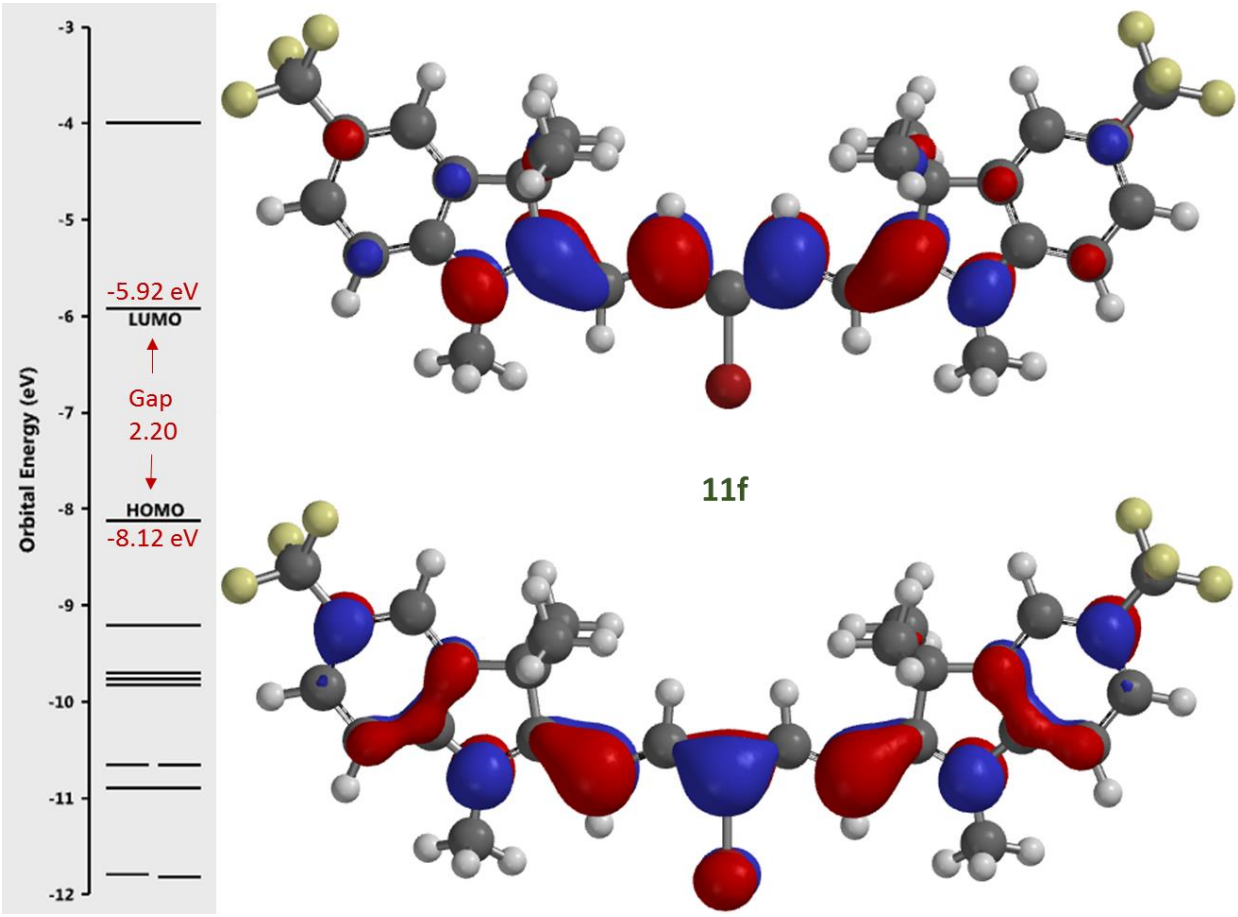
Orbital Energy (eV)
-3
-4
-5
-6
-7
-8
-9
-10
-11
-12
-5.92 eV
LUMO
Gap
2.20
HOMO
-8.12 eV
11f